MOLECULAR ENGINEERING OF HIGH AFFINITY T-CELL RECEPTORS FOR BISPECIFIC THERAPEUTICS

A Thesis submitted in requirement of

Cardiff University for the Degree of Doctor of Philosophy

*****

Nathaniel Liddy

2013

School of Medicine

ACKNOWLEDGMENTS

I owe my supervisors Professor Andrew Sewell and Dr. Bent Jakobsen a huge debt of gratitude for giving me the opportunity to realise a lifetime's ambition. Bent Jakobsen has been a constant source of support, encouragement and inspiration and has fuelled my interest for T-cell biology. Thanks go to Peter Molloy, Annelise Vuidepot and Namir Hassan (Immunocore Limited) for innumerable discussions, advice and scientific input into my work. I would like to pay special thanks to my wife, Karen whose love, support and sacrifice have made this possible and to my sons, Noah and Arthur, who have provided a distraction and a sense of perspective. Finally, I would like to thank my Mum and Dad who reminded me to never give up.

DECLARATION

This work has not previously been accepted in substance for any degree and is not concurrently submitted in candidature for any degree.

Signed …… (candidate) Date ……

STATEMENT 1

This thesis is being submitted in partial fulfillment of the requirements for the degree of PhD

Signed …… (candidate) Date ……

STATEMENT 2

This thesis is the result of my own independent work/investigation, except where otherwise stated. Other sources are acknowledged by explicit references.

Signed …… (candidate) Date ……

STATEMENT 3

I hereby give consent for my thesis, if accepted, to be available for photocopying and for inter-library loan, and for the title and summary to be made available to outside organisations.

Signed …… (candidate) Date ……

ABSTRACT

Cytotoxic T lymphocytes are able to identify malignant cells by scanning for aberrant peptides presented on cell surface human leukocyte antigen (HLA) Class I molecules by virtue of an antigen binding receptor called the T-cell receptor (TCR). Peptides presented by HLA Class I complexes represent the largest array of tumour associated antigens (TAAs) and are therefore ideal targets for immunotherapeutic reagents. Cancer patients frequently mount T-cell responses to tumour-specific antigens, but these are in most cases ineffective at clearing the tumour. This is in part due to the low affinity of TCRs for self-antigens coupled with low-level expression of target peptides on the surface of cancer cells. To harness the exquisite antigen recognition property of TCRs for use as potential therapeutic proteins, the principal goal of this thesis was to generate ultra-high affinity TCRs against three clinically relevant HLA Class I melanoma-specific epitopes, including peptides derived from Melan-A/MART-$1_{(26-35)}$, $gp100_{(280-288)}$ and MAGE-$A3_{(168-176)}$. TCRs are membrane-bound disulphide (ds)-linked heterodimers consisting of an alpha and a beta chain. Each chain comprises three hypervariable or complementarity-determining region (CDR) loops, which assemble to form the antigen binding domains. As a general rule the CDR3 loops, and to a lesser extent the CDR1 loops, contact the peptide bound in the HLA groove and as such specificity is largely attributable to the CDR3 loops. The remaining CDR loops interact with the HLA surface and not the bound peptide. Each CDR loop was mutagenised using degenerative NNK oligonucleotides and expressed on the surface of bacteriophage as fusions to the phage coat protein pIII. Through a Darwinian process of *in vitro* evolution using pHLA ligand as the target molecule, mutated TCRs with improved affinity for pHLA were identified. TCRs engineered by phage display were produced as soluble ds-linked proteins and the contribution to affinity of each mutated CDR was measured by surface plasmon resonance (SPR). Using a combinatorial strategy, individual mutated CDRs were spliced into the same TCR molecule in a stepwise manner to further increase binding affinity. The final combination of mutated CDRs was shown to bind their cognate pHLA antigen with substantially improved K_D values of 18 pM (Melan-A/MART-$1_{(26-35)}$), 11 pM ($gp100_{(280-288)}$) and 58 pM (MAGE-$A3_{(168-176)}$), representing an increase over the wild-type TCR of approximately 1.8 million-fold, 1.7 million-fold and 3.7 million-fold respectively. In addition, having discovered an off-target binding profile for the high affinity MAGE-A3 TCR, the phage display methodologies were explored to

reestablish the specificity of this molecule. These results are significant because this has provided a platform on which, for the first time, to make TCR-based therapeutics. For example, the affinity enhanced gp100 TCR is currently undergoing clinical evaluation in a Phase I/II trial.

PUBLICATIONS AND PATENTS

Aleksic M, **Liddy N**, Molloy PE, Pumphrey N, Vuidepot A, Chang KM, Jakobsen BK. Different affinity windows for virus and cancer-specific T-cell receptors: Implications for therapeutic strategies. *Eur J Immunol.* 2012 Sep 5.

Liddy N, Bossi G, Adams KJ, Lissina A, Mahon TM, Hassan NJ, Gavarret J, Bianchi FC, Pumphrey NJ, Ladell K, Gostick E, Sewell AK, Lissin NM, Harwood NE, Molloy PE, Li Y, Cameron BJ, Sami M, Baston EE, Todorov PT, Paston SJ, Dennis RE, Harper JV, Dunn SM, Ashfield R, Johnson A, McGrath Y, Plesa G, June CH, Kalos M, Price DA, Vuidepot A, Williams DD, Sutton DH, Jakobsen BK. Monoclonal TCR-redirected tumor cell killing. *Nat Med.* 2012 Jun;18(6):980-7.

Plesa G, Zheng L, Medvec A, Wilson CB, Robles-Oteiza C, **Liddy N**, Bennett AD, Gavarret J, Vuidepot A, Zhao Y, Blazar BR, Jakobsen BK, Riley JL. TCR affinity and specificity requirements for human regulatory T-cell function. *Blood.* 2012 Apr 12;119(15):3420-30.

Liddy N, Molloy PE, Bennett AD, Boulter JM, Jakobsen BK, Li Y. Production of a soluble disulfide bond-linked TCR in the cytoplasm of Escherichia coli trxB gor mutants. *Mol Biotechnol.* 2010 Jun;45(2):140-9.

Purbhoo MA, Li Y, Sutton DH, Brewer JE, Gostick E, Bossi G, Laugel B, Moysey R, Baston E, **Liddy N,** Cameron B, Bennett AD, Ashfield R, Milicic A, Price DA, Classon BJ, Sewell AK, Jakobsen BK. The HLA A*0201-restricted hTERT(540-548) peptide is not detected on tumor cells by a CTL clone or a high-affinity T-cell receptor. *Mol Cancer Ther.* 2007 Jul;6(7):2081-91.

Li Y, Moysey R, Molloy PE, Vuidepot AL, Mahon T, Baston E, Dunn S, **Liddy N,** Jacob J, Jakobsen BK, Boulter JM. Directed evolution of human T-cell receptors with picomolar affinities by phage display. *Nat Biotechnol.* 2005 Mar;23(3):349-54.

Hendry E, Taylor G, Grennan-Jones F, Sullivan A, **Liddy N,** Godfrey J, Hayakawa N, Powell M, Sanders J, Furmaniak J, Smith BR. X-ray crystal structure of a monoclonal antibody that binds to a major autoantigenic epitope on thyroid peroxidase. *Thyroid.* 2001 Dec;11(12):1091-9.

High Affinity Melan-A/MART-1 T-Cell Receptors (PCT/GB2006/001980), Jakobsen BK and **Liddy N**

High Affinity gp100 T-Cell Receptors (PCT/GB2010/001277), Jakobsen BK, Harwood N and **Liddy N**

High Affinity MAGE-A3 T-Cell Receptors (PCT/GB2010/01433), Jakobsen BK and **Liddy N**

TABLE OF CONTENTS

ABBREVIATIONS

Ab	Antibody
Abs	Absorbance
AP	Alkaline phosphatase
APC	Antigen presenting cells
β_2-m	β_2-microglobulin
BCR	B-cell receptor
BiTE	Bispecific T-cell Engager
BSA	Bovine serum albumin
C	Constant domain of T-cell receptor or B-cell receptor
CD (number)	Cluster of differentiation (number)
cDNA	Complementary deoxyribonucleic acid
CDR	Complementarity determining regions
CH1	Constant heavy chain 1
CH2	Constant heavy chain 2
CH3	Constant heavy chain 3
CL	Constant light chain
CLIP	Class II associated invariant chain peptide
cm	Centimetre
CM5	Carboxymethylated dextran
cfu	Colony forming units
CTLA-4	Cytotoxic T-lymphocyte antigen-4
DMSO	Dimethyl sulfoxide
DN	Double negative
DNA	Deoxyribonucleic acid
dNTP	Deoxyribonucleic triphosphate
DP	Double positive
E. coli	*Escherichia coli*
EDC	N-ethyl-N'-(dimethylamiopropyl) carbodiimide
EDTA	Ethylenediaminetetra-acetic acid
ELISA	Enzyme linked immunosorbent assay
ELISpot	Enzyme linked immunospot
ER	Endoplasmic reticulum
Fv	Variable fragment
Fab	Fragment of antigen-binding
FDA	Food and Drug Administration
FPLC	Fast protein liquid chromatography
g	Gram
HBS	HEPES buffered saline
HPSF	High purity salt free (oligonucleotides)
HLA	Human leucocyte antigen
ICAM-1	Intracellular adhesion molecule-1
IFN-γ	Interferon gamma
Ig	Immunoglobulin
IPTG	Isopropyl-1-thio-β-D-galactopyranoside
k(bp)	(Kilo) base pair
K_D	Dissociation constant
KDa	Kilodalton
kg	Kilogram
k_{off}	Dissociation off-rate

k_{on}	Dissociation on-rate
l	Litre
LB	Luria Bertani medium
LFA-1	Leukocyte function associated antigen-1
m	Metre
M	Molar
mg	Milligram
min	Minute
ml	Millilitre
MPBS	Marvel PBS
MHC I	Major Histocompatibility Class I
MHC II	Major Histocompatibility Class II
mAb	Monoclonal antibody
mTCR	Monoclonal T cell receptor
MW	Molecular weight
nM	Nanomolar
OD	Optical Density
pHLA	Peptide HLA
pMHC	Peptide MHC
Pan	Biopanning
PBMC	Peripheral blood mononuclear cells
PBS	Phosphate buffered saline
PBST	Phosphate buffered saline tween
PCR	Polymerase chain reaction
PEG	Polyethylene glycol
PE	Phycoerythrin
pM	Picomolar
pmol	Picomole
RPM	Revolutions per minute
RU	Response unit
scFv	Single chain variable fragment
SDS-PAGE	Sodium Dodecyl Suphate-Polyacrylamide Gel Electrophoresis
Sec	Second or s
SOC	Super optimal catabolities
SOE	Splice by overlap extension
SPR	Surface plasmon resonance
T	Tween
$T_{1/2}$	Dissociation half-life
TAP	Transporter associated with antigen processing
TCR	T-cell receptor
TdT	Terminal deoxynucleotidyl transferase
U	Unit
V	Variable domain of T-cell receptor or B-cell receptor
VH	Variable heavy chain
VL	Variable light chain
v/v	Volume per unit volume
w/v	Weight per unit volume
α	Alpha TCR chain
β	Beta TCR chain
μg	Microgram

µl	Microlitre
µg	Microgram
°C	Degrees Celsius

Amino Acids

A	Ala	Alanine
C	Cys	Cysteine
D	Asp	Aspartic acid
E	Glu	Glutamic acid
F	Phe	Phenylalanine
G	Gly	Glycine
H	His	Histidine
I	Ile	Isoleucine
K	Lys	Lysine
L	Leu	Leucine
M	Met	Methionine
N	Asn	Asparagine
P	Pro	Proline
Q	Gln	Glutamine
R	Arg	Arginine
S	Ser	Serine
T	Thr	Threonine
V	Val	Valine
W	Trp	Tryptophan
Y	Tyr	Tyrosine

INTRODUCTION

1.1 Introduction

The mainstay of cancer treatment, except in cases where the disease is too far progressed, has for many decades been surgery. More recently, this has been combined with chemo- or radiation therapy which, although it does not have spectacular efficacy and is associated with severe toxicity, has improved survival and time to progressive disease in many indications. Most chemo- and radiation therapies attempt to exploit the highly proliferative characteristic of cancer cells by inducing damage in the replicating cell ultimately leading to cell death. This is rarely a targeted approach and typically highly proliferative normal, healthy cells such as those in the bone marrow, digestive tract and hair follicles are also affected.

The limited efficacy and severe side-effects of chemo- and radiation type therapies has in recent decades prompted considerable efforts to develop therapies that are targeted more specifically to cancer cells. Extensive research has uncovered molecules that are specifically involved in tumour survival and growth. Many proteins have also been identified that, although of unknown function, are characteristic to a smaller or larger extent of cancer cells, because they are overexpressed or, in some cases, exclusively expressed, in these. All these molecules represent potential targets for anti-cancer drugs.

Targeted cancer therapies raise the possibility of more efficacious and less toxic treatment and include small molecule drugs and monoclonal antibodies that act in a variety of ways: blocking signal transduction pathways involved in the proliferation of cancer cells, sequestering proteins required for tumour spread and apoptosis of malignant cells via a toxic ‘pay load’ or by recruitment of components of the immune system e.g. bispecific antibodies which target the cancer cell via one arm and T-cells via the other. In recent years immunotherapy more than any other type of therapy has begun to show the capacity to eradicate tumours leading to long-term clinical

remission and the potential promise of a cure. In the majority of patients however, a cure remains elusive due to active immune evasion by cancers.

Cancer cells arise from normal tissue cells and, despite the devastating threat they pose to a patient's health, differ only marginally from their parental origin. However, they do contain gene mutations and exhibit abnormal expression of certain genes that make them stand out from 'self'. A group of potential cancer targets are the tumour associated antigens (TAAs) which can elicit an immune response by antibodies or by T-cells. Cancer antigens vary in the pattern of their expression and can be divided into several distinct groups. Overexpressed antigens are expressed in normal tissue but are upregulated in tumours. Mutated self-antigens arise from random point mutations within genes that can be specific to a particular tumour of a particular individual. Cancer/testis antigens are widely spread in many different cancers but their normal expression is restricted to male germline cells in the testis. Expression of differentiation antigens is restricted to one particular tissue-type and by cancer cells derived from that tissue-type.

The dominant immunotherapeutic protein scaffold in clinical development is antibody-based. The last two decades has seen notable successes with this type of framework, such as trastuzumab (Herceptin) in metastatic breast cancer, bevacizumab (Avastin) in metastatic colorectal cancer and rituximab (Rituxan) in Non-Hodgkin's lymphoma. The targets for antibody-based therapies against cancer cells are integral-membrane proteins; however, the majority of TAAs are intracellular and therefore inaccessible to antibodies. Therefore, the continued development of these types of drugs may be hindered by the limited number of amenable cancer targets.

Cellular proteins, including TAAs, are continuously undergoing a process of degradation in the cytosol and are loaded onto major histocompatibility complexes

(MHC in the murine system and human leukocyte antigen, HLA in the human system) as short peptide fragments. The surface presentation of peptides provides the immune surveillance system a means to scan and screen the protein composition of the cell. Cytotoxic $CD8^+$ T-cells recognise endogenously-derived peptide fragments presented in the context of MHC molecules via a surface-bound protein called the T-cell receptor (TCR); a molecule homologous both in structure and function to the B-cell receptor (BCR) displayed on the surface of B-cells.

A number of clinical observations have provided evidence supporting the role of natural immunity to cancer. Although rare, in some cases, spontaneous regression of melanoma lesions accompanied by the clonal expansion of T-cells has been observed as reviewed in (Bindea, Mlecnik et al. 2010; Vesely, Kershaw et al. 2011). These anti-tumour responses manifest in the absence of specific immunotherapy supporting the role of the immune system in the detection of malignant cells. Further evidence for cancer immunosurveillance (i.e. the recognition and destruction of cancerous cells by the immune system) is provided by reports that have identified tumour-reactive T-cells in human cancer patients (Bindea, Mlecnik et al. 2010; Vesely, Kershaw et al. 2011). Additionally, studies of melanoma, ovarian and colon cancer have demonstrated that improved prognosis correlates with increased numbers of intratumoural infiltrating lymphocytes (TILs). More specifically, it is the T-cell phenotype, quantity and location within the tumour that collectively are associated with patient survival (Bindea, Mlecnik et al. 2010; Vesely, Kershaw et al. 2011). However, in the majority of cancer cases presented T-cells are ineffective at controlling tumour growth. Failure to eliminate cancer cells is due in part to the depletion of T-cells that recognise self-peptides with high affinity during the process of negative selection in the thymus. T-cells that move into the periphery will present

TCRs with low antigen-binding affinity for self-antigen and as a result may fail to recognise and destroy malignant cells presenting these peptides.

Whilst antibodies cannot recognise intracellular TAAs, the unique ability of TCRs to do so, makes this class of molecule an ideal candidate for therapeutic tumour targeting. For TCRs to be suitable as cancer therapeutic agents several challenges have to be addressed. TCRs are naturally membrane-bound and would therefore have to be produced as a soluble molecule. The number of tumour associated peptide antigens TAPAs presented on the surface of tumour cells is low necessitating engineering of the TCR for high affinity for which there is no precedent.

1.2 Antibody structure and function

Since the Nobel Prize-winning achievements of Georges Kohler and Cesar Milstein in 1975 (Kohler and Milstein 1975) in generating monoclonal antibody hybridomas, this class of molecule has proven invaluable in both the research and clinical arena. The literature on this subject is almost endless, providing numerous lessons in areas such as protein engineering, design and expression, tumour targeting and drug development.

The lessons learned from the engineering of antibody fragments are very relevant when exploring the engineering of TCRs. Both TCRs and antibodies are members of the immunoglobulin superfamily and retain a good degree of structural homology. Strategies devised for antibody stabilisation, reconfiguration and expression have the potential to inform or be directly applied to TCR engineering.

Antibodies play a crucial role in the body's response to encounters with foreign antigens; they are used by the immune system to identify and neutralise foreign pathogens. Antibodies can be secreted in a soluble form from activated B-cells called plasma cells or remain membrane bound. There are 5 classes (or isotypes) of

antibodies called immunoglobulins: IgA, IgD, IgE, IgG and IgM which differ in size and antigen-binding capacity (Murphy, Travers et al. 2008). The intact format of IgG is used by almost all approved antibody drugs (Beck, Wurch et al. 2011). Figure 1.1 depicts an IgG molecule.

The principal unit is Y-shaped (150 kilodaltons, KDa), bivalent (can bind two identical antigens) and has a modular structure containing a total of twelve domains (Padlan 1994). It comprises four chains: two identical heavy (H) chains and two identical light (L) chains (either a lambda-λ or a kappa-κ light chain) held together by disulphide bonds.

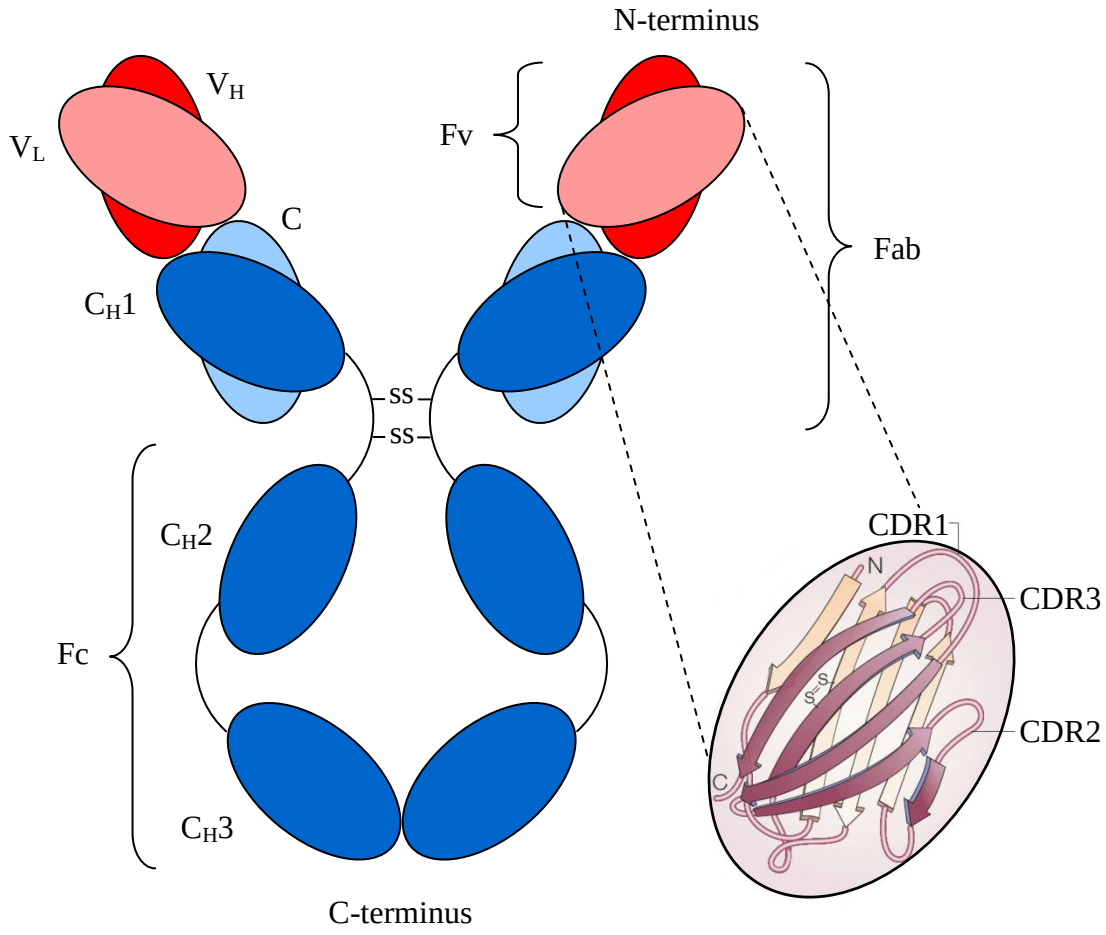

Figure 1.1. Schematic representation of an antibody IgG structure. An IgG molecule comprises two distinct modules in relation to activity: an antigen-binding end (the Fab region) and a biological mediated end (the Fc region). The IgG molecule consists of two identical heavy (H) chains and two identical light (L) chains (either an lambda λ chain or a kappa κ chain) held together by disulphide bonds. The H chain is formed by one variable (V) domain and three constant (C) domains (C_H1, C_H2 and C_H3). The light chain consists of one V domain and only a single C domain. The Fv fragment consists of a covalently bonded variable heavy (V_H) and variable light (V_L) domain. The N-terminus of the V domains contain three hypervariable loops or complementarity determining regions (CDR1, 2 and 3) where the highest level of sequence variability is concentrated; the most variable part is the third CDR. The pairing of the two V domains creates a single hypervariable site called the antigen-binding site. Adapted from (Brekke and Sandlie 2003; Holliger and Hudson 2005).

The heavy chains of IgG comprise three constant (C_H1, C_H2, C_H3) domains and one variable (V_H) domain, whilst the light chains contain a constant (C_L) domain and a single variable (V_L) domain. Each domain comprises two β-sheets packed tightly against each other in an antiparallel β-barrel to form the so-called immunoglobulin (Ig) fold. The smallest unit of an antibody that still retains the antigen-binding site is the Fv (fragment, variable) domain which encompasses the variable region of the heavy and light chain. The antibody is divided into two distinct function-related portions. The Fab (fragment, antigen-binding) domain comprises of one variable domain and one constant domain from each of the two chains. The variable region is responsible for antigen recognition and binding affinity. The "tip" (N-terminus) of the V_L and V_H domains is formed from a total of six hypervariable loops or complementarity determining regions (CDRs); three loops from the variable domain of each chain (V_H-CDR1, CDR2, CDR3 and V_L-CDR1, CDR2, CDR3). Each set of loops is supported by nine β-strands arranged in two sheets of four and five strands. The enormous diversity in antigen-binding capacity is generated by genetic recombination events that occur during B-cell maturation and somatic hypermutation of the variable regions in the activated B-cell. Recombination events in the precursor B-cell lead to a single heavy chain and a single light chain gene, each with a specific V region. Whilst antigen specificity of V_H CDR3 results from the recombination of variable (V), diversity (D) and junctional (J) gene segments, V_L CDR3 antigen specificity results from VJ gene recombination (Storb, Shen et al. 2001). Antigen-binding capability is also derived from germline encoded CDR1s and CDR2s. There are seven human kappa (κ) light chains and eleven human lambda (λ) light chains. Further diversity is generated through variation in CDR-L1, CDR-H1 and CDR-H2 lengths (Tomlinson, Walter et al. 1992; Lefranc, Giudicelli et al. 1999). The tail of the

molecule (domains two and three of each of the heavy chain constant regions), is termed the Fc (fragment, crystallisable) region and mediates effector functions through interaction with Fc receptors expressed on various effector cells, including macrophages and natural killer (NK) cells or with components of the complement system leading to the destruction of antibody-coated target cells.

1.3 Engineered Antibody fragments

The modular structure of antibodies with the scaffold-like properties of the Ig fold lends itself to reconfiguration into various other simplified structural formats, including Fab (Fragment of antigen-binding), Fv (Fragment variable) and scFv (Single-chain Fv). The reduced size of these fragments confers a number of advantages, in certain circumstances over the parent IgG. For example, Fab fragments are more easily crystallised and in the context of molecular evolution strategies, Fab and other antibody fragments are better expressed in microbial systems. In terms of therapeutic potential, the smaller formats exhibit improved pharmacokinetics allowing a more rapid and efficient penetration of tissues inaccessible to intact IgGs. Numerous approaches have been devised to generate alternative recombinant antibody scaffolds for facile expression in microbial systems (yeast and *E. coli*). There are various ways of employing subunits of the antibody complex for engineering smaller fragments that can be used therapeutically; a number of which are undergoing preclinical and clinical evaluation (Holliger and Hudson 2005).

1.3.1 Fragment of antigen-binding (Fabs)

The Fab fragment (50 KDa), at one-third the size of the complete IgG, retains the antigen-binding capacity of the parent antibody making it an attractive molecule in terms of expression and potential therapeutic application. Chimeric mouse-human

Fabs that comprise mouse V domains fused to human C domains have been expressed as functional fragments in both yeast (Horwitz, Chang et al. 1988) and *E. coli* (Better, Chang et al. 1988; Skerra and Pluckthun 1991).

1.3.2 Single-chain Fvs (scFvs)

A smaller engineered antibody fragment is called Fv (Fragment variable). Variable V_H and V_L domains which are expressed as separate polypeptides assemble into Fv fragments through non-covalent association (Skerra and Pluckthun 1988; Pluckthun and Skerra 1989; Ward, Gussow et al. 1989). The production of Fv fragments, however, was hampered by improper folding and a tendency to form aggregates. In an effort to overcome the issues of instability and poor yields, the V_H and V_L domains of an Fv fragment can be linked to generate molecules called single-chain Fvs (scFvs) via a flexible peptide linker (Bird, Hardman et al. 1988; Huston, Levinson et al. 1988), typically between 10 and 25 amino acids in length or by introducing a disulphide bond in the framework region of the V_H and V_L domains (disulphide-stabilised Fvs; dsFvs) (Brinkmann, Reiter et al. 1993).

1.3.3 Multivalent scFvs

In terms of therapeutic promise, antibody molecules need to fulfil certain pharmacokinetic requirements such as low antigen dissociation rates and high retention times on the target tumour. Whilst monovalent antibody fragments such as scFvs, dsFvs and Fvs do not satisfy these criteria, they can be multimerised (scFv dimers, trimers and tetramers) as a means to increase functional affinity (avidity) (Holliger and Hudson 2005). Multivalency can be achieved by varying the length of the linker between the V_H and V_L domains. Shortening the linker to between 5-15 (Holliger, Prospero et al. 1993; Kortt, Lah et al. 1997; Arndt, Muller et al. 1998;

Nielsen, Adams et al. 2000), <5 or between 0-2 residues forces the scFv to self-associate into dimeric (dimer), trimeric (trimer) or tetrameric (tetramer) antibody fragments respectively (Dolezal, De Gori et al. 2003).

1.4 *In vitro* affinity maturation of antibodies

It is not fully understood what affinity is necessary to deliver maximal therapeutic potential in terms of potency and efficacy. Although it has been shown that improvements in affinity correlate with greater antibody-mediated cytotoxicity and target cell lysis (McCall, Shahied et al. 2001), it has also been demonstrated that lower affinity antibodies are capable of efficient tumour targeting and tumour retention (Adams, Schier et al. 1998). Additionally, ultra-high affinity antibodies may not always be desired as, in some cases, diffusion from the vasculature into solid tumours, is impaired. It therefore seems apparent that an affinity plateau is reached above which tumour retention reduces (Adams, Schier et al. 2001).

Display technologies have proven to be a powerful and efficient method to isolate and engineer antibodies *in vitro*. An examination of the techniques and strategies used to improve the affinity of antibodies has direct implications for the directed evolution of TCRs for high affinity. The *in vitro* directed evolution of antibody affinity follows a well-defined process akin to Darwinian evolution that starts with genetically manipulating the antibody sequence to generate huge libraries of variants from which binders with improved affinity for the target antigen are selected. A variety of display formats have been employed to engineer tighter binding antibodies each with advantages and disadvantages. The three major display formats are shown in Figure 1.2 and include cell-free systems such as ribosomal display and cell-based systems such as yeast display and phage display. The fundamental principal of each display

strategy is the link between the phenotype (protein) and the genotype (genetic information) (Bradbury, Sidhu et al. 2011).

Ribosome display was established by Hanes and Pluckthun (Hanes and Pluckthun 1997) as a technique to identify scFv fragments specific for target ligands. The DNA construct for ribosomal display includes a T7 promoter, the gene to be displayed and a spacer region near the codon for the carboxy-terminus lacking a terminal stop codon. The library DNA is transcribed and translated *in vitro* (cells are not used any stage). The spacer domain enables the complete exit of the nascent polypeptide from the ribosomal tunnel whilst absence of a 3' stop codon leaves the protein tethered to the ribosome accessible for interaction with antigen. Using this approach, scFvs against bovine insulin with affinities up to 82 pM (Hanes, Schaffitzel et al. 2000) and scFvs against the human death-receptor Fas with 22-fold affinity gains (Chodorge, Fourage et al. 2008) have been engineered. The major attraction of ribosomal display is the size of the libraries that can be generated. Because there is no transformation step, diversity is not restricted as in cell-based systems; libraries of more than $1x10^{13}$ members are routinely produced. Cell-free systems such as ribosomal display are, however, limited to the display of antibody scFv fragments and have not been successful in the display of intact full-length IgGs. Ribosomal display of antibodies has been recently reviewed (Pluckthun 2012).

In yeast display recombinant proteins are displayed on the surface of *S. cerevisiae* as fusions to the a-agglutinin yeast adhesion cell surface receptor (Boder and Wittrup 1997). The receptor comprises two proteins, Aga1 and Aga2. Aga1 is embedded in the cell membrane and Aga2 binds Aga1 through two disulphide bonds. Recombinant antibodies are fused in frame to the *AGA2* gene.

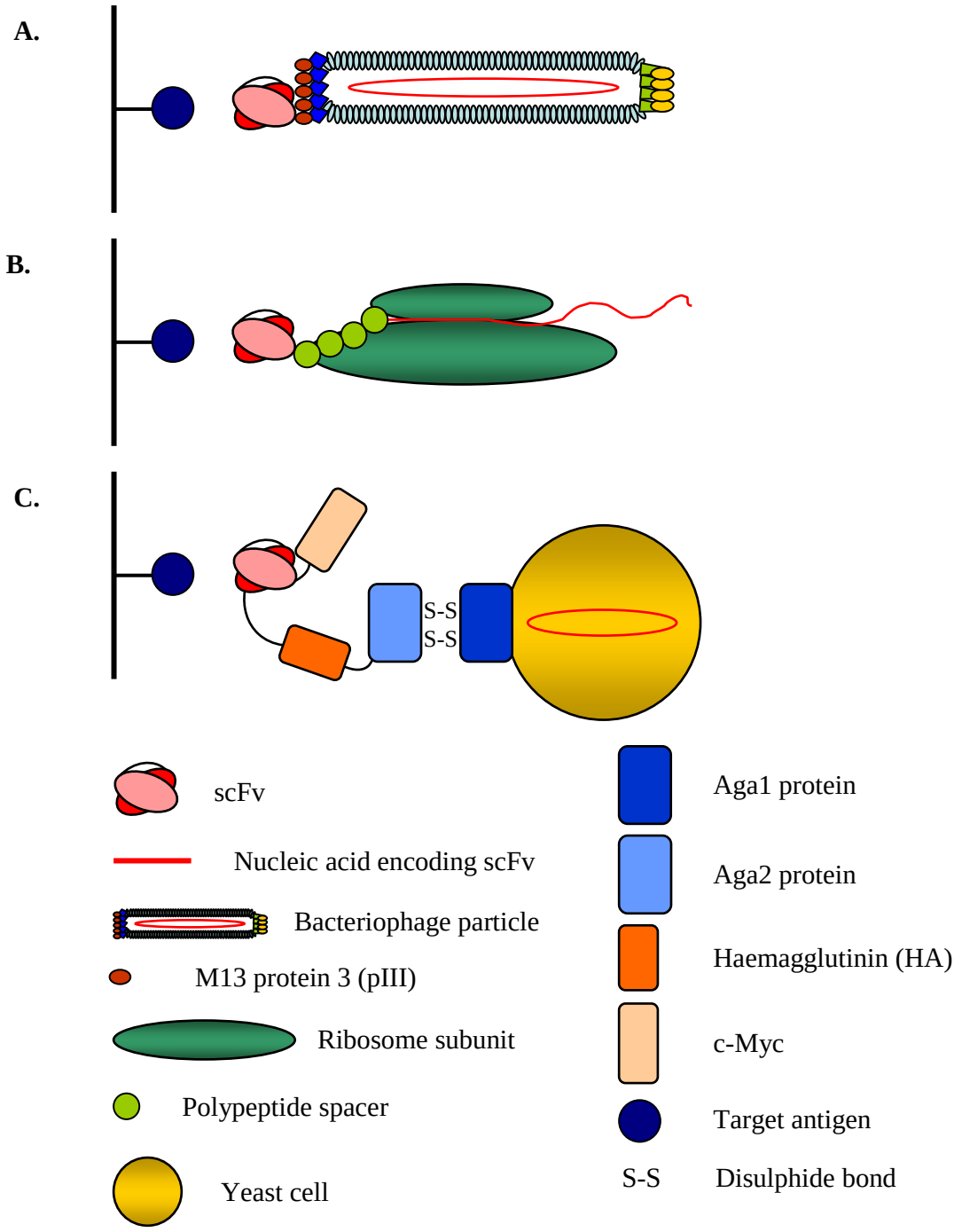

Figure 1.2. *In vitro* display formats. (A). Phage display. The recombinant protein (in this case an scFv) is displayed on the surface of a bacteriophage particle fused to a phage coat protein (in this case pIII). **(B).** Ribosome display. The DNA library is fused to a spacer sequence lacking a stop codon. The spacer sequence when translated remains tethered to the ribosome allowing the protein of interest (e.g. an scFv) to protrude out of the ribosome and interact with target antigen. The genetic information is recovered by reverse transcriptase PCR. **(C).** Yeast display. The gene of interest is fused to the Aga2 gene. The fusion cassettes are transformed into a strain of *S. cerevisiae* (producing endogenous Aga1 protein). Association of Aga1 and Aga2-scFv fusion through two disulphide (S-S) bonds results in display on the yeast cell surface. Expression is monitored using antibodies to the HA or c-Myc tags. Adapted from (Weisser and Hall 2009).

In the yeast display cloning vector the gene of interest is flanked with a C-terminal c-myc and N-terminal HA epitope tag. This facilitates monitoring of the level of recombinant antibody display through FACS-sorting using fluorescently labelled antibodies recognising either of the epitope tags. Flow cytometry techniques also allow the isolation and enrichment of populations of yeast cells displaying antibodies with desired antigen-binding characteristics. Although yeast display library size is limited by the relatively low transformation efficiency of yeast cells, there have been numerous antibody engineering successes. In addition to affinity maturing an anti-fluorescein scFv more than 17,000-fold to 48 fM (one of the highest affinity antibodies reported) (Boder, Midelfort et al. 2000), the Wittrup lab has also evolved the dissociation half-life of an anti-carcinoembryonic antigen (CEA) antibody up to 7 days at 37ºC (Graff, Chester et al. 2004). Application of yeast display over the past 15 years for engineering of antibodies has been recently summarised (Boder, Raeeszadeh-Sarmazdeh et al. 2012).

Although both ribosome and yeast display have been used successfully to engineer antibodies, phage display technology remains the most widely used method of improving antibody affinity and binding properties; both are pivotal to the development of effective therapeutic molecules.

Antibody fragments can be displayed on the surface of filamentous bacteriophage fused to one of the phage coat proteins, commonly protein III (pIII). A detailed description of the phage display machinery will be discussed in section 1.5. The antibody fragments can be displayed as Fab fragments, in which one of the two domains is fused to bacteriophage pIII and expressing the other unfused and secreting into the periplasm of *E. coli* (Hoogenboom, Griffiths et al. 1991; Barbas, Bjorling et al. 1992; Barbas, Crowe et al. 1992), as Fv fragments (Riechmann and Weill 1993)

and as scFv fragments (Marks, Hoogenboom et al. 1991). The increased stability of the Fab fragment compared to scFv and Fv fragments, presumably a consequence of the additional constant region interface, has seen it become the more popular display scaffold in recent libraries.

An antibody phage library is a population of phage that displays on their surface a repertoire of antibody variants. Novel antibody clones specific for a particular target antigen can be isolated from several types of phage library including immunised, naïve and synthetic and will be discussed in section 1.5.4. In terms of *in vitro* affinity maturation (lead optimisation), which aims to mimic *in vivo* somatic hypermutation and clonal selection, sequence diversity is introduced into an antibody clone in a number of ways. The most commonly used are CDR walking (site directed mutagenesis), light and heavy chain shuffling and random mutagenesis of the variable domains. Molecular evolution techniques follow three steps: first, generation of diversity, second, introduction of a selective pressure and third, amplification of improved variants.

1.4.1 CDR walking

CDR walking is a targeted approach to introduce diversity within regions of the molecule that are known to interact with the antigen, principally the CDR loops. Affinity improvements can be achieved using a parallel or sequential approach.

In a parallel strategy, Fab antibody libraries have been constructed in which every residue in all of the CDRs is separately mutated, one at a time. Using degenerative NNS oligonucleotides (where N = nucleotides G, A, T or C in an equal molar ratio and S = nucleotides G or C in an equal molar ratio) (Wu, Beuerlein et al. 1998) or NNK oligonucleotides (where K = nucleotides T or G in an equal molar ratio) (Wu, Pfarr et al. 2005) each residue is targeted. Combinations of individual mutations

selected from these libraries often confer a step wise improvement in affinity into the low nanomolar range.

A parallel (Yang, Green et al. 1995) and a sequential (Schier, McCall et al. 1996) approach have been used to affinity mature an antibody for the HIV gp120 antigen. The parallel approach involved building five Fab libraries targeting four CDRs (Yang, Green et al. 1995) and combining independently isolated mutations. Whilst not all mutations combined in an additive manner, a 420-fold affinity improvement was achieved over the parent antibody. Marks and colleagues (Schier, McCall et al. 1996) addressed the non-cooperation frequently observed between mutants by using a sequential library strategy. Firstly, a high affinity clone was isolated from an NNS designed LCDR3 library. Using this clone as template for mutagenesis of the HCDR3, further variants were identified. Recruitment of mutated HCDR3 segments into the already high affinity LCDR3 segment conferred a 1230-fold improvement in affinity over the parent clone. In this example, the sequential approach proved to be a more efficient means of achieving high affinity compared with the parallel approach.

There are numerous examples of CDR mutagenesis for the isolation of high affinity antibodies, including Fab-based libraries where affinity improvements of 228-fold are observed from CDR3 targeting (Lowe, Gerhardt et al.) and 5000-fold from LCDR3 and HCDR2 targeting (Steidl, Ratsch et al. 2008).

Affinity improvements are also possible through extending the length of germ line encoded HCDR2 loops (Lamminmaki, Pauperio et al. 1999). Inserting two, three or four NNS-encoded residues into the loop of HCDR2 created new antigen-binding contacts and conferred up to 12-fold improvements in affinity over the wild-type antibody.

1.4.2 Chain shuffling

Chain shuffling exploits the enormous natural sequence diversity of antibody variable chains (Tomlinson, Walter et al. 1992; Timmers, Hermans et al. 1993; Williams and Winter 1993) and is another strategy for selecting high affinity antibodies. In this approach, one of the chains is replaced by a repertoire of genes and combined with the static partner (Marks, Griffiths et al. 1992; Kwong, Baskar et al. 2008). A chain shuffling strategy was used to improve the affinity of an already high affinity anti-HIV gp120 antibody (Thompson, Pope et al. 1996). Whilst shuffling the light chain yielded little improvement in affinity, two residues in HCDR2 and one in the heavy chain framework, resulted in reduced off-rate from the gp120 antigen. Subsequently, the HCDR3 was randomised by a synthetic oligonucleotide spiking approach. Finally, the residues in the heavy chain each conferring a reduction in off-rate were randomised by site-directed mutagenesis to yield a mutant with a 7-fold improvement over the parent antibody.

1.4.3 Guided mutagenesis

Further strategies to engineer improvements in affinity rely on either antibody-antigen structural information or on protein alignment of antibody germline sequences to identify hot spots frequently mutated in the natural antibody repertoire. Structural information can guide the identification of contact points at the antibody-antigen interface and so can direct the engineering of antibodies through a targeted approach (Chen, Wiesmann et al. 1999). In this study, the wild-type antibody crystal structure identified the HCDR3 loop as making greatest contact with antigen. Focusing mutagenesis within this region uncovered variants with between two and five-fold improvements in affinity compared to the parent molecule with a further improvement in affinity when combined. In a similar approach, instructed by crystallography, a hot

spot of amino acids in the contact zone were targeted using degenerative oligonucleotides that yielded mutated antibodies with improved potency both *in vitro* and *in vivo* over the wild-type antibody (Li, Xi et al. 2009).

Ho et al. (Ho, Kreitman et al. 2005) used NNS-directed mutagenesis of residues frequently mutated *in vivo* by somatic mutation to identify two hot-spots within LCDR1 that conferred a 7-fold improvement over the wild-type antibody. Whilst this study failed to demonstrate additivity of the mutations, Ducancel and co-workers (Muller, Savatier et al. 2011) successfully showed that independently identified CDR hot-spot mutations combined to bestow further affinity improvements over the parent antibody.

1.4.4 Random mutagenesis

Affinity maturation can also be accomplished using a non-targeted approach. Mutations are randomly introduced into either the variable genes or framework regions using error-prone PCR (Foote and Winter 1992; Hawkins, Russell et al. 1992) or using a bacterial mutator strain (Irving, Kortt et al. 1996; Low, Holliger et al. 1996). Hawkins et al. (Hawkins, Russell et al. 1992) introduced mutations randomly into the antibody genes of an anti-hapten antibody using error prone PCR and identified mutations with a 4.5-fold increase in affinity over the parent molecule. Winter and co-workers (Low, Holliger et al. 1996) used a similar approach to isolate mutations with up to 100-fold improvement in affinity over the wild-type antibody. From the studies reported here, it appears that the CDR walking approach is most successful in generating the largest increases in antibody affinity and as such deserves consideration as a strategy to engineer TCRs for high affinity.

1.5 Phage Display

Phage display is an *in vitro* selection technique that allows the isolation and enrichment of proteins and peptides with particular biochemical characteristics from vast pools (libraries) of variants. Phage display was first reported over twenty-five years ago in George Smith's seminal paper (Smith 1985) that demonstrated that peptides, fused to one of the phage coat proteins could be enriched over normal phage through binding to a target antibody. It was later shown that antibody fragments could also be displayed on phage opening up the technology to antibody engineering (McCafferty, Griffiths et al. 1990).

1.5.1 Filamentous phage structure

The filamentous bacteriophages are a group of viruses capable of infecting many Gram negative bacteria. The best studied filamentous phages belong to Ff class of phages (f1, M13, fd) whose genomes are more than 98% homologous. The Ff phage particle is approximately 6.5 nm in diameter and 930 nm in length (see Figure 1.3). The 6440-nucleotide circular single-stranded DNA genome (ssDNA) encodes eleven proteins, of which five are the coat proteins (pIII, pVI, pVII, pVIII and pIX) and the remainder are the non-structural proteins involved in DNA replication (pII, pV and pX) and virion assembly (pI, pIV and pXI). The filament-shaped structure which encapsulates the phage DNA comprises almost 2700 copies of the major coat protein, pVIII. One end of the particle is capped by five copies each of pVII and pIX. The other end of the particle consists of between four to five copies each of pIII and pVI.

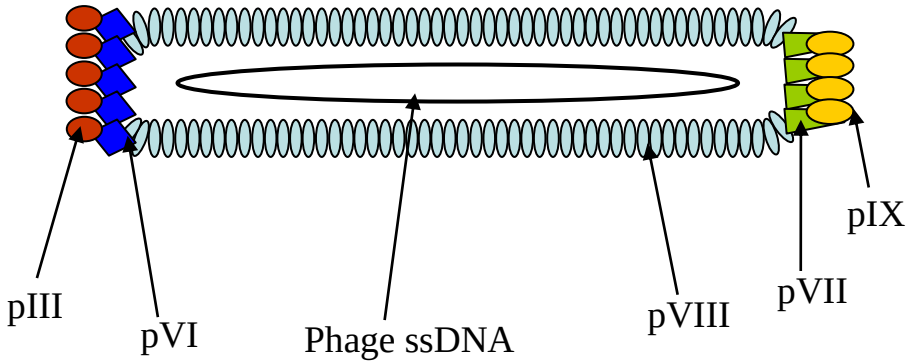

Figure 1.3. Filamentous phage Ff structure. Filamentous phage are cylindrical structures with a diameter of about 6.5 nm and a length of about 900 nm containing a circular single-stranded (ss) DNA genome comprising 6407 nucleotides, encapsulated by approximately 2700 copies of the major coat protein pVIII. The particle is capped at the pointed end by five copies each of pIII and pVI. The blunt end contains three to five copies of pVII and pIX.

1.5.2 The life cycle of filamentous phage

Ff phages most efficiently infect male bacteria as they use the *E. coli* F pilus (encoded by the F plasmid) as a receptor during the infection process. The infection and assembly process is illustrated in Figure 1.4. Infection is mediated through the interaction of pIII and the F pilus. The pIII consists of three domains: two N-terminal, N1 and N2 (which are intramolecularly linked) and one C-terminal, CT. The three domains are connected by a flexible glycine-rich linker. Infection is initiated when the N2 domain binds to the F pilus on an *E. coli* cell. The pilus subsequently retracts bringing the phage particle to the *E. coli* periplasm. Interaction of the pilus with pIII leads to the dissociation of N1 from N2 allowing it to bind with the bacterial TolA protein. The F pilus acts as a receptor and the TolA protein as a co-receptor for pIII binding and infectivity. The presence of pIII in the bacterial membrane confers the cell with resistance to further infection from filamentous phage. Two additional bacterial proteins, TolQ and TolR, are essential for phage infectivity facilitating the

disassembly of the phage coat proteins into the cytoplasmic membrane and injection of the phage ssDNA into the bacterial cytoplasm, although the exact mechanism of this process remains unclear. Once in the cytoplasm, the viral (+) ssDNA is converted into a double-stranded, supercoiled molecule that is referred to as the Replicative Form (RF) DNA. The (-) strand of the RF DNA acts as the template for transcription and the synthesis of all eleven phage proteins. Of particular importance to further phage genome replication is pII which serves as a nicking-closing enzyme. It first nicks the (+) strand of the RF in a non-coding intergenic region. The (-) strand of the RF acts as a template to elongate the nicked (+) strand via a rolling-circle mode of action. Once a round of replication has finished, the nicked (+) strand is recircularised by pII and converted into RF. The process of RF DNA synthesis continues until a level of pV is reached where it starts to bind to viral (+) ssDNA blocking its conversion to RF DNA. All phage proteins are synthesised simultaneously. Each of the eight proteins involved in phage assembly are inserted into the cytoplasmic (pIII, pVI, pVII, pVIII, pIX, pI and pXI) or outer membrane (pIV). The remaining three phage proteins (pII, pX and pV) are located in the cytoplasm. Assembly of the virus particle is a multi-step process that takes place in the cytoplasmic membrane. It involves the removal of pV from phage genomic DNA and encapsulation by the phage capsid proteins. The eventual extrusion of phage particles from the bacterial cell occurs via the assembly point (comprising pI, pXI and pIV) where the cytoplasmic and outer membrane become in close contact and a pIV-mediated channel is formed. Once the end of the DNA is reached, as the phage particle exits through the pIV channel, assembly is terminated by the addition of pIII and pVI. During the first hour about 1000 phage progeny are secreted from the bacterial cell (Webster 2001).

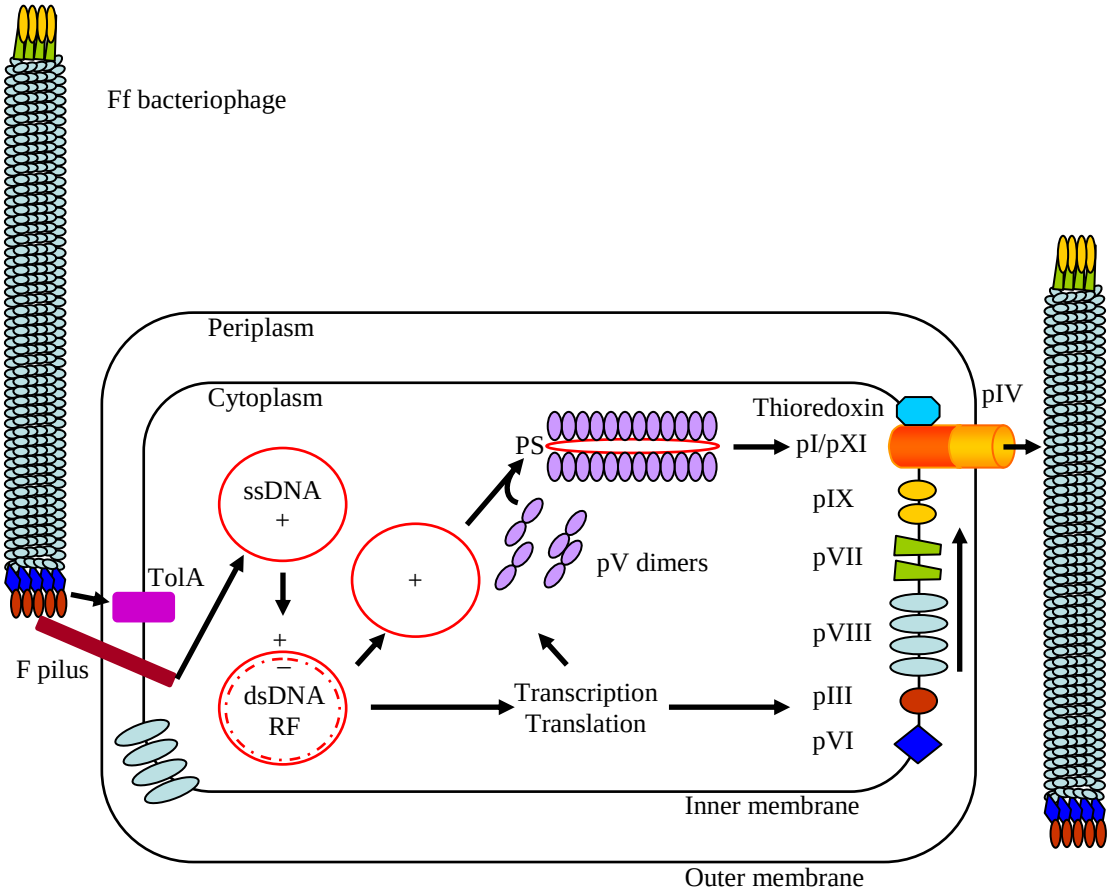

Figure 1.4. Life cycle of filamentous Ff phage. Sequential binding of the N2 domain of pIII with the *E. coli* F pilus and the Tol A protein leads to retraction of the pilus and transfer of the phage genome (the + strand) into the cytoplasm of the bacterial cell. The major pVIII coat protein integrates into the inner membrane. The viral ssDNA is converted to a double-stranded Replicative Form (RF) DNA mediated by host enzymes and acts as the template for the phage gene expression. Newly synthesised viral ssDNA is coated with pV (except the packaging sequence hairpin (PS) which protrudes from one end) preventing conversion to RF. The pV/ssDNA complex is the substrate for phage assembly. Phage proteins are expressed simultaneously. Multiple copies of pIV assemble in the outer membrane of the bacteria host cell, whilst pI and pXI proteins assemble in the inner membrane. An assembly point is formed where the inner and outer membrane come into close proximity. The formation of the pI, pXI, pIV (thioredoxin) transport complex provides a route through which the phages are secreted from the *E. coli* cell. Interaction of pIX and pVII with the pV/ssDNA complex at the PS leads to the replacement of pV with pVIII. Secretion is terminated by capping of the phage particle with pIII and pVI. Adapted from (Russel, Lowman et al. 2004).

1.5.3 Phage display formats

Whilst all of the phage coat proteins have been used to display various peptides, antibodies and other proteins (Velappan, Fisher et al. 2010) the most widely used phage proteins for display are pIII and pVIII. Phage vectors that encode foreign DNA as pIII or pVIII fusions are called type 3 or type 8 respectively (Smith and Petrenko 1997). In type 3 or 8, the foreign DNA is inserted into the phage genome as N-terminal fusions so that all copies of either pIII (five copies) or pVIII (2700 copies) display the foreign peptide. With regards to type 8 vectors the number of peptides that can be displayed is dependent on the size of the peptide and is restricted to short fragment insertions (5-6 residues), possibly due to the space constraints resulting from the tight packing of the pVIII coat proteins or because large pVIII fusions may be unable to pass through the pIV pore during virion assembly (Greenwood, Hunter et al. 1991). Display on pIII molecules can accommodate larger insertions although infectivity can be affected.

To overcome the size restriction of the foreign peptide (about six residues) in type 8 vectors there is a second group of phage vector, type 3 3 or 8 8, in which the phage genome contains two copies of genes III or VIII, one wild-type and one recombinant. This gives rise to phage particles displaying a mixture of wild-type and recombinant pIII or pVIII molecules (with the majority of pIII or pVIII molecules being wild-type).

Type 3+3 or 8+8 is different from 3 3 or 8 8 in that the wild-type and recombinant genes III or VIII are encoded by two separate genomes. Type 3 or 8 and 3 3 or 8 8 vectors are termed phage vectors and type 3+3 and 8+8 vectors are called phagemid vectors or just phagemids.

Phage vectors bear the entire phage genome and so possess all the necessary viral machinery for the replication and assembly of new virus particles. Foreign peptides

are inserted in frame at the C-terminus of the coat protein signal peptide sequence and at the N-terminus of the coat protein (pIII or pVIII) sequence. This results in polyvalent display in which all copies of the coat proteins display the foreign peptide (Scott and Smith 1990; McLafferty, Kent et al. 1993).

In contrast, phagemids do not contain the genes required for the production of new virus particles. A phagemid is a small plasmid that contains an antibiotic resistance gene to allow the selection of plasmid-bearing cells, an *E. coli* origin of replication for plasmid propagation in bacteria and a filamentous phage (Ff) origin of replication which enables the synthesis of single-stranded vector DNA. The Ff origin remains inactive until the phagemid-bearing *E. coli* cells are superinfected with a helper phage.

A helper phage is a phage particle which provides all the necessary genetic information for the assembly and propagation of new virus particles including the wild-type coat proteins. The phage replication protein encoded by the helper phage acts *in trans* on both the helper phage and phagemid Ff origin of replication. The foreign peptide is cloned between the coat protein signal sequence, and the fusion coat protein sequence is under the control of a weak promoter. Phagemid-bearing *E. coli* are grown in glucose-containing media to repress the expression of pIII which would prevent superinfection with helper phage. Helper phage contain an antibiotic selection marker (commonly kanamycin) different from that encoded by the phagemid allowing the selection of *E. coli* cells that contain both the helper phage and phagemid genomes. In the *E. coli* cell proteins from both the helper phage (wild-type) and the phagemid (recombinant) are produced. Wild-type pIII competes with recombinant pIII for incorporation into the assembling virus particle. The majority of phage produced from the phagemid system will display only wild-type pIII on their surface

derived from the helper phage (referred to as bald phage), with less than 10% displaying one copy of the fusion, resulting in monovalent display. This is due to the excess expression of wild-type pIII and its preferential assembly into the virus particle over the recombinant version. However, it is important to note that helper phage contain a defective Ff origin of replication and packaging signal and so phagemid DNA is preferentially packaged over helper phage DNA so that the link between the phenotype and the genotype of the protein displayed is maintained.

It is possible to increase the valency of display with the phagemid system by using a modified gene III-deleted helper phage called Hyperphage (Rondot, Koch et al. 2001). Such phages display the pIII phenotype but contain a phage vector that does not code the gene III sequence. So the phage particles have to be produced in an *E. coli* cell line that provides pIII for helper phage assembly. This means that the only source of pIII is from the phagemid vector and so multivalent display is possible.

The type of phage display system employed dictates the number of recombinant fusion proteins displayed on the phage surface that are accessible to interaction with the target antigen. Polyvalency of the phage vector system in which 3-5 identical copies of the fusion protein are displayed leads to the selection of low affinity binders (by virtue of avidity effects). In contrast, the monovalent phagemid system, due to the lack of avidity effects, more often select for high affinity binders and as such are typically used in affinity maturation projects.

An overview of the processes involved in the construction of and selection from TCR phage display libraries is illustrated in Figure 1.14 (page 99).

1.5.4 Isolation of antibody variable domains

In addition to the affinity maturation of antibodies, phage display has proven an effective tool for the generation and isolation of antibodies with particular binding

specificities. Antibodies are a naturally diverse group of molecules and so provide an excellent scaffold for engineering. A variety of strategies have been employed to isolate V domains against any given antigen. These include isolating antibodies from immunised animals, from repertoire (naïve) libraries or from synthetic or semi-synthetic libraries.

Antibody libraries can be constructed from an immunised source by firstly challenging the animal with a particular antigen and then amplifying the V_L and V_H domains from reverse-transcribed splenocyte RNA (Clackson, Hoogenboom et al. 1991). A drawback, in addition to the time demands and technical challenges of animal immunization, is that the antibody specificities are restricted to that of the antigen used and so new libraries have to be built for each new antigen.

The construction of naïve libraries from repertoires of V-genes addresses this limitation. Oligonucleotide primer sets for each of the V_L and V_H genes are used to PCR amplify the repertoire of V-genes from a non-immunised source of PBMCs. The random combination of variable chains generates a library of diverse antibodies with the potential to recognise any target antigen. Libraries with a relatively limited diversity of $>10^7$ have yielded antibodies with affinities in the low micromolar range (Marks, Hoogenboom et al. 1991). By comparison, naïve libraries with 10^{10} clones (Vaughan, Williams et al. 1996) and 6.5×10^{10} clones (Griffiths, Williams et al. 1994) have yielded antibodies with subnanomolar and low nanomolar affinities respectively.

Synthetic V_H/V_L libraries are constructed by design and can vary from being semi-synthetic to fully synthetic depending on the ratio of antibody genes of synthetic or natural origin. The Winter lab has utilised semi-synthetic and fully synthetic libraries to select antibodies against desired antigens by introducing randomised mutations into HCDR3 of all 49 V_H genes; either 5-8 residues (Hoogenboom and Winter 1992) or 4-

12 residues (Nissim, Hoogenboom et al. 1994) and combining with a single V_L domain.

Knappik et al. (Knappik, Ge et al. 2000) constructed fully synthetic Human combinatorial antibody libraries (HuCAL). They combined 7 V_H and 7 V_L chain genes to generate 49 V_H/V_L (*E. coli* optimised) frameworks and then randomised the CDR3 loops. A recent permutation is the HuCAL GOLD library in which all six CDRs are randomised (Rothe, Urlinger et al. 2008). The quality of the CDR randomisation libraries was optimised using trinucleotides where there is a greater control over the inserted mutations compared to the more common mononucleotides. There are many further examples of synthetic libraries in which the number of antibody frameworks is restricted. The ETH-2 library built on one germline heavy chain and two germline light chains, diversified through random mutagenesis of HCDR3 (4-6 positions) and LCDR3 (6 positions) (Viti, Nilsson et al. 2000) has been mined for anti-CEA antibodies (Pavoni, Flego et al. 2006). Another synthetic library was constructed by combining 49 germline V_H chains and 7 light chains coupled with randomisation of HCDR3 (de Kruif, Boel et al. 1995). Additionally, libraries have been devised that combine repertoire-derived variable CDR3 genes with synthetically engineered variable CDR1 and CDR2 domains (Hoet, Cohen et al. 2005).

1.5.5 *In vitro* selection methods

In theory it should be possible to directly screen antigen-binding phage-displayed particles from the original phage display library but this is impractical because of the number of phage particles that would have to be analysed. For this reason methods have been developed to enrich for antigen-binding molecules over non-binding phage particles. Because the genotype encoding the displayed protein is carried within the

phage particle, once proteins have been selected, the DNA sequence can be readily determined by sequencing.

The selection process called “biopanning” involves multiple steps: incubation of phage antibodies with their target, washing to remove clones that do not bind, elution of antigen-binding phage antibodies from their target and infection of *E. coli* cells with the eluted phage (Figure 1.5).

Each of these steps can be performed in a variety of ways. The selection step is the process whereby antigen-binding phage is separated from non-binding phage; this requires purified antigen. The quality of antigen is paramount in order to prevent the selection of antibodies to antigens other than the target peptide. Selections are performed in a blocking media such as bovine serum albumin, milk powder or gelatin to reduce the binding of non-specific phage. To maximise the capture of antigen binders the first selection cycle (“pan”) is usually carried out under conditions that are not too stringent. The antigen is immobilised onto solid supports such as petri dishes or plastic tubes (Marks, Hoogenboom et al. 1991) or can be tagged, biotinylated and captured in solution as phage-antigen complexes with streptavidin-coated paramagnetic beads and a magnet (Hawkins and Winter 1992).

Several features of the process can be fine-tuned to enrich for clones with the desired binding properties, including antigen concentration, the number of washes, the type of elution agent and the total number of panning cycles. The selection efficiency is also dependent on other factors such as folding of the protein in the periplasm during phage assembly and potential toxicity of the protein to the bacterial host cell. Both of these can affect the level of display on the phage surface.

Antigen concentration can be decreased and the number of washes increased through each round of panning to encourage the selection of higher affinity antigen

binders. The selection of higher affinity antibodies from an already high affinity parent molecule requires greater stringency (i.e. panning of second generation libraries). In off-rate selection antibody-phage is mixed with biotinylated antigen until equilibrium is reached. A molar excess of non-biotinylated antigen is added to capture antibodies with faster dissociation times. Antibodies with slower off-rates remain bound to the biotinylated antigen and are isolated (Hawkins, Russell et al. 1992).

A number of treatments can be used to elute antibodies bound to antigen: acidic (0.1 M HCl or 0.2 M Glycine, pH 2.5) (De Pascalis, Gonzales et al. 2003), basic (0.1 M triethylamine) (van Wyngaardt, Malatji et al. 2004) or enzymatic (a trypsin protease cleavage site is engineered between antibody and pIII) (Kristensen and Winter 1998). In the next step, the eluted phage is then used to infect *E. coli* cells and plated onto selective agar. The selective output is amplified through several rounds of replication in liquid media and the enriched antigen-binding phage particles re-enter the panning cycle. Following several rounds of panning (typically three to five) individual antibiotic-resistant colonies are picked, phage prepared and screened for antigen-binding by ELISA.

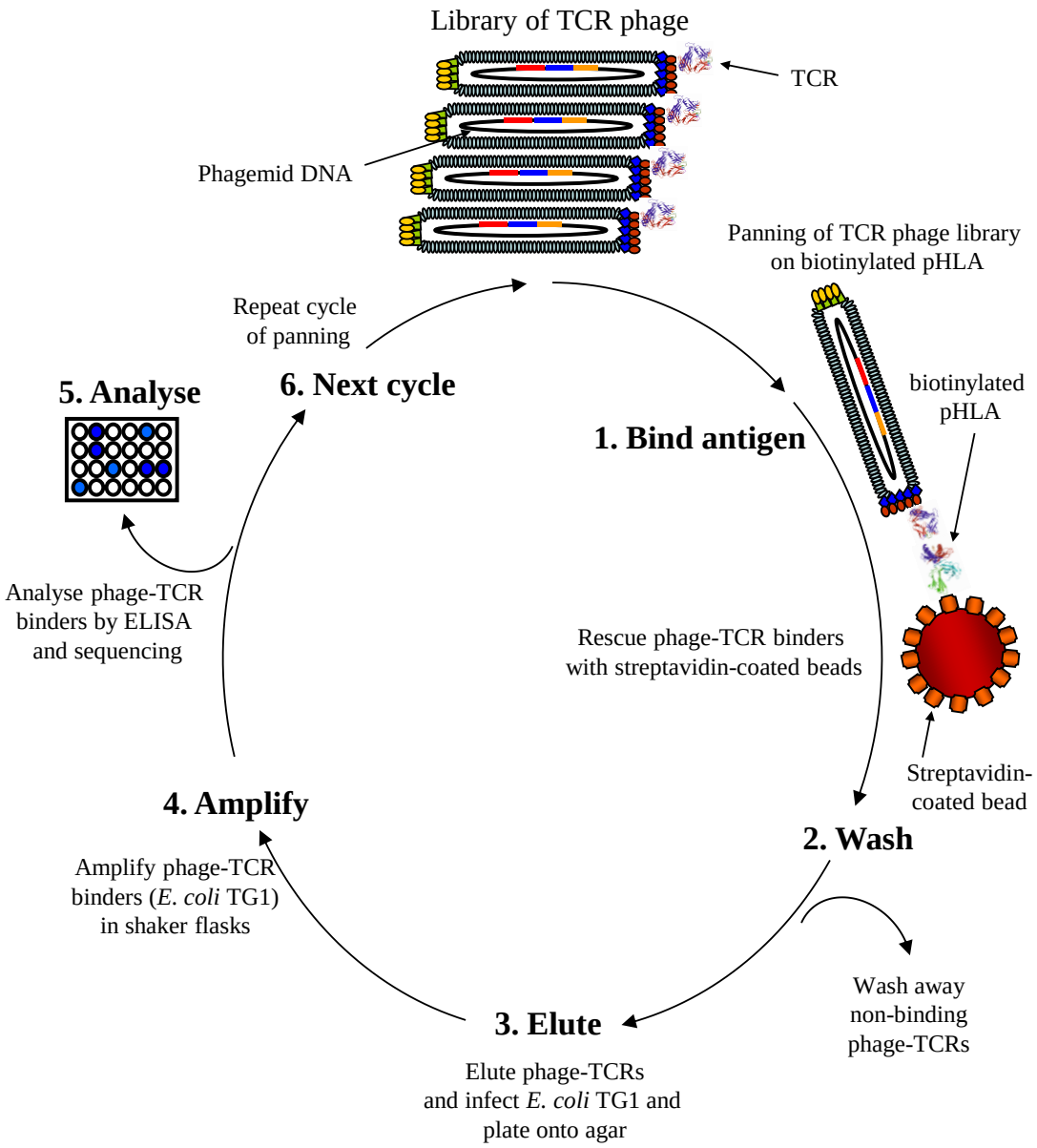

Figure 1.5. Schematic representation of the biopanning process. A phagemid vector that encodes a recombinant protein (in this example a TCR) fused to pIII is propagated in *E. coli* with a helper phage. The library of protein variants is displayed on the surface of the phage particles and is incubated with the target antigen in a binding step. Antigen is either immobilised onto a solid surface or is tagged (biotinylated) and added in solution (as shown here). In solution panning, antigen-binding phages are rescued using streptavidin-coated beads and a magnet. Following a wash step to remove non-specific phage particles, specific antigen-binding phage are eluted from the binding matrix and used to re-infect *E. coli* and re-enter the next round of panning. Following several rounds of enrichment individual clones are analysed by ELISA and sequencing.

1.6 Cellular immune responses

The potent capacity of the immune system to combat diseases is demonstrated by its ability to prevent infection from the barrage of pathogens we are exposed to during our lifetime. The human body is protected from infection with foreign pathogens and from the growth of tumour cells by a collection of interdependent cells that comprise the immune system. The immune system comprises two main subdivisions, the innate and the adaptive immune system. The innate system which is the first line of defence provides a physical barrier (skin and mucosal epithelia) to many pathogenic agents but also includes cells such as macrophages and neutrophils that eliminate pathogens through an active process called phagocytosis. Only when this barrier is breached does the second line of defence, the adaptive immune system, come into play. The adaptive immune response is distinguished from the innate system in a number of ways. First, the innate system acts immediately to protect against invading pathogens, whereas the adaptive response requires sufficient time for the clonal expansion and differentiation of antigen-specific lymphocytes. Second, whereas the cells of the adaptive immune system use highly diverse antigen-specific receptors that have undergone genetic rearrangement, the innate receptors are germ-line encoded and recognise surface molecules displayed on pathogens. Third, the adaptive system affords immunological memory against re-infection with the same pathogen, whereas the innate system does not result in lasting memory of specific pathogens. The adaptive immune response is characterised by specific recognition of foreign pathogens by T and B lymphocytes. B-cells contribute to the humoral response by secreting antigen-specific antibodies that recognise, inactivate and destroy pathogens. T-cells recognise antigens presented on the surface of cells bound to MHC molecules. T-cells are the key players in cell-mediated immune response. Recognition of antigen fragments bound to MHC molecules is through the heterodimeric T-cell receptor

(TCR) which consists of and an alpha and a beta (α or β) chain. The work described in this thesis is focused on the recognition of peptide-MHC by the $\alpha\beta$ TCR and so $\gamma\delta$ TCRs will not be considered further.

Effector $\alpha\beta$ T-cells are divided into two distinct subsets: cytotoxic T-cells (Tc) and helper T-cells (T_H). Cytotoxic T-cells express on their surface the CD8 co-receptor and recognise and kill pathogen-infected or tumour cells largely through two mechanisms. First, perforin/granzyme-mediated killing: perforin molecules released from the Tc insert into the target cell membrane to form a pore through which granule proteases (granzymes) pass. Granzymes cleave intracellular substrates to activate signalling pathways leading to apoptosis. Second, Fas Ligand (FasL)/Fas protein killing: activated Tc upregulate the expression of a transmembrane protein designated FasL. Target cells express a receptor for FasL called the Fas protein. Interaction of FasL and Fas leads to apoptosis of the target cell. The work described in this thesis is focussed on $CD8^+$ T-cells as these have the ability to recognise intracellular antigens. CD4 T-cells orchestrate the immune system by recognising MHC class II and will not be considered further. T-cells also express on their surface CD3, which contains the γ, δ, ε and ζ proteins used for cell signalling when a T-cell encounters cognate antigen presented on MHC molecules. In the context of cancer, many components of the immune response are not recruited and consequently the disease progresses. Therapeutic approaches that are designed to harness some or all of these mechanisms have great promise to provide potent long-term effective treatment.

1.7 The Major Histocompatibility Complex

There are two classes of MHC molecules: class I and class II. The genes that encode the MHC class I and class II molecules are clustered on the short arm of human

chromosome 6 occupying 4-6 megabases. The α chain of MHC class I and the α and β chains of MHC class II are tightly linked within the MHC region of chromosome 6 whilst the β_2-microglobulin (β_2-m) of class I molecules is located on chromosome 15. There are three "classical" MHC class I genes in humans: Human Leukocyte Antigen (HLA)-A, -B and -C which are highly polymorphic, and three "non-classical" class I genes HLA-E, -F and -G which are far less polymorphic. MHC class I molecules are present on almost all nucleated cells.

The class II molecules (HLA-DR, -DQ and -DP) are encoded by a cluster of genes located within the MHC class II region of the MHC on human chromosome 6. The HLA-DR, -DQ and -DP chain genes are all highly polymorphic. The cellular distribution of MHC class II molecules is more restricted than for class I molecules being normally found on B lymphocytes, dendritic cells and macrophages but not on other cells.

The function of the MHC molecule is to capture peptides and display them on the cell surface for recognition by T-cells. MHC class I molecules present peptides that are derived from the cytosol and are recognised by cytotoxic T-cells expressing the CD8 co-receptor. MHC class II molecules present peptides produced in intracellular vesicles and are recognised by helper T-cells expressing the CD4 co-receptor. T-cells only recognise antigens presented on the cell surface bound to MHC in the form of short peptides (on average 9 amino acids in length). Binding of T-cells to peptide-MHC (pMHC) molecules evoke cytotoxic and helper T-cell responses.

Class I molecules are formed from the association of a membrane-bound heavy chain and soluble β_2-m. Class II molecules comprise a membrane-bound α and β chain. The class II heterodimer is formed by a non-covalent association of an α chain (α1 and α2 domains) and a β chain (β1 and β2 domains). The peptide-binding groove

is formed from the dimer of the membrane-distal domains α1 and β1. Structurally the α1 and β_2-m of class I molecules are similar to the α1 and α2 domains of class II molecules. Likewise the α2 and α3 domains of class I are similar to the β1 and β2 domains. One main difference between the structure of the peptide-binding grooves is that in class I molecules it is blocked at both ends by bulky amino acid side chains whereas in class II molecules it is open ended and able to accommodate longer peptides (15 amino acids) (Madden 1995).

Our lab is focused on the engineering of MHC class I-restricted T-cell receptors and therefore the structural analysis sections will be restricted to these molecules.

1.7.1 Structure of MHC molecules

The first three-dimensional structure of the MHC class I HLA-A2 protein was determined to 3.6-Å and provided information on the domain arrangement of MHC class I molecules (Bjorkman, Saper et al. 1987; Bjorkman, Saper et al. 1987). MHC class I molecules comprise a heavy chain (43 KDa), which spans the membrane, complexed non-covalently to a light chain known as β_2-m (12 KDa). The heavy chain consists of three domains, called α1, α2 and α3 (each of ~90 amino acids). The structure of the pMHC class I complex ectodomain is shown in Figure 1.7.

The α3 and β_2-m are fairly conserved and form immunoglobulin-like folds. The α1 and α2 membrane-distal domains comprise of two α helices that rest on a seven-stranded beta sheet to form a cleft or groove (~30 Å long and 12 Å wide) (Figure 1.6). It was presumed, from the initial solved structure (Bjorkman, Saper et al. 1987) that electron density within the groove that was not of heavy chain origin represented bound antigen.

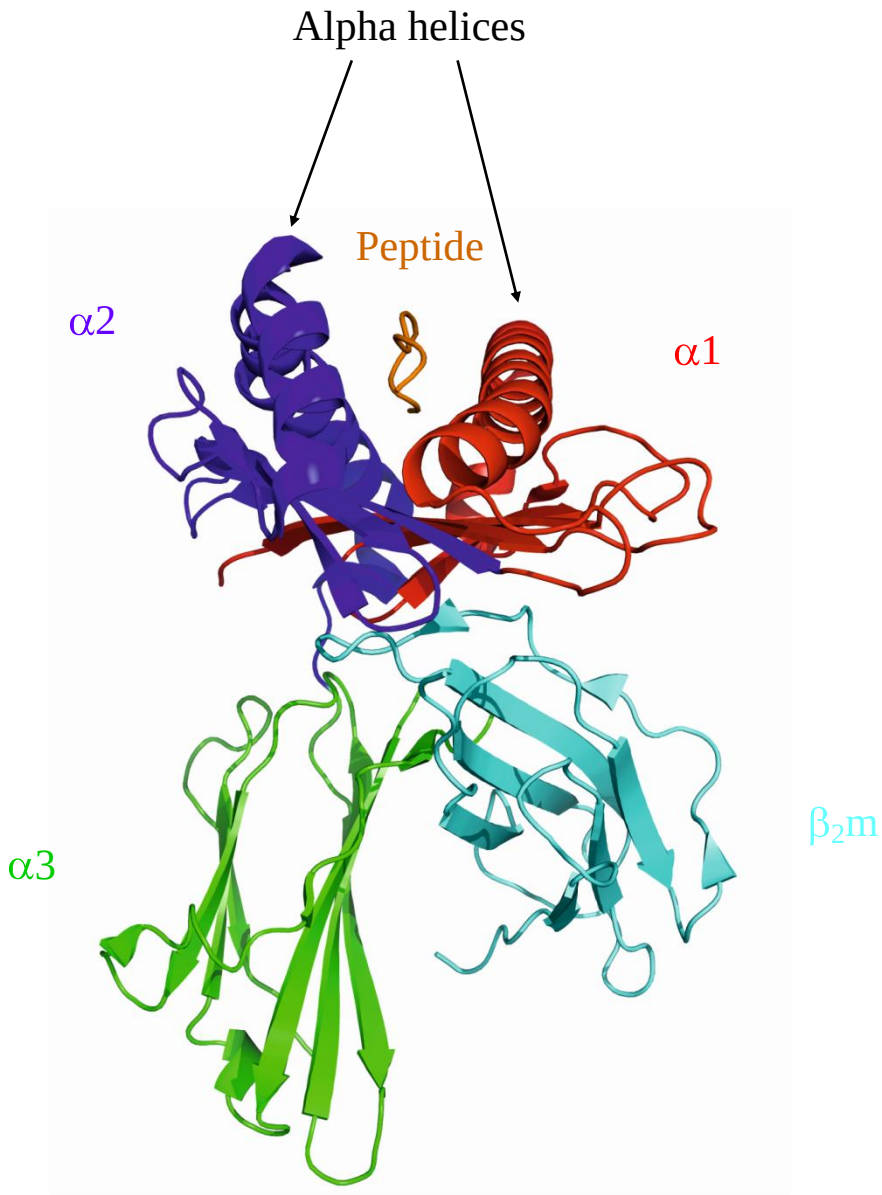

Figure 1.6. Structure of the ectodomain of the class I molecule HLA-A*0201-NY-ESO-1$_{(157-165)}$ (SLLMWITQC). The HLA heavy chain consists of three domains: alpha 1 (α1 red), alpha 2 (α2 purple) and alpha 3 (α3 green); α1 and α2 associate as a dimer comprising two α-helices to form the antigen-binding groove. The peptide (brown) is positioned between the two α-helices extending the whole length of the cleft. The light chain or β_2-m (pale blue) is linked to the heavy chain through non-covalent interactions. The figure is based on the crystal structure reported in (Chen, Stewart-Jones et al. 2005) and was constructed in PyMOL version 1.5. (PDB: 2BNR).

1.7.2 Peptide-MHC binding

Further crystal structures of the MHC class I complex confirmed the presence of peptide bound in the cleft of the molecule (Madden, Gorga et al. 1991; Saper, Bjorkman et al. 1991; Fremont, Matsumura et al. 1992; Silver, Guo et al. 1992). All crystal structures showed that the peptide lies the length of the $\alpha1\alpha2$ groove in an elongated conformation in a constrained orientation. Whether a peptide will bind to the groove depends on the amino acids that line the groove. Because class I molecules are polymorphic, different class I molecules will bind different peptides. Variations of the residues lining the pockets along the peptide-binding groove that are conferred by different class I alleles alter the peptide-binding specificity or binding motif of each MHC molecule.

There are six specificity pockets (A to F) that line the class I peptide-binding groove creating an irregular surface necessary to accommodate a plethora of peptide side chains. Although the peptide-binding groove is highly polymorphic, at either end of the cleft reside two clusters of residues (pockets A and F) that are conserved between most class I molecules. The amino acid residues forming pockets B to E are not as conserved and are described as being polymorphic in sequence. Hydrogen bonds form between the conserved residues of the A pocket and the N-terminus of the bound peptide. Likewise hydrogen bonds form between conserved residues lining the F pocket and the C-terminus of the peptide. A network of hydrogen bonds form between the peptide main chain and the conserved residues at either end of the MHC cleft so-called side chain sequence-independent interactions. Hydrogen bonds also form between polymorphic residues in the groove and the peptide main chain. Additional contacts form between the MHC and the side chains of the central peptide residues. In combination, this extensive network of interactions account for the tight

binding affinity between peptide and the MHC molecule (Stern and Wiley 1994; Madden 1995). The stability of peptide binding is achieved through water-mediated hydrogen bonds between the peptide and the MHC molecule. The importance of groove-based water molecules to fill the gap between the floor of the binding cleft and the peptide has been demonstrated (Meng, von Grafenstein et al. 1997).

Although class I molecules can accommodate a vast spectrum of peptide sequences (with a strong preference for nonameric peptides), peptides must fulfil certain criteria to bind into the groove. MHC molecules show a preference for certain amino acid residues at particular positions in the peptide before binding will occur. So-called anchor residues in the peptide, in most cases at or near the amino and carboxy-terminal end of the peptide, are buried deep in the peptide-binding groove and stabilise the complex. Anchor residues are usually at position 2 (P2) at the N-terminus and the C-terminal (PC) residue but can also be the third (P3) or fifth (P5) residue depending on the class I allele. HLA-A*0201 (HLA-A2) has a preference for leucine or methionine at P2 and with a preference for leucine or valine at PC (Hunt, Henderson et al. 1992; Parker, Bednarek et al. 1992). HLA-A*0101 preferentially binds nonapeptides with the anchor residues asparagine or glutamic acid at P3 and tyrosine at P9 (DiBrino, Tsuchida et al. 1993; Falk, Rotzschke et al. 1994).

In addition to binding of nonomeric peptides, the class I peptide-binding groove can accommodate longer peptides of 11 (Guo, Jardetzky et al. 1992) and 13 (Tynan, Borg et al. 2005) amino without loss of the fixed binding at the N- and C-terminus. This is achieved by a significant conformational change in the central region of the peptide which points out of the groove. The central core of the peptide is exposed for direct interaction with the TCR. It is therefore the peptide that dictates the antigenic identity of the MHC complex.

A structural comparison of five different peptides bound to the class I HLA-A2 molecule showed that although the peptide amino and carboxy-termini bound similarly within the groove, the conformation of the central peptide core varied greatly in relation to its sequence. The central peptide residue side chains can point up for some peptides, down or sideways for others (Madden, Garboczi et al. 1993). This demonstrated that both the length and sequence of the peptide is important for creating unique structural landscapes that can be recognised by specific T-cell receptors and moreover, the driving force of TCR recognition is the central core of the peptide.

A remarkable feature of the pMHC complex is that whilst a high level of polymorphism exists within the residues lining the antigen-binding groove (Bjorkman, Saper et al. 1987), the overall architecture of MHC class I molecules is conserved. This structural conservation is demonstrated in Figure 1.7. Figure 1.7 A-C depict the HLA-A*0201 heavy chain in complex with three different peptides, demonstrating the capacity of the HLA complex to accommodate peptide variation within the groove with minimal alteration to the global organisation of the structure. Figure 1.7 D shows the HLA-B*0801 heavy chain in complex with an EBV-derived peptide, illustrating that the fold structure is maintained throughout. Moreover, it demonstrates the remarkable capacity of TCRs to distinguish between different antigenic targets that vary by only a handful of amino acid residues.

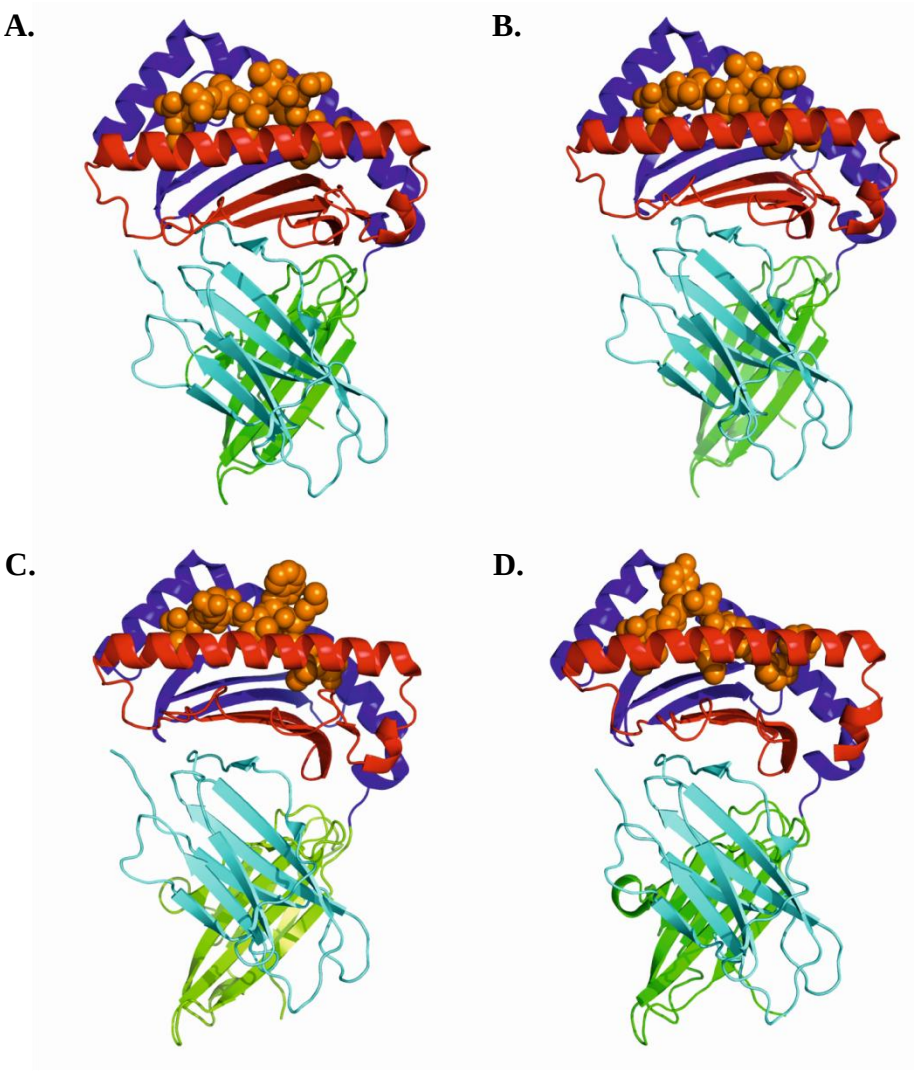

Figure 1.7. Comparison of the structure of two different HLA class I molecules in complex with four different peptides. (A). HLA-A2-GAG $_{(77\text{-}85)}$ (SLYNTVATL) (PDB: 1T21) (Martinez-Hackert, Anikeeva et al. 2006). **(B).** HLA-A2-GAG $_{(77\text{-}85)}$ variant (SLFNTIAVL) (PDB: 1T1W) (Martinez-Hackert, Anikeeva et al. 2006). **(C).** HLA-A2-NY-ESO-1 $_{(157\text{-}165)}$ (SLLMWITQC) (PDB: 2BNR) (Chen, Stewart-Jones et al. 2005). **(D).** HLA-B8-Epstein Barr nuclear Ag 3A $_{(193\text{-}201)}$ (FLRGRAYGL) (PDB: 1M05) (Kjer-Nielsen, Clements et al. 2002). MHC class molecules comprise a three domain heavy chain (α1 shown in red, α2 shown in blue and α3 shown in green) and a light β2-m chain (shown in pale blue). The peptide-binding groove is formed from two α-helices and the peptide shown in brown lies in the cleft. The configuration of the MHC class I molecule is largely unchanged irrespective of the MHC isoform (HLA-A or HLA-B) or the sequence of the bound peptide. The figure was constructed in PyMOL version 1.5.

1.8 Antigen processing and presentation: Class I pathway

The ability of T-cells to distinguish between healthy and diseased cells (pathogen-infected or tumour cells) is pivotal to their protective immune function. Antigens are processed within the cell into peptide fragments through two distinct pathways (class I and class II). The work described in this thesis is focussed on the αβ TCR recognition of MHC class I derived peptides and so the peptide loading of MHC class II molecules will not be discussed further. MHC class I molecules transport endogenous peptides originating from the cytosol to the cell surface. Proteins, both normal self-proteins and foreign or abnormal proteins are degraded in the cytoplasm. This constant turnover provides an abundance of potential MHC class I peptides. MHC class I heavy chains assemble into a complex with β_2-m in the lumen of the ER where they are retained until they are loaded with a peptide. Proteins are degraded in the cytosol by a mutlicatalytic protease complex called the proteasome. Two subunits of the proteasome are encoded within the MHC by the LMP2 and LMP7 genes and are inducible by IFN-γ. Incorporation of these subunits alters the enzymatic specificity of the complex favouring the cleavage of peptides after hydrophobic residues and inhibiting cleavage after acidic residues, thus producing peptides that are suited to binding MHC class I molecules. The TAP (transporter associated with antigen processing) complex transports peptides from the cytosol to the ER. The complex forms a peptide-binding channel through which peptides can pass (peptides of 8-13 residues are favoured). The TAP complex associates with the MHC class I molecule and peptides are loaded into the peptide-binding groove to complete the folding and assembly of the MHC class I complex. The peptide-MHC complex then leaves the ER and is transported to the cell surface.

1.9 T-cell receptors

T-cell receptors recognise both the bound peptide and the polymorphic variation within the MHC molecule; a feature of T-cell antigen-binding termed MHC restriction (Zinkernagel and Doherty 1974). T-cell receptors (TCRs) share many common structural and functional characteristics with antibodies. The domain structures of TCRs are very similar to those of antibodies and so are classified as members of the immunoglobulin superfamily. As antigen-specific receptors TCR and antibodies also share a common function. The organisation of the variable domains of the TCR into an antigen-recognition site resembles the Fab fragment of antibodies. Although they share these features, TCRs differ in several ways from antibodies. First, they only exist as membrane-bound proteins expressed on the surface of T-cells and are not found in a soluble form as antibodies are. Second, antibodies have two antigen-binding sites whereas TCRs only have one. Third, the affinity of interaction between TCR and its antigen is far weaker than for antibodies. Fourth, TCRs have to recognise both the antigen and the MHC molecule into which it is bound.

1.9.2 T-cell receptor gene rearrangement

As with Ig light and heavy chains, TCR α and β chains contain a variable (V), a joining (J) and a constant (C) region. The TCR β chain, like the Ig heavy chain, also contain diversity (D) segments (Davis and Bjorkman 1988). The gene encoding the TCR α chain is found on chromosome 14 and has 47 Vα gene segments (TRAV, nomenclature assigned by the immunogenetics database, IMGT (Lefranc, Giudicelli et al. 1999)), 61 Jα segments (TRAJ) and 1 C segment. The β chain locus is on chromosome 7 and has 54 Vβ (TRBV) segments, 2 Dβ (TRBD) segments, 14 Jβ (TRBJ) segments and 2 C segments.

Functional TCRs result from α and β chain gene rearrangement, in which a TCR α protein chain comprises only one V, J and C segment and the TCR β protein chain consists of only one V, D, J and C segments spliced together (Figure 1.8). TCR diversity is generated, as with Igs, through the CDRs. CDRs 1 and 2 are encoded by the germline V gene itself, whereas CDR3 is formed by the junction of V and J for α chains and V, D and J for β chains. For the α chain a V gene segment rearranges to a J gene segment to create a functional Vα region exon. The β chain undergoes a two-step rearrangement: first, D to J and then V to DJ to form the functional Vβ region exon. The rearranged V gene segments are transcribed and spliced with the constant segment to yield the TCR α and β chains. This process takes places in the thymus.
The mechanics of rearrangement and splicing of TCR and Ig DNA are similar. TCR diversity is generated not only by a combinatorial process of V(D)J gene segment rearrangement, but also through addition of nucleotides at the junctions between V, D and J segments during rearrangement. Palindrome (P) and non-template-encoded (N) nucleotides can be added or deleted.

As a consequence of VDJ gene rearrangement occurring in immature thymocytes, in the thymus a theoretical pool of 10^{15} TCRs with differing specificities could generated in the mouse (Davis and Bjorkman 1988). The theoretical number of possible TCR in humans is likely to be substantially larger due to the larger number of TCR Vβ genes (Sewell 2012). To prevent mounting an immune response to self-antigens whilst maintaining recognition of self-MHC, naïve T-cells proliferate and then undergo a process of clonal selection in the thymus (Starr, Jameson et al. 2003) that substantially reduces the TCR diversity in the circulation to perhaps 25 million (Arstila, Casrouge et al. 1999).

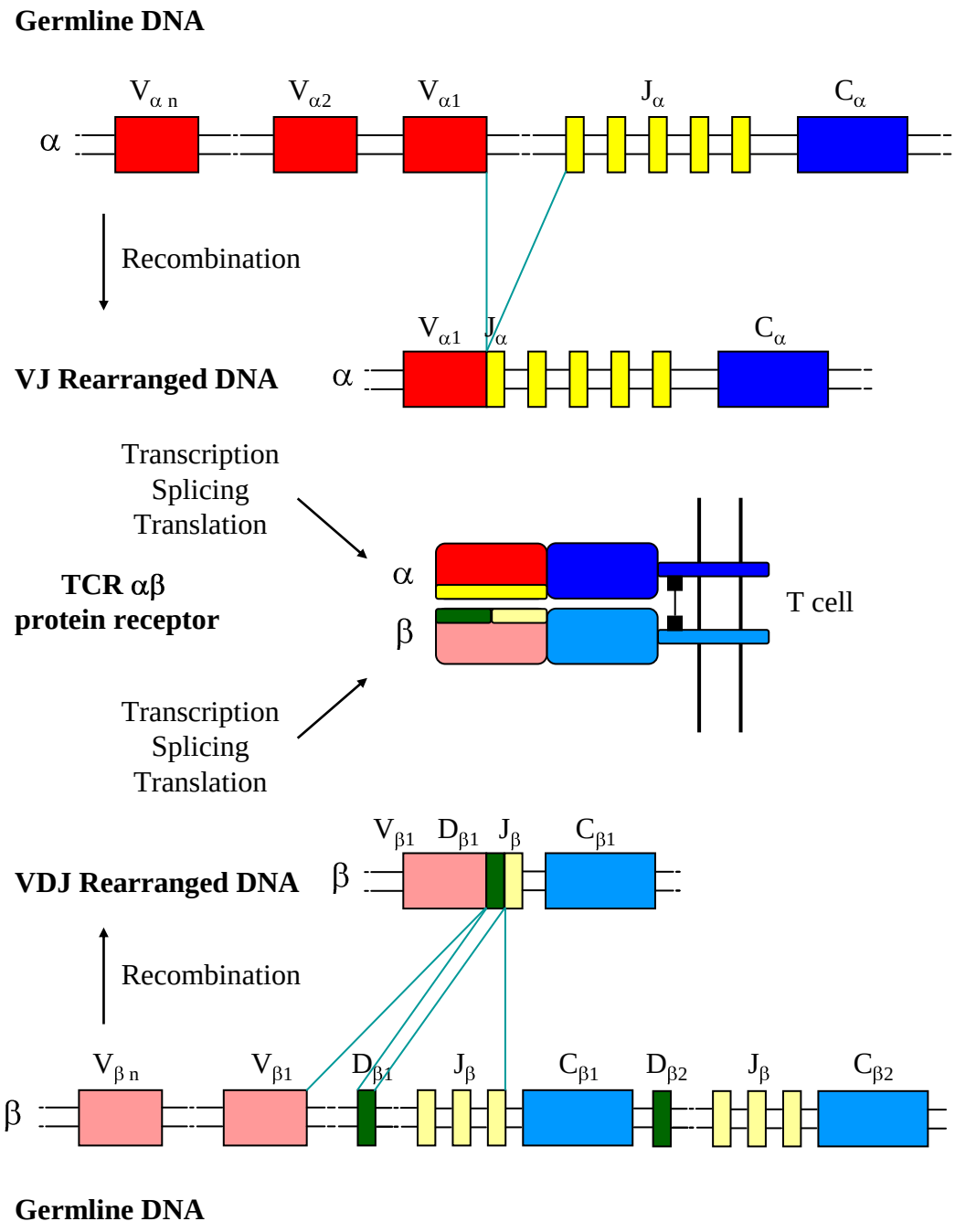

Figure 1.8. T-cell receptor α and β chain gene recombination and expression. For the α chain, a V segment rearranges to a J segment to create a V region exon. Transcription and splicing to a C segment generates the final mRNA encoding the TCR α chain protein. For the β chain, D-J rearrangement takes place first. The selection of Cβ1 or Cβ2 is determined by the selection of the Jβ1 or Jβ2 gene. In the second step, the V segment rearranges with the DJ segment. The V-DJ exon is transcribed and spliced to a C segment to produce the final mRNA sequence encoding the TCR β chain protein. The α and β chain proteins pair to form the αβTCR heterodimer. Not all V and J segments are shown and the V segment leader sequences are omitted for simplicity. Adapted from (Janeway, Travers et al. 2001).

1.9.3 Selection of the T-cell repertoire

Upon entering the thymus TCR α and β chain genes are rearranged to produce a functional αβTCR heterodimer. The earliest population of thymocytes do not express CD4, CD8 or TCRs and are called "double-negative" (DN: $CD4^-$ $CD8^-$) T-cells. Productively rearranged β chains are expressed on the T-cell surface and associate with the pre-TCR invariant surrogate α chain (pTα) to form the pre-TCR heterodimer. Thymocytes undergo rapid proliferation and CD4 and CD8 are co-expressed on the same cell. The α chain genes rearrange and are expressed on the cell surface where they pair with the β chain. These cells are called "double-positive" (DP: $CD4^+$ $CD8^+$) thymocytes. Successive attempts at rearranging a productive α chain continue until positive selection takes place.

In positive selection (or MHC restriction) T-cells that bind self-MHC molecules expressed on cortical thymic epithelial cells (cTECs) are retained. Thymocytes that express a rearranged αβTCR and fail to recognise self-MHC (does not bind or binds too weakly) are deleted by apoptosis (Kisielow and Miazek 1995). Thymocytes that interact with MHC class I molecules will express only CD8 and T-cells that bind MHC class II molecules express only CD4 and are known as "single-positive" (SP: $CD4^-$ $CD8^+$ or $CD4^+$ $CD8^-$) T-cells.

In negative selection SP-T-cells are screened for recognition of self-peptides associated with self-MHC to prevent autoimmune disorders (Finkel, Cambier et al. 1989). SP-T-cells migrate from the cortex to the medulla where they encounter self-MHC displaying a spectrum of peripheral self-peptides on medullary thymic epithelial cells (mTECs). So called self-reactive T-cells that bind with too high affinity for self-peptides are deleted presumably leaving a repertoire of T-cells with low affinity for self-antigens but with the potential to recognise foreign antigens with higher affinity.

Those T-cells that do not bind the self-peptide MHC molecules are retained and allowed to further mature.

1.9.4 Structure of the αβ T-cell receptor

This work will focus on the αβ TCRs. A wealth of structural data of the TCR molecule alone or in complex with cognate pHLA have provided an insight into the domain organisation of the molecule; this is reviewed extensively in (Rudolph, Stanfield et al. 2006).

TCRs were predicted to have a Fab-like structure and it was presumed that as they shared a high degree of similarity in the organisation of their protein domains they would also possess a similar folding pattern (Claverie, Prochnicka-Chalufour et al. 1989). As predicted from sequence homologies, subsequent three-dimensional structures of a monomeric TCR β chain (Bentley, Boulot et al. 1995) and a V α domain homodimer (Fields, Ober et al. 1995) confirmed structural homology to immunoglobulins (Igs) with the hypervariable region forming loops all pointing in one direction.

Amino-terminal V domains, which comprise VDJ gene encoded protein (as discussed earlier) are formed from the association of six CDR loops; three from both α and β chains. Collectively the CDRs form the antigen-binding site at the membrane-distal end of the molecule. A carboxy-terminal constant (C) region with homology to the Ig C domain is positioned at the membrane-proximal end of the protein. Each chain contains a short stalk region including a cysteine proximal to the transmembrane domain that forms an inter-chain disulphide bond followed by a positively charged transmembrane domain and a cytoplasmic tail (Figure 1.9).

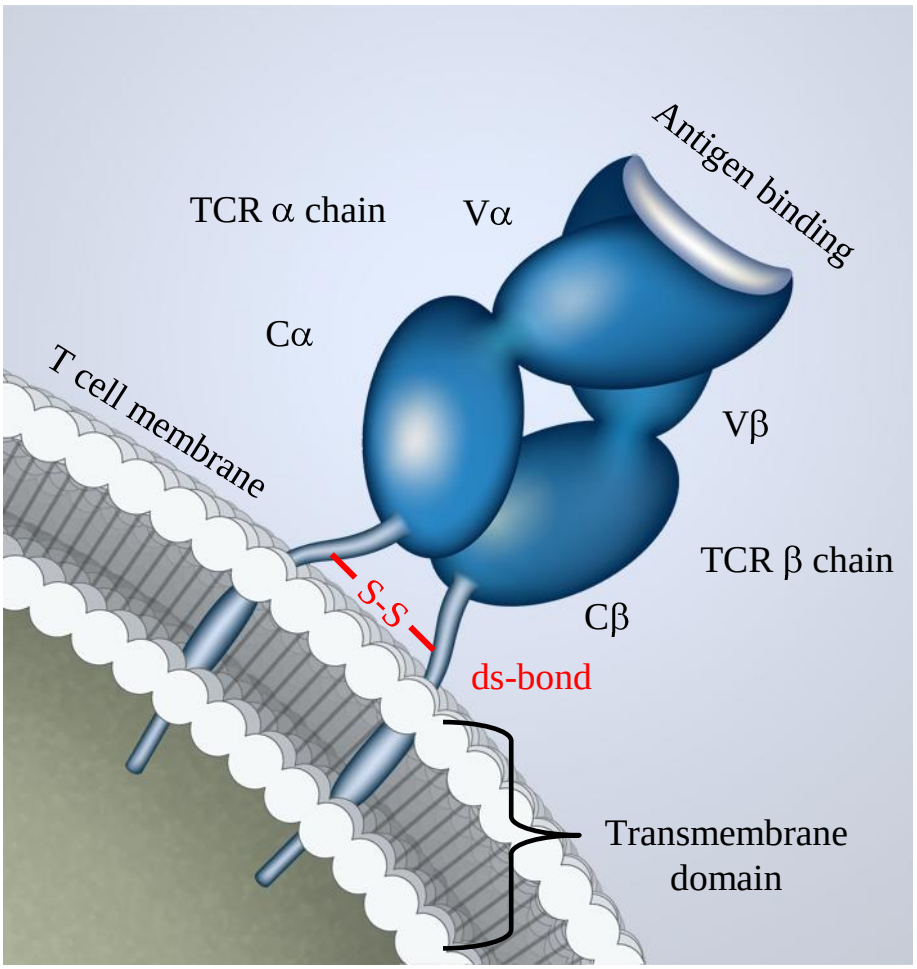

Figure 1.9. Cartoon structure of the membrane-bound TCR. The TCR comprises four domains: variable alpha (Vα), constant alpha (Cα), variable beta (Vβ) and constant beta (Cβ). The αβ TCR heterodimer is tethered to the T-cell through a transmembrane domain. The Vα and Vβ regions form the antigen-binding surface. The alpha and beta chains are stabilised by a membrane-proximal disulphide bond (ds-bond) (highlighted in red).

To date, the structures of ten (free) TCRs have been solved (uncomplexed to pMHC). The structural information obtained from the first TCRs to be solved, an αβ murine TCR designated 2C (in complex with H-2K^{b}-dEV8 peptide) (Garcia, Degano et al. 1996) and a human αβ TCR designated A6 (in complex with HLA-A2-Tax peptide) (Garboczi, Utz et al. 1996) provided a structural template that subsequent TCRs followed. The TCR consists of four domains characterised by a series of

antiparallel β strands held together by disulphide bonds (Figure 1.10). Three of the four domains, Vα, Vβ and Cβ are related to Ig domains; the Cα domain however, is structurally unrelated to the normal Ig fold and represents the most disordered region of the TCR. The Cα c, f and g strands that comprise the top β sheet are structurally unrelated to Ig C-type folds. The Cα domain consists of one half of the classical β-barrel with the remainder of the domain exhibiting random coils. The buried interface between the Cα-Cβ domains is more extensive than in antibodies. The interface is highly polar with a high proportion of acidic residues on Cα and basic residues on Cβ. Carbohydrate moieties associated with the Cα domain form hydrogen bonds with the Cβ domain. The relatively parallel association of the Cα and Cβ domains gives the TCR its 'squat' structure. The V and C domains interact extensively. The Vβ-Cβ interaction is highly polar with many interdomain hydrogen bonds whilst the Vα-Cα contact area is mainly through van der Waals' interactions. The CDR loops align fairly closely with antibody loops, with the exception of CDR2α which is almost at right angles to the equivalent loop in antibodies. The antigen-binding surface is relatively flat lacking protruding side chains presumably facilitating closer contact between TCR and pMHC. It does contain a hydrophobic cleft formed between the two CDR3s which is believed to accommodate side chains extending from the peptide bound into the MHC antigen-binding groove.

Although all TCRs share these common features subtle differences can be observed between TCRs including, variation in the CDR loop length (Bulek, Cole et al.; Reiser, Gregoire et al. 2002) and at the interface between the α and β chains of different V-region families, which can alter the local structure and affect the orientation of the two chains respectively.

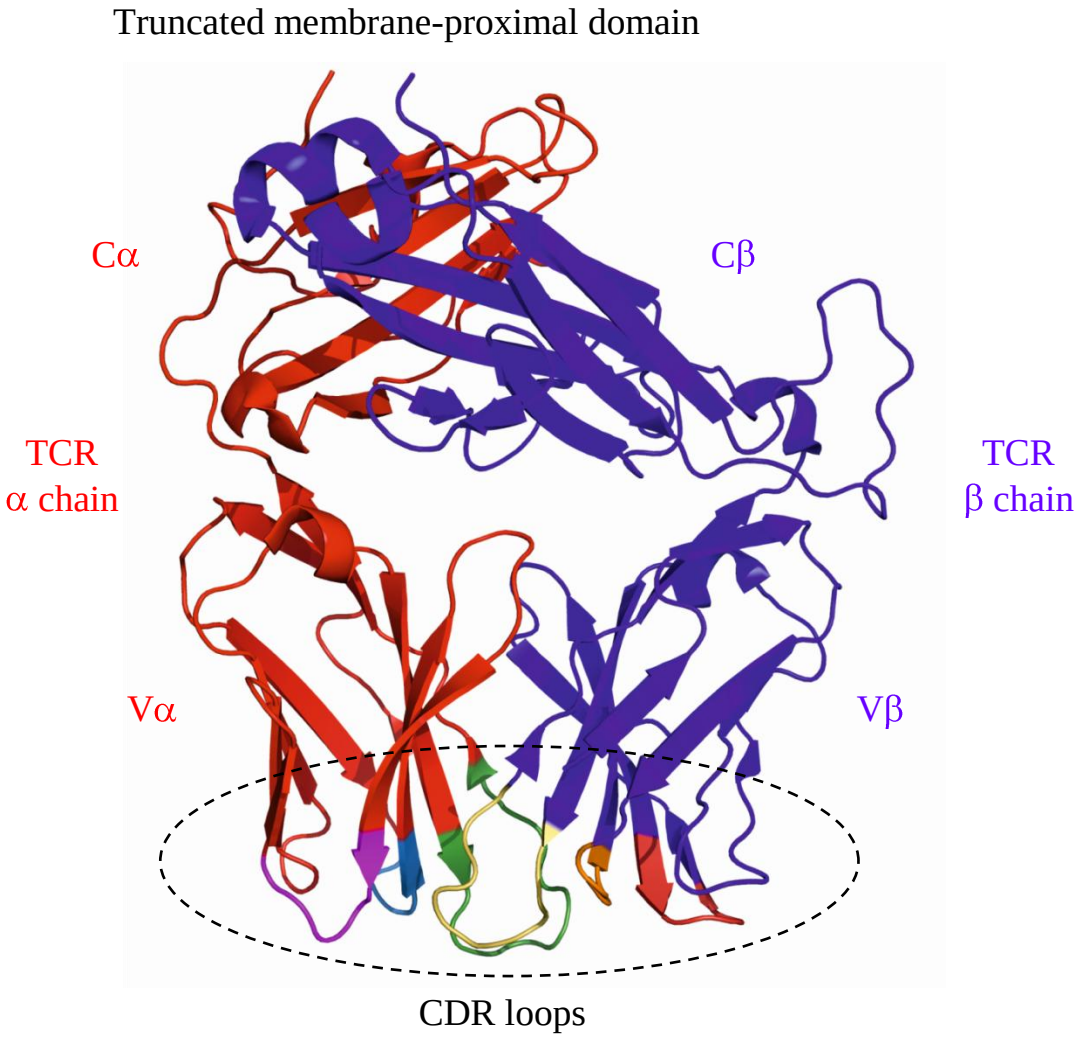

Figure 1.10. Domain organisation of the ectodomain of the αβ TCR. The TCR depicted is the 1G4 TCR. The TCR consists of four domains characterised by a series of antiparallel β strands: two variable (Vα and Vβ) and two constant (Cα and Cβ) regions. The truncated membrane-proximal domain is highlighted. The antigen-binding portion of the molecule (highlighted with a dashed circle) is formed from the six complimentarity determining region (CDR) loops: CDR1α (dark blue), CDR2α (magenta), CDR3α (dark green), CDR1β (orange), CDR2β (red), CDR3β (yellow). This figure was constructed in PyMOL version 1.5. (PDB: 2BNR) (Chen, Stewart-Jones et al. 2005).

1.9.5 Structure of the T-cell receptor-peptide-MHC complex

An extensive collection of structural data has amassed over the last 15 years on the complex of TCR bound to peptide-MHC (pMHC) molecules and a number of common features have emerged (Rudolph, Stanfield et al. 2006). These include the mode of docking onto the pMHC, the positioning of the CDR loops in relation to the MHC helices and the peptide and the significant interface between the TCR and MHC that buries the peptide beneath the TCR footprint.

The first TCR-pMHC complexes were published in quick succession over 15 years ago; the A6 TCR/HLA-A2-Tax complex from the Wilson lab (Garcia, Degano et al. 1996) and the 2C TCR/ H-2K^{b}-dEV8 complex from the Wiley lab (Garboczi, Utz et al. 1996). In general, the mode of interaction between TCR and pMHC is similar irrespective of the MHC allele or class. The TCR docks on the pMHC in a conserved diagonal to orthogonal binding orientation relative to the peptide-binding groove (Figure 1.11). The maintained docking orientation is demonstrated by two TCRs in complex with the same pHLA. The A6 (Garboczi, Ghosh et al. 1996) and B7 (Ding, Smith et al. 1998) TCRs bind the HLA-A2-Tax complex in a similar diagonal docking orientation across the peptide-binding groove despite sharing only one contact residue at the TCR-HLA interface.

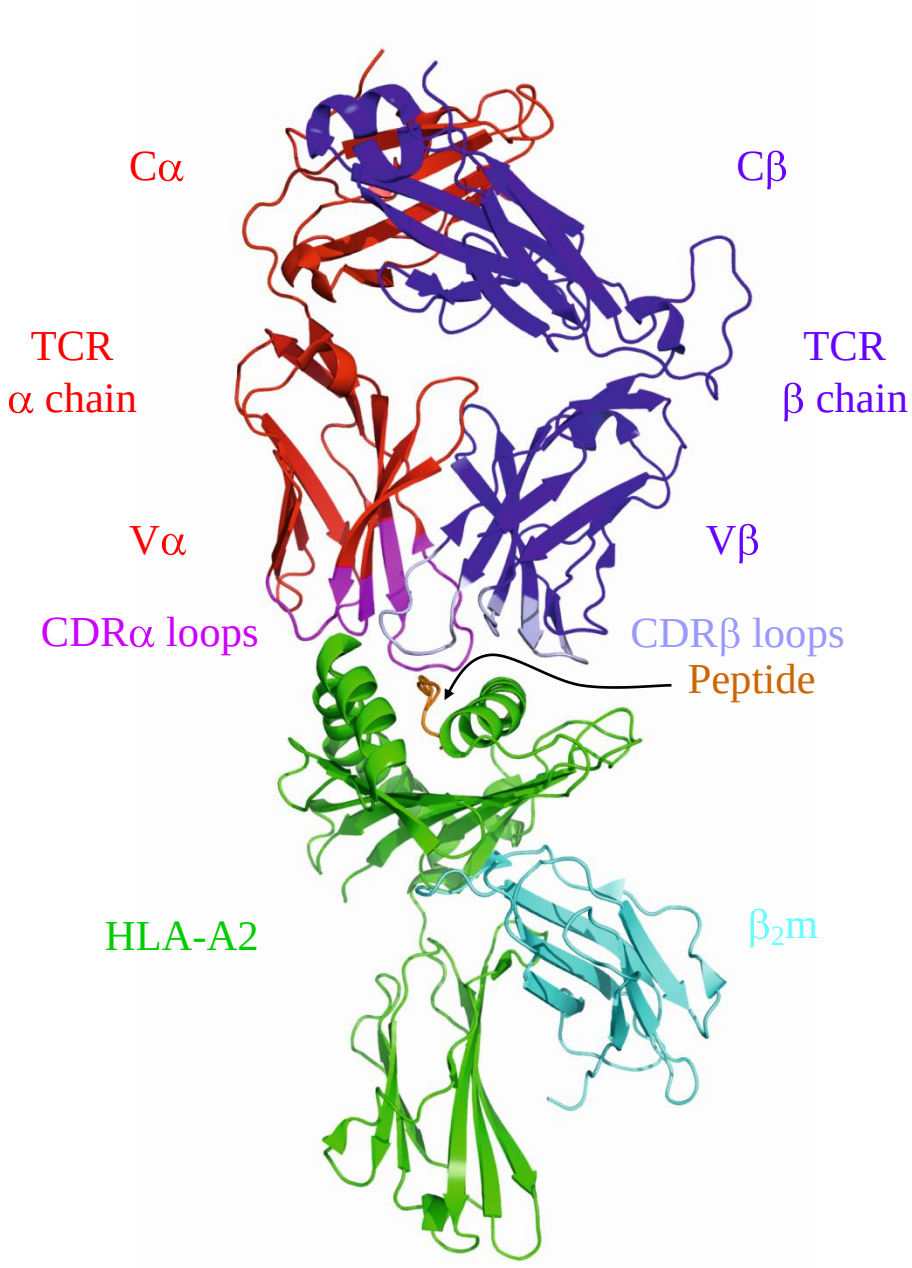

Figure 1.11. Architecture of the complex formed between class I HLA and αβ TCR. The TCR depicted is the 1G4 TCR in complex with HLA-A*0201 tumour epitope NY-ESO-$1_{(157\text{-}165)}$ (SLLMWITQC). The TCR sits directly on top of the HLA molecule in a diagonal orientation with the primary contacts between the TCR and the HLA mediated through the CDR alpha (CDRα pink) and CDR beta (CDRβ pale purple) loops which point down towards the HLA alpha helices (green) and the bound peptide (brown). The binding interface is formed between the TCR CDR loops and the HLA heavy chain α helices and peptide. The β_2-microglobulin (β_2-m) is shown in pale blue. This figure was constructed in PyMOL version 1.5. (PDB: 2BNR) (Chen, Stewart-Jones et al. 2005).

The Vα domain lies more over the N-terminal end of the peptide and the Vβ over the C-terminal end. Vα CDR1 is positioned over the N-terminal end of the pMHC α1 helix and over the N-terminal end of the peptide. Vα CDR2 lies predominantly over the C-terminal end of the pMHC α2 helix. Vβ CDR2 mainly lies over the C-terminal end of the pMHC α1 helix with slight contact with the C-terminal end of the peptide. Vβ CDR1 mostly covers the N-terminal end of the pMHC α2 helix with some contact with the C-terminal end of the peptide. The most diverse loops of the TCR (CDR3α and CDR3β) predominantly make contact with the peptide making minimal contact with the MHC framework (Figure 1.12).

Positioning of the less diverse germline encoded CDR1 and CDR2 loops over the MHC helices coupled with the placement of the more diverse CDR3 loops over the peptide provide a possible structural explanation for MHC restriction and moreover, indicate that specificity of antigen-binding is largely governed by the CDR3α and CDR3β loops. Whilst this suggests that engineering of the CDR1 and CDR2 loops for improved binding to the MHC helices may lead to diminished peptide specificity, a recent study by Dunn et al. (Dunn, Rizkallah et al. 2006) demonstrated that affinity enhancing mutations in CDR2 loops retained specificity for their cognate pMHC.

A further pattern that characterises TCR-pMHC complex formation is the large buried surface area at the TCR-pMHC interface (~1200-2000 $Å^2$). The Vα and Vβ contribution to this footprint varies widely between different TCRs. It can be split equally between the α and β chains as seen with the 1G4 TCR in complex with HLA-A2-NY-ESO 9C (47% and 53% respectively), skewed towards the α chain with the A6 TCR/HLA-A2-Tax (Y8A) (65% and 35%) or towards the β chain with the BM3.3/H-$2K^b$-pBM1 complex (37% and 63%) (Rudolph, Stanfield et al. 2006).

Whilst the orientation of TCR-pMHC docking is stringently conserved with respect to the positioning of the CDR loops relative to the bound peptide and MHC helices, examples exist that vary from this generality. The BM3.3-H2Kb-pBM1 TCR complex is one such example (Reiser, Darnault et al. 2000). The CDR3α loop, rather than aligning over the peptide, flares out from the peptide binding groove; the cavity being occupied by ~30 water molecules. It can be envisaged that engineering of the BM3.3 TCR for high affinity may require extension of the CDR3α loop to facilitate contact with the pMHC complex.

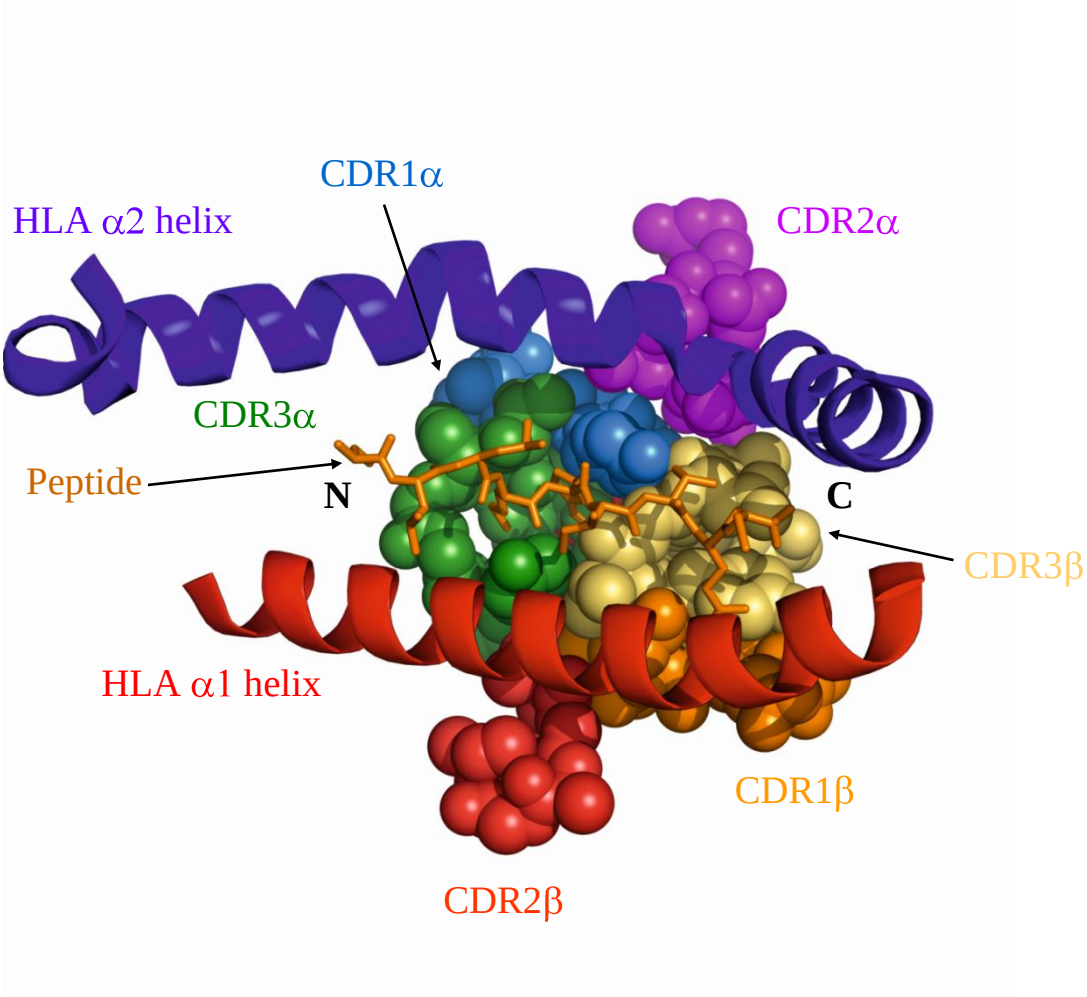

Figure 1.12. A view of 1G4 TCR binding to HLA-A*0201 tumour epitope NY-ESO-1$_{(157-165)}$ (SLLMWITQC) from beneath the peptide binding groove. The TCR contains six CDR loops: CDR1α (dark blue), CDR2α (magenta), CDR3α (dark green), CDR1β (orange), CDR2β (red), CDR3β (yellow). As a general rule the CDR3 loops and to a lesser extent the CDR1 loops contact the peptide bound in the HLA groove and as such it is the CDR3 loops that largely confer specificity. The CDR2 loops interact predominantly with the HLA surface and not the bound peptide. Whilst the Vα domain interacts predominantly with the N-terminus of the peptide, the Vβ contacts the C-terminus. The peptide amino and carboxy termini are shown with an N and a C respectively. This figure was constructed in PyMOL version 1.5. (PDB: 2BNR) (Chen, Stewart-Jones et al. 2005).

1.9.6 T-cell receptor conformational changes upon ligand binding

Although the crystallographic database contains more than 40 TCR-pMHC complexes, only ten free TCR structures have been solved. Nonetheless, using this limited set of uncomplexed structures, has revealed the conformational changes that occur following TCR-pMHC ligation (Armstrong, Piepenbrink et al. 2008).

Many reports have shown that the CDR loops possess a degree of flexibility or plasticity in order to bind pMHC. This has been exemplified by studies of a single TCR bound to different peptides (Garcia, Degano et al. 1996; Ding, Baker et al. 1999; Degano, Garcia et al. 2000). In general, moderate changes in the orientation of the CDR loops are sufficient to generate a degree of cross-reactivity or TCR degeneracy. Conformational differences are predominantly within the CDR3 loops that make adjustments to accommodate the varying peptide side chains.

For example, the CDR3β loop of the LC13 TCR undergoes a 2.5 Å rigid body shift accompanied by a 38º rotation that increases the contact with the peptide. Upon ligation, the CDR3α loop undergoes an 8Å shift to form a "crumpled" structure that enables contact with the HLA α1 helix (Kjer-Nielsen, Clements et al. 2003). A similar degree of repositioning of the CDR3α and CDR3β loops (~5 Å each) has also been reported for the JM22 TCR (Ishizuka, Stewart-Jones et al. 2008). More dramatically, a ~15.1 Å conformational shift of the (unusually long) CDR3β loop has been observed for the KB5-C20 TCR upon pMHC engagement (Reiser, Gregoire et al. 2002).

Whilst the majority of TCR-pMHC complexes studied to date have shown that greatest conformational changes occur in the hypervariable CDR3 loops, examples exist that break from this convention. For the LC13 TCR-HLA-B8-EBV complex, major conformational shifts also occur in the germline encoded CDR1α and CDR2α

loops (in addition to the CDR3 loops) with the CDR2α loop pointing in the opposite direction upon ligation (Kjer-Nielsen, Clements et al. 2003).

Significant conformational disruption of the CDR3s is not always observed. The CDR3 loops of the 1G4 TCR undergo only minor shifts upon pMHC binding. Here, accommodation of the peptide is achieved through a preexisting cavity formed between the CDR1α, CDR3α and CDR3β domains (Chen, Stewart-Jones et al. 2005).

It can be surmised that upon TCR-pMHC ligation, the CDR3α loop undergoes greatest shift in conformation and the CDR1β loop undergoes the least. To generalise, the following magnitude of conformational shift occurs: CDR3α > CDR3β > CDR1α > CDR2α > CDR2β > CDR1β (Armstrong, Piepenbrink et al. 2008).

1.9.7 TCR degeneracy

It has been estimated that there are $>10^{15}$ potential peptides that can be presented on MHC dwarfing the 2.5×10^{7} different TCRs within the naïve T-cell pool (Arstila, Casrouge et al. 1999). This poses a significant conundrum for the immune system assuming the clonal selection theory that one T-cell is specific for a single pMHC antigen. One theory to satisfy this predicament is that significant TCR degeneracy exists in the immune system that enables the limited diversity of TCRs in the naïve pool to respond to the multitude of displayed peptides (Mason 1998). Indeed, it has recently been estimated that a single TCR (designated 1E6) isolated from a patient with type I diabetes can respond to more than 1 million distinct peptides (Wooldridge, Ekeruche-Makinde et al. 2012).

A number of mechanisms have been proposed that permit this degree of promiscuity; a perspective of which has been presented recently (Sewell 2012). One solution that focuses on the TCR molecule, argues that it is the considerable flexibility

of the TCR antigen-binding loops (most strikingly in the CDR3 regions), that enables binding to an array of divergent peptides. The conformational plasticity of the TCR facilitates inspection of different pMHC landscapes and is supported by numerous TCR crystal structures in their bound and unbound states (Rudolph, Stanfield et al. 2006; Armstrong, Piepenbrink et al. 2008).

However, flexibility of the CDR loops does not satisfy the degeneracy of the 1E6 TCR, which upon pMHC ligation does not undergo conformational adjustment (Bulek, Cole et al. 2012; Wooldridge, Ekeruche-Makinde et al. 2012). Rather, degeneracy is achieved through a conserved pair of residues within the peptide that is sufficient for TCR engagement; permitting inclusion of divergent residues at all other positions (so-called peptide-centric binding).

Molecular mimicry that allows a TCR to bind to molecularly similar peptides has also been advocated (Borbulevych, Piepenbrink et al. 2011). The A6 TCR binds both the Tax peptide (sequence LLFGYPVYV) from the HTLV-1 virus and a self-peptide from the neuronal protein HuD (sequence LGYGFVNYI). It has been postulated that if T-cells react with a foreign peptide that shares sufficient sequence homology to a self-peptide, autoimmune pathologies may ensue. Baker and colleagues (Borbulevych, Piepenbrink et al. 2011) showed that shared homology of the Tax and HuD peptides at positions 4, 5 and 8 permitted recognition of both, by the A6 TCR, albeit with a 70-fold reduced binding affinity.

In addition to conformational changes occurring in the TCR, structural adjustments of the pMHC complex upon ligation have also been observed (Garboczi, Utz et al. 1996; Tynan, Reid et al. 2007) and more recently have been implicated as a potential mechanism of TCR cross-reactivity (Borbulevych, Piepenbrink et al. 2009). Cross-reactive binding of the A6 TCR towards the yeast peptide mimic Tel1p (sequence

MLWGYLQYV) is mediated through cooperative conformational changes in the TCR CDR3 loops, the peptide and the HLA-α2 helix. The phrase 'conformational melding' has been introduced to describe the process of structural adjustments occurring at the pMHC-TCR interface that allows the TCR to sample all conformational variations searching for a suitable fit.

It therefore appears likely that a cooperative flexibility and subsequent structural rearrangement of the TCR, the peptide and the HLA molecule all contribute to a level of T-cell promiscuity that is essential for an effective cellular immune response.

1.9.8 T-cell receptor binding affinities and kinetics

Until the advent of techniques to produce high levels of soluble TCR, studies of the interactions of the TCR and the pMHC were difficult. Over the last twenty years technologies, such as surface plasmon resonance (SPR), have been developed as a powerful tool to measure protein-protein interactions. TCR-pMHC interactions are characterised by a low affinity (0.1-400 μM) compared to antibodies. Since the first determined TCR/pMHC affinity measurements were published using BIAcore (Matsui, Boniface et al. 1994), a wealth of data has accumulated and is reviewed in (Willcox, Gao et al. 1999; van der Merwe and Davis 2003; Cole, Pumphrey et al. 2007; Stone, Chervin et al. 2009; Bridgeman, Sewell et al. 2011). The interaction of TCR and pMHC is a reversible reaction involving an association rate constant (k_{on}) (which measures the binding speed), a dissociation rate (k_{off}) (which measures the dissociation speed), a half-life of interaction ($t_{1/2}$) calculated from the k_{off} and a dissociation constant (K_D, affinity) determined by a ratio of k_{off}/k_{on}.

A recent study by Cole et al. (Cole, Pumphrey et al. 2007) directly compared the binding affinity of 8 class I and 6 class II MHC-restricted TCRs. Their data supports

the body of work that demonstrates that low affinity is the result of a fast dissociation rate constant and a slow association rate constant (van der Merwe and Davis 2003). The mean k_{on} values of the class I MHC (TCR-I) and the class II MHC (TCR-II)-restricted TCRs for their cognate antigen were 3.3 x 10^4 M^{-1} s^{-1} and 4.1 x 10^4 M^{-1} s^{-1} respectively. The mean TCR-I k_{off} was 0.22 s^{-1} and the mean TCR-II k_{off} was 0.3 s^{-1}. The slow on rates may be a consequence of the conformational changes that take place in the antigen-binding CDR loops upon pMHC ligation prior to stabilisation of the complex (Willcox, Gao et al. 1999).

From the accumulated data it is possible to propose a number of common features regarding the biophysical properties of the TCR-pMHC interaction. First, TCRs bind to MHC class I molecules with a higher affinity (five times greater affinity) compared to MHC class II-restricted TCRs. This may indicate that $CD4^+$ T-cells have a lower activation threshold compared with $CD8^+$ T-cells or that the signal mediated by the TCR-pMHC class II is stronger than by the TCR-MHC class I interaction. Second, class I TCRs demonstrate faster on rates than class II TCRs, with conserved off rates irrespective of the MHC restriction and antigenic origin (Cole, Pumphrey et al. 2007). The faster on rates conferred by the class I molecules may suggest that the interaction with TCR is more favourable than for class II complexes. The class I peptides tend to bulge from the peptide binding groove providing a structural feature on which to bind. The conserved off rates is consistent with crystal structures that shows the number of contacts between TCR/MHC class I and class II are similar (Rudolph, Stanfield et al. 2006). Third, self-reactive TCRs bind with lower affinity and shorter half-lives compared to TCRs binding to non-self-peptides (Aleksic, Liddy et al. 2012). In this recent report the binding of 24 TCRs to their cognate pMHC complexes were analysed, of which 10 peptides were of viral origin and 14 were tumour associated

peptide antigens (TAPAs). The mean K_D = ~108 μM and mean $t_{1/2}$ <1.9 s for TCRs binding to cancer associated peptides; mean K_D = ~8 μM and mean $t_{1/2}$ 8.4 s for TCRs binding to viral peptides). This clear correlation in binding parameters between self-reactive and non-self-reactive TCRs could be the consequence of clonal selection in the thymus. Those T-cells bearing TCRs that bind too tightly to self-pMHC are deleted in a process of negative selection thus leaving TCRs with low affinity for self-pMHC in the periphery. In contrast, T-cells will not have encountered virally-derived peptides during thymic selection, and so high affinity TCRs for these non-self-antigens will be present in the periphery.

1.10 Engineering T-cell receptors

TCRs have been engineered for improvements in stability and antigen-binding affinity using a variety of display platforms previously applied to antibody engineering. TCRs and antibodies share a similar domain organisation. This structural relatedness would imply that the display strategies employed successfully for antibodies would be amenable to TCRs (e.g. yeast display, mammalian display and phage display). However, the success of surface-displayed TCRs has been limited. The difficulties may be related to the inherent instability of the TCR molecule in which the α and β chains have a reduced ability to associate (i.e. a low affinity for each other) as compared to the heavy and light antibody chain counterparts. Symptomatic of this is the tendency of TCRs to misfold and form aggregates.

1.10.1 Yeast display of TCRs

The Kranz lab pioneered TCR engineering using yeast display (Kieke, Shusta et al. 1999). Whilst antibodies are readily displayed on the surface of yeast, TCRs are not. In general, wild-type TCRs cannot be detected on the yeast cell surface and must be

engineered to identify a variant exhibiting improved folding properties. In this study, an *E. coli* mutator strain was used to introduce random mutations throughout both chains of the murine 2C TCR. The mutant single chain Vβ-linker-Vα TCRs (scTCRs), analogous to the V_H-linker-V_L scFv, were transfected into yeast and mutant scTCRs with improved folding properties were selected with clonotypic anti-TCR antibodies by flow cytometry. The majority of mutations that improved the level of display were concentrated at the Vα/Vβ interface away from the antigen-binding regions and so had little effect on antigen-binding kinetics.

To further improve the stability and soluble expression efficiency of the murine 2C TCR a directed-evolution strategy using the yeast display system was devised (Shusta, Holler et al. 2000). A mixture of the wild-type 2C scTCR and four stabilised mutant 2C scTCRs previously identified (Kieke, Shusta et al. 1999) were subjected to random mutagenesis using error-prone PCR. The yeast-displayed mutant scTCR library was screened in parallel at two temperatures: a 46°C incubation library sort to isolate mutants with improved stability and a 37°C incubation induction step to screen for higher expression. Mutants isolated from both strategies were combined and demonstrated an additive effect in improving thermal stability, display levels and solubility of purified protein.

In addition to the murine 2C TCR, the yeast cell format has been successfully used to display correctly folded human TCRs as an scTCR (Aggen, Chervin et al. 2011). Three high affinity TCRs (previously identified by phage display) were used in the study: the A6 TCR, the 1G4 TCR (Li, Moysey et al. 2005; Dunn, Rizkallah et al. 2006) and the 868 TCR (Varela-Rohena, Molloy et al. 2008). In contrast to the selection of yeast-displayed 2C TCR where a clonotypic antibody capable of recognising correctly folded Vα and Vβ domains is available; here they used soluble

peptide-HLA-A2 tetramers. Remarkably, the 868 scTCR was detected on the yeast cell surface without necessitating a random mutagenesis step; the first time this had been observed for a TCR. However, random mutagenesis of the A6 scTCR was required to select mutants that folded properly in yeast cells, but was not sufficient to isolate yeast-displayed 1G4 scTCR. Because the A6 and 1G4 TCRs share the TRBV6-5 β chain, the Vβ mutations that permitted display of the A6 TCR were transferred into the 1G4 TCR framework but were not sufficient to allow surface display of the 1G4 TCR.

In spite of the efforts to identify common mutations within the V-domains that allow the surface expression of TCRs (Weber, Donermeyer et al. 2005; Richman, Aggen et al. 2009; Aggen, Chervin et al. 2011), the results were ineffectual, suggesting that an *in vitro* evolution strategy, employing scattergun muatagenesis, is the most effective approach to select TCRs that can be displayed on the surface of yeast.

Yeast display has also been used to select mutated TCRs with improved binding affinity for their cognate peptide-MHC. In the first example the CDR3α loop of the murine 2C TCR was targeted for mutagenesis using NNS oligonucleotides to mutate five codons (Holler, Holman et al. 2000). Using the stabilised mutant 2C TCR previously isolated (Kieke, Shusta et al. 1999) as the template, a library of 10^5 variants was constructed from which CDR3α mutants with up to 100-fold higher affinity for the pMHC were isolated. As a continuation of this work, the other CDR loops (CDR1α, CDR2α, CDR1β, CDR2β and CDR3β) of the 2C scTCR were subjected to mutagenesis using NNS oligonucleotides (Chlewicki, Holler et al. 2005). In the context of the CDR3α clone, mutants were isolated in CDR2α, CDR1β and

CDR3β that conferred up to 750-fold affinity improvements over the wild-type 2C scTCR with no loss of peptide specificity.

Isolation of high-affinity class II-restricted murine (3.L2) TCR mutants has also been demonstrated (Weber, Donermeyer et al. 2005). Using a yeast display stabilised mutant (mutated in CDR1α) as a template for mutagenesis of the CDR3 loops, mutants were selected with up to an 800-fold improvement in affinity compared to the TCR containing no CDR mutations.

1.10.2 Mammalian cell surface display of TCRs

There have been two reports of the display and engineering of TCRs on the surface of TCR-negative T-cells using retroviral transduction (Kessels, van Den Boom et al. 2000; Chervin, Aggen et al. 2008). An advantage of this technique over yeast display is that the TCRs are expressed as full-length heterodimeric proteins in their native conformation rather than in a single-chain format. A significant drawback, however, is the limited sequence diversity that can be generated as a consequence of low retroviral transformation efficiency (~10^4 surface TCR-expressing cells). An additional technical challenge in the process is the ability to tightly control the transformation conditions in order to minimise the number of target cells containing multiple TCRs.

Whilst the first report (Kessels, van Den Boom et al. 2000) was successful in demonstrating surface TCR display, mutants were isolated on the basis of altered binding specificity rather than with improved binding affinity. In a subsequent study reported from the Kranz lab (Chervin, Aggen et al. 2008), high affinity variants of the murine 2C TCR were isolated using retroviral display. The CDR3α loop was targeted for mutagenesis using a single five codon NNS degenerative oligonucleotide.

Following only two cycles of sorting, enrichment of a single clone (m100) was achieved. Interestingly, the m100 clone was distinct from a 2C TCR mutant (m33) isolated from a CDR3α yeast display library (Holler and Kranz 2003). Whilst both clones contained a conserved proline indicating its importance to the binding affinity, the determined equilibrium binding constants showed the yeast display isolate (m33) to exhibit a ~50-fold higher affinity compared to the mammalian display isolate (m100); K_D value of 32 nM for m33 and 1.8 μM for m100. These experiments illustrate the influence of the display format on the selection output.

1.10.3 Phage display of TCRs

Green and co-workers first described the phage display of TCRs (Onda, LaFace et al. 1995). An atypical TCR Vα chain was fused to the N-terminus of the bacteriophage coat protein pVIII. It was shown that the TCR Vα chain could be enriched from a library "spiked" with an irrelevant TCR indicating the promise of this display strategy. In a later study, a 3-domain single-chain murine DO11.10 TCR (Vα-linker-VβCβ) was displayed on the surface of phage fused separately to the N-terminus of pIII and pVIII (Weidanz, Card et al. 1998). Display of the TCR on the phage surface was confirmed with an anti-TCR antibody. The DO11.10 phage-displayed TCR was "spiked" into a phage display single-chain antibody library. Selections using anti-TCR antibodies or an anti-Vβ-specific antibody resulted in a 2,500-fold enrichment in the percentage of phage displaying the DO11.10 scTCR. In this study, however, neither affinity maturation nor functionality of the TCR was demonstrated.

Li et al. (Li, Moysey et al. 2005) first demonstrated phage display directed evolution of human TCRs for high-affinity. This approach used VαCα/VβCβ heterodimers and included the stabilising non-native disulphide bond introduced into

the C-domains, so-called monoclonal TCRs (mTCRs) (Boulter, Glick et al. 2003). The CDR3 loops of the A6 TCR, specific for the human T-cell lymphotrophic virus type 1 (HTLV-1) tax_{11-19} peptide-HLA-A*0201, and the 1G4 TCR, specific for the NY-ESO-$1_{157-165}$ peptide-HLA-A*0201, were targeted for mutagenesis using degenerative NNK oligonucleuotides. Libraries of mutated TCRs were fused to the N-terminus of the bacteriophage protein pIII. Following on from this work the germline-encoded CDR2 loops of the 1G4 TCR were targeted for mutagenesis using degenerative oligonucleuotides (Dunn, Rizkallah et al. 2006). The highest-affinity A6 TCR after a single round of selection had a K_D of 2.5 nM representing a >700-fold improvement over the wild-type TCR. The highest-affinity 1G4 TCR obtained following a second round of engineering had a K_D of 26 pM equating to >1 million-fold increase over the wild-type counterpart.

The display of TCRs on the surface of bacteriophage has recently been further interrogated with the hope to optimise the levels of display (Loset, Lunde et al. 2007). The TCR fusion format (scTCR, Fab and dsTCR), fusion mode (α or β domain fused to pIII) and phage system (phage vector and phagemid vector) were explored. In total, six constructs were generated: scTCR (VαVβ-pIII or VβVα-pIII), cFab (chimeric Fab VαC_H/VβC_L-pIII or VαC_L/VβC_H-pIII) and dsTCR (VαCα/VβCβ-pIII or VβCβ/VαCα-pIII). It was demonstrated that in addition to the format and domain orientation, the primary sequence of the TCR greatly influences the level of display.

1.10.4 Production of soluble TCRs

The production of soluble TCRs in sufficient quantities and of consistent quality has been a considerable challenge. Although many expression systems and TCR

constructs have been explored no single method was applicable to all TCRs (Fremont, Rees et al. 1996; Rudolph, Stanfield et al. 2006).

An early approach took advantage of the shared structural homology of antibodies and TCRs by making chimeric TCR-Ig proteins ($V\alpha C_L$ and $V\beta C_L$) but failed to produce correctly folded heterodimer (Gascoigne, Goodnow et al. 1987). To facilitate the production of properly folded heterodimer the TCR constant (C) domains were included in the TCR-Ig constructs ($V\alpha C\alpha C_L$ and $V\beta C\beta C_L$) (Gregoire, Rebai et al. 1991). Another approach was to mimic the scFv antibody format and refold single-chain scTCRs (Vα-linker-Vβ) (Novotny, Ganju et al. 1991; Hoo, Lacy et al. 1992; Hilyard, Reyburn et al. 1994) or disulphide-stabilised scTCRs (Reiter, Kurucz et al. 1995) from *E. coli* inclusion bodies. Alternatively scTCRs have been expressed in the periplasm of *E. coli* (Ward 1991; Wulfing and Pluckthun 1994). Three-domain single-chain scTCRs (Vα-linker-VβCβ) have also been expressed on the surface of αβTCR-negative T-cells linked to a glycosyl phosphatidylinositol (GPI) anchor with soluble TCR obtained by enzymatic cleavage with a phosphatidylinositol-specific phospholipase (Chung, Wucherpfennig et al. 1994).

Although the single-chain format did show promise in the production of soluble TCR, it is far from ideal because they do not include the entire extracellular region of the TCR. Soluble heterodimeric VαCα/VβCβ TCRs have been produced in a number of expression systems: in *Drosophila melanogaster* cells (Garcia, Degano et al. 1996), secreted from Chinese hamster ovary (CHO) cells (Strong, Penny et al. 1994) or refolded from *E. coli* inclusion bodies (Garboczi, Hung et al. 1992; Garboczi, Utz et al. 1996; Ding, Smith et al. 1998). These methods rely on weak noncovalent interactions between the α and β chains and so the TCRs tend to be rather unstable. To stabilise the TCR structure Wilcox et al. (Willcox, Gao et al. 1999) attached the

jun/fos heterodimerisation domains to the C-terminal end of the α and β chains, respectively, and refolded the TCR from *E. coli* inclusion bodies. The TCR was shown to be correctly folded and specific for its cognate peptide-HLA ligand as measured by surface plasmon resonance. Whilst this method is highly successful in producing a wide variety of different TCRs the inclusion of the non-native leucine zipper fusion partners makes it unsuitable for use as a therapeutic reagent. Boulter et al. (Boulter, Glick et al. 2003) introduced a non-native inter-chain disulphide bond between the Cα and Cβ domains and TCRs were refolded from *E. coli* inclusion bodies (mTCRs). Soluble TCRs produced with either the engineered disulphide bond or the jun/fos coiled coil fusion showed comparable binding affinities to their cognate peptide-HLA molecules. This approach provides a generic method to produce soluble, stable and functional TCRs and has been used extensively as a research tool (Chen, Stewart-Jones et al. 2005; Tynan, Borg et al. 2005; Cole, Pumphrey et al. 2007; Purbhoo, Li et al. 2007). It has also been shown that the high-affinity A6c134 TCR (Li, Moysey et al. 2005) can be produced as a functional, soluble, disulphide-linked protein in the cytoplasm of *trx*B *gor* mutant *E. coli* strains (Liddy, Molloy et al. 2010).

1.11 Bispecific antibodies

As has been alluded to earlier, multispecific antibodies offer numerous advantages over their monospecific counterparts. Bispecific antibody molecules can bind two targets at the same time; either two different antigens or two different epitopes on the same antigen i.e. dual binding specificity in a single construct. Antibody fragments can be engineered with two different antigen specificities by connecting each separate scFv polypeptide via a middle peptide linker (tandem scFv or bispecific scFv)

(Mallender and Voss 1994; Korn, Nettelbeck et al. 2004). Bivalent $(scFv)_2$ antibodies can also be produced by introducing C-terminal cysteines (Adams, McCartney et al. 1993; Kipriyanov, Dubel et al. 1994) commercialised by Macrogenics as Dual-Affinity Re-Targeting (DART) platform antibodies (Moore, Zhang et al. 2011). However, they have no or, at best, limited therapeutic potential because they are devoid of the Fc region of a full-IgG and require reformatting to interact either with Fc-related or cytotoxic effector cells. Single-chain Fv IgG-like antibodies have been produced by fusing an scFv fragment with one antigen-binding specificity to a full-length IgG molecule with a second antigen-binding specificity. Fusion of the scFv can either be at the N-terminus (Alt, Muller et al. 1999; Michaelson, Demarest et al. 2009) or C-terminus (Orcutt, Ackerman et al.; Coloma and Morrison 1997; Dong, Sereno et al. 2011) of either the IgG heavy or light chain. Fusion to a full-IgG molecules ensures that the Fc effector function of the antibody is retained. Whilst fusion to an Fc domain confers an effector function through triggering a multifaceted cellular immune cascade leading to target cell death, a more direct killing approach is through conjugation of the antibody to molecules such as cellular toxins, radioisotopes and cytokines.

1.11.1 Anti-TCR/Anti-tumour antibody bispecifics

Almost three decades ago it was first demonstrated by two groups that bispecific or "hybrid" antibodies with dual specificity for the T-cell receptor and a chosen target antigen could redirect T-cells to the target site (Perez, Hoffman et al. 1985; Staerz, Kanagawa et al. 1985). In subsequent studies it was shown that cross-linked anti-tumour/anti-TCR antibody bispecifics could specifically lyse target tumour cells (Perez, Titus et al. 1986) and that T-cell triggering was dependent on dual antibody binding to both TCR and target antigen (Roosnek and Lanzavecchia 1989). More

recently, bispecific anti-tumour antigen/anti-CD3 scFvs showed great promise in redirecting T-cells to specifically lyse tumour cells in vitro (Loffler, Kufer et al. 2000; Withoff, Bijman et al. 2001; Dreier, Lorenczewski et al. 2002).

This approach has been exploited commercially by German biotech Micromet (recently acquired by Amgen) who have developed a new class of bispecific antibody called bispecific T-cell engager (BiTE) antibodies which comprise the V_H and V_L domain from an anti-CD3 IgG antibody attached to a V_H and V_L domain from an anti-tumour IgG antibody via a peptide linker (Figure 1.13). Dual engagement of a T-cell and a tumour cell results in T-cell activation and tumour cell killing through apoptosis (Baeuerle and Reinhardt 2009). Several BiTE molecules have demonstrated significant efficacy in controlling and in some cases eradicating tumour tissue using human xenograft mouse models. Anti-tumour efficacy has been confirmed using BiTE molecules targeting different tumour antigens, e.g. epithelial cell adhesion molecule (Ep-CAM) (Schlereth, Fichtner et al. 2005) and EpHA2 receptor tyrosine kinase (Hammond, Lutterbuese et al. 2007). Blinatumomab (MT103), a bispecific antibody targeting CD19 positive cells of various B-cell malignancies is currently undergoing clinical appraisal for a number of indications. In a Phase I study for the treatment of Non-Hodgkin's Lymphoma (NHL) a median duration of response in all patients of 508 days was observed (Dhimolea and Reichert 2012). A Phase II clinical trial evaluating the efficacy of blinatumomab for the treatment of patients with minimal residual disease B-cell acute lymphoblastic leukaemia (MRD B-ALL) showed an 80% complete molecular response rate (Topp, Kufer et al. 2011).

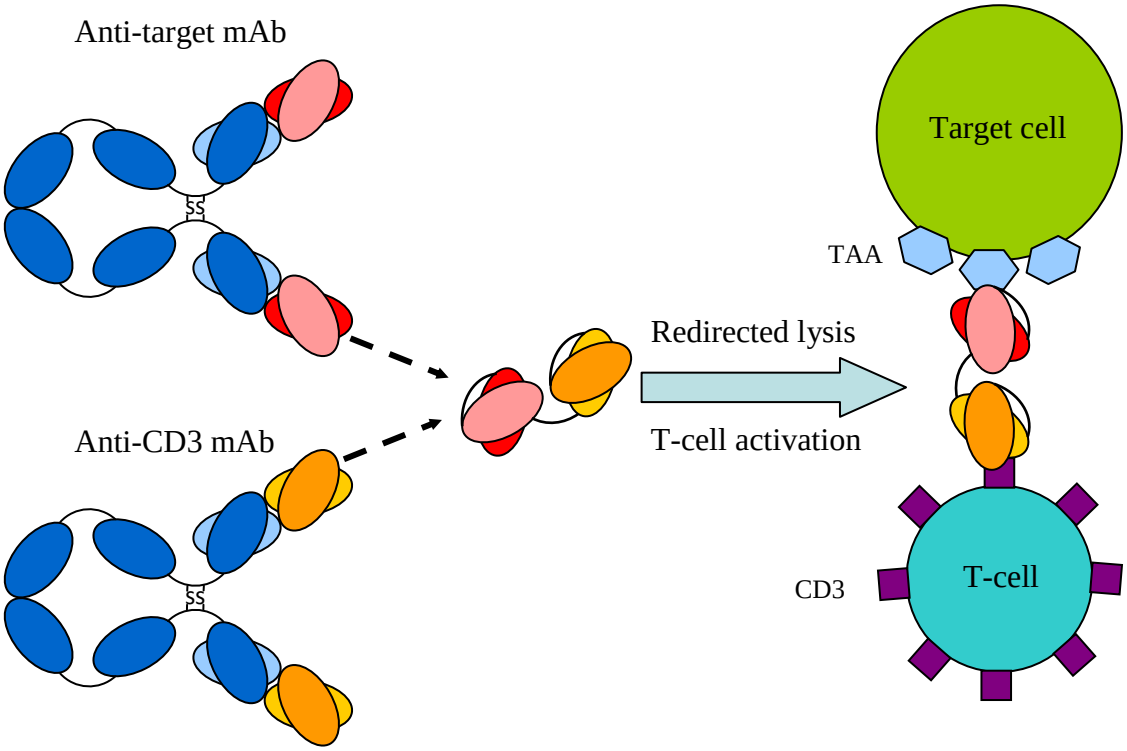

Figure 1.13. The BiTE antibody structure and mode of action. The BiTE molecule comprises the V_H and V_L domains from two different mAbs, one specific for a tumour associated antigen (TAA) and one specific for the CD3 moiety of the T-cell receptor complex. The TAA-specific arm binds to the target antigen and the anti-CD3 arm binds to T-cells. Interaction of both arms with their targets leads to T-cell activation and redirected lysis of the attached tumour cell. Adapted from (Baeuerle and Reinhardt 2009)).

1.12 Tumour associated antigens

1.12.1 Antibody TAA targets

A key challenge has been the identification of suitable antigen targets. Genomic, proteomic and bioinformatic databases in combination with serology and immunohistochemistry have identified antigens that are overexpressed in cancer cells or expressed in a modified form compared with normal tissues. Many TAAs targeted by therapeutic monoclonal antibodies are growth factors and growth factor receptors that are overexpressed on tumour cells and can be divided into distinct groups (reviewed in (Scott, Wolchok et al. 2012). (1) Haematopoietic differentiation antigens, usually associated with cluster of differentiation (CD) antigens: CD20, CD30, CD33 and CD52; (2) Glycoproteins expressed on solid tumours: EpCAM, CEA (carcinoembryonic antigen) and PSMA (prostate specific membrane antigen); (3) Angiogenesis-related antigens: VEGF (vascular endothelial growth factor) and VEGFR (vascular endothelial growth factor receptor); (4) Growth and differentiation signalling antigens: EGFR (epidermal growth factor receptor) and Her2; (5) Stromal and extracellular matrix antigens: FAP (fibroblast activation protein) and Tenascin. A total of twelve mAbs targeting many of these surface proteins have being given FDA approval for the treatment of various solid and haematological tumours and a multitude of others are being analysed in early and late-stage clinical trials (Scott, Wolchok et al.).

Whilst the overall clinical benefit of these mAbs has in general been fairly modest, several have become blockbusters. Trastuzumab (Herceptin) is a humanised IgG used in the treatment of breast cancer. It targets the HER2 gene which is amplified in 25-30% of breast cancers and the encoded protein is expressed in abnormally elevated levels in tumour cells. In combination with chemotherapy, trastuzumab can prolong the life of patients by 4-5 months compared to patients on chemotherapy alone

(Slamon, Leyland-Jones et al. 2001). Bevacizumab (Avastin) is a humanised mAb against VEGF and is used in the treatment of metastatic colorectal cancer and can prolong the survival of patients by 4-5 months compared to patients on chemotherapy and placebo (Hurwitz, Fehrenbacher et al. 2004). Rituximab is a chimeric mAb that targets CD20 on B-cells and is used for the treatment of Non-Hodgkin's Lymphoma. Treatment with rituximab significantly improved time to progressive disease (3.7 versus 1.3 years) compared to treatment with chemotherapy alone (van Oers, Van Glabbeke et al. 2010).

1.12.2 T-cell TAA targets

It is over 100 years since Paul Ehrlich proposed his magic bullet theory to selectively target tumour cells (Ehrlich 1906) and whilst there have been a number of success stories for the treatment of cancer, there still remains a clear unmet need for more effective targeted therapies.

A major limitation of antibody-based therapies against cancer cells is the nature and location of the target antigens. The majority of TAAs are expressed as intracellular proteins and are therefore inaccessible to antibodies. This greatly reduces the pool of potential antigens that antibodies can target. Modification to the protein makeup of the cell that results from genetic mutations and altered gene expression, distinguishes cancer cells from normal cells. These differences are reflected at the cell surface in the degradation products (epitopes) presented by MHC molecules, thus providing a mechanism for T-cells to distinguish between normal and malignant cells. Aberrant peptides can be recognised by cytotoxic T-cells resulting in target cell lysis.

Several strategies have been employed to identify tumour associated T-cell antigens/epitopes (reviewed in (Paschen 2009)). The first is to generate tumour-specific T-cells. Tumour-specific cytotoxic T-cells can be isolated by stimulating

lymphocytes from a cancer patient with an autologous tumour cell line. Stimulated T-cells are then used to screen HLA-matched target cells transfected with tumour-derived cDNA libraries. The second approach is to use reverse immunology. Computer software using predictive algorithms analyse proteins of interest for HLA-binding motifs. Predicted peptides are synthesised and their ability to bind MHC measured. Dendritic cells loaded with the candidate peptides are used to prime autologous T-cells. Peptide-specific T-cells are used to confirm reactivity against the predicted peptide by lysis of pulsed antigen presenting cells or peptide-matched tumour cells. A third method elutes the repertoire of peptides bound to MHC from the surface of cancer cells. Eluted peptides are separated by a combination of chromatography with mass spectroscopy and the peptide tissue distribution on normal and malignant cell analysed. A fourth strategy uses DNA microarray technology to compare gene expression profiles in normal and tumour cells (Paschen 2009). These methods have been used to identify four main classes of human tumour antigens: cancer-testis antigens, differentiation antigens, overexpressed antigens and unique antigens and are reviewed in (Linley, Ahmad et al.; Novellino, Castelli et al. 2005; Lucas and Coulie 2008; Paschen 2009).

The focus of this study is the engineering for high affinity three HLA class I-restricted TCRs targeting peptides derived from Melan-A/MART-1, gp100 and MAGE-3 antigens and as such each will be discussed in detail.

1.12.2.1 Cancer testis antigens

The cancer-testis (CT) antigens or tumour-specific shared antigens are the products of genes that are silent in normal cells and are reactivated in malignant cells. Expression of these antigens in normal tissue is restricted to MHC-negative testicular germ cells

and placenta trophoblasts which cannot present antigens to T-cells. For this reason the CT antigens represent ideal candidates for targeted immunotherapy.

1.12.2.1.1 MAGE

Van der Bruggen et al. (van der Bruggen, Traversari et al. 1991) identified the gene encoding the TAA MAGE-1 and demonstrated that the antigen, initially called MZ2-D was recognised by CTLs from a melanoma patient. They subsequently identified a nonapeptide presented by HLA-A1 recognised by the same CTLs (Traversari, van der Bruggen et al. 1992). They later reported that a structurally-related antigen (73 % sequence homology to MAGE-1) is expressed on the same tumour, named MAGE-3 (Gaugler, Van den Eynde et al. 1994).

The MAGE-3 nonapeptide presented in the context of HLA-A1 corresponded to codons 168-176 (EVDPIGHLY) of the large open reading frame and is the best characterised MAGE-3 epitope (Celis, Tsai et al. 1994). Since it is HLA-A1-restricted it is commonly referred to as MAGE-3.A1. T-cells specific for the MAGE-3 peptide elicits cytotoxic activity toward peptide-pulsed, HLA-A1 positive target cells and toward two MAGE-3-expressing HLA-A1 melanoma cell lines (Celis, Tsai et al. 1994).

The expression of the MAGE-3 gene by tumour tissues was measured by RT-PCR (Gaugler, Van den Eynde et al. 1994). It was shown that it is expressed in a variety of tumour samples and tumour cell lines including in 69 % (72 out of 105) of melanomas, 81 % (50/62) of melanoma cell lines, 82 % (18/22) of head and neck squamous cell carcinoma tumour samples, 30 % (14/46) non small cell lung carcinoma tumour samples, 2 out 3 small cell lung carcinoma tumour samples and in 82 % (18/22) of cell lines.

MAGE-A3 has also been detected in the bone marrow of multiple myeloma (MM) patients (Jungbluth, Ely et al. 2005; Atanackovic, Luetkens et al. 2009). In these studies the percentage of MAGE-A3 positive samples from Stage III MM patients was higher compared to Stage I/II (50-100 % compared to 33-50 % respectively). Thus there appears to be a correlation between cancer progression and MAGE-A3 expression. It has also been shown that a CTL clone (CTL 434/1) that recognises MAGE-A3 can specifically lyse a MM cell line (EJM) which is both HLA-A1+ and MAGE-A3 + (van Baren, Brasseur et al. 1999).

The identification of the MAGE family of CT antigens paved the way for the discovery of a multitude of other CT gene families, including BAGE, GAGE and NY-ESO, and are reviewed in (Scanlan, Simpson et al. 2004).

1.12.2.2 Differentiation antigens

This group describes TAAs that are shared between tumours and the normal tissue from which the tumour arose. They are also called shared lineage antigens and are mainly found on melanomas and normal melanocytes (Anichini, Maccalli et al. 1993). Following oncogenic transformation the antigens are significantly overexpressed.

1.12.2.2.1 Melan A/MART-1

The Melan-A (melanoma antigen A) or MART-1 (melanoma antigen recognised by T-cells 1) was one of the first TAAs to be cloned. CTLs were isolated from either peripheral blood mononuclear cells from a melanoma patient (Coulie, Brichard et al. 1994) or from tumour infiltrating lymphocytes (TILs) from metastatic melanoma patients (Kawakami, Eliyahu et al. 1994). To identify potential immunogenic peptides twenty-three peptides from MART-1 were synthesised (Kawakami, Eliyahu et al.

1994). Specific lysis of peptide-pulsed T2 cells by more than ten TIL populations identified two HLA-A2 overlapping peptides mapped to residues 27-35 (AAGIGILTV) and 26-35 (EAAGIGILTV); it has been argued that the decapeptide (EAAGIGILTV) represents the major HLA-A2 epitope (Romero, Gervois et al. 1997). They showed that the decapeptide was more efficiently recognised by polyclonal tumour-infiltrated lymph nodes (TILNs) and monoclonal CTL clones derived from a melanoma patient than the nonapeptide. Mass spectrometry later identified the nonapeptide (AAGIGILTV) but not the decapeptide (EAAGIGILTV) on the surface of melanoma cells eluted from HLA-A2 molecules (Skipper, Gulden et al. 1999).

On the basis that both of these peptides contain a nonoptimal P2 alanine anchor residue, artificial variants, substituting alanine for leucine, were designed (Valmori, Fonteneau et al. 1998). Artificial variant (or heteroclitic) peptides of the nonapeptide (AL<u>L</u>GIGILTV) and decapeptide (EL<u>L</u>AGIGILTV) were synthesised (the substituted alanine for leucine are underlined). Recognition of the peptide analogues by either Melan-A-specific tumour infiltrated lymph node cells (TILNs) or Melan-A-specific CTL were in agreement. Although the Ala28Leu nonapeptide variant bound with higher affinity to HLA-A2, recognition by Melan-A-specific TILNs and CTLs was greatly diminished. In contrast, the Ala27Leu decapeptide variant which also bound with higher affinity to HLA-A2, was more efficiently recognised by Melan-A-specific TILNs and CTLs than both the wild-type and variant nonapeptides.

Overexpression of Melan-A/MART-1 in tumour tissue has been extensively evaluated. It has been demonstrated that, at the mRNA level as measured by RT-PCR, that 100 % of (26/26) melanoma samples were positive for Melan-A/MART-1 (Coulie, Brichard et al. 1994). Immunohistochemistry (IHC) using anti-MART-1

antibodies has also been a valuable technique to measure the level of Melan-A/MART-1 expression. Positive staining of melanoma tumour samples for Melan-A/MART-1 has been 89 % (193 out of 217 samples) (Cormier, Hijazi et al. 1998); 82 % (103 out of 126 samples) (Zubovits, Buzney et al. 2004) and 83 % (285 out of 345 samples) (Reinke, Koniger et al. 2005).

1.12.2.2.2 gp100

A second melanoma differentiation antigen, called gp100 (also known as Pmel17) that shares a similar expression pattern in normal and malignant tissue to that of Melan-A/MART-1 has also been identified (Bakker, Schreurs et al. 1994; Kawakami, Eliyahu et al. 1994).

Multiple HLA-A2 naturally-processed gp100 epitopes have been detected on the surface of melanoma cells by mass spectrometry and includes a peptide mapped to residues 280-288, $G9^{280}$ (YLEPGPVTA) (Cox, Skipper et al. 1994; Skipper, Gulden et al. 1999). Several of these peptides, including the $G9^{280}$ peptide were used to generate CTL derived from peripheral blood lymphocytes (PBLs) of HLA-$A2^{+}$ melanoma patients. These CTLs were shown to kill both peptide-pulsed T2 cells and HLA-$A2^{+}$, $gp100^{+}$ melanoma cell lines (Salgaller, Afshar et al. 1995).

As was observed with the Melan-A/MART-1 wild-type peptides, the $G9^{280}$ peptide also contains a nonoptimal HLA-A2 anchor residue. In the case of the $G9^{280}$ peptide it contains an alanine at P9. Through peptide-binding assays it was determined that the $G9^{280}$ has an intermediate binding affinity to HLA-A*0201 (Kawakami, Eliyahu et al. 1995). To improve both the HLA-binding affinity and immunogenicity, the alanine was substituted for a valine at this position (Parkhurst, Salgaller et al. 1996). The 9V variant bound HLA-A*0201 with a ten-fold increase in affinity compared to the

parent peptide. This correlated with enhanced immunogenicity and CTLs were induced against the modified peptide more efficiently than against the unmodified peptide. Stimulation of melanoma patient PBMCs with the $G9^{280}$ peptide induced tumour-specific CTL from only one of seven patients, compared to six out of seven with the 9V variant.

Overexpression of gp100 in malignant melanoma has been well documented. Expression has been assessed by RT-PCR and has shown that 100 % (10 out of 10) (Jager, Ringhoffer et al. 1996) and (6 out of 6) (Spagnoli, Schaefer et al. 1995) of melanoma samples were positive for gp100 mRNA. IHC staining with anti-gp100 antibodies has also been used to analyse gp100 expression in melanoma tissue with reports of 76 % (165 out of 217 samples) (Cormier, Hijazi et al. 1998) and 82 % (Trefzer, Hofmann et al. 2006) gp100 positive staining.

1.12.2.3 Overexpressed antigens

Overexpression can mean two different things: either a gene is expressed at higher levels in malignant cells than in normal cells or that a higher percentage of tumour cells express the antigen compared to normal cells so that at the single cell level the amount of gene expression is the same. Tumour overexpressed antigens include HER-2/neu, PRAME, telomerase, surviving, MUC-1 and WT-1. Each of these proteins are expressed in both normal and tumour cells and although they represent potential targets for immunotherapy the possibility for autoimmunity against normal cells must be considered (Lucas and Coulie 2008; Paschen 2009; Linley, Ahmad et al. 2011).

1.12.2.4 Unique antigens

Unique antigens in tumour cells arise from somatic mutations in normal genes and as such can be considered tumour-specific. This group of TAAs is exemplified by Ras where the peptide is altered by point mutations. These TAAs are ideal for immunotherapy targeting because of their truly tumour-specific localisation. However, because the mutations are generally restricted to the tumour of a particular individual, immunotherapeutic agents would be needed for each patient, i.e. personalised medicine (Lucas and Coulie 2008; Paschen 2009; Linley, Ahmad et al. 2011).

1.13 Considerations on TCRs as bispecifics

In order to exploit the exquisite antigen recognition capacity of the TCR for use as a soluble immunotherapeutic reagent, three properties of the TCR molecule need addressing: first, TCRs are naturally membrane-bound proteins; second, soluble versions of TCRs would be devoid of effector domains; third, TCRs have an intrinsic low affinity for cognate pMHC.

The challenge of producing soluble TCR has been successfully achieved by expressing the α and β chains paired by a non-native ds-bond in *E. coli* (Boulter, Glick et al. 2003) and has been discussed earlier in Section 1.10.4.

The choice of effector domain has been largely influenced by the recent success of the bispecific scFv antibodies (BiTES) which possess dual specificity for target antigen and the CD3 domain of the TCR complex (Baeuerle, Kufer et al. 2009; Baeuerle and Reinhardt 2009). Fusing a human anti-CD3 scFv to the TCR would facilitate the redirection and activation of T-cells to lyse tumour cells in a mode of action analogous to the BiTE molecules.

In the context of my thesis, the third and most relevant feature of the TCR that limits its therapeutic potential is the inherent low affinity of interaction with pMHC. The repertoire of T-cells is generated during thymic selection. T-cells in the periphery express TCRs with low affinities for pMHC to minimise autoreactivity. The majority of T-cells that recognise self-antigen presented on MHC with too high an affinity will have been deleted during negative selection. Many TAAs are derived from self-antigens and so those T-cells that are present in the periphery will express TCRs with low affinity for these TAAs reducing their targeting and killing capabilities.

Engagement of a T-cell with a cognate antigen presenting cell (APC) leads to substantial reorganisation of receptors involved in antigen recognition and adhesion. It is at the T-cell:APC contact interface that supramolecular activation clusters (SMAC) or bullseye-shaped immunological synapses are formed (Monks, Freiberg et al. 1998; Grakoui, Bromley et al. 1999). Clustered within the central region, cSMAC, are molecules for T-cell signalling such as CD28 or cytotoxic T-lymphocyte antigen-4 (CTLA-4) on the T-cell that bind pMHC and CD80/CD86 on the APC respectively. This is surrounded by a peripheral ring, pSMAC, of adhesion molecules such as leukocyte function associated antigen-1 (LFA-1) and intracellular adhesion molecule-1 (ICAM-1) on T-cell and APC respectively, that function to strengthen the T-cell:APC interaction. Phosphorylation of TCR/CD3 intracellular domains following ligation of the TCR with pMHC initiates a signalling cascade that regulates gene expression of immune modulating cytokines that ultimately determines cell fate. Although the mechanisms responsible for triggering these signalling cascades are not fully understood, several models exist as reviewed in (van der Merwe and Dushek 2011). The aggregation model proposes that the aggregation of more than one TCR-CD3 molecule increases the proximity of signalling proteins (e.g. Lck) with their

substrate. The conformational change model proposes that ligation of TCR with cognate pMHC leads to conformational changes that are transmitted to the CD3 domain enhancing phosphorylation events. The segregation model suggests that exclusion from the TCR:pMHC contact zone of large ectodomain inhibitory phosphatases, CD45 and CD148, favours phosphorylation and thus signalling to occur.

In a cellular context, the low affinity TCR-pMHC interaction is adequate to induce cytotoxicity of target cells bearing as few as three pMHC complexes (Purbhoo, Irvine et al. 2004). Whilst the processes that permit such remarkable sensitivity are not fully understood, the role of the co-receptor CD8 expressed on the surface of cytotoxic T-cells is pivotal. The CD8 effect described by Cole et al. in a recent review (Cole, Laugel et al. 2012) suggests that at low TCR-pMHC affinity T-cell activation is dependent on CD8 cooperation, whereas at high TCR-pMHC affinity T-cell stimulation is CD8 independent. This hypothesis has direct implication on the biological activity of a soluble TCR reagent in which the antigen-binding function is uncoupled from the intrinsic co-receptor participation. Binding to pMHC through a soluble high affinity TCR may negate the absolute requirement for CD8 contribution; a parameter that has as yet not been explored.

In addition to abrogating the complete requirement for CD8 co-receptor assistance, engineering a soluble TCR reagent for high affinity could also compensate for loss of avidity effects necessary to target low numbers of pMHC. Antigen expression on tumour cells that act as targets for antibody therapeutics is in great contrast to the number of peptide epitopes available for recognition by TCR therapeutics. For example, Baeuerle and colleagues have determined the level of Ep-CAM expression on the surface of several tumour cell lines and included: Kato III (gastric cell line)

900,000 sites per cell, SW480 (colon) 510,000 sites per cell and PC3 (prostate) 114,000 sites per cell (Brischwein, Schlereth et al. 2006). The number of pMHC complexes on the cell surface has been estimated using a variety of methods each in agreement that the level of presented epitopes is extremely low. Peptides bound to HLA-A*0201 have been eluted from the surface of tumour cells and quantified by mass spectrometry with estimates of 85 to 125 copies per cell of the YLDPQQNL epitope (derived from an unknown member of the zinc finger protein) (Wang, Gulden et al. 1997) and 18 copies per cell for the KVLEYVIKV epitope (derived from the MAGE-A1 protein) (Pascolo S Cancer Res 2001 61:4072). Antibody fragments isolated from nonimmunised phage-Fab libraries with anti-pHLA specificity have also been used to quantitate the cell surface expression of peptide antigens (Chames, Hufton et al. 2000; Cohen, Hoffmann et al. 2002). More recently, tetramers of soluble TCRs (Laugel, Boulter et al. 2005) or high-affinity TCR monomers (Purbhoo, Sutton et al. 2006) have been used. In the latter study, Jakobsen and colleagues determined by single-molecule fluorescence microscopy, that SK-MEL-37 and Mel-264 melanoma cells presented an average of ~25 and ~45 target antigens per cell respectively.

Although tumour cells can be recognised and killed by the body's cytotoxic T-cells, most tumours are not eliminated. Cancer cells have developed escape mechanisms that enable evasion of the immune system. The display of peptides on MHC are targets for T-cells; aberrant peptides will be recognised and the cell destroyed. Down-regulation or complete loss of expression of MHC on tumour cells provides a method to avoid detection by T-cells and therefore a survival advantage. The mechanisms for loss of MHC include β2-m mutations, alterations in the antigen

processing machinery, HLA class I mutations and deletion of segments of chromosome 6 and are reviewed in (Tait 2000).

T-cell avidity is a measure of the strength of interaction between a T-cell and its target antigen and is affected by TCR expression levels, TCR-pMHC binding affinity and expression of other co-stimulatory and co-inhibitory receptors on T-cells. Although for some, binding affinity provides the most important contribution, there does not appear to be a clear relationship between binding affinity, avidity and tumour cell killing. High avidity T-cells can have TCRs of low affinity and conversely, low avidity T-cells can have high affinity TCR. Both populations of T-cells still retain the capacity to recognise tumour cells as reviewed in (McKee, Roszkowski et al. 2005).

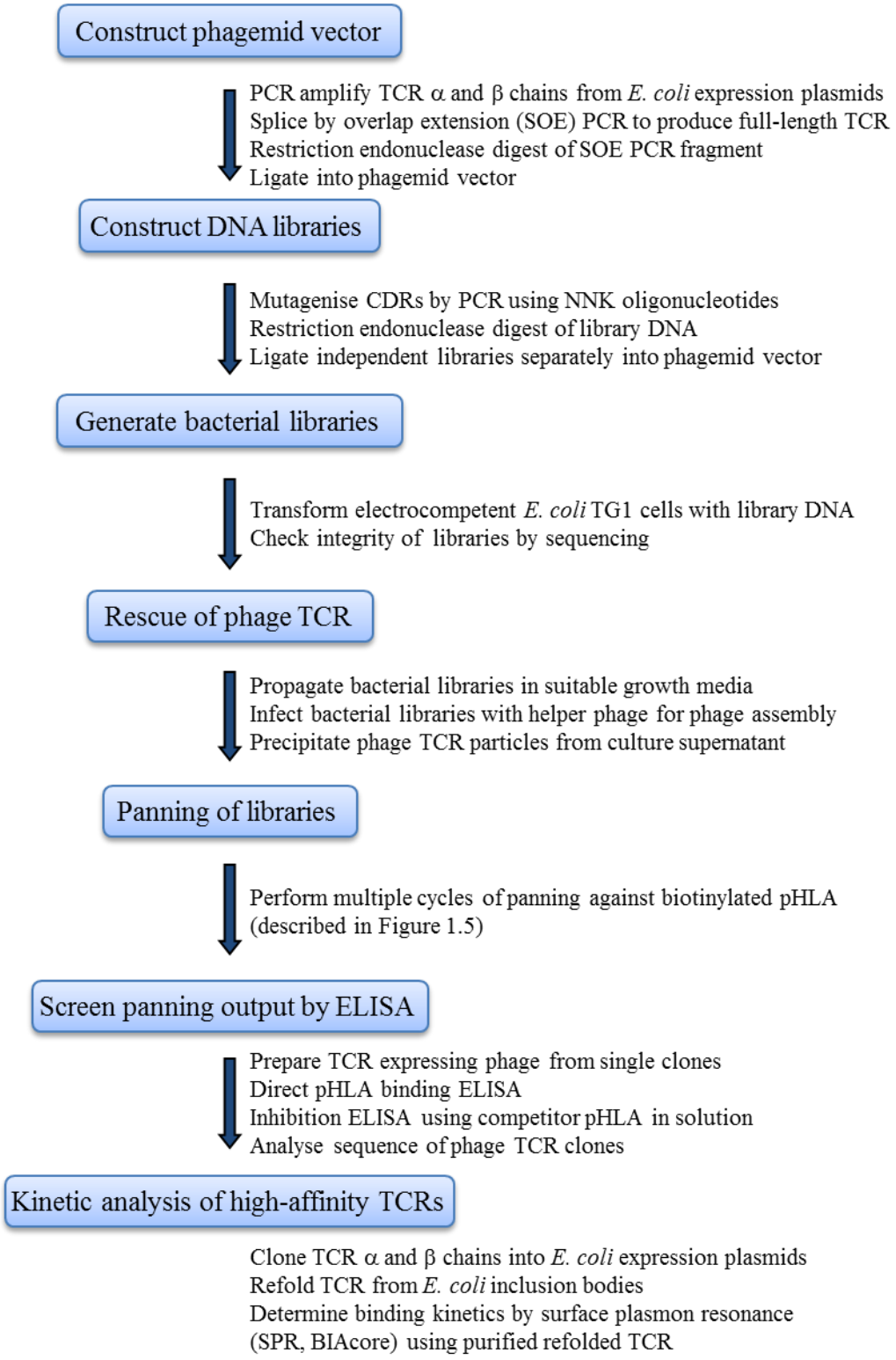

Figure 1.14. Schematic representation of the processes involved in the affinity maturation of TCRs by phage display.

1.14 Aims of the thesis

Peptides presented by HLA Class I complexes represent antigenic barcodes that T-cells scan to distinguish malignant cells from healthy cells and are therefore ideal targets for immunotherapeutic reagents. Although natural T-cell immunity can lead to regression of malignant lesions in a minority of patients, these are in most cases ineffective at clearing the tumour. An effectual anti-tumour T-cell-mediated immune response is hampered in part by the low affinity of TCRs for self-antigens and by the low-level expression of target antigens presented on cancer cells. To harness the inherent antigen recognition property of TCRs for use as potential therapeutic proteins, the principal goal of this thesis was to generate ultra-high affinity TCRs.

The specific aims include:

1. Using phage display to engineer for high affinity TCRs that recognise peptides derived from Melan-A/MART-1_{26-35}, $gp100_{280-288}$ and MAGE-$A3_{168-176}$.
2. Developing a generic and robust phage display process for the targeted mutagenesis and *in vitro* selection of TCRs with improved binding kinetics.
3. Exploring the phage display methodologies to isolate high affinity TCRs, including
    a. The format of the TCR; investigating the effect of the position of the inter-chain constant region cysteines (native versus mTCR).
    b. The number of consecutive CDR residues randomised (5-NNK versus 6-NNK).
    c. The use of subtractive panning of phage libraries on mammalian cells to remove off-target binders and enrich for target-specific binders.

MATERIALS AND METHODS

2.1 Reagents and buffers

2.1.1 Bacterial culture media

Media	Ingredients
Luria Bertani Medium (LB)	Tryptone 10 g/l (Oxoid) Yeast Extract 5 g/l (Sigma) NaCl 10 g/l (Sigma)
Super Optimal Broth (SOB)	Tryptone 20 g/l Yeast Extract 5 g/l NaCl 10 g/l KCl 2.5 mM (Sigma)
TYP Medium	Tryptone 16 g/l Yeast Extract 16 g/l NaCl 5 g/l K_2HPO_4 1 g/l (Sigma)
2xYeast Extract Tryptone Medium (2xYT)	Tryptone 16 g/l Yeast Extract 10 g/l NaCl 5 g/l
LB Agar	LB medium + BactoAgar 16 g/l (Appleton Woods)
YTE Agar	2xYT medium + BactoAgar 16 g/l

2.1.2 Bacterial strains and vectors

Strain	Product details
E. coli XL1-Blue	Agilent Technologies: *RecA endA1 gyrA96 thi-1 hsdR17supE44 relA1 lac (F proAB lacIq^{Z} M15 Tn10 (Tet^{r})*
E. coli TG1	Lucigen: [F´ *traD36 proAB lacIq^{Z} Δ M15*] *supE thi-1 Δ (lac-proAB) Δ (mcrB-hsdSM)5(rK^{-}mK^{-})*
E. coli BL21 (DE3) pLysS	Novagen: F^{-} *omp*T *hsd*S$_B$ (r_B-, m_B-) *dcm gal* λ(DE3) pLysS Cm^{r}
E. coli Rosetta (DE3) pLysS	Novagen: F^{-} *omp*T *hsd*S$_B$ (r_B-, m_B-) *dcm gal* λ(DE3) pLysS RARE2 Cm^{r}

Plasmid	Description
pLitmus28	NEB: pUC19 origin of replication *bla* (Ap^{R}) M13 origin of replication promoter *lacZα*
[ab]pEX922	Wild-type A6 αβ TCR
[ac]pG484	Undisclosed TCR
[ab]pG125	Wild-type Mel-5 TCR
[ab]pG396	Enhanced-affinity Mel-5 TCR clone MELa1
[ab]pG397	Enhanced-affinity Mel-5 TCR clone MELa1c
[ab]pGPb7	Enhanced-affinity gp100 TCR clone GPb7
[ac]pIM160	Wild-type MAGE-A3 TCR (native format)
[ac]pIM194	Enhanced-affinity MAGE-A3 TCR clone MAGEa6a
[ac]pIM195	Enhanced-affinity MAGE-A3 TCR clone MAGEb2a
[ab]pLAS0282	Wild-type MAGE-A3 TCR
pEX954	pGMT7-based vector for T7 driven bacterial expression containing the α chain constant region including the introduced mutant cysteine at position TRAC48 (Boulter, Glick et al. 2003)
pEX821	pGMT7-based vector for T7 driven bacterial expression the β chain constant region including the introduced mutant cysteine at position TRBC57 (Boulter, Glick et al. 2003)
pG190	pEX954-based vector encoding wild-type Mel-5 TCR α chain
pG176	pEX821-based vector encoding wild-type Mel-5 TCR β chain
pG246	pEX954-based vector encoding enhanced-affinity MELa1 Mel-5 TCR α chain

[a]pLitmus28-based phagemid vector; [b]mTCR format; [c]Native format

2.1.3 Buffer compositions: *E. coli* inclusion body preparation and TCR refolds

Buffer	Ingredients
Lysis buffer	EDTA (pH 8) 10 mM (Sigma) Tris-HCl (pH 8.1) 10 mM (Sigma) NaCl 150 mM (Sigma) Glycerol 10% (v/v) (Sigma)
Triton wash buffer	EDTA (pH 8) 10 mM Tris-HCl (pH 8.1) 50 mM NaCl 100 mM Triton X-100 0.5% (v/v) (Sigma)
Resuspension buffer	EDTA (pH 8) 10 mM Tris-HCl (pH 8.1) 50 mM NaCl 100 mM
Guanadine Buffer	Guanadine-HCl 6 M (Apollo Scientific) EDTA (pH 8) 10 mM Tris-HCl (pH 8.1) 50 mM NaCl 100 mM
TCR refold Buffer	Urea 5 M (VWR) Tris (pH 8.1) 100 mM L-arginine HCl 400 mM (Sigma) β-mercaptoethylamine 6.5 mM (Sigma) Cystamine 3.7 mM (Sigma)

2.2 Preparation of phagemid vectors pEX922 and pG484

E. coli TG1 glycerol stocks bearing the phagemid vectors pEX922 (Li, Moysey et al. 2005) (kindly provided by Dr. Y. Li) and pG484 (kindly provided by Dr. R. Webster) were used to inoculate 50 ml 2xYT media (in a sterile 250 ml conical flask) supplemented with 100 μg/ml ampicillin (Fisher Scientific) and 2% (w/v) glucose (media designated 2xYTag) and incubated with shaking at 250 rpm (Innova 4430 incubator) for 16 hours at 37ºC. DNA was isolated from the overnight culture using a QIAprep spin miniprep kit (Qiagen). Overnight cultures were pelleted at 3,360 x g for 10 minutes at room temperature. The pellets were thoroughly respuspended in 400 μl resuspension buffer. Cells were lysed by inverting with 400 μl cell lysis buffer and

neutralised by inverting with 560 μl neutralisation buffer. The cell lysate was centrifuged at 16,200 x g for 10 minutes at room temperature and the supernatant applied to a Qiagen miniprep spin column. Following a 1 minute centrifugation at 16,200 x g at room temperature, the column was washed with 400 μl binding buffer followed by two washes with 750 μl wash buffer. After the second wash step, the columns were re-centrifuged at 16,200 x g for 1 minute at room temperature to remove residual buffer. The DNA was eluted from the column using 50 μl nuclease-free water (Qiagen) into a clean 1.5 ml sterile centifugation tube. The absorbance of the eluted DNA was measured at 260 nm using a Nanodrop ND-1000 spectrophotometer (Thermo Scientific) and the concentration calculated using the Beer-Lambert law.

2.3 Generating phagemid TCR templates

2.3.1 PCR oligonucleotides

The oligonucleotides used to PCR amplify the variable (V) and constant (C) regions specific to the Mel-5 and MAGE-A3 TCRs are listed below. Primers Nat22 and J185 were used to PCR amplify the Mel-5 TRAV12-2 and TRBV30 genes respectively. Primers J135 and J155 were used to PCR amplify the MAGE-A3 TRAV21 and TRBV5-1 genes respectively. The phagemid vector, pGPb7, encoding the first-generation enhanced-affinity gp100 TCR mutant GPb7 was kindly provided by Dr. N. Harewood. High purity salt free (HPSF) oligonucleotides were ordered from Eurofins MWG.

Phagemid molecular cloning primers

Nat22	5’-gcccagccggccatggcccaaaaagaagttgaa-3’
J185	5’-ctattctcacagcgcgcagtctcagactattcatcaatgg-3’
J135	5’-gcccagccggccatggccaaacaggaggtgacgcaga-3’
J155	5’-ctattctcacagcgcgcagaaggctggagtcactcaaac-3’
YOL236	5’-ccgtgtaccagctgagagactc-3’
YOL237	5’-gagtctctcagctggtacacgg-3’
YOL238	5’-gcgcgctgtgagaatagaaag-3’
YOL239	5’-cacacccaaaaggccacact-3’
YOL240	5’-agtgtggccttttgggtgtg-3’
YOL13	5’-tcacacaggaaacagctatg-3’
YOL22	5’-cattttcagggatagcaagc-3’
J195	5’-tccagaagacaccttcttcc-3’
MAGEa6aFwd	5’-ttagtgcgtccgtatcagag-3’
MAGEa6aRev	5’-ctctgatacggacgcactaacagagatgtgag-3’
MAGEb2aFwd	5’-acgttgagaaacaaaggaaacttc-3’
MAGEb2aRev	5’-gtttccttgtttctcaacgtcatatccgtgtattc-3’

2.3.2 PCR of TCR α and β chains

With the exception of the MAGE-A3 TCR α and β chains which were amplified from the cDNA isolated from the MAGE-A3-EB103 T-cell clone (kindly provided by Dr. B. Cameron), the TCR V regions were amplified from *E. coli* expression plasmids containing the TCR α and β chains. The TCR constant regions were amplified from either phagemid vector pEX922 containing TCR αβ chains including the non-native constant domain cysteines at position TRAC threonine 48 and TRBC serine 57 (Boulter, Glick et al. 2003) (engineered mTCR format) or from phagemid vector

pG484 containing TCR αβ chains including the native membrane-proximal cysteines at position TRAC 95 and TRBC 131 and the wild-type residue at positions TRAC 48 and TRBC 57 (native format). Vα PCR fragments were designated fragment A; Vβ PCR fragments were designated fragment B; Cα PCR fragments were designated fragment C; Cβ PCR fragments were designated fragment D. For the Mel-5 TCR the α chain *E. coli* expression vector was pG190 and the β chain *E. coli* expression was pG176 (both vectors kindly provided by E. Gostick). In addition to wild-type α and β chains, several affinity enhanced α and β chains were cloned into the phagemid vector. The Mel-5 TCR Vα region (fragment A) encoding the enhanced-affinity CDR3α clone MELa1c was amplified from *E. coli* expression vector pG246 (Section 2.6.3). MAGE-A3 TCR Vα (MAGEa6a) and Vβ (MAGEb2a) mutations were introduced into the wild-type MAGE-A3 TCR using two pairs of complimentary primers to generate fragments E and F and will be described separately. All phagemid-TCR vectors were constructed with the mTCR constant regions with the exception of the MAGE-A3 TCR-phagemids which were prepared with both mTCR and native constant regions. All reactions were performed in sterile PCR tubes. The reaction components and volumes for the amplification of the TCR Vα and Cα domains were as follows: Fragment A (TCR Vα): 1 μl [a]DNA, 1 μl dNTP mix (10 mM each; NEB), 1 μl [b]Vα forward primer (10 pmol/μl), 1 μl YOL237 (10 pmol/μl), 5 μl 10 X Polymerase buffer (Roche), 3.5 U Expand DNA polymerase (Roche) in a final volume of 50 μl. Fragment B (TCR Vβ): 1 μl [c]DNA, 1 μl dNTP mix (10 mM each), 1 μl [d]Vβ forward primer (10 pmol/μl), 1 μl YOL240 (10 pmol/μl), 5 μl 10 X Polymerase buffer, 3.5 U Expand DNA polymerase in a final volume of 50 μl. Fragment C (TCR Cα): 5 ng [e]DNA, 1 μl dNTP mix (10 mM each), 1 μl YOL236 (10

pmol/μl), 1 μl YOL238 (10 pmol/μl), 5 μl 10 X Polymerase buffer, 3.5 U Expand DNA polymerase in a final volume of 50 μl. Fragment D (TCR Cβ): 5 ng [f]DNA, 1 μl dNTP mix (10 mM each), 1 μl YOL239 (10 pmol/μl), 1 μl YOL22 (10 pmol/μl), 5 μl 10 X Polymerase buffer, 3.5 U Expand DNA polymerase in a final volume of 50 μl.

[a]TCR Vα templates were: *E. coli* expression plasmid pG190 for the wild-type Mel-5 α chain; *E. coli* expression plasmid pG246 for the MELa1c CDR3α enhanced-affinity clone; cDNA isolated from the MAGE-A3-EB103 T-cell clone for the wild-type MAGE-A3 α chain; [b]TCR Vα specific forward primers were: Nat22 for the Mel-5 TCR; J135 for the MAGE-A3 TCR; [c]TCR Vβ templates were: *E. coli* expression plasmid pG176 for the Mel-5 β chain; cDNA isolated from the MAGE-A3-EB103 T-cell clone for the wild-type MAGE-A3 β chain; [d]TCR Vβ specific forward primers were: J185 for the Mel-5 TCR; J155 for the MAGE-A3 TCR; [e]TCR Cα templates were: phagemid plasmid pEX922 for the mTCR constant domains; phagemid plasmid pG484 for the native constant domains; [f]TCR Cβ templates were: phagemid plasmid pEX922 for the mTCR constant domains; phagemid plasmid pG484 for the native constant domains; [a,c]*E. coli* expression plasmids were diluted to 5 ng/μl and the T-cell clone was diluted 1:10 in nuclease-free H_2O.

MAGEa6a and MAGEb2a

All reactions were performed in sterile PCR tubes. The reaction components and volumes were as follows: Fragment E: 5 ng pIM160 (Section 2.1.2), 1 μl dNTP mix (10 mM each), 1 μl YOL13 (10 pmol/μl), 1 μl [a]Reverse primer (10 pmol/μl), 10 μl 5 X Phusion Polymerase buffer (NEB), 2 U Phusion DNA polymerase (NEB) in a final volume of 50 μl. Fragment F: 5 ng pIM160, 1 μl dNTP mix (10 mM each), 1 μl [b]Forward primer (10 pmol/μl), 1 μl YOL22 (10 pmol/μl), 10 μl 5 X Phusion Polymerase buffer, 2 U Phusion DNA polymerase in a final volume of 50 μl.

[a]Reverse primer either MAGEa6aRev or MAGEb2aRev; [b]Forward primer either MAGEa6aFwd or MAGEb2aFwd.

The PCR conditions to amplify the TCR fragments (A-F) were as follows using a Biometra PCR thermocycler: Step 1: 94ºC for 2 min; Step 2: 94ºC for 16 sec; Step 3: 53ºC for 16 sec; Step 4: 72ºC for 50 sec/kbp (Expand; Roche) or 25 sec/kbp (Phusion; NEB); Step 5: 4ºC pause. Step 2 to 4 repeated 26 times.

2.3.3 Purification of TCR variable and constant domains for cloning into the phagemid vector

PCR amplified TCR gene fragments were resolved on a 1.5% (w/v) agarose (Bio-Rad) gel containing 2.5 μl ethidium bromide (Sigma) in 50 ml agarose gel. DNA bands of the expected size were excised from the gel and purified using the Zymoclean DNA gel recovery kit (Zymo Research). The gel slices were weighed and three times the volume of the excised gel slice was added. Following melting of the gel slices at 50ºC using a heating block, each mixture was added to a separate Zymo column. The columns were centrifuged at 16,200 x g for 30 seconds at room temperature and the flow through discarded. The columns were washed with 500 μl wash buffer and centrifuged at 16,200 x g for 30 seconds at room temperature. The washing step was repeated with 250 μl wash buffer and the columns were centrifuged at 16,200 x g for 30 seconds at room temperature. After the second wash step, the columns were centrifuged at 16,200 x g for 1 minute at room temperature to remove residual buffer. The DNA was eluted from the column using 15 μl nuclease-free water into a clean 1.5 ml sterile centrifugation tube. The concentration of the eluted DNA was determined using a Nanodrop ND-1000 spectrophotometer.

2.3.4 Generating full-length αβ TCR constructs using splice by overlap extension PCR (SOE-PCR) for cloning into phagemid vector

The DNA fragments (A, B, C and D or E and F) were assembled using SOE-PCR to generate a 1700-1800 bp fragment. The primers for the ABCD SOE-PCR were the TCR Vα specific forward primer (used to generate fragment A) and YOL22 and for the EF SOE-PCR were primers YOL13 and YOL22. The fragments were diluted to give an equimolar ratio in a 1 μl volume of each. Fragment A/B/C/D: 2-6 ng each of fragments A, B, C and D, 1 μl dNTPs (10 mM each), 1 μl ^{a}Vα forward primer (10

pmol/μl), 1 μl YOL22 (10 pmol/μl), 5 μl 10 X polymerase buffer, 3.5 U Expand polymerase in a final volume of 50 μl.

[a]TCR Vα specific forward primers were: Nat22 for the Mel-5 TCR and J135 for the MAGE-A3 TCR.

Fragment E/F: 2 ng each of fragments E and F, 1 μl dNTPs (10 mM each), 1 μl YOL13 (10 pmol/μl), 1 μl YOL22 (10 pmol/μl), 10 μl 5 X polymerase buffer, 1 U Phusion polymerase in a final volume of 50 μl. The cycling parameters are outlined in Section 2.3.2 except with an extension time of 80 seconds (A/B/C/D) or 45 seconds (E/F) and repeating steps 2 to 4 thirty times. The amplified SOE-PCR 1700-1800 bp product was resolved on a 1% (w/v) agarose gel and gel-purified using the Zymoclean DNA gel recovery kit. DNA was eluted using 15-20 μl nuclease-free water.

2.3.5 Restriction digests of the SOE-PCR product and pEX922 and ligation into phagemid vector

The SOE-PCR fragment and phagemid vector pEX922 were mixed with 10 U each of the restriction enzymes *Nco*I and *Not*I (NEB) and buffer according the manufacturer's recommendations in a final volume of 40-50 μl and incubated at 37ºC for 3 hours. Following incubation at 37ºC, the digested DNA fragments were resolved on a 1% (w/v) agarose gel. Bands of the expected size were excised from the gel and purified using the Zymoclean DNA gel recovery kit. The concentration of the eluted DNA was determined using a Nanodrop ND-1000 spectrophotometer. The purified SOE-PCR product was ligated (using the Rapid ligation kit; Roche) into the purified phagemid vector pEX922 using a molar ratio of 3:1 (insert to vector) following conditions: typically, 40 ng pEX922, 40 ng SOE-PCR fragment, 1 μl DNA Dilution Buffer 5 X, 5 μl DNA Ligation Buffer 2 X, 5 U T4 DNA ligase in a final volume of 10 μl.

Following incubation at room temperature for 10 minutes, residual salt was removed from the ligation mixture using the DNA clean and concentrator kit (Zymo research). The ligation mixture was mixed with 100 µl DNA binding buffer and added to a Zymo spin column. The columns were centrifuged at 16,200 g for 30 seconds at room temperature and the flow through discarded. The columns were washed with 500 µl wash buffer and centrifuged at 16,200 x g for 30 seconds at room temperature. The washing step was repeated with 250 µl wash buffer and the columns were centrifuged at 16,200 x g for 30 seconds at room temperature. After the second wash step, the columns were centrifuged at 16,200 x g for 1 minute at room temperature to remove residual buffer. The DNA was eluted from the column using 12 µl nuclease-free water into a clean 1.5 ml sterile centrifugation tube.

2.3.6 Preparation of electrocompetent *E. coli* TG1 cells

A 40 ml volume of LB medium was inoculated with a single *E. coli* TG1 colony picked from a freshly streaked minimal salt agar plate and grown overnight at 37ºC at 250 rpm. From the overnight starter culture, 12 ml was used to inoculate 800 ml LB medium (in a 2 litre flask). The culture was incubated at 37ºC at 250 rpm until the optical density (OD_{600}) reached 0.2; at which point the culture was transferred to an incubator set at 18ºC and grown for a further 1 hour with shaking (250 rpm). Incubation at 18ºC continued until the OD_{600} reached 0.7. The conical flasks were then chilled on ice for 30 minutes with gentle swirling. The culture was then split between two 500 ml centrifuge bottles and centrifuged at 3,360 g for 20 minutes at 4ºC. The supernatant was discarded and the pellets were resuspended (by gentle agitation) in 50 ml ice-cold sterile molecular grade water. Once the cells were resuspended, the volume was increased to 400 ml (the original culture volume) ice-

cold sterile molecular grade water. The samples were centrifuged at 3,360 x g for 20 minutes at 4ºC. The supernatant was discarded and the pellets were resuspended (by gentle agitation) in 50 ml ice-cold sterile molecular grade water. Once the cells were resuspended, the volume was increased to 400 ml (the original culture volume) ice-cold sterile molecular grade water. The samples were centrifuged at 3,360 x g for 20 minutes at 4ºC. The supernatant was discarded and each pellet was resuspended in 40 ml ($1/10^{th}$ the original volume) ice-cold filter-sterilised 10% (v/v) glycerol (Sigma) solution. The cell suspension (80 ml volume) was transferred to four sterile 50 ml centrifuge tubes and centrifuged at 3,360 x g for 20 minutes at 4ºC. The supernatant was discarded and each pellet was resuspended in 0.5 ml ice-cold filter-sterilised 10% (v/v) glycerol solution (2 ml final volume). Following 20 minutes incubation on ice, the cells were transferred to sterile 1.5 ml centrifugation tubes, flash frozen in liquid nitrogen and stored at -80ºC.

2.3.7 Electroporation of *E. coli* TG1 cells with a TCR-containing phagemid vector

Electrocompetent *E. coli* TG1 cells were transformed with the purified ligation reaction (Section 2.3.5) using a MicroPulser electroporation system (Bio-Rad). The *E. coli* TG1 cells were thawed on ice and 40 μl was transferred to a sterile 1.5 ml centrifugation tube containing 2.5-3 μl of the purified ligation mixture. After gentle mixing with a pipette tip, the *E. coli* TG1 cell/DNA mixture was transferred into a chilled electroporation cuvette without introducing bubbles. The electroporation cuvette was gently tapped to deposit the cells across the bottom of the chamber and then placed in the ShockPod (Bio-Rad) and the lid closed. A 1.8 kV pulse was passed through the cell suspension and 0.96 ml of prewarmed (37ºC) SOC media (Sigma) was used to collect the contents of the chamber into a sterile 50 ml centrifugation

tube. The transformed cells were incubated at 37ºC at 250 rpm for 1 hour. Using a sterile inoculation loop the transformed *E. coli* TG1 cells were streaked onto an YTE agar plate supplemented with 100 μg/ml ampicillin and 2% glucose (w/v) to obtain single colonies. The plate was incubated at 30ºC overnight.

2.3.8 Colony PCR screen of *E. coli* TG1 cells transformed with a TCR-containing phagemid vector

A total of 8 colonies were screened. Five ml 2xYTag media was inoculated with a single ampicillin-resistant *E. coli* TG1 colony and incubated at 37ºC at 250 rpm until the culture was visibly cloudy. At this point, 1 μl of each was screened by colony PCR with primers YOL13 and YOL22. The cultures were incubated at 37ºC at 250 rpm until reaching the desired cell density (OD_{600} ~0.8). Bacterial stocks were prepared for each of the 8 cultures by mixing in a sterile 1.5 ml centrifugation tube 0.6 ml of culture with 0.4 ml 50% glycerol-supplemented media; 20% (v/v) glycerol final. Tubes were snap frozen on dry-ice and stored at -80ºC. The PCR mixture for each colony was assembled as follows: 1 μl *E. coli* culture (or *E. coli* colony), 1 μl dNTP mix (10 mM each), 1 μl YOL13 (10 pmol/μl), 1 μl YOL22 (10 pmol/μl), 5 μl 10 X Polymerase buffer (NEB), 2.5 U Taq DNA polymerase (NEB) in a final volume of 50 μl. The cycling parameters are outlined in Section 2.3.2 with an extension time of 120 seconds and repeating steps 2 to 4 thirty times. The PCR products were purified using the DNA clean and concentrator kit. DNA was eluted in 30 μl of nuclease-free water and purified DNA sequenced with primers YOL13, YOL22 and J195 using the Sanger sequencing method (GATC Biotech).

2.4 Construction of TCR phage display libraries

Phagemid vector DNA (listed in Section 2.3.1) was isolated from the *E. coli* TG1 bacterial stock of a sequence verified phagemid vector-TCR clone (Section 2.3.8). 20 ml of 2xYTag media was inoculated with 5 µl of the *E. coli* TG1 bacterial stock and incubated at 26ºC overnight at 250 rpm. DNA was isolated from the overnight culture using a QIAprep spin miniprep kit (Qiagen). The eluate was re-purified using the DNA clean and concentrator kit (Zymo research). The concentration of the eluted DNA was determined using a Nanodrop ND-1000 spectrophotometer. As a modification to the Mel-5 TCR library construction, phagemid vector templates, pGPb7 (gp100 TCR) and pIM160, pIM194, pIM195 and pLAS0282 (MAGE-A3 TCR) were linearised separately with *Nco*I and *Not*I. Restriction digests were typically performed using ~1.5 µg DNA, 25 U of the required enzyme and buffer in accordance with manufacturer's guidelines (NEB) in a final volume of 20 µl. Digestions were incubated at 37 °C for 2-4 hours. After incubation DNA was resolved on a 1% (w/v) agarose gel and bands of the predicted size were purified using the Zymoclean DNA gel recovery kit. The concentration of the eluted DNA was determined using a Nanodrop ND-1000 spectrophotometer.

2.4.1 Mel-5 TCR phage display libraries

Mutagenised Mel-5 TCR libraries were constructed in which the DNA encoding the CDRs was mutated with degenerative 4- or 5-NNK oligonucleotides (where N = 25% mix each of nucleotides A, C, G and T; K = 50% mix each of nucleotides G or T). High purity salt free (HPSF) oligonucleotides were ordered from Eurofins MWG. First-generation libraries were built in the context of the wild-type Mel-5 TCR framework and all 6 CDRs were targeted. Second-generation libraries were constructed in the context of two enhanced-affinity CDR3α frameworks (MELa1 and

MELa1c) and only CDR1α, CDR2α, CDR2β and CDR3β regions were mutated. The methods used to identify the enhanced-affinity templates (MELa1 and MELa1c) will be described in Section 2.6.3. This section will focus on phage display library construction. The primers are shown below and the PCR strategies employed for the first and second-generation library construction are depicted in Figure 2.1 and Figure 2.2.

Mel-5 TCR library primers

Nat1	5'-gtcactgtaagtgcagttgag-3'
Nat2	5'-aactgcacttacagtgacNNKNNKNNKNNKTccttcttctggtacagacaa-3'
Nat3	5'-tccttcttctggtacagacaatat-3'
Nat4	5'-gaacattatcaactcagggca-3'
Nat5	5'-cctgagttgataatgttcNNKNNKNNKNNKggtgacaaagaagatgg-3'
Nat6	5'-ggtgacaaagaagatggaaggttt-3'
Nat29	5'-agccacctacctctgtNNKNNKNNKNNKNNKggcaaatcaacctttg-3'
Nat30	5'-cacctacctctgtgccNNKNNKNNKNNKNNKaaatcaacctttgggg-3'
Nat31	5'-cctctgtgccgtgaacNNKNNKNNKNNKNNKacctttggggatggga-3'
Nat32	5'-ctgtgccgtgaacgttNNKNNKNNKNNKNNKtttggggatgggacta-3'
Nat37	5'-acagaggtaggtggctgaatc-3'
Nat38	5'-ggcaaatcaacctttggggat-3'
Nat39	5'-ggcacagaggtaggtggctga-3'
Nat40	5'-aaatcaacctttggggatggg-3'
Nat41	5'-gttcacggcacagaggtaggt-3'
Nat42	5'-acctttggggatgggactacg-3'
Nat43	5'-aacgttcacggcacagaggta-3'
Nat44	5'-tttggggatgggactacgctc-3'

Nat23	5’-tccctccacagtgcactccagaga-3’
Nat24	5’-tgcactgtggagggaNNKNNKNNKNNKaacctatactggtaccga-3’
Nat25	5’-aacctatactggtaccgacaggct-3’
Nat26	5’-ggagtagaagagcagctggaggcc-3’
Nat27	5’-ctgctcttctactccNNKNNKNNKNNKcagatcagctctgaggtg-3’
Nat28	5’-cagatcagctctgaggtgccccag-3’
Nat33	5’-tggcttctatctctgtNNKNNKNNKNNKNNKgggttaggcaccgggg-3’
Nat34	5’-ctatctctgtgcctggNNKNNKNNKNNKNNKggcaccggggagctgt-3’
Nat35	5’-ctgtgcctggtccgagNNKNNKNNKNNKNNKggggagctgttttttg-3’
Nat36	5’-gtccgagacagggttaNNKNNKNNKNNKNNKttttttggagaaggct-3’
Nat45	5’-acagagatagaagccagagtc-3’
Nat46	5’-gggttaggcaccggggagctg-3’
Nat47	5’-ccaggcacagagatagaagcc-3’
Nat48	5’-ggcaccggggagctgtttttt-3’
Nat49	5’-ctcggaccaggcacagagata-3’
Nat50	5’-ggggagctgtttttggagaa-3’
Nat51	5’-taaccctgtctcggaccaggc-3’
Nat52	5’-ttttttggagaaggctctagg-3’
Nat209	5’-actgtaagtgcagttgagaga-3’
Nat212	5’-caactgcacttacagtNNKNNKNNKNNKcagtccttcttctggt-3’
Nat215	5’-cagtccttcttctggtacaga-3’
Nat227	5’-ggagtgcactgtggagNNKNNKNNKNNKcccaacctatactggt-3’
Nat224	5’-ctccacagtgcactccagaga-3’
Nat230	5’-cccaacctatactggtaccga-3’
Nat239	5’-tgcctggtccgagacaNNKNNKNNKNNKNNKgagctgtttttggag-3’

Nat242	5’-tgtctcggaccaggcacagag-3’
Nat245	5’-gagctgtttttggagaaggc-3’
Nat241	5’-cgagacagggttaggcNNKNNKNNKNNKNNKtttggagaaggctcta-3’
Nat244	5’-gcctaaccctgtctcggacca-3’
Nat247	5’-tttggagaaggctctaggctg-3’

2.4.1.1 Generating ‘black’ and ‘red’ library PCR fragments

First-generation library PCRs used phagemid vector pG125 (wild-type Mel-5 TCR) as the template. Second-generation α chain library PCRs used either phagemid vector pG396 (MEla1) or pG397 (MELa1c) as template. Second-generation β chain library PCRs used phagemid vector pG125 as template. All reactions were performed in sterile PCR tubes. The reaction components and volumes for the amplification of the Mel-5 TCR alpha and beta ‘black’ and ‘red’ PCR fragments (Figure 2.1 and Figure 2.2) are shown below.

A.

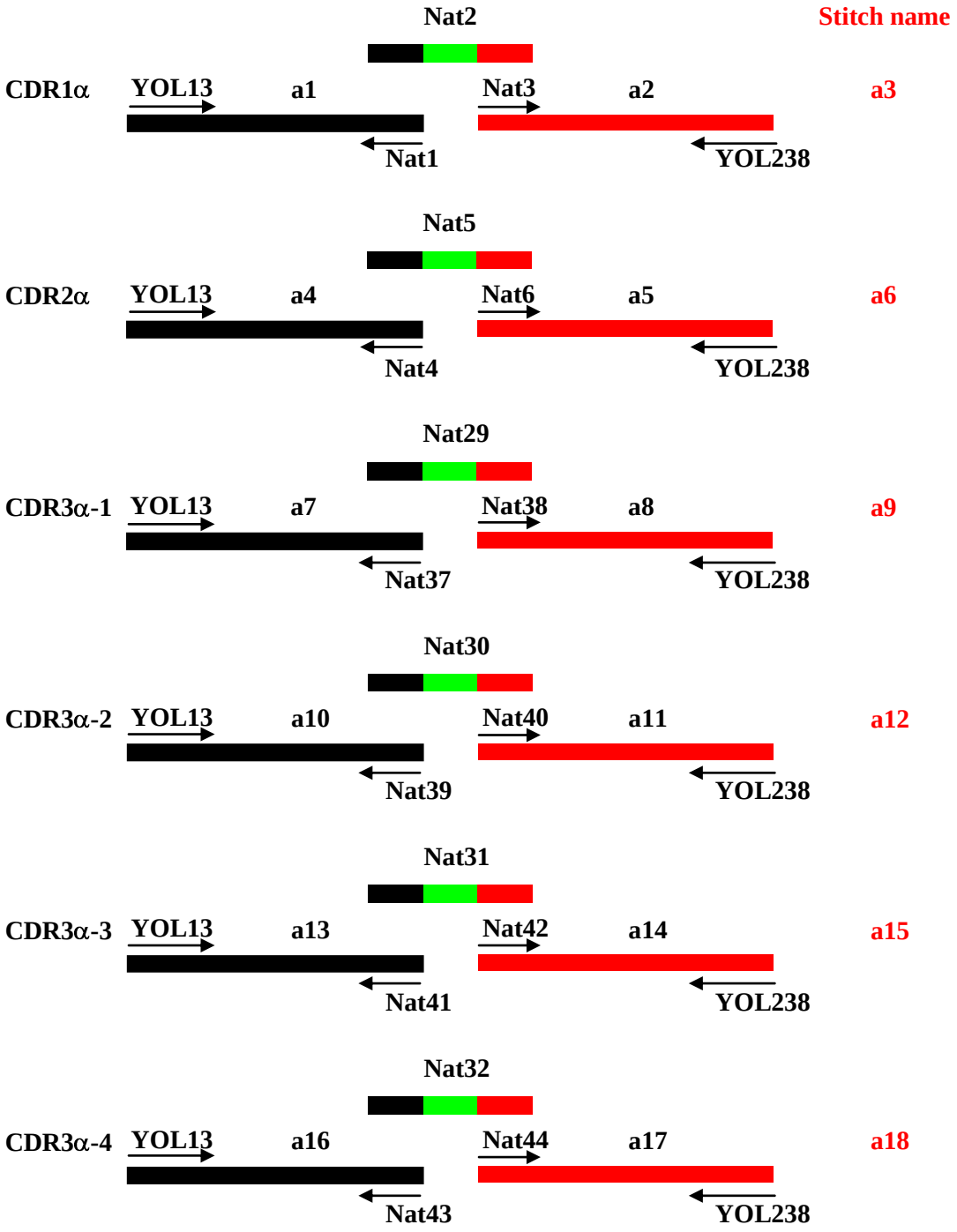
Nat2
Stitch name
CDR1α
YOL13
a1
Nat3
a2
a3
Nat1
YOL238
Nat5
CDR2α
YOL13
a4
Nat6
a5
a6
Nat4
YOL238
Nat29
CDR3α-1
YOL13
a7
Nat38
a8
a9
Nat37
YOL238
Nat30
CDR3α-2
YOL13
a10
Nat40
a11
a12
Nat39
YOL238
Nat31
CDR3α-3
YOL13
a13
Nat42
a14
a15
Nat41
YOL238
Nat32
CDR3α-4
YOL13
a16
Nat44
a17
a18
Nat43
YOL238

B.

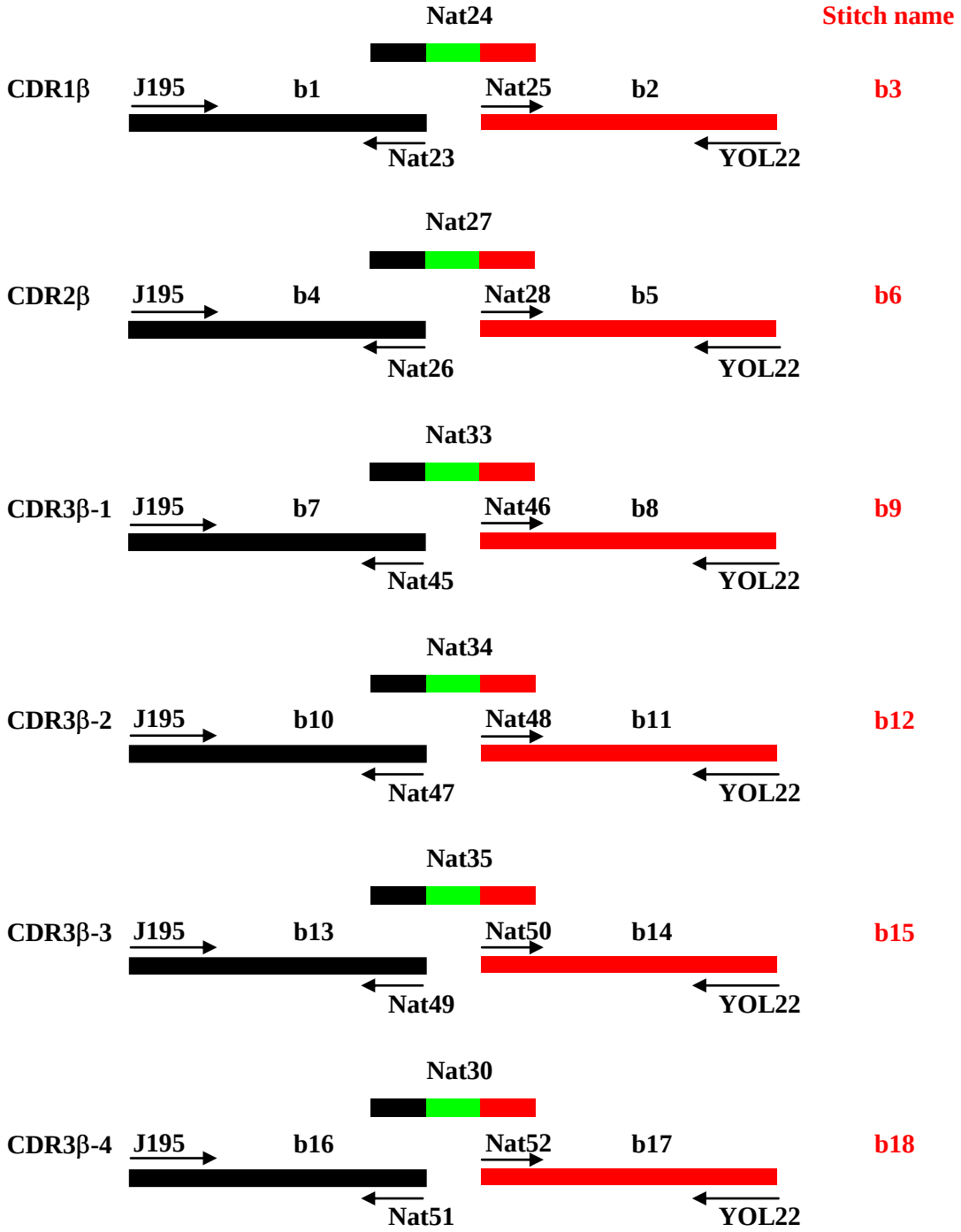

Figure 2.1. Schematic representation of the strategy for constructing first-generation mutagenised Mel-5 TCR fragments. (A). α chain library. **(B).** β chain library. Two PCR fragments are generated for each CDR library (a black and a red fragment). The two fragments are assembled by addition of an NNK oligonucleotide (bright green corresponds to the mutagenised NNK region; black and red sections will anneal to the corresponding coloured fragments) and amplification with the external primers. The α chain fragments are named: a1, a2, a4, a5, a7, a8, a10, a11, a13, a14, a16 and a17. The β chain fragments are named: b1, b2, b4, b5, b7, b8, b10, b11, b13, b14, b16 and b17. α chain SOE-PCR fragments are named: a3, a6, a9, a12, a15 and a18. β chain SOE-PCR fragments are named: b3, b6, b9, b12, b15 and b18.

A.

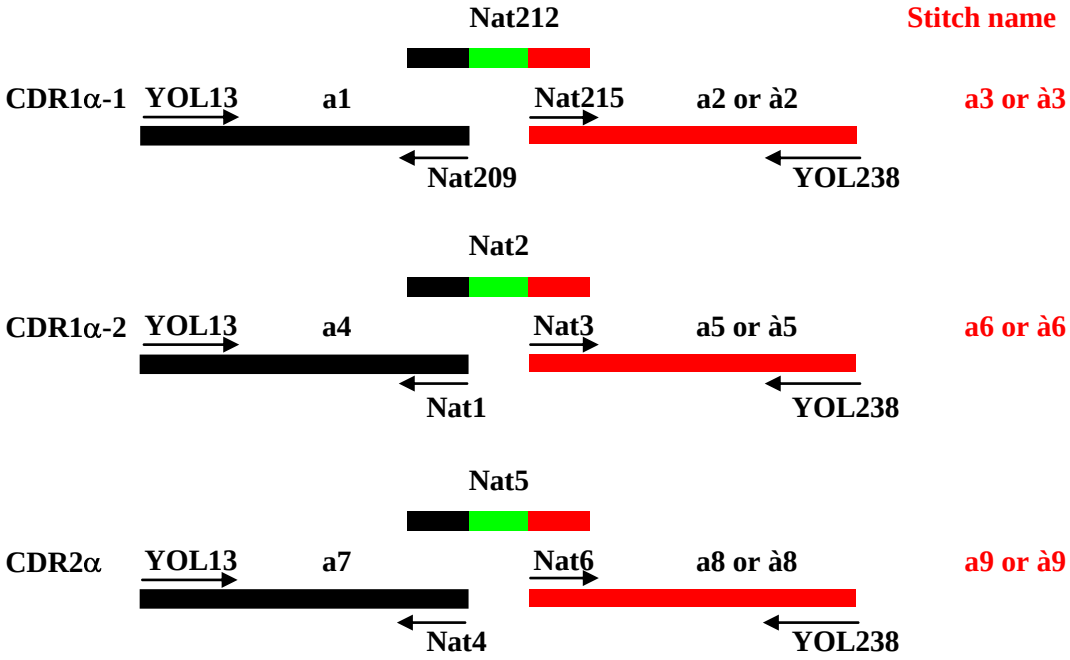
Nat212
Stitch name
CDR1α-1
YOL13
a1
Nat215
a2 or à2
a3 or à3
Nat209
YOL238
Nat2
CDR1α-2
YOL13
a4
Nat3
a5 or à5
a6 or à6
Nat1
YOL238
Nat5
CDR2α
YOL13
a7
Nat6
a8 or à8
a9 or à9
Nat4
YOL238

B.

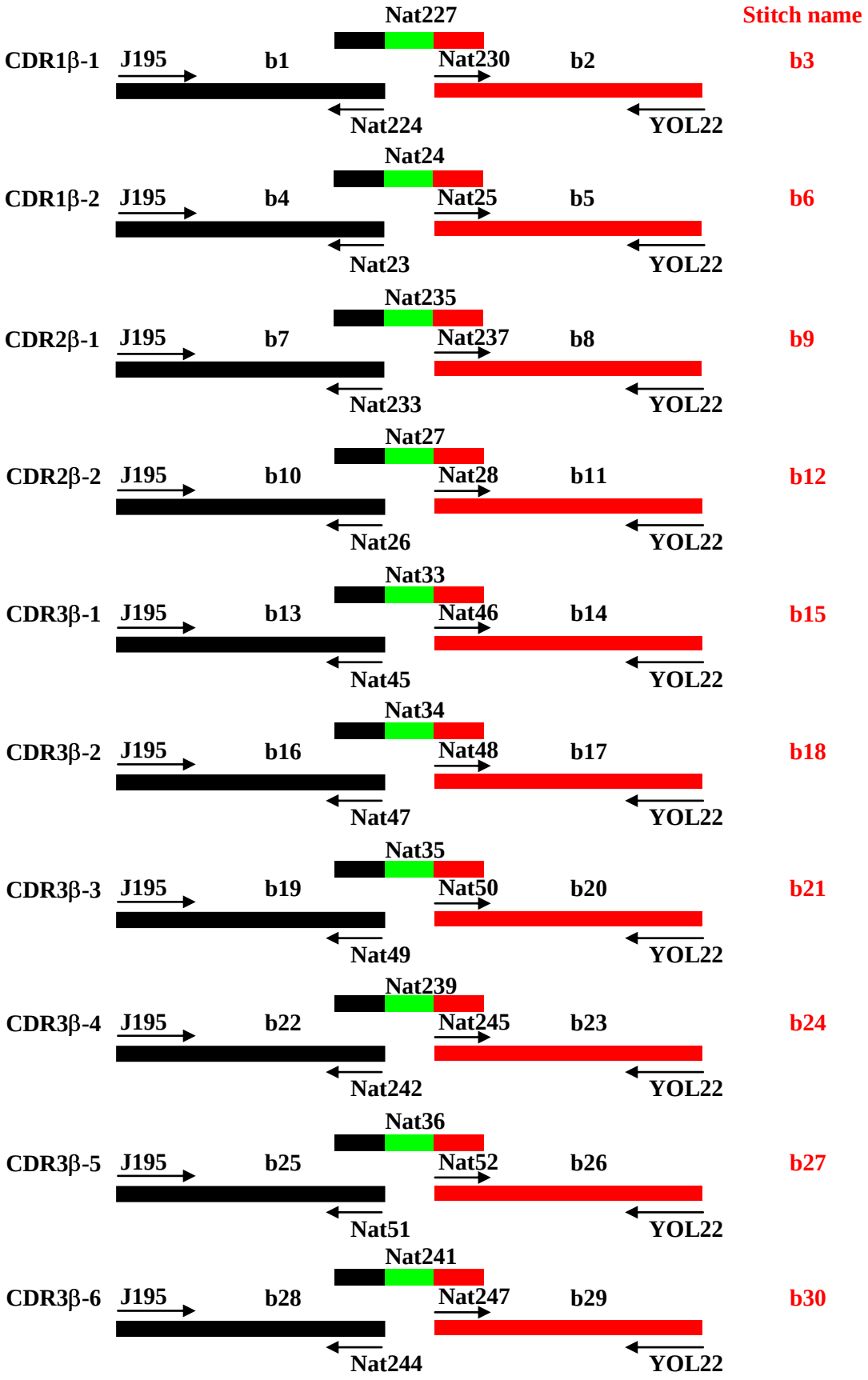
Stitch name
CDR1β-1
J195
b1
Nat227
Nat230
b2
b3
Nat224
YOL22
CDR1β-2
J195
b4
Nat24
Nat25
b5
b6
Nat23
YOL22
CDR2β-1
J195
b7
Nat235
Nat237
b8
b9
Nat233
YOL22
CDR2β-2
J195
b10
Nat27
Nat28
b11
b12
Nat26
YOL22
CDR3β-1
J195
b13
Nat33
Nat46
b14
b15
Nat45
YOL22
CDR3β-2
J195
b16
Nat34
Nat48
b17
b18
Nat47
YOL22
CDR3β-3
J195
b19
Nat35
Nat50
b20
b21
Nat49
YOL22
CDR3β-4
J195
b22
Nat239
Nat245
b23
b24
Nat242
YOL22
CDR3β-5
J195
b25
Nat36
Nat52
b26
b27
Nat51
YOL22
CDR3β-6
J195
b28
Nat241
Nat247
b29
b30
Nat244
YOL22

Figure 2.2. Schematic representation of the strategy for constructing second-generation mutagenised Mel-5 TCR fragments by overlapping PCR. (A). α chain library schematic. **(B).** β chain library schematic. Two PCR fragments were generated for each CDR library (a black and a red fragment). The two fragments were assembled by addition of an NNK oligonucleotide and amplified with the external primers. The α chain fragments are named: a1, a2 or à2, a4, a5 or à5, a7, a8 or à8. Fragments generated using pG396 (MELa1) as template are shown as "a" and fragments generated using pG397 (MELa1c) as template are shown as "à". The β chain fragments are named: b1, b2, b4, b5, b7, b8, b10, b11, b13, b14, b16, b17, b19, b20, b22, b23, b25, b26, b28 and b29. α chain SOE-PCR fragments are named: a3, a6 and a9. β chain SOE-PCR fragments are named: b3, b6, b9, b12, b15, b18, b21, b24, b27 and b30.

Alpha chain 'black' PCR fragments:

Component	Volume
[a]Phagemid vector ~2 ng/μl	1 μl
dNTP mix (10 mM each)	1 μl
YOL13 (10 pmol/μl)	1 μl
[b]Nat Rev primer (10 pmol/μl)	1 μl
10 X Polymerase buffer	5 μl
Expand DNA polymerase	1 μl
Nuclease-free H_2O	40 μl
	50 μl

[a]First-generation libraries: pG125; second-generation α chain libraries: pG396 or pG397; [b]First-generation libraries: Nat Rev primer refers to the following primers (Figure 2.1A): Nat1, Nat4, Nat37, Nat39, Nat41 and Nat43; [b]Second-generation libraries: Nat Rev primer refers to the following primers (Figure 2.2A): Nat209, Nat1, Nat4.

Alpha chain 'red' PCR fragments:

Component	Volume
[a]Phagemid vector ~2 ng/μl	1 μl
dNTP mix (10 mM each)	1 μl
[b]Nat Fwd primer (10 pmol/μl)	1 μl
YOL238 (10 pmol/μl)	1 μl
10 X Polymerase buffer	5 μl
Expand DNA polymerase	1 μl
Nuclease-free H_2O	40 μl
	50 μl

[a]First-generation libraries: pG125; second-generation α chain libraries: pG396 or pG397; [b]First-generation libraries: Nat Fwd primer refers to the following primers (Figure 2.1A): Nat3, Nat6, Nat36, Nat40, Nat42 and Nat44; [b]Second-generation libraries: Nat Fwd primer refers to the following primers (Figure 2.2A): Nat215, Nat3, Nat6.

Beta chain 'black' PCR fragments:

Component	Volume
[a]Phagemid vector ~2 ng/μl	1 μl
dNTP mix (10 mM each)	1 μl
J195 (10 pmol/μl)	1 μl
[b]Nat Rev primer (10 pmol/μl)	1 μl
10 X Polymerase buffer	5 μl
Expand DNA polymerase	1 μl
Nuclease-free H_2O	40 μl
	50 μl

[a]First and second-generation libraries: pG125; second-generation β chain libraries: pG125; [b]First-generation libraries: Nat Rev primer refers to the following primers (Figure 2.1B): Nat23, Nat26, Nat45, Nat47, Nat49 and Nat51; [b]Second-generation libraries: Nat Rev primer refers to the following primers (Figure 2.2B): Nat224, Nat23, Nat233, Nat26, Nat45, Nat47, Nat49, Nat242, Nat51, and Nat244.

Beta chain 'red' PCR fragments:

Component	Volume
[a]Phagemid vector ~2 ng/μl	1 μl
dNTP mix (10 mM each)	1 μl
[b]Nat Fwd (10 pmol/μl)	1 μl
YOL22 (10 pmol/μl)	1 μl
10 X Polymerase buffer	5 μl
Expand DNA polymerase	1 μl
Nuclease-free H_2O	40 μl
	50 μl

[a]First-generation libraries: pG125; second-generation β chain libraries: pG125; [b]First-generation libraries: Nat Fwd primer refers to the following primers (Figure 2.1B): Nat25, Nat28, Nat46, Nat48,

Nat50 and Nat52; [b]Second-generation libraries: Nat Fwd primer refers to the following primers (Figure 2.2B): Nat230, Nat25, Nat237, Nat28, Nat46, Nat48, Nat50, Nat245, Nat52 and Nat247.

PCR extension times were adjusted according to the expected size based on the manufacturer's (Roche) recommended extension times. The reactions were performed using the following PCR cycling conditions: Step 1: 94ºC for 2 min; Step 2: 94ºC for 16 sec; Step 3: 55ºC for 16 sec; Step 4: 72ºC for 40 sec/kbp; Step 5: 4ºC pause. Step 2 to 4 repeated 25 times.

Following PCR cycling, 20 U of *Dpn*I (NEB) endonuclease were added to each PCR tube, mixed by gentle pipetting and incubated at 37ºC for 2 hours using a Biometra PCR thermocycler. PCR amplified Mel-5 TCR 'black' and 'red' alpha and beta fragments were resolved on a 1.6% (w/v) agarose gel. DNA bands of the expected size were excised from the gel and purified using the Zymoclean DNA gel recovery kit. The DNA was eluted from the column using 10-30 μl nuclease-free water into a clean 1.5 ml sterile centrifugation tube. The concentration of the eluted DNA was determined using a Nanodrop ND-1000 spectrophotometer. Additionally, to assess purity of the excised bands 1 μl of each was resolved on a 1-1.5% (w/v) agarose gel.

2.4.1.2 Generating full-length Mel-5 TCR α and β chain library PCR fragments

Full-length α and β chain library PCR fragments were assembled by SOE-PCR using the mutagenic NNK oligonucleotides (Section 2.3.1) to join the 'black' and the 'red' PCR fragments and amplification with primers YOL13 and YOL238 for the α chain fragments and J195 and YOL22 for the β chain fragments. In addition, control PCRs were set up, identical except for the omission of the linking NNK primer. 'Black' and 'red' purified PCR fragments were diluted to a concentration so that 1 μl of each

would give a 1:1 molar ratio in a total of 10-12 ng DNA. The reaction components and volumes for the amplification of the full-length Mel-5 TCR α and β PCR fragments were as follows (note that the components of the control PCRs are not provided). Alpha chain: 1 μl each of 'black' and 'red' fragments, 1 μl dNTPs (10 mM each), 1 μl YOL13 (10 pmol/μl), 1 μl YOL238 (10 pmol/μl), 1 μl [a]NNK oligonucleotide (1 pmol/μl), 5 μl 10 X polymerase buffer, 3.5 U Expand polymerase in a final volume of 50 μl. Beta chain: 1 μl each of 'black' and 'red' fragments, 1 μl dNTPs (10 mM each), 1 μl J195 (10 pmol/μl), 1 μl YOL22 (10 pmol/μl), 1 μl [a]NNK oligonucleotide (1 pmol/μl), 5 μl 10 X polymerase buffer, 3.5 U Expand polymerase in a final volume of 50 μl.

[a]The nomenclature of the NNK oligonucleotides are shown in Figure 2.1 and Figure 2.2.

The reactions were performed using the PCR cycling conditions outlined in Section 2.4.1.1 using an extension time of 80 seconds and repeating steps 2 to 4 thirty times. After successful amplification, the full-length mutagenised Mel-5 TCR α and β chain fragments were resolved on a 1% (w/v) agarose gel and DNA bands of the expected size were excised from the gel and purified using the Zymoclean DNA gel recovery kit. The DNA was eluted from the column using 20-50 μl nuclease-free water. The concentration of the eluted DNA was determined using a Nanodrop ND-1000 spectrophotometer. To assess purity of the excised bands 1 μl of each was resolved on a 1.4% (w/v) agarose gel.

2.4.1.3 Restriction digests of the Mel-5 TCR SOE-PCR products and pG125

First-generation libraries were cloned into pG125 as *Sfi*I fragments for the α chains and as *Bss*HII-*Not*I fragments for the β chain fragments. Second-generation α chain

libraries (built on either MELa1 or MELa1c DNA templates) were cloned into pG125 as *Sfi*I fragments. Second-generation β chain libraries were cloned into both pG396 and pG397 as *Bss*HII-*Not*I fragments. Restriction digests of 2-3 μg of SOE-PCR fragments were set up with 20-30 U each of the appropriate enzyme(s), using the manufacturer's recommended buffer in a final volume of 50-60 μl. Restriction digest of 60-100 μg of phagemid vectors were set up with 300-500 U each of the appropriate enzyme(s), using the manufacturer's recommended buffer in a final volume of 600-700 μl and incubating at 37ºC (*Not*I) or 50ºC (*Bss*HII or *Sfi*I). *Sfi*I digests were performed at 50ºC for 6 hours. *Not*I digests were performed at 50ºC for 6 hours followed by incubation with *Bss*HII for a further 6 hours at 50ºC.

2.4.1.4 Transformation and electroporation of Mel-5 TCR libraries

Digested DNA were gel-purified from a 1% (w/v) agarose gel using the Zymoclean DNA gel recovery kit and the concentrations determined on a Nanodrop ND-1000 spectrophotometer. To assess purity of the excised bands 1 μl of each was resolved on a 1% (w/v) agarose gel. For the first-generation libraries the efficiency of the insert and vector digests was monitored by small-scale pilot ligations using the Rapid ligation kit (Roche) and a total of ~80 ng DNA based on a ratio of 3:1 (insert to vector) following the conditions described in Section 2.3.5. Control ligations of digested vector only were also set up. Subsequently, large-scale ligations were prepared using T4 DNA ligase (NEB) overnight at 16ºC as shown below and in Table 2.1.

First-generation libraries

Alpha chain libraries : 4 μg pG125, 1.4 μg α chain fragment, 12 μl 10 X ligase buffer, 2000 U T4 DNA ligase (NEB) in a final volume of 120 μl.

Beta chain libraries : 5 μg pG125, 2 μg α chain fragment, 15 μl 10 X ligase buffer, 2000 U T4 DNA ligase (NEB) in a final volume of 150 μl.

Library	Ligation	CDR	SOE-PCR fragment
1	1	CDR1α	a3
	2	CDR2α	a6
2	3	CDR3α	a9
	4		a12
	5		a15
	6		a18
3	7	CDR1β	b3
	8	CDR2β	b6
4	9	CDR3β	b9
	10		b12
	11		b15
	12		b18

Table 2.1. Mel-5 TCR first-generation affinity maturation library ligations. Refer to Figure 2.1 for nomenclature of fragments.

Second-generation libraries

Second-generation library ligations were set up using a ratio of 3:1 (insert:vector) with the total amount of DNA indicated in Table 2.2 according to the following ratio of reagents: 300 U T4 ligase (NEB) for 1 μg of total DNA in a final volume of 100 μl and incubating overnight at 16ºC.

Library	Ligation	Framework	CDR	SOE-PCR fragments	Phagemid	V + I (μg)
1	1	MELa1	CDR1α	a3, a6	pG125	7
	2	MELa1	CDR2α	a9	pG125	4
2	3	MELa1c	CDR1α	à3, à6	pG125	6.5
	4	MELa1c	CDR2α	à9	pG125	4
-	[a]5	MELa1	CDR1β	b3, b6	pG396	5.6
	[a]6	MELa1	CDR2β	b9, b12	pG396	7
3	7	MELa1c	CDR1β	b3, b6	pG397	5.1
	8	MELa1c	CDR2β	b9, b12	pG397	6.8
-	[a]9	MELa1	CDR3β	b15, b18, b21, b24, b27, b30	pG396	11
4	10	MELa1c	CDR3β	b15, b18, b21, b24, b27, b30	pG397	15

Table 2.2. Mel-5 TCR second-generation affinity maturation library ligations. Refer to Figure 2.2 for nomenclature of fragments. [a]The β chain libraries, CDR1β, CDR2β and CDR3β (ligations 5, 6 and 9), built on the MELa1 framework were contaminated with the MELa1 template and were not taken forward into the phage panning experiments. V = vector; I = insert.

After ligation, the mixtures were purified using the Zymo DNA clean and concentrator kit. DNA was eluted in 20-40 μl of nuclease-free water. Transformation of electrocompetent *E. coli* TG1 cells followed the protocol described in Section 2.3.7 except that following recovery at 37ºC the entire 1 ml suspension volume was spread uniformly onto YTE agar (Square BioAssay dish 245 mm x 245 mm; Corning) supplemented with 100 μg/ml ampicillin and 2% glucose (w/v). For second-generation libraries, commercially prepared electrocompetent *E. coli* TG1 cells were used (≥4 x 10^{10} cfu/μg; Lucigen). For the first-generation libraries, 1 electroporation for each ligation was performed. For the second-generation libraries, 2 transformations for each ligation were performed except for ligation 9 and ligation 10 in which 6 and 10 transformations were performed respectively. Serial dilutions of the transformed library were performed by diluting the library in SOC media and

spreading 100 µl of each dilution on YTE agar plates supplemented with 100 µg/ml ampicillin and 2% glucose (w/v). The plates were incubated at 30ºC overnight. Individual colonies were counted on the dilution plates and the library sizes were calculated. Individual ampicillin-resistant colonies from each library were screened by PCR with Taq polymerase (NEB) using primers YOL13 and YOL22 and following the protocol described in Section 2.3.8. PCR products were purified using the DNA clean and concentrator kit and were sequenced with primers YOL13 and YOL22 (GATC Biotech). The transformed colony large plates were scraped using a spreader into 15% (v/v) glycerol-supplemented 2xTY media. The scraped bacterial suspension from multiple transformations belonging to the same CDR library were pooled and incubated on ice for ~15 minutes with gentle mixing. The 12 first-generation individual transformations were pooled into 4 libraries (Table 2.1). The 10 second-generation ligation transformations were pooled into 6 libraries (Table 2.2). All bacterial library stocks were transferred to sterile 1.5 ml centrifugation tubes and snap frozen on dry-ice. The cell stocks were stored at -80ºC.

2.4.2 gp100 TCR phage display libraries

First-generation gp100 TCR libraries were constructed by Dr. N. Harwood who provided the phagemid-gp100 TCR vector (pGPb7) encoding the enhanced-affinity clone GPb7 (Section 2.4). Second-generation libraries were built using pGPb7 as template targeting CDR2α, CDR3α and CDR3β regions for mutagenesis. Second-generation libraries were constructed according to the protocols outlined in Section 2.4-2.4.1.4 with some modifications. The primers are shown below and the PCR strategy employed for the library construction is depicted in Figure 2.3.

gp100 TCR library primers

Nat53 5’-taaaattaggtggacaag

Nat54 5’-cttgtccacctaattttaNNKNNKNNKNNKNNKagagagaaacacagtggaag-3’

Nat55 5’-cttgtccacctaattttaataNNKNNKNNKNNKNNKgagaaacacagtggaag

Nat56 5’-acagaagtaagaagcagtgtc

Nat57 5’-gacactgcttcttacttctgtNNKNNKNNKNNKNNKacacctcttgtctttgg

Nat58 5’-cgtagcacagaagtaagaagc

Nat59 5’-gcttcttacttctgtgctacgNNKNNKNNKNNKNNKcttgtctttggaaagggcacaag-3’

Nat60 5’-tccgtccgtagcacagaagtaag

Nat61 5’-cttacttctgtgctacggacggaNNKNNKNNKNNKNNKtttggaaagggcacaag-3’

Nat62 5’-acagagatagaaagctgtcgg

Nat63 5’-ccgacagctttctatctctgtNNKNNKNNKNNKNNKggcccctacgagcagtac

Nat64 5’-actggcacagagatagaaagctgtc

Nat65 5’-gacagctttctatctctgtgccagtNNKNNKNNKNNKNNKtacgagcagtacttcg

Nat66 5’-tatactactggcacagagatag

Nat67 5’-ctatctctgtgccagtagtataNNKNNKNNKNNKNNKcagtacttcgggccgg

Nat68 5’-gccccctatactactggcacag

Nat69 5’-ctgtgccagtagtataggggggcNNKNNKNNKNNKNNKttcgggccgggcaccaggctc-3’

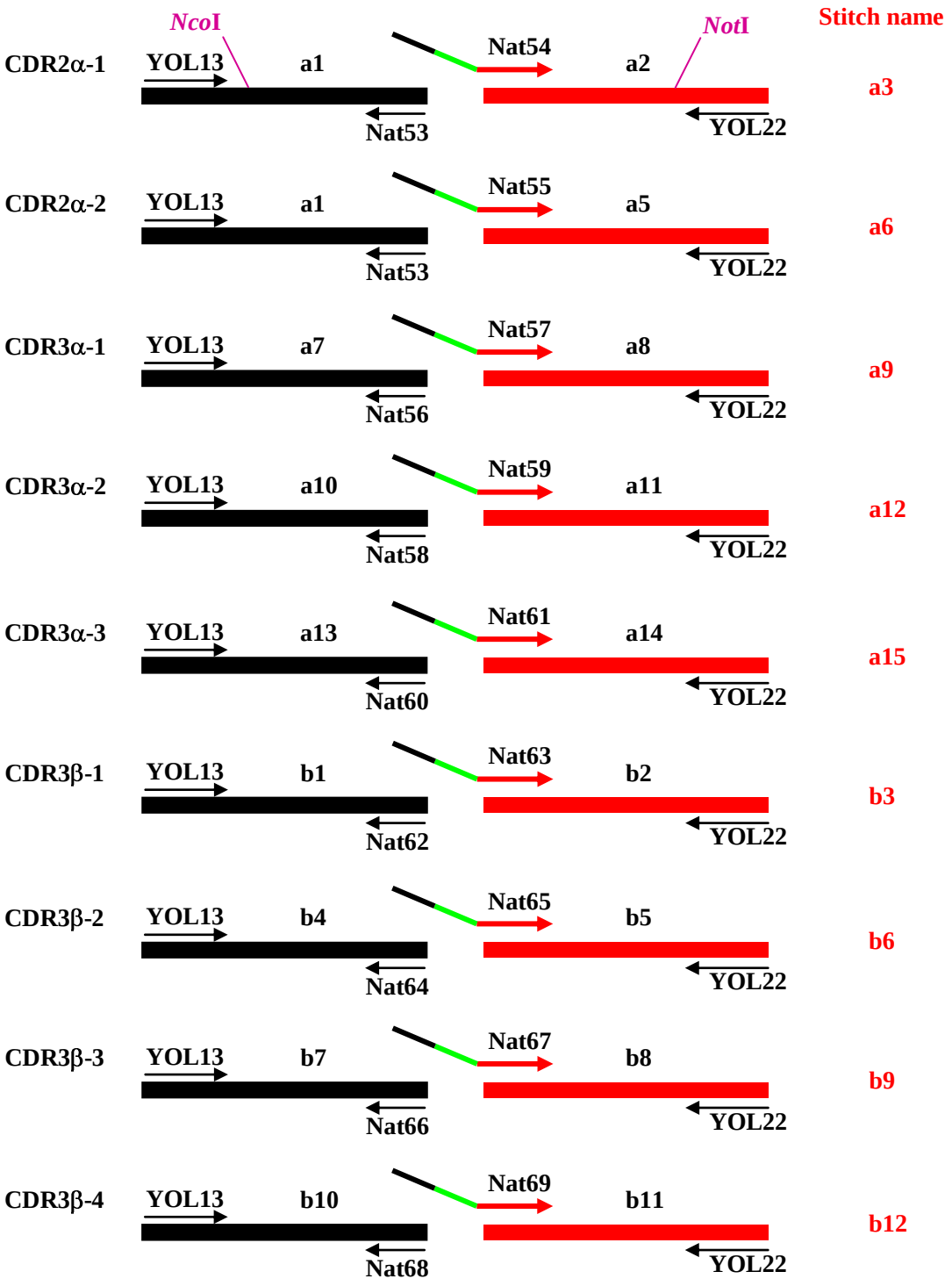

Figure 2.3. Schematic representation of the strategy for constructing second-generation mutagenised gp100 TCR fragments by overlapping PCR. Two PCR fragments are generated for each CDR library (a black and a red fragment). The red fragment is generated with a forward primer containing the NNK motif. The two fragments are assembled by SOE-PCR with primers YOL13-YOL22 (bright green primer segment corresponds to the mutagenised NNK region and the black primer region will anneal to the corresponding black PCR fragment). The α and β chain fragments are denoted by the letter a or b respectively. *Nco*I-*Not*I restriction sites are shown in purple.

2.4.2.1 Generating 'black' and 'red' library PCR fragments

Second-generation library PCRs used *Nco*I or *Not*I linearised phagemid vector pGPb7 (Section 2.4) as the template. 'Black' fragments: 2 ng pGPb7 (*Not*I linearised), 1 μl dNTPs (10 mM each), 1 μl YOL13 (10 pmol/μl), 1 μl [a]Nat Rev primer (10 pmol/μl), 5 μl 10 X polymerase buffer, 3.5 U Expand polymerase in a final volume of 50 μl. 'Red' fragments: 2 ng pGPb7 (*Nco*I linearised), 1 μl dNTPs (10 mM each), 1 μl [b]Nat Fwd primer (10 pmol/μl), 1 μl YOL22 (10 pmol/μl), 5 μl 10 X polymerase buffer, 3.5 U Expand polymerase in a final volume of 50 μl.

[a]Nat Rev primer refers to the following primers shown in Figure 2.3: Nat53, Nat56, Nat58, Nat60, Nat62, Nat64, Nat66, Nat68. [b]Nat Fwd primer refers to the following primers shown in Figure 2.3: Nat54, Nat55, Nat57, Nat59, Nat61, Nat63, Nat65, Nat67, Nat69.

The reactions were performed using the following PCR cycling conditions: Step 1: 94ºC for 2 min; Step 2: 94ºC for 16 sec; Step 3: 53ºC for 16 sec; Step 4: 72ºC for 50 sec/kbp; Step 5: 4ºC pause. Step 2 to 4 repeated 26 times. *Dpn*I treatment and gel-purification of PCR fragments followed the protocol described in Section 2.4.1.1. To assess purity of the excised bands 1 μl of each was resolved on a 1% (w/v) agarose gel.

2.4.2.2 Generating full-length gp100 TCR library PCR fragments

In contrast to the three-fragment SOE-PCR assembly of the Mel-5 TCR libraries, gp100 TCR libraries were assembled by two-fragment SOE-PCR. Full-length αβ TCR library fragments were assembled using SOE-PCR amplification of the 'black' and 'red' PCR fragments with primers YOL13 and YOL22. 'Black' and 'red' purified PCR fragments were diluted to a concentration so that 1 μl of each would give a 1:1 molar ratio in a total of 10-12 ng DNA. Multiple PCRs were set up for each

stitch reaction to generate sufficient PCR product required for ligations. Control PCRs were set up using only the 'black' or 'red' fragment as template; the composition of the control PCRs is not provided. The PCR mixture for the SOE-PCRs was assembled as follows: 1 µl 'black' fragment, 1 µl 'red' fragment, 1 µl dNTP mix (10 mM each), 1 µl YOL13 (10 pmol/µl), 1 µl YOL22 (10 pmol/µl), 5 µl 10 X Polymerase buffer (NEB), 2.5 U Taq DNA polymerase (NEB) in a final volume of 50 µl. The reactions were performed using the PCR cycling conditions outlined in Section 2.4.2.1 with an extension time of 80 seconds and repeating steps 2 to 4 thirty rimes. PCR products were resolved by agarose gel electrophoresis and bands of the expected size were purified using the Zymoclean DNA gel recovery kit. To assess purity of the excised bands 1 µl of each was resolved on a 1% (w/v) agarose gel. To monitor the integrity of the library PCR fragments, purified PCRs were sequenced with primers YOL13 and J195 (GATC) ('polyclonal sequencing').

2.4.2.3 Restriction digests of the gp100 TCR SOE-PCR products and pEX922

Purified SOE-PCR fragments: typically, 6-8 µg DNA, 50 U each of *Nco*I and *Not*I (both NEB), buffer in accordance with manufacturer's guidelines (NEB) in a final volume of 80 µl. Phagemid vector pEX922: typically, 100 µg DNA, 500 U each of *Nco*I and *Not*I (both NEB), buffer in accordance with manufacturer's guidelines (NEB) in a final volume of 1 ml and incubation at 37ºC for 5 hours.

2.4.2.4 Ligation and transformation of gp100 TCR libraries

Digested DNA were gel-purified from a 1% (w/v) agarose gel using the Zymoclean DNA gel recovery kit and the concentrations determined on a Nanodrop ND-1000

spectrophotometer. To assess purity of the excised bands 1 μl of each was resolved on a 1% (w/v) agarose gel. Transformations were prepared using T4 DNA ligase overnight at 16ºC. Alpha chain libraries : ~5 μg pEX922, ~5 μg [a]α chain fragments, 80 μl 10 X ligase buffer, 4000 U T4 DNA ligase (NEB) in a final volume of 800 μl. Beta chain libraries : ~10 μg pEX922, ~10 μg [b]β chain fragments, 160 μl 10 X ligase buffer, 8000 U T4 DNA ligase (NEB) in a final volume of 1.6 ml.

[a]α chain library fragments: library 1 (CDR2α) comprised PCR fragments a3 and a6; library 2 (CDR3α) comprised PCR fragments a9, a12 and a15; [b]β chain library fragments: library 3 (CDR3β) comprised PCR fragments b3, b6, b9 and b12.

After ligation, the mixtures were purified using the Zymo DNA clean and concentrator kit. DNA was eluted in 20 μl of nuclease-free water. Multiple transformations of electrocompetent *E. coli* TG1 cells (Lucigen) were performed for each library (library 1: 12; library 2: 12; library 3: 20) as described in Section 2.4.1.4. Preparation of bacterial glycerol stocks and sequencing of library clones followed the methods described in Section 2.4.1.4.

2.4.3 MAGE-A3 TCR phage display libraries

First-generation libraries were built in the context of the wild-type MAGE-A3 TCR framework and all 6 CDRs were targeted. Second-generation libraries targeted only CDR3 regions and were constructed in the context of two enhanced-affinity frameworks (MAGEa6a and MAGEb2a) (Section 2.3). Construction of first and second-generation libraries followed the protocols outlined in Section 2.4.2. The template for amplification of the 'black' and 'red' fragments (Figure 2.4 and Figure 2.5) was *Nco*I or *Not*I linearised phagemid vector pIM160 (for first-generation libraries), pIM194 and pIM195 (for second-generation libraries). 'Black' fragments: 2

ng phagemid vector (*Not*I linearised), 1 μl dNTPs (10 mM each), 1 μl YOL13 (10 pmol/μl), 1 μl [a]Nat Reverse primer (10 pmol/μl), 5 μl 10 X polymerase buffer, 1 U Phusion polymerase (NEB) in a final volume of 50 μl. 'Red' fragments: 2 ng phagemid vector (*Nco*I linearised), 1 μl dNTPs (10 mM each), 1 μl [b]Nat Forward primer (10 pmol/μl), 1 μl YOL22 (10 pmol/μl), 5 μl 10 X polymerase buffer, 1 U Phusion polymerase in a final volume of 50 μl. [a]Nat Reverse and [b]Nat Forward primers see Figure 2.4 and 2.5. PCR cycling as shown in Section 2.4.2 (extension time of 25 seconds/kbp). Assembly of αβ TCR fragments by SOE-PCR followed the protocol outlined in Section 2.4.2.2 (extension time of 45 seconds). Construction of second-generation Strategy 2 libraries followed a unique set of protocols and will be described separately. The primers are shown below and the PCR strategies employed for the first and second-generation library construction are depicted in Figure 2.4, Figure 2.5 and Figure 2.6. Second-generation Strategy 3 libraries were kindly provided by Dr. Y. Li.

MAGE-A3 TCR library primers

Nat70 5'-ctcaactgcagtttcactNNKNNKNNKNNKNNKaacctccagtggtttaggcag-3'

Nat71 5'-agtgaaactgcagttgagaacc-3'

Nat72 5'-caactgcagtttcactgatNNKNNKNNKNNKNNKctccagtggtttaggcaggac-3'

Nat73 5'-atcagtgaaactgcagttgag-3'

Nat74 5'-ggtctcacatctctgttgNNKNNKNNKNNKNNKcagagagagcaaacaagtggaag-3'

Nat75 5'-caacagagatgtgagacctttccc-3'

Nat76 5'-gccacctacctctgtgctNNKNNKNNKNNKNNKgctgggagttaccaactcac-3'

Nat77 5'-agcacagaggtaggtggctgag-3'

Nat78 5'-cctacctctgtgctgtgaggNNKNNKNNKNNKNNKagttaccaactcactttcggg-3'

Nat79 5’-cctcacagcacagaggtagg-3’

Nat80 5’-cctctgtgctgtgaggccgNNKNNKNNKNNKNNKtaccaactcactttcgggaagg-3’

Nat81 5’-cggcctcacagcacagaggtagg-3’

Nat82 5’-gtgctgtgaggccgggagggNNKNNKNNKNNKNNKctcactttcgggaaggggacc-3’

Nat83 5’-ccctcccggcctcacagcacag-3’

Nat84 5’-gaggccgggaggggctgggNNKNNKNNKNNKNNKttcgggaaggggaccaaactc-3’

Nat85 5’-cccagcccctcccggcctcac-3’

Nat86 5’-ctgagctgctcccctatcNNKNNKNNKNNKNNKgtatcctggtaccaacagacc-3’

Nat87 5’-gataggggagcagctcagtgtc-3’

Nat88 5’-ccttcagttcctctttgaaNNKNNKNNKNNKNNKcagagaaacaaaggaaacttccc-3’

Nat89 5’-ttcaaagaggaactgaaggcc-3’

Nat90 5’-cttcagttcctctttgaatacNNKNNKNNKNNKNNKagaaacaaaggaaacttccctg-3’

Nat91 5’-gtattcaaagaggaactgaagg-3’

Nat92 5’-gccctttatctttgcgccNNKNNKNNKNNKNNKgccgacgagcagtacttcggg-3’

Nat93 5’-ggcgcaaagataaagggccgagtc-3’

Nat94 5’-ctttatctttgcgccagcagcNNKNNKNNKNNKNNKgagcagtacttcgggccgggc-3’

Nat95 5’-gctgctggcgcaaagataaagg-3’

Nat96 5’-ctttgcgccagcagcccgNNKNNKNNKNNKNNKcagtacttcgggccgggcacc-3’

Nat97 5’-cgggctgctggcgcaaagataaag-3’

Nat98 5’-cgccagcagcccgaacatgNNKNNKNNKNNKNNKttcgggccgggcaccaggctc-3’

Nat99 5’-catgttcgggctgctggcgcaaag-3’

Nat100 5’-ctcagccacctacctctgtNNKNNKNNKNNKNNKggggctgggagttaccaactc-3’

Nat101 5’-acagaggtaggtggctgagtc-3’

Nat102 5’-ctcggccctttatctttgcNNKNNKNNKNNKNNKatggccgacgagcagtacttc-3’

Nat103 5’-gcaaagataaagggccgagtc-3’

A.

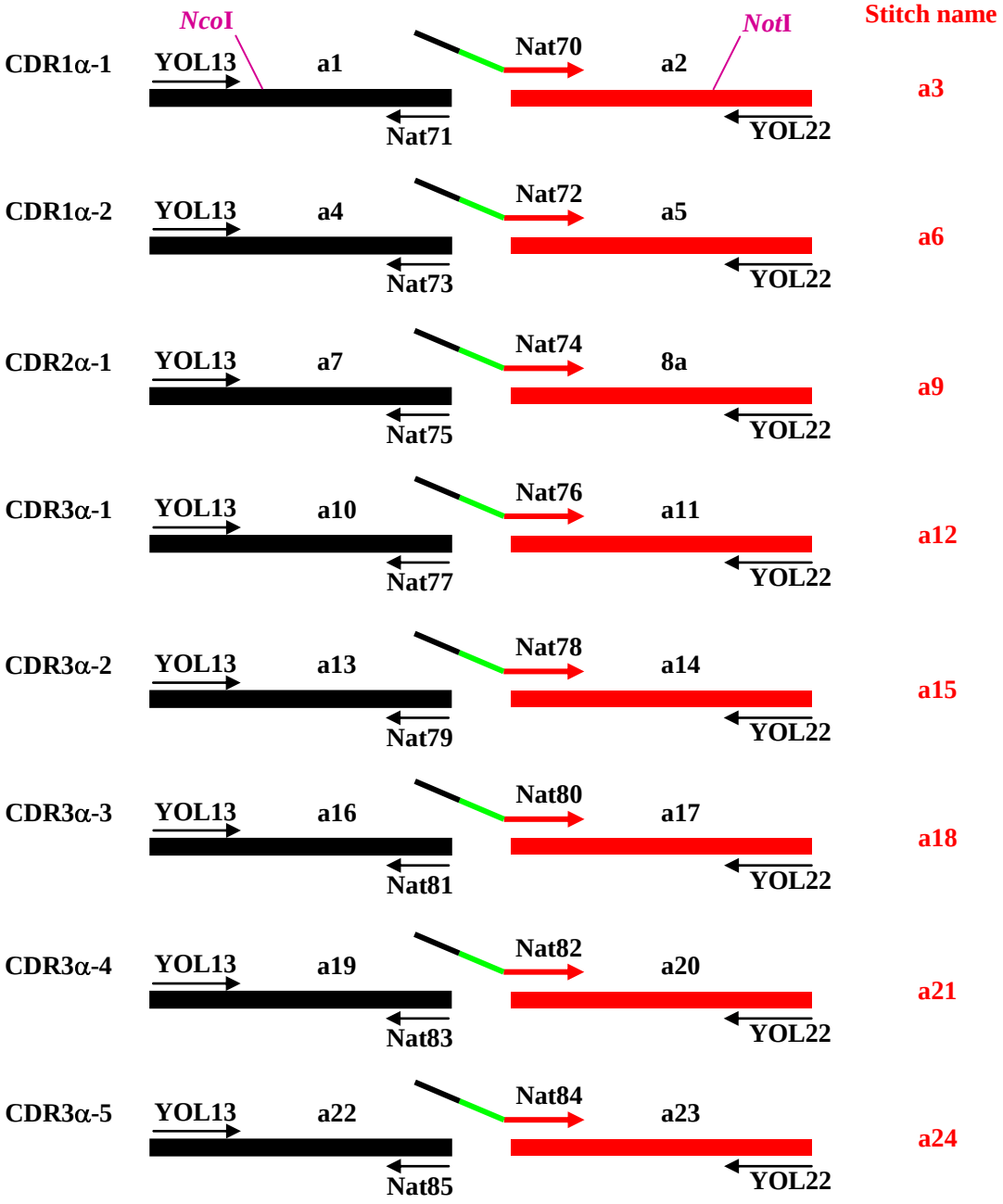
NcoI
NotI
Stitch name
CDR1α-1
YOL13
a1
Nat70
a2
a3
Nat71
YOL22
CDR1α-2
YOL13
a4
Nat72
a5
a6
Nat73
YOL22
CDR2α-1
YOL13
a7
Nat74
8a
a9
Nat75
YOL22
CDR3α-1
YOL13
a10
Nat76
a11
a12
Nat77
YOL22
CDR3α-2
YOL13
a13
Nat78
a14
a15
Nat79
YOL22
CDR3α-3
YOL13
a16
Nat80
a17
a18
Nat81
YOL22
CDR3α-4
YOL13
a19
Nat82
a20
a21
Nat83
YOL22
CDR3α-5
YOL13
a22
Nat84
a23
a24
Nat85
YOL22

B.

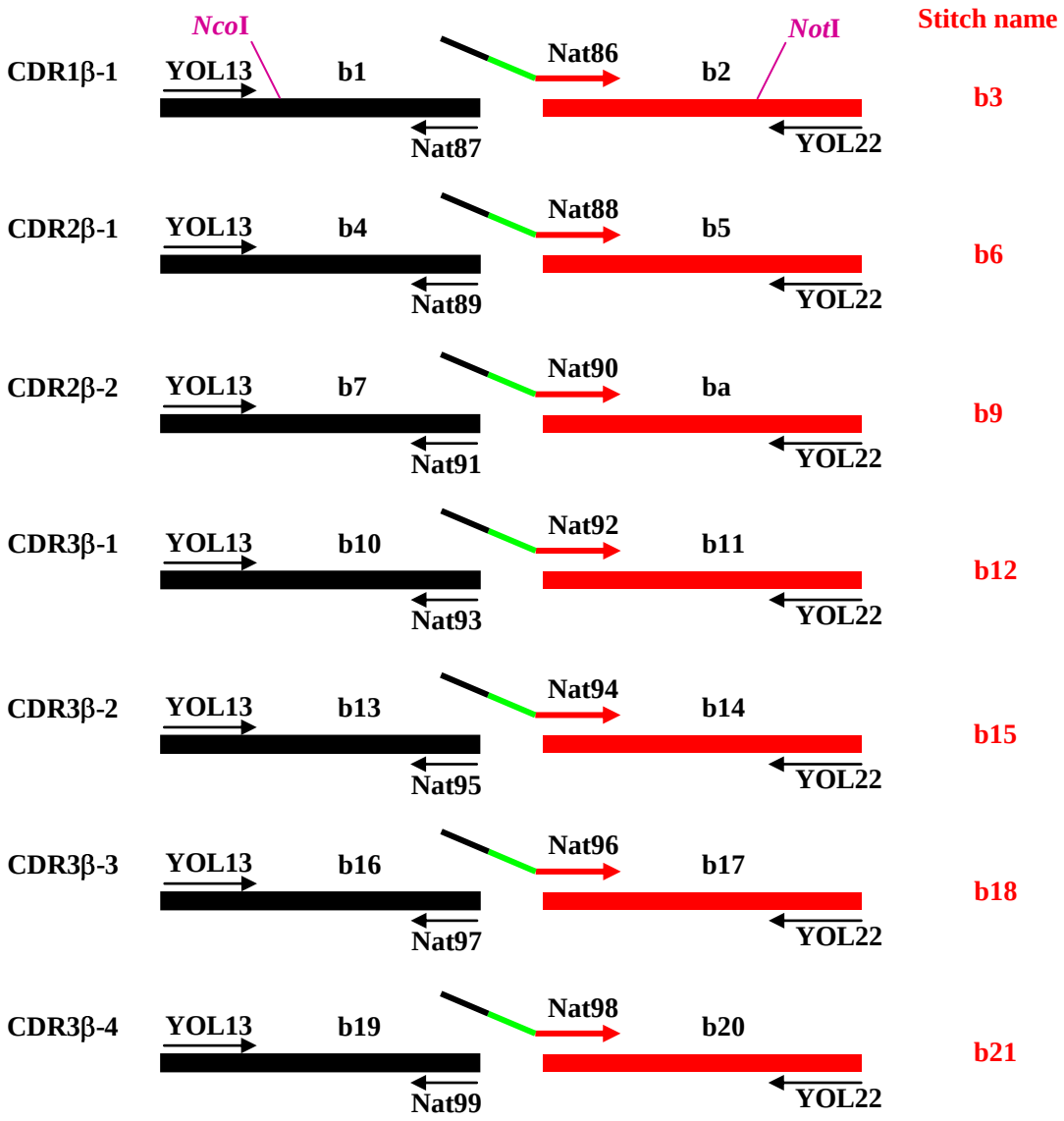

Figure 2.4. Schematic representation of the strategy for constructing first-generation mutagenised MAGE-A3 TCR fragments by overlapping PCR. (A). α chain library schematic. **(B).** β chain library schematic. Two PCR fragments are generated for each CDR library (a black and a red fragment). The red fragment is generated with a forward primer containing the NNK motif. The two fragments are assembled by SOE-PCR with primers YOL13-YOL22 (bright green primer segment corresponds to the mutagenised NNK region and the black primer region will anneal to the corresponding black PCR fragment). The α and β chain fragments are denoted with an a or b respectively.

A.

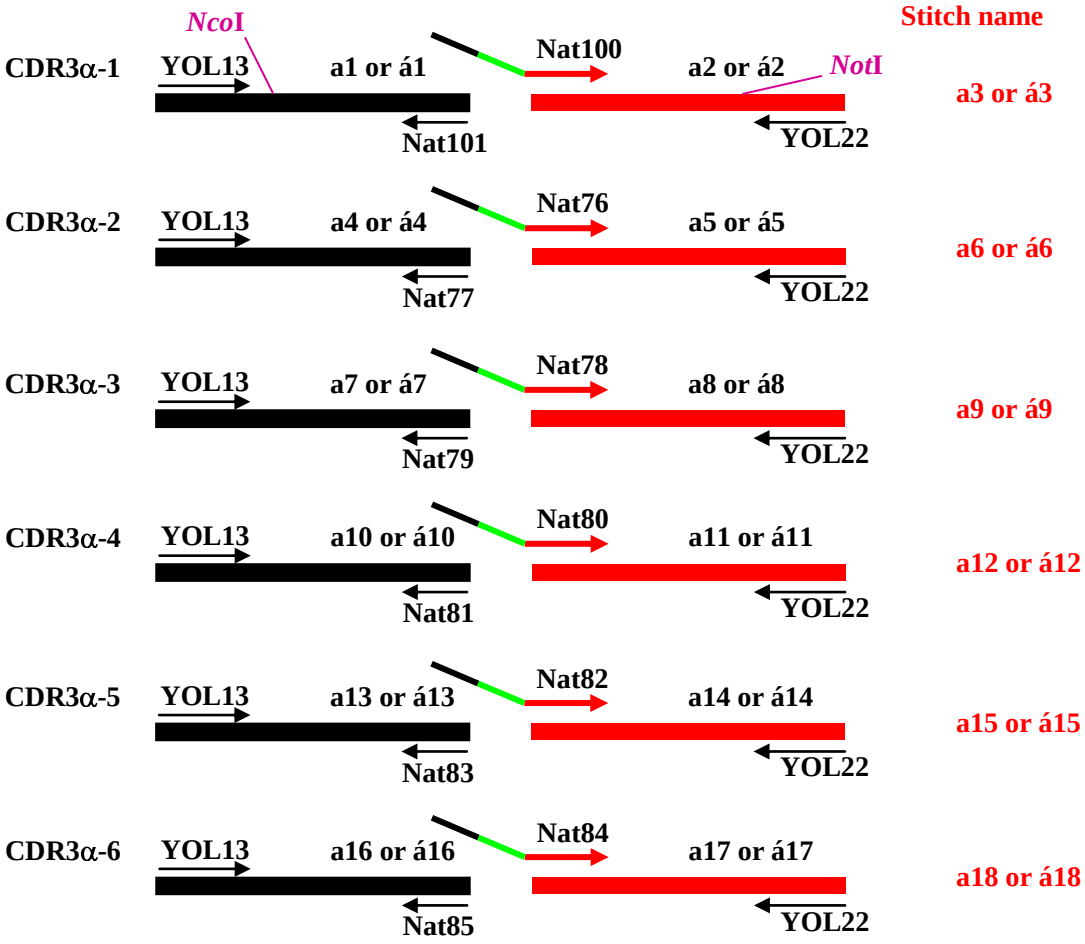
NcoI
Stitch name
CDR3α-1
YOL13
a1 or á1
Nat100
a2 or á2
NotI
a3 or á3
Nat101
YOL22
CDR3α-2
YOL13
a4 or á4
Nat76
a5 or á5
a6 or á6
Nat77
YOL22
CDR3α-3
YOL13
a7 or á7
Nat78
a8 or á8
a9 or á9
Nat79
YOL22
CDR3α-4
YOL13
a10 or á10
Nat80
a11 or á11
a12 or á12
Nat81
YOL22
CDR3α-5
YOL13
a13 or á13
Nat82
a14 or á14
a15 or á15
Nat83
YOL22
CDR3α-6
YOL13
a16 or á16
Nat84
a17 or á17
a18 or á18
Nat85
YOL22

B.

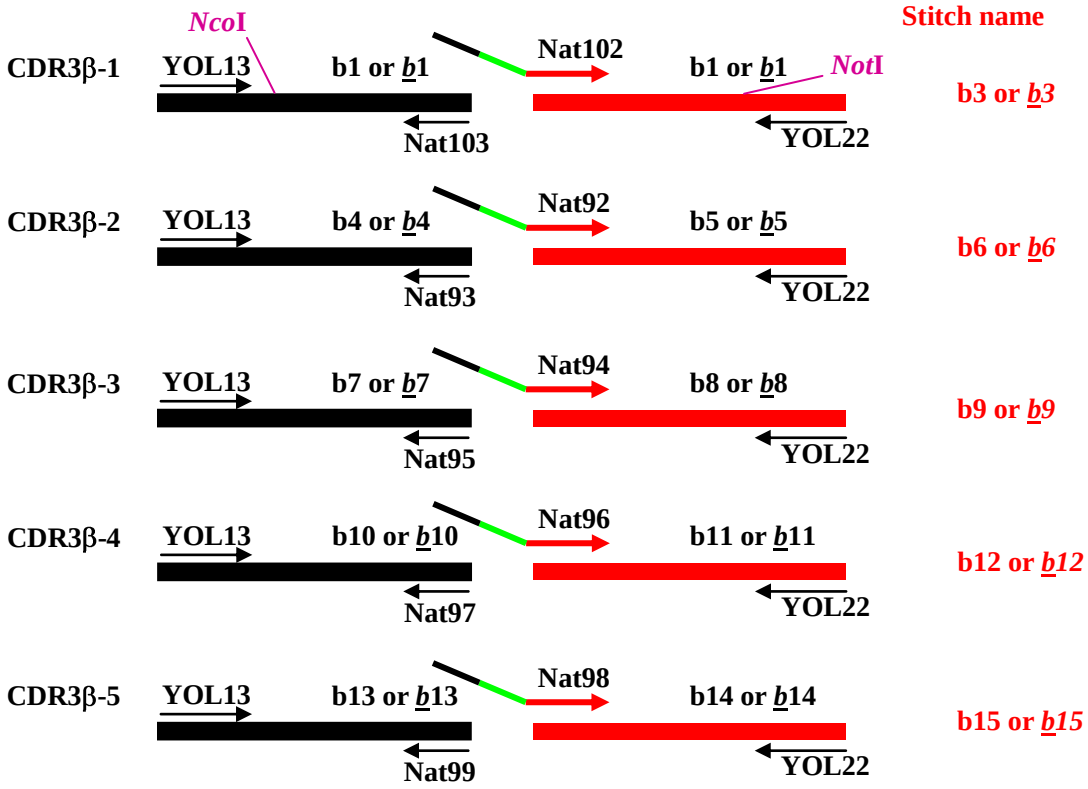

Figure 2.5. Strategy 1: schematic representation of the strategy used for constructing mutagenised second-generation MAGE-A3 TCR CDR3 fragments in the context of the enhanced-affinity CDR2 mutant clones MAGEa6a and MAGEb2a. (A). CDR3α library schematic. **(B).** CDR3β library schematic. Two PCR fragments are generated for each CDR library (a black and a red fragment). The red fragment is generated with a forward primer containing the NNK motif. The two fragments are assembled by SOE-PCR with primers YOL13-YOL22 (bright green primer segment corresponds to the mutagenised NNK region and the black primer region will anneal to the corresponding black PCR fragment). The α and β chain library fragments are amplified from either phagemid vector template pIM194 (encoding the CDR2α MAGEa6a back-mutant) or pIM195 (encoding the CDR2β MAGEb2a back-mutant). The α chain PCR products generated from pIM194 and pIM195 template are named "a" and "á" respectively. The β chain PCR products generated from pIM194 and pIM195 template are named "b" and "*b*" respectively. Phagemid vector templates pIM194 and pIM195 contain constant region cysteines located in the native format.

2.4.3.1 Ligation and transformation of MAGE-A3 TCR libraries

Digests were performed according to the conditions outlined in Section 2.4.2.3: 2-7 μg of each SOE-PCR fragment, 5 U/μg DNA each of *Nco*I and *Not*I (both NEB), buffer in accordance with manufacturer's guidelines (NEB) in a final volume of 30-50 μl. Ligations were set up using a 3:1 ratio of insert to vector with 400 U T4 DNA ligase (NEB) per 1 μg total DNA and 1X T4 ligase buffer in a final volume of 80 μl and incubated overnight at 16ºC. The total amount of vector and library insert DNA used in the ligation reactions is outlined below:

First-generation library ligations (total DNA shown)

Library 1: CDR1α (PCR fragment a3, a6) 10 μg

Library 2: CDR2α (PCR fragment a9) 5 μg

Library 3: CDR3α (PCR fragment a12, a15, a18, a21, a24) 20 μg

Library 4: CDR1β (PCR fragment b3) 5 μg

Library 5: CDR2β (PCR fragment b6, b9) 10 μg

Library 6: CDR3β (PCR fragment b12, b15, b18, b21) 20 μg

Refer to Figure 2.4 for nomenclature of PCR fragments.

Second-generation Strategy 1 library ligations

Library 1: CDR3α:MAGEa6a (PCR fragment a3, a6, a9, a12, a15, a18) 6 μg

Library 2: CDR3α:MAGEb2a (PCR fragment à3, à6, à9, à12, à15, à18) 6 μg

Library 3: CDR3β:MAGEa6a (PCR fragment b3, b6, ba9, b12) 5 μg

Library 4: CDR3β:MAGEb2a (PCR fragment *b*3, *b*6, *b*a9, *b*12) 5 μg

Refer to Figure 2.5 for nomenclature of PCR fragments.

After ligation, the mixtures were purified using the Zymo DNA clean and concentrator kit. DNA was eluted in 20 μl (first-generation) or 12 μl (second-generation) of nuclease-free water. Multiple transformations of electrocompetent *E. coli* TG1 cells (Lucigen) were performed following the protocol described in Section 2.4.1.4. For the first-generation libraries: 6 each for library 2 and 4; 10 each for library 1 and 5; 20 each for library 3 and 6. Five transformations of each second-generation library were performed. Preparation of bacterial glycerol stocks and sequencing of library clones followed the methods described in Section 2.4.1.4. The scraped bacterial suspension from multiple transformations belonging to the same library were pooled.

2.4.3.2 Construction of MAGE-A3 TCR first-generation CDR2α:CDR2β crossing libraries

The Pan 3 mutated CDR2α and CDR2β regions that were selected from first-generation libraries 2 and 5 (Section 2.4.3.1) were spliced by SOE-PCR to generate a library of TCRs mutated in both CDR2 loops. TG1 *E. coli* glycerol stocks of first-generation Pan 3 library 2 and library 5 (Section 2.4.3.1) were used to inoculate separately 25 ml 2xYT media to an OD_{600} of ~1.0. Cell suspensions were pelleted at 3,360 x g for 10 minutes at room temperature. The pellets were thoroughly respuspended in 25 ml STE buffer (10 mM Tris, pH 8.1, 1 M EDTA, pH 8.0, 100 mM NaCl). After a second wash step (under the same conditions) DNA was isolated from the cultures using the QIAprep spin miniprep kit (Qiagen). The concentration of the eluted DNA was determined using a Nanodrop ND-1000 spectrophotometer. DNA isolated from library 2 and library 5 (10 μg) was digested with 50 U each of restriction enzymes *Nco*I and *Avr*II (both NEB) and buffer in accordance with

manufacturer's guidelines (NEB) in a final volume of 270 µl. Digestions were incubated at 37ºC for 5 hours. Digested library fragments were resolved on a 1% (w/v) agarose gel and a ~640 bp band from library 2 and ~6200 bp from library 5 DNA were gel-purified using the Zymo DNA clean and concentrator kit. Ligation reactions using appropriately digested (gel-purified) DNA insert and vector were set up using a 3:1 molar ratio of insert:vector (5 µg total DNA), 2000 U of T4 DNA Ligase (NEB), 1X ligation buffer in a final volume of 400 µl and incubated overnight at 16ºC. Three transformations of electrocompetent TG1 *E. coli* cells (Lucigen) were performed with 2.5 µl of the PCR-purified ligation as described in Section 2.4.1.4. The scraped cell suspension from each of the 3 transformations was pooled and stored at -80Cº.

2.4.3.3 Construction of MAGE-A3 TCR second-generation Strategy two libraries

Four previously constructed MAGE-A3 TCR libraries (Section 2.4.3.1) were converted from the native to the engineered disulphide C-region cysteine framework (mTCR). These were the preselected (Pan 0) first-generation library 3 and library 6 and the Pan 0 second-generation library 1 and library 4 (Section 2.4.3.1). DNA was isolated from the scraped bacterial glycerol stocks as described in Section 2.4.3.2. The concentration of the eluted DNA was determined using a Nanodrop ND-1000 spectrophotometer. The primers used to introduce the mTCR constant region cysteines are shown below and the PCR library construction strategy is depicted in Figure 2.6.

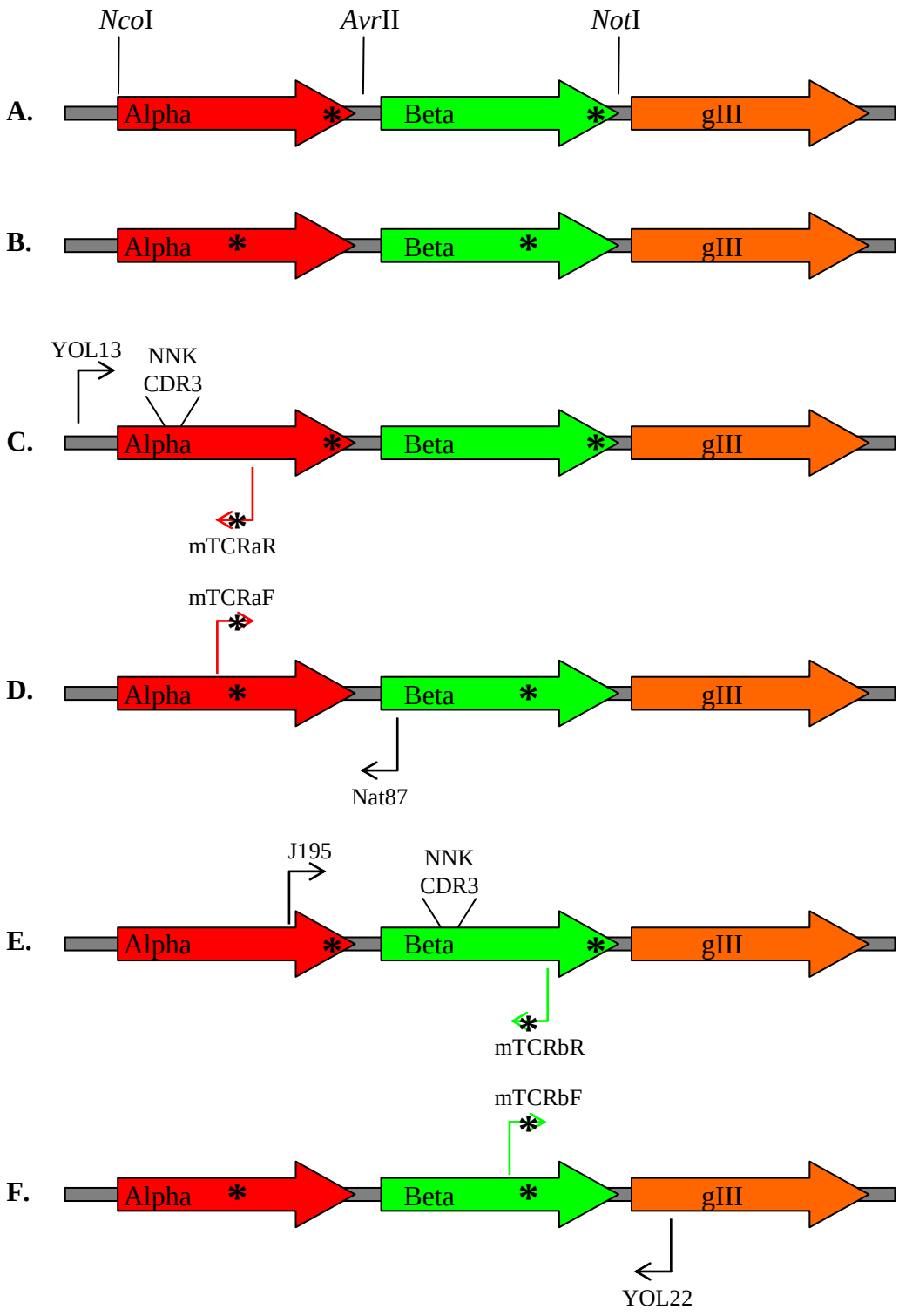

Figure 2.6. Schematic representation of the strategy to convert MAGE-A3 TCR CDR3 libraries from native format into mTCR format. (A). TCR α and β chains containing membrane proximal C domain cysteines (*) in native format. **(B).** TCR α and β chains containing introduced constant domain cysteines (*) (membrane proximal cysteines removed) in mTCR format. **(C).** Introduction of mTCR α chain cysteine into CDR3α library segments. Templates: library 3 CDR3α built on wt framework (section 5.2.2) and library 1 CDR3α built on MAGEa6a framework

(section 5.8.2) (both containing native cysteine). **(D).** PCR amplification of MAGE-A3 TCR Cα domain. Template: wt MAGE-A3 TCR in mTCR format. **(E).** Introduction of mTCR β chain cysteine into CDR3β library segments. Templates: library 6 CDR3β built on wt framework (section 5.2.2) and library 4 CDR3β built on MAGEb2a framework (section 5.8.2) (both containing native cysteine). **(F).** PCR amplification of MAGE-A3 TCR Cβ domain. Template: wt MAGE-A3 TCR in mTCR format. SOE-PCR fragment from (C) and (D) generates full-length Vα/Cα product including the mTCR cysteines. Digested (E) and (F) SOE-PCR product generates full-length Vβ/Cβ product including the mTCR cysteines. gIII, M13 geneIII.

MAGE-A3 TCR second-generation Strategy 2 library primers

mTCRaR 5'-gtctagcacacatttgtctgtgatatacacatc-3'

mTCRbR 5'-cgggtctgtgcagaccccactgtgcacctccttc-3'

mTCRaF 5'-gacaaatgtgtgctagacatgaggtctatg-3'

mTCRbF 5'-ggggtctgcacagacccgcagcccctcaag-3'

The reaction components and volumes were as follows: Fragment C: 15 ng [a]phagemid library, 1 μl dNTPs (10 mM each), 1 μl YOL13 (10 pmol/μl), 1 μl mTCRaR (10 pmol/μl), 5 μl 10 X polymerase buffer, 1 U Phusion polymerase in a final volume of 50 μl. Fragment D: 2 ng [b]pLAS0282, 1 μl dNTPs (10 mM each), 1 μl mTCRaF (10 pmol/μl), 1 μl Nat87 (10 pmol/μl), 5 μl 10 X polymerase buffer, 1 U Phusion polymerase in a final volume of 50 μl. Fragment E: 15 ng [c]phagemid library, 1 μl dNTPs (10 mM each), 1 μl J195 (10 pmol/μl), 1 μl mTCRbR (10 pmol/μl), 5 μl 10 X polymerase buffer, 1 U Phusion polymerase in a final volume of 50 μl. Fragment F: 2 ng [b]pLAS0282, 1 μl dNTPs (10 mM each), 1 μl mTCRbF (10 pmol/μl), 1 μl YOL22 (10 pmol/μl), 5 μl 10 X polymerase buffer, 1 U Phusion polymerase in a final volume of 50 μl.

[a]MAGE-A3 TCR-phagemid library template (Section 2.4.3.1): library 3 (first-generation) or library 1 (second-generation); [b]pLAS0282 (wild-type MAGE-A3 TCR mTCR format) from Section 2.4; [c]MAGE-A3 TCR-phagemid library template (Section 2.4.3.1): library 6 (first-generation) or library 4 (second-generation).

The reactions were performed using the PCR cycling conditions outlined in Section 2.4.2.1 (20 second extension time). PCR products (C, D, E, F) were resolved on a 1.5% (w/v) agarose gel and bands of the expected size were gel-purified using the Zymo DNA clean and concentrator kit. Full-length α (C/D) or β (E/F) chains were assembled as follows: Fragment C/D: 10 ng fragment C, 5 ng fragment D, 1 μl dNTPs

(10 mM each), 1 μl YOL13 (10 pmol/μl), 1 μl Nat87 (10 pmol/μl), 5 μl 10 X polymerase buffer, 1 U Phusion polymerase in a final volume of 50 μl. Fragment E/F: 10 ng fragment E, 5 ng fragment F, 1 μl dNTPs (10 mM each), 1 μl J195 (10 pmol/μl), 1 μl YOL22 (10 pmol/μl), 5 μl 10 X polymerase buffer, 1 U Phusion polymerase in a final volume of 50 μl. The reactions were performed using the PCR cycling conditions outlined in Section 2.4.2.1 (30 second extension time). SOE-PCR products (C/D and E/F) were resolved on a 1.5% (w/v) agarose gel and bands of the expected size were gel-purified using the Zymo DNA clean and concentrator kit. Fragment C/D was digested with restriction enzymes *Nco*I and *Avr*II (both NEB); Fragment E/F was digested with restriction enzymes *Avr*II and *Not*I (both NEB). Phagemid pLAS0282 (20 μg) was digested separately with *Nco*I-*Avr*II and AvrII-*Not*I. Restriction digests were performed using 10 U (for the inserts) or 50 U (for the vector) of the required enzymes and buffer in accordance with manufacturer's guidelines (NEB) in a final volume of 50 μl (inserts) or 300 μl (vector). Digestions were incubated at 37ºC for 5 hours. Digested vector and PCR fragments were resolved on a 1% (w/v) agarose gel and bands of the expected size were gel-purified using the Zymo DNA clean and concentrator kit. Fragments C/D and E/F (1 μg) were ligated separately into phagemid vector pLAS0282 using T4 DNA ligase at a ratio of 3:1 (insert:vector) overnight at 16ºC following the conditions described in Section 2.4.3.1. Electrocompetent *E. coli* TG1 cells (Lucigen) were transformed with PCR-purified ligations as described in Section 2.3.7 to generate 4 libraries: library 1, CDR3α on the wild-type MAGE-A3 TCR framework; library 2, CDR3α on the MAGEa6a TCR framework; library 3, CDR3β on the wild-type MAGE-A3 TCR framework; library 2, CDR3β on the MAGEb2a TCR framework.

2.5 Phage selections and screening

2.5.1 Rescue of TCR-displaying phages

For the rescue of TCR-displaying phages, 250 ml 2xYTag media in a conical flask was inoculated with an aliquot of the phage glycerol stocks to an initial OD_{600} ~0.05-0.08 and incubated at 37ºC with shaking at 250 rpm until the mid-exponential growth phase (OD_{600} ~0.4-0.5) was reached. At which point, helper phage M13K07 (>1 x 10^{11} pfu/ml; Invitrogen) was added to 50 ml of culture at an infection ratio of 20:1 (phage:bacteria), mixed by inversion and incubated at 37ºC in a water-bath for 30 minutes (without shaking). The cultures were pelleted at 2,900 g for 10 minutes at 16ºC and the supernatant discarded. The pellets were resuspended in 100 ml 2xYT media in a conical flask supplemented with ampicillin (100 μg/ml) and kanamycin (Apollo Scientific Limited) (25 μg/ml) (helper phage resistance gene) (designated 2xYTak) and incubated overnight at 26ºC with shaking at 250 rpm. The quantity of reagents was adjusted according to the culture volume. Monoclonal phage TCRs were rescued from panning master-plates (Section 2.5.4) by inoculating 100 μl 2xYTag media in a sterile 96-well tissue culture plate (Falcon) with 5 μl of each well of the master-plate and incubating at 37ºC with shaking for 2-3 hours. Helper phage M13K07 was added 20:1 (phage:bacteria) and incubated at 37ºC for 1 hour without shaking. The cultures were centrifuged, the supernatant discarded and the pellets resuspended in 400 μl 2xYTak media and incubated overnight at 26ºC with shaking at 250 rpm.

2.5.2 Precipitation of phage-displayed fragments using PEG/NaCl

The 100 ml culture was centrifuged at 11,200 x g for 20 minutes at 4ºC and the bacterial pellet discarded. The supernatant was transferred to a fresh centrifugation tube and the phage was precipitated by adding 20 ml polyethylene glycol (PEG)/NaCl

(20% w/v PEG 8000; Sigma, 2.5 M NaCl), mixing thoroughly by inversion and incubating on ice for 1 hour. Following incubation the tubes were centrifuged for 10 minutes at 3,360 x g at 4ºC. The supernatant was discarded and the tubes briefly respun to remove the remaining supernatant. The TCR-phage pellet was resuspended in 10 ml phosphate buffered saline (PBS; Sigma) and spun at 11,200 x g for 10 minutes at 4ºC. The supernatant was transferred to a fresh tube and the phage was precipitated once more by adding 2.5 ml PEG/NaCl solution, mixing thoroughly by inversion and incubating on ice for 20-30 minutes. After incubation the tubes were spun for 10 minutes at 3,360 x g at 4ºC and the supernatant discarded. Following a final brief spin to remove the remaining supernatant the TCR-phage pellets were resuspended in 1 ml PBS and transferred to a sterile 1.5 ml centrifuge tube. The TCR-phage solution was centrifuged twice at 16,200 x g for 15 minutes at 4ºC; TCR-phage supernatant was transferred to fresh tubes between spins. The supernatant containing phage TCR was stored on ice at 4ºC until required for panning experiments. The quantity of reagents was adjusted accordingly for the precipitation of TCR-displaying phages from other culture volumes.

2.5.3 Preparation of debiotinylated Marvel (db-M) solution

BioMag streptavidin-coated magnetic beads (2 ml) (Qiagen) were washed 5 times with 1 ml PBS using a magnet to collect the beads between each wash. The washed beads were added to 3% (w/v) Marvel dried milk powder and incubated at room temperature for 2 hours with mixing. After the incubation the beads were collected using a magnet. The milk solution was transferred to a fresh tube and place on the magnet. This step was repeated at least 5 times to remove the remaining beads. To the db-M 1.5 ml 0.5 M EDTA, pH 8.0 was added and transferred to prewashed dialysis tubing and dialysed against 5 litres of PBS. The dialysis buffer was changed to fresh

PBS and stored overnight at 4ºC. The next day, the dialysis buffer was changed to fresh PBS and dialysed for a further 2-3 hours. After dialysis the db-M was filter sterilised through a 0.22 μM filter (Sartorius Stedim Biotech) and divided into 1 ml aliquots for storage at -20ºC.

2.5.4 Selection of antigen-binding TCR-displaying phage using solution-based biopanning

Rescued phage (from Section 2.5.2) (50-100 μl) was added to 1 ml 3% db-M and incubated at room temperature for 90 minutes with rotation[a]. After this blocking step 1 μl Tween-20 (Sigma) together with biotinylated pHLA (kindly provided by Dr. B. Cameron) at the desired concentration and incubated at room temperature for 1 hour with gentle rotation[b]. Dynabeads M-280 streptavidin-coated magnetic beads (Invitrogen) were washed 5 times with PBS and 50-100 μl was used to rescue the phage-TCR-pHLA complexes. Following a 7 minute incubation at room temperature with rotation the bead-phage-TCR-pHLA complexes were captured using a magnet. The collected beads were washed by resuspension using a fresh pipette tip and a fresh centrifuge tube between each wash. The washing conditions for the first cycle of panning were typically: 2 times with 3% (w/v) Marvel-PBS (MPBS); 3 times PBS-Tween-20 (PBST) (0.1%, v/v final); 2 times PBS. After discarding the final wash solution the TCR phage were eluted by adding 0.5 ml triethylamine (Sigma) and incubating at room temperature for 8 minutes with rotation. The beads were collected using a magnet and the supernatant containing eluted phage TCRs transferred to a sterile 1.5 ml centrifuge tube containing 0.25 ml 1 M Tris-HCl, pH7.4 (Sigma) for neutralisation purposes. Ten ml mid-exponential growth phase (OD_{600} ~0.4-0.5) TG1 *E. coli* cells (grown in 2xYT supplemented with 2%, w/v glucose) were infected with 0.6 ml of the eluted phage, mixed by inversion and incubated at 37ºC for 30 minutes

in a water-bath (without shaking). After incubation the culture was centrifuged at 2,900 x g for 10 minutes at room temperature and the pellet respuspended in 1 ml fresh 2xYT media and spread onto YTE agar plates (Square BioAssay dish 245 mm x 245 mm; Corning) supplemented with ampicillin (100 μg/ml) and 2% (w/v) glucose and incubated at 30ºC overnight. Input and output titres of phage were performed by infecting TG1 *E. coli* cells and performing serial dilutions of the phage. The infected cells were incubated for 30 min at 37ºC and 100 μl of each dilution spread on 2xYT agar plates containing ampicillin (100 μg/ml) and 2% (w/v) glucose and incubated at 30ºC overnight. Alternatively, input phage titres were determined using an absorbance at 260 nm based method (Lee, Iorno et al. 2007). Precipitated input phage was diluted 50-fold in PBS and the OD_{260nm} measured. Using the empirical formula: phage ml^{-1} = OD_{260} x phage dilution x 22.14 x 10^{10} the phage titre was estimated (Lee, Iorno et al. 2007). The input and output titres were calculated by counting the number of cells present on the dilution plates. The stock plates containing the eluted phage were scraped using 2xYT media containing 20% (v/v) glycerol for the next cycle of panning. After the final round of panning individual ampicillin-resistant TG1 *E. coli* cells were used to inoculate 100 μl 2YT media containing ampicillin (100 μg/ml) and 2% (w/v) glucose in a sterile 96-well tissue culture plate (Falcon) and incubated at 37ºC overnight with shaking. Following incubation 30 μl 2xYT media containing 50% (v/v) glycerol was added to each well and stored at -80ºC until required for monoclonal phage ELISAs (master-plate).

[a]Subtractive panning on human primary cells: before selection on biotinylated pHLA the TCR-phage was subjected to a depletion step. The 1 ml blocked TCR-phage solution was used to resuspend ~2 x 10^6 HEP2 (human hepatocyte) or HDMEC3 (human microvascular endothelial) cells (kindly provided by Dr. N. Hassan). After 1 hour room temperature incubation with rotation the tubes were centrifuged at 3,360 g for 10 minutes at room temperature to remove the human cell pellet. [b]Off-rate selections: after 45 minutes incubation with biotinylated pHLA, 0.1-1 μM of nonbiotinylated pHLA (same antigenic identity as the biotinylated pHLA) was added and incubated for a further 15 minutes with rotation.

2.5.5 Phage ELISA - Monoclonal and inhibition

An ELISA plate was incubated with 100 μl streptavidin (5 μg/ml final; Sigma) overnight at 4ºC. All subsequent steps were performed at room temperature. The plate was washed 2 times with PBS, 100 μl biotinylated pHLA (5 μg/ml final) added and incubated for 30 minutes with shaking. After 3 washes with PBS the plate was blocked with 400 μl 3% (w/v) MPBS for 1 hour. In a separate sterile 96-well plate 70 μl phage supernatant[a] was mixed with 70 μl 6% (w/v) MPBS[b] and incubated for 1 hour with shaking. The blocked ELISA plate was washed 3 times with PBS and 100 μl blocked rescued monoclonal phage TCRs were added and the plate incubated for 1 hour with shaking. After incubation the plate was washed 3 times with PBST. After washing the wells 4 times with PBST, 100 μl of 1:1,000 dilution of a anti-M13 antibody (Sigma) in 1% (w/v) BSA-PBS was added and the plate incubated for 1 hour with shaking. After washing the wells 5 times with PBST, 100 μl of 1:15,000 dilution of a phosphatase-labelled anti-rabbit IgG monoclonal antibody (Sigma) in 1% (w/v) BSA-PBS was added and the plate incubated for 1 hour with shaking. Antigen-binding phage was detected using 100 μl BluePhos (KPL) as substrate for alkaline phosphatase. This solution was left to develop for 20-30 minutes and the absorbance was read at 650 nm.

[a]Phage: phage supernatant was used neat; PEG precipitated phage was first diluted in PBS before adding to 6% (w/v) MPBS. [b]Inhibition ELISA: nonbiotinylated pHLA was added to 6% (w/v) MPBS at a concentration that was twice the desired final concentration to account for the diluting effect from adding an equal volume of the phage solution.

2.6 Protein expression

2.6.1 Making chemically competent bacterial cells

Bacterial cells were streaked out onto an LB agar plate and incubated overnight at 37ºC. 200 ml of SOB media (supplemented with tetracycline Sigma, 12.5 μg/ml final

and 300 mM NaCl) was inoculated with a single colony and grown to an OD_{600} of ~0.4. Cells were pelleted by centrifugation at 3,360 x g for 10 minutes in a Heraeus Megafuge 2.0 R centrifuge at 4ºC. The pellet was resuspended in 68 ml of ice-cold FSB, pH 6.4 (10 mM KOAc, 44 mM $MnCl_2$, 100 mM KCl, 10 mM $CaCl_2$, 3 mM $HACoCl_3$ and 10% v/v glycerol) and incubated on ice for 15 minutes. After pelleting by centrifugation at 840 x g for 10 minutes at 4ºC, the bacterial cells were resuspended in 16 ml ice-cold FSB (containing 3.5% v/v DMSO; Sigma). Cells were then aliquoted into pre-chilled centrifugation tubes, snap frozen on dry-ice and stored at -80ºC.

2.6.2 Transformation of chemically competent *E. coli* cells

Aliquots of competent bacteria were thawed on ice. 100-200 ng of plasmid DNA (*E. coli* BL21-DE3 pLysS) or 10 µl ligation reaction mixture (*E. coli* XL1-Blue) was added to 100 µl thawed competent bacteria, incubated on ice for 20 minutes, before being transferred to 42ºC for 45 seconds and replaced on ice for 2 minutes. Following heat-shock, the cells were streaked out on LB agar plates supplemented with 100 µg/ml ampicillin and incubated overnight at 37ºC.

2.6.3 Cloning mutated Mel-5 TCR CDR3α chains into *E. coli* expression vector

The Mel-5 TCR CDR3α mutants (MELa1-MEL-a9) were amplified from the *E. coli* TG1 Pan 3 master-plate (Section 2.5.4) and the Mel-5 TCR CDR3α back-mutants (MELa1a-MELa1d) were amplified from *E. coli* expression vector pG161 (encoding MELa1) using the primers listed below:

Mel-5 TCR *E. coli* expression vector primers

TRAV12-2 5’-agatataatgcatgcaaaaagaagttgaacaaaattctggacccc-3’

SalI Rev	5’-ttgtcagtcgacttagagtctctcagctggtacacg-3’	
Nat102	5’-acgacccccaacgttcacggcacagaggtag-3’	MELalaR
Nat103	5’-gccgtgaacgttgggggtcgtcttacctttg-3’	MELalaF
Nat104	5’-aagacgacccgcatcgttcacggcacagagg-3’	MELalbR
Nat105	5’-cgtgaacgatgcgggtcgtcttacctttgggg-3’	MELalbF
Nat106	5’-aaaggtaagtttacccccatcgttcacggcac-3’	MELalcR
Nat107	5’-cgatgggggtaaacttacctttggggatggg-3’	MELalcF
Nat108	5’-cccaaaggtagaacgacccccatcgttcacg-3’	MELaldR
Nat109	5’-gggggtcgttctacctttggggatgggactac-3’	MELaldF
T7	5’-taatacgactcactataggg-3’	
OX281	5’-cagcaaaaaacccctcaag-3’	

MELa1-MELa9: 1 μl *E. coli* culture, 1 μl dNTPs (10 mM each), 1 μl TRAV12-2 (10 pmol/μl), 1 μl SalI Rev (10 pmol/μl), 5 μl 10 X polymerase buffer, 3.5 U Expand polymerase in a final volume of 50 μl. MELa1a-MELa1c: Fragment A: 5 ng pG161, 1 μl dNTPs (10 mM each), 1 μl T7 (10 pmol/μl), 1 μl [a]Reverse primer (10 pmol/μl), 5 μl 10 X polymerase buffer, 3.5 U Expand polymerase in a final volume of 50 μl. Fragment B: 5 ng pG161, 1 μl dNTPs (10 mM each), 1 μl [b]Forward primer (10 pmol/μl), 1 μl OX281 (10 pmol/μl), 5 μl 10 X polymerase buffer, 3.5 U Expand polymerase in a final volume of 50 μl.

[a]Reverse primer: Nat102, Nat104, Nat106, Nat108. [b]Forward primer: Nat103, Nat105, Nat107, Nat109. PCR amplification parameters followed those outlined in Section 2.3.2.

All PCR products were resolved by agarose gel electrophoresis and bands of the expected size were purified using the Zymoclean DNA gel recovery kit. MELa1a-MEa1c fragments A/B were assembled by SOE-PCR using 10 ng each of fragment A

and B, 1 μl dNTPs (10 mM each), 1 μl T7 (10 pmol/μl), 1 μl OX281 (10 pmol/μl), 5 μl 10 X polymerase buffer, 3.5 U Expand polymerase in a final volume of 50 μl and using PCR cycling parameters outlined in 2.3.2. DNA was resolved agarose gel electrophoresis and purified using the Zymoclean DNA gel recovery kit. Restriction enzymes *Cla*I-*Sal*I or *Xba*I-*Hind*III were used to digest fragments MELa1-a9 and MELa1a-MELa1d respectively. Vector pEX954 was separately digested with *Cla*I-*Xho*I and *Xba*I-*Hind*III 2 μg DNA, 20 U of the required enzymes and buffer in accordance with manufacturer's guidelines (NEB) in a final volume of 40 μl. Digestions were incubated at 37ºC for ~6 hours. Ligation reactions using appropriately digested (gel-purified) DNA insert and vector were set up using a 3:1 molar ratio of insert:vector (typically 100 ng insert DNA, 70 ng vector) as outlined in Section 2.3.5 and ligations were transformed into chemically competent XL1-Blue *E. coli* cells (as described in Section 2.6.2). Sequence-verified plasmid DNA was used to transform *E. coli* BL21-DE3 pLysS bacteria as described above.

2.6.4 Expression of TCR α and β chains in bacterial cell culture

A single colony from freshly transformed BL21 (DE3) pLysS bacteria was used to inoculate 10 ml TYP media supplemented with 100 μg/ml ampicillin and incubated for 4 hours at 37ºC with shaking. The 10 ml starter culture was used to inoculate 1 litre of TYP media supplemented with 100 μg/ml ampicillin and incubated for ~7 hours at 37ºC with shaking until the OD_{600} reached 0.6-1.0. Protein expression was induced by adding 0.5 ml 1 M isopropyl-1-thio-β-D-galactopyranoside (IPTG; Generon). The culture was incubated overnight at 37ºC with shaking. The following morning, the culture was pelleted at 3,360 x g for 30 minutes at 4ºC and the supernatant discarded.

2.6.5 Inclusion body preparation

The composition of all buffers is listed in Section 2.1.3. Inclusion bodies were purified from 1 litre IPTG-induced *E. coli* as follows. The bacterial pellet was resuspended in 40 ml lysis buffer supplemented 2 mM dithiothreitol (DTT; Sigma), DNAse (Sigma) to a final concentration of 0.2 mg/ml and 200 mM $MgCl_2$ and incubated at room temperature with mixing for 30 minutes. The bacterial suspension was transferred to a 50 ml centrifuge tube (Falcon) and subjected to 2-3 repeated freeze/thaw cycles. The bacteria was pelleted at 3,360 x g for 30 minutes at 4ºC and the supernatant discarded. Inclusion bodies were purified in 50 ml triton wash buffer supplemented with 2 mM DTT using a homogeniser to resolubilise the pellet. Inclusion bodies were pelleted at 3,360 x g for 30 minutes at 4ºC and the supernatant containing bacterial cell debris discarded. This step was repeated 2-3 times and the inclusion body pellet resuspended in 5 ml resuspension buffer supplemented with 2 mM DTT using a homogeniser.

2.6.6 Sodium dodecyl sulphate-polyacrylamide gel electrophoresis (SDS-PAGE)

Mel-5 TCR α chain inclusion bodies (MELa1a-MELa1c) were prepared for SDS-PAGE analysis as follows: 80 μl of purified inclusion bodies was pelleted, the supernatant discarded and then resuspended in 0.32 ml Laemmli sample buffer (Bio-rad) containing 5% β-mercaptothanol (Bio-rad). Refolded TCR samples collected from anion exchange and size exclusion chromatography were mixed at a ratio of 1:1 in Laemmli sample buffer with and without reducing agent. The inclusion body samples (5 μl and 10 μl) or refolded TCR anion exchange and size exclusion samples (15 μl) and molecular weight marker (Prestained SDS-PAGE marker, Bio-Rad) were loaded into separate wells of a Novex 4-20% Tris-Glycine SDS-PAGE gel

(Invitrogen). Gels were run at 200 volts for 1 hour and subsequently stained with Coomasie Blue staining solution (40% methanol (Fisher), 7% acetic acid (Sigma), 0.025% Brilliant Blue R (Sigma) for 1 hour with mixing. Gels were destained with destain solution (10% methanol, 10% acetic acid) for at least 1 hour with mixing.

2.6.7 Estimating protein concentration by UV spectrophotometry

Samples were diluted 1 in 100 in 6 M guanidine buffer (Section 2.1.3) for inclusion bodies and undiluted for refolded TCR proteins. Absorbance at 280 nm was measured using either 6 M guanidine buffer or PBS accordingly as reference blanks. Concentrations were calculated using the predetermined extinction coefficient values calculated from the amino acid sequence of the proteins using Vector NTI (Invitrogen).

2.6.8 Production of soluble Mel-5 TCRs

For the preparation of soluble TCRs, 15 mg of TCR α chain (MELa1a-MELa1c) and 7.5 mg of wild-type TCR β chain inclusion bodies were denatured in 10 ml 6 M guanidine buffer (Section 2.1.3) supplemented with 10 mM DTT at 37ºC for 30 minutes. Refolding was initiated by adding the denatured αβ chain mixture to 0.5 litre of pre-chilled TCR refold buffer (Section 2.3.1) and mixing vigorously for 2 hour at 4ºC. The refold solution was poured into 12 kDa dialysis tubing and dialysed against 20 litres of distilled H_2O overnight then 20 litres 10 mM Tris, pH 8.1 for 24 hours (with 2 changes of 10 mM Tris, pH 8.1). The refold was filtered through a 0.8 μM filter (Whattman) and loaded onto a Poros50HQ column equilibrated with 10 mM Tris, pH 8.1 and the protein eluted with a salt gradient (0-500 mM NaCl over 10 minutes/10 mM Tris, pH 8.1). After analysis of the eluted samples by SDS-PAGE, the fraction containing correctly folded TCR was purified by gel-filtration (size

exclusion) on a Superdex 75PG 26/60 (S75) column equilibrated with HEPES-buffered-saline-EP (HBS-EP, GE Healthcare) solution. HBS contains 10 mM HEPES (pH 7.4), 150 mM NaCl, 3.4 mM EDTA and 0.005% surfactant P20. Fractions containing correctly folded TCR, as checked by SDS-PAGE, were pooled and stored at 4ºC until required for biophysical analysis by surface plasmon resonance (SPR) using a BIAcore 3000. Production of all TCR α and β chains followed a similar method.

2.7 Surface plasmon resonance (SPR) kinetic studies

2.7.1 SPR equilibrium analysis

Streptavidin was covalently linked to Research Grade CM-5 sensor chips (BIAcore) via primary amines using the standard amino-coupling kit according to the manufacturer's instructions (BIAcore). Streptavidin was injected at 0.2 mg/ml in 10 mM sodium acetate (pH 4.5) until a saturation of response units (RU) was achieved. Biotinylated pHLA proteins were diluted to ~5 μg/ml and flowed over the relevant sensor flow cells at a flow rate of 10 μl/min. Approximately 1000 RU of pHLA ligand were bound to each flow cell. TCRs were concentrated to approximately 5 to 10-fold above the expected K_D. Ten serial doubling dilutions of TCR were prepared and injected (5 μl/min) over the relevant flow cells at 25ºC and the response values at equilibrium for each protein concentration measured using the BIAevaluation 3.1 software. Using Origin 6.1 software the equilibrium binding constant (K_D) values were determined using a non-linear curve fit ($y = (P_1 x)/(P_2 + x)$).

2.7.2 SPR kinetic analysis

Chip and reagent preparation was the same as for equilibrium analysis. Flow cells were coated with ~100 RU of pHLA ligand. TCRs were concentrated to

approximately 5 to 10-fold above the expected K_D and were flowed over the sensor surface at 50 μl/min in a total volume of 300 μl using a kinetic injection. Kinetic binding parameters K_{on} and K_{off} were determined assuming 1:1 Langmuir binding using BIAevaluation 3.1 software.

ENGINEERING FOR HIGH AFFINITY A CLASS I HLA-A2 RESTRICTED T CELL RECEPTOR AGAINST THE MELAN-A/MART-1$_{(26-35)}$ TUMOUR ASSOCIATED ANTIGEN BY PHAGE DISPLAY

3.1 Introduction

This chapter describes in detail the processes involved in engineering TCRs for high affinity through directed molecular evolution using phage display. The chapter is divided into three principal sections: (1) isolating high affinity TCRs from first generation phage display libraries; (2) identifying a suitable clone from the first generation libraries on which to build subsequent libraries; (3) isolating high affinity TCRs from second generation libraries.

In this chapter, the affinity maturation of the Mel-5 TCR that recognises the melanoma-specific epitope derived from Melan-A/MART-1_{26-35} (Kawakami, Eliyahu et al. 1994) will be described. The Mel-5 TCR was isolated from a Melan-A-specific $CD8^+$ T cell clone that recognises the ELAGIGILTV peptide in complex with HLA-A*0201 and was kindly provided by Andy Sewell (Cardiff University, UK) (Cole, Yuan et al. 2009). The wild-type Mel-5 TCR binds to HLA-A*0201-Melan-A/MART-1_{26-35} with an affinity of 18 μM as determined by surface plasmon resonance (SPR) equilibrium binding measurements (Cole, Pumphrey et al. 2007).

Affinity maturation of the Mel-5 TCR involved targeted mutagenesis of each of the six CDR loops using degenerative NNK oligonucleotides. Mutated TCR chains were expressed on the surface of bacteriophage as fusions to the phage coat protein pIII to facilitate selection on soluble pHLA antigen. Enrichment for enhanced-affinity clones was measured by phage inhibition ELISA. Affinity maturation of the Mel-5 TCR required the construction of second generation libraries, using as template an improved affinity clone from the first generation libraries. The CDR-walking mutagenesis approach which has been successfully used for the affinity maturation of antibodies was adopted here to isolate mutations in further CDRs (Yang, Green et al. 1995; Schier, McCall et al. 1996).

3.2 Design and construction of first generation Mel-5 TCR libraries

3.2.1 Cloning the wild-type Mel-5 TCR into the phagemid vector

The phagemid/helper phage system was used to isolate high affinity TCRs. Unlike in a phage vector system where recombinant protein is expressed as fusion proteins to all 5 copies of pIII, in the phagemid vector system only 1 to 3 copies of recombinant protein are displayed. Whereas a phage vector system, through multivalent display, supports the selection of low-affinity binders, the phagemid vector system encourages the enrichment for high affinity binders through, predominantly, monovalent display.

Although scFvs have been successfully engineered by phage display, the phage display of scTCRs has proved more challenging (probably due to problems of folding) (Weidanz, Card et al. 1998). We hypothesised that the introduced inter-chain ds-bond at the constant region interface would overcome these folding problems and facilitate the display of full-length TCR on the phage surface.

The phagemid vector pG125 for the phage display of the Mel-5 TCR was constructed by splicing by overlap extension PCR (SOE-PCR) as described in Section 2.3 of Materials and Methods. A four-way PCR stitch product was assembled as follows: the TCR Vα domain (TRAV12-2, nomenclature according to (Lefranc, Giudicelli et al. 1999)) was amplified from the *E. coli* expression vector pG190 (cloned by E. Gostick) containing the TCR α chain with forward primer Nat22 (to introduce an *Nco*I restriction site) (Section 2.3.1 of Materials and Methods) and reverse primer YOL237 to generate fragment A; TCR Cα plus the bacteriophage geneIII leader sequence was amplified from the phagemid vector, pEX922 (pLitmus 28a, based on pUC19 phagemid vector containing the α and β A6 TCR genes) (Li, Moysey et al. 2005) with forward primer YOL236 and reverse primer YOL238 to generate fragment C; the TCR Vβ (TRBV30, nomenclature according to (Lefranc,

Giudicelli et al. 1999) was amplified from the *E. coli* expression vector pG176 (cloned by E. Gostick) containing the TCR β chain with forward primer J185 and reverse primer YOL240 to generate fragment B; TCR Cβ plus ~200 base pairs (bp) of bacteriophage geneIII was amplified from pEX922 with forward primer YOL239 and reverse primer YOL22 to generate fragment D (encoding a *Not*I site). The TCR α and β constant regions include the introduced cysteines at position TRAC threonine 48 and TRBC serine 57 (Boulter, Glick et al. 2003). The PCR fragments were resolved on a 1.6 % (w/v) agarose gel (Figure 3.1 A). The fragments migrated to the expected sizes: PCR fragment A ~390 base pairs (bp); fragment B ~450 bp; fragment C ~370 bp; fragment D ~550 bp. A four-way SOE-PCR was performed with equimolar amounts of purified fragments A, B, C and D and amplified with external primers Nat22 and YOL22 to generate the desired ~1700 bp fragment (Figure 3.1 B).

A.

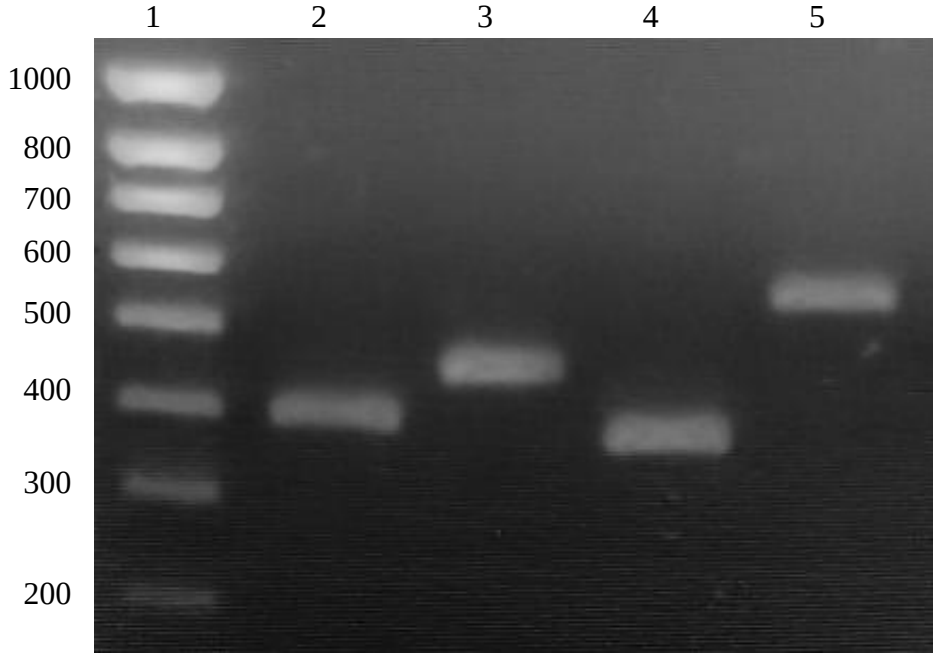

B.

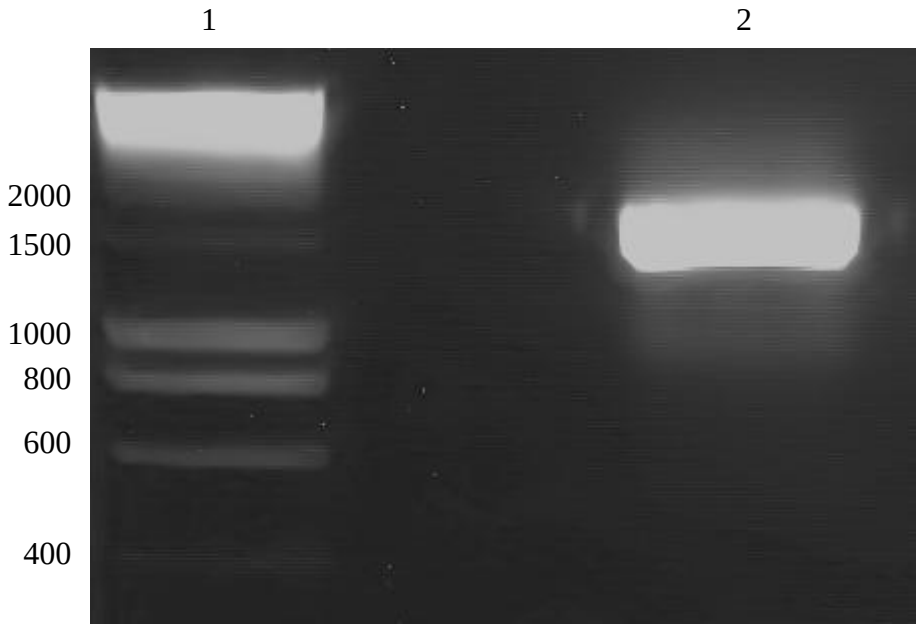

Figure 3.1. Generating the wild-type Mel-5 TCR PCR fragment for cloning into the phagemid vector. (A). Photo of ethidium bromide agarose gel electrophoresed wild-type Mel-5 TCR PCR products were gel-purified and 1 μl loaded onto a 1.6 % (w/v) agarose gel for quantitation. Lane 1, Hyperladder (HYP) IV size of bands in bp; lane 2, PCR fragment A; lane 3, fragment B; lane 4, fragment C; lane 5, fragment D. **(B).** Ethidium bromide stained agarose gel photo of the PCR-assembled Mel-5 wt TCR. A four-way SOE-PCR was set up with equimolar amounts of each of the fragments (A-D). Lane 1, HYP I; lane 2, assembled PCR product (A/B/C/D). Stitch PCR was resolved on a 1 % (w/v) agarose gel.

Both the PCR-assembled full-length Mel-5 TCR fragment and the phagemid vector, pEX922 (containing a human αβ TCR) were digested with the restriction enzymes *Nco*I and *Not*I and resolved on a 1.4 % (w/v) agarose gel (Figure 3.2 A). Digestion of the pEX922 vector excised a ~1500 bp fragment corresponding to a full-length αβ TCR. The upper band, equating to the linearised phagemid vector was gel-purified. Digestion of the Mel-5 TCR stitch PCR product generated two fragments: one of ~1500 bp, corresponding to the Mel-5 TCR fragment and one of ~200 bp, corresponding to the *Not*I-YOL22 fragment. Following gel-purification, 1 μl of each digested DNA fragment was resolved on a 1.2 % (w/v) agarose gel for quantitation (Figure 3.2 B). Using a molar ratio of 1:3 of vector:insert and T4 ligase, the Mel-5 αβ TCR fragment was ligated into pEX922.

A.

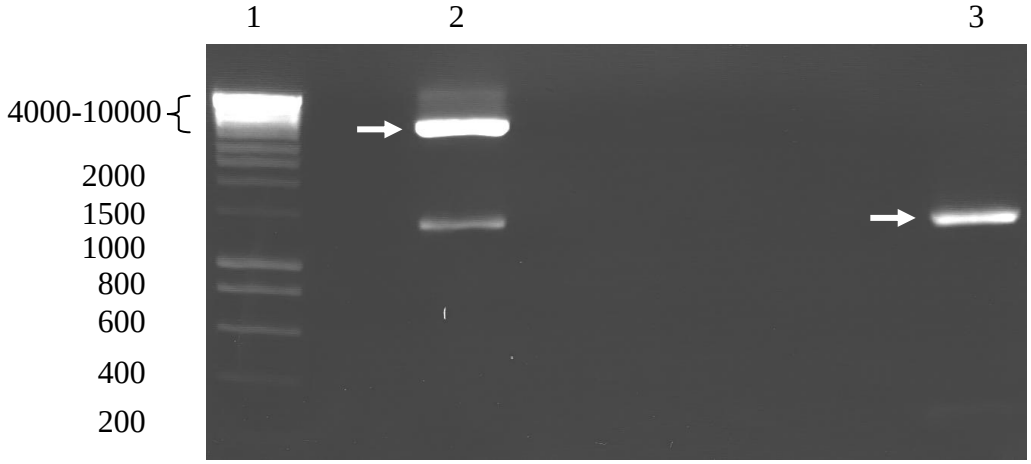

B.

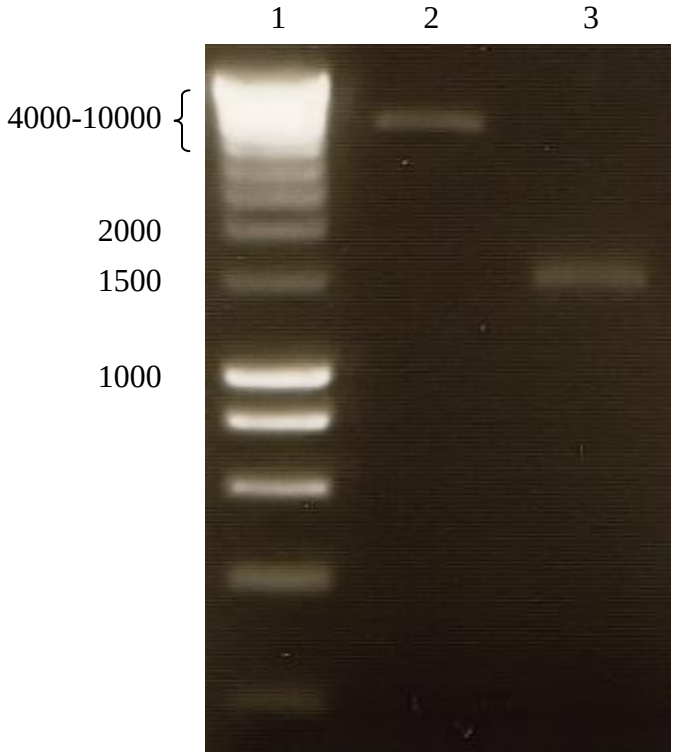

Figure 3.2. Generating the digested Mel-5 wild-type TCR PCR fragment and phagemid vector. (A). Ethidium bromide stained agarose gel photo of the *Nco*I-*Not*I digested Mel-5 TCR PCR and phagemid vector, pEX922. Lane 1, HYP I; lane 2, *Nco*I-*Not*I digest of pEX922 vector; lane 3, *Nco*I-*Not*I digest of the Mel-5 TCR PCR fragment. The high molecular weight band for both digests (indicated with an arrow) was excised and gel-purified. **(B).** Ethidium bromide stained agarose gel photo of gel-purified *Nco*I-*Not*I digested Mel-5 TCR PCR and pEX922. Lane 1, HYP I; lane 2, *Nco*I-*Not*I pEX922 vector fragment; lane 3, *Nco*I-*Not*I Mel-5 αβ TCR fragment.

Following transformation of chemically-competent *E. coli* XL1-Blue cells, DNA from ampicillin-resistant colonies was isolated and sequenced with primers YOL13 and YOL22 (Figure 3.4). Figure 3.3 shows the DNA and protein sequence of the Mel-5 TCR cloned into the phagemid vector, named pG125. The Mel-5 TCR α chain V domain is encoded by TRAV12-2*01 and TRAJ27*01 gene segments. The Cα region is encoded by the TRAC*01 gene segment (International Immunogenetics (IMGT) nomenclature (Lefranc, Giudicelli et al. 1999)). The Mel-5 TCR β chain V domain is encoded by TRBV30, TRBJ2-2*01 and TRBD1*01 gene segments. The Cβ region is encoded by the TRBC1*01 gene segment. The locations of the six CDR loops are highlighted.

In the final pG125 construct, the TCR α chain contains the engineered ds-bond mutation and is truncated N-terminal of the natural membrane-proximal cysteine. The TCR β chain contains the ds-bond mutation and is truncated at the equivalent position. The 3' end of the β chain is fused in frame to the 5' end of the geneIII coat protein of bacteriophage M13. The pelB and geneIII leader sequences are fused to the 5' end of the α and β chains, respectively, and expression of both chains is under the control of the same *lacZ* promoter (Figure 3.4 A). Figure 3.4 B illustrates the location of the primers and restriction sites used for cloning the mutagenic libraries into the phagemid vector pEX922.

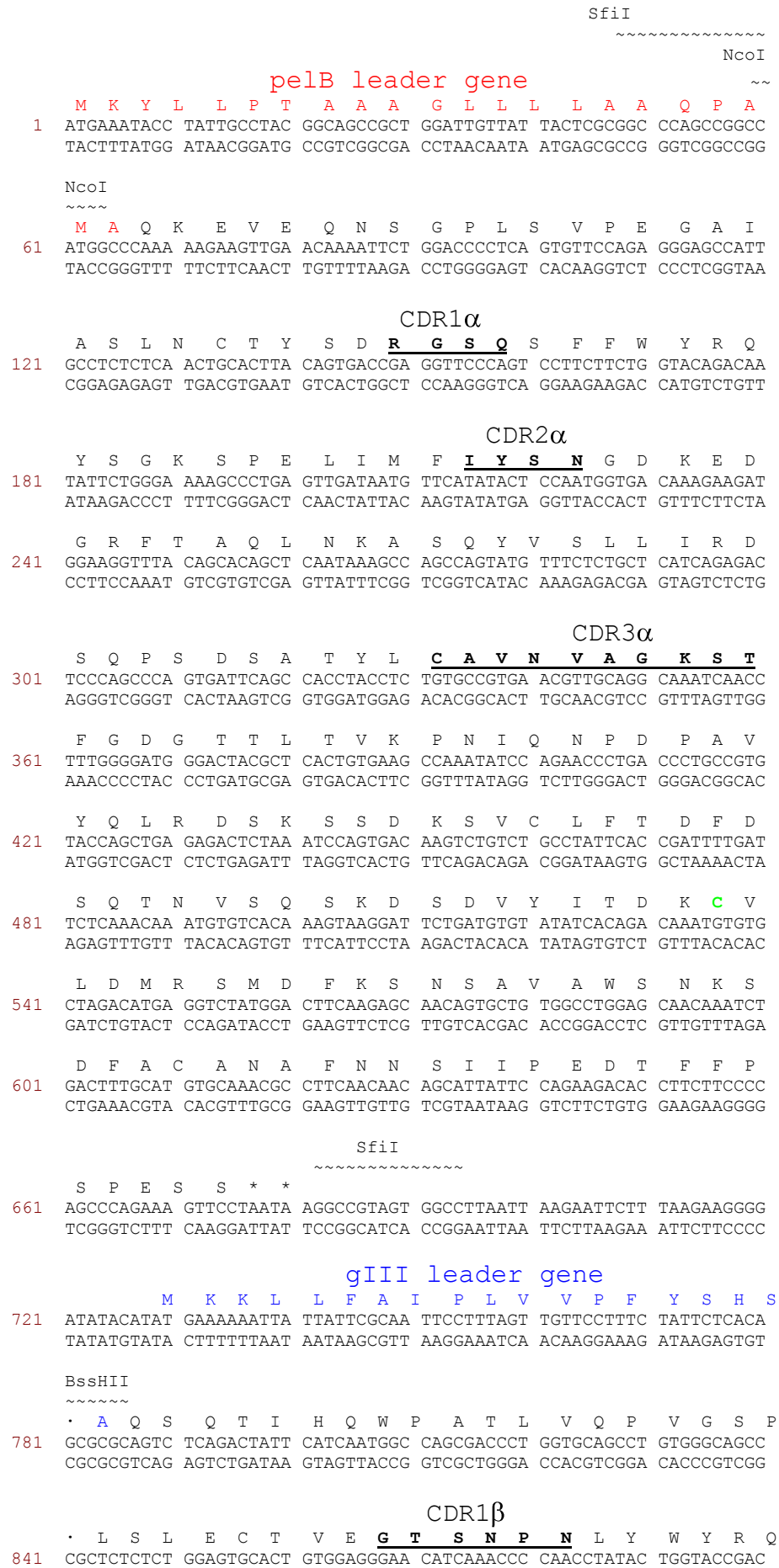
SfiI
NcoI
pelB leader gene
NcoI
CDR1α
CDR2α
CDR3α
SfiI
gIII leader gene
BssHII
CDR1β

Figure 3.3. Sequence of Mel-5 wild-type TCR cloned into the phagemid vector pEX922. The amino acid residues encoding the pelB and bacteriophage M13 geneIII leader genes are highlighted in red and blue respectively. The six CDR loops, designated by the International Immunogenetics (IMGT) database (Lefranc, Giudicelli et al. 1999), are in bold and underlined. The TCR membrane-proximal cysteines in both the α and β chains have been removed. The introduced TCR stabilising constant region cysteines (at positions TRAC Thr 48 and TRBC Ser 57) are highlighted in green. The restriction enzyme sites used for molecular cloning are highlighted (*Nco*I, *Sfi*I, *BssH*II and *Not*I). Asterisks show the location of stop codons including an amber codon (TAG) at the C-terminus of the beta chain. In suppressor (*sup*E) strains of *E. coli* such as TG1 cells (as used in this work) protein translation continues through amber codons (at a reduced efficiency) with substitution of Gln. The TCR is linked to the hexahistidine tag. The sequence was analysed with Vector NTI Advance 11 (Invitrogen).

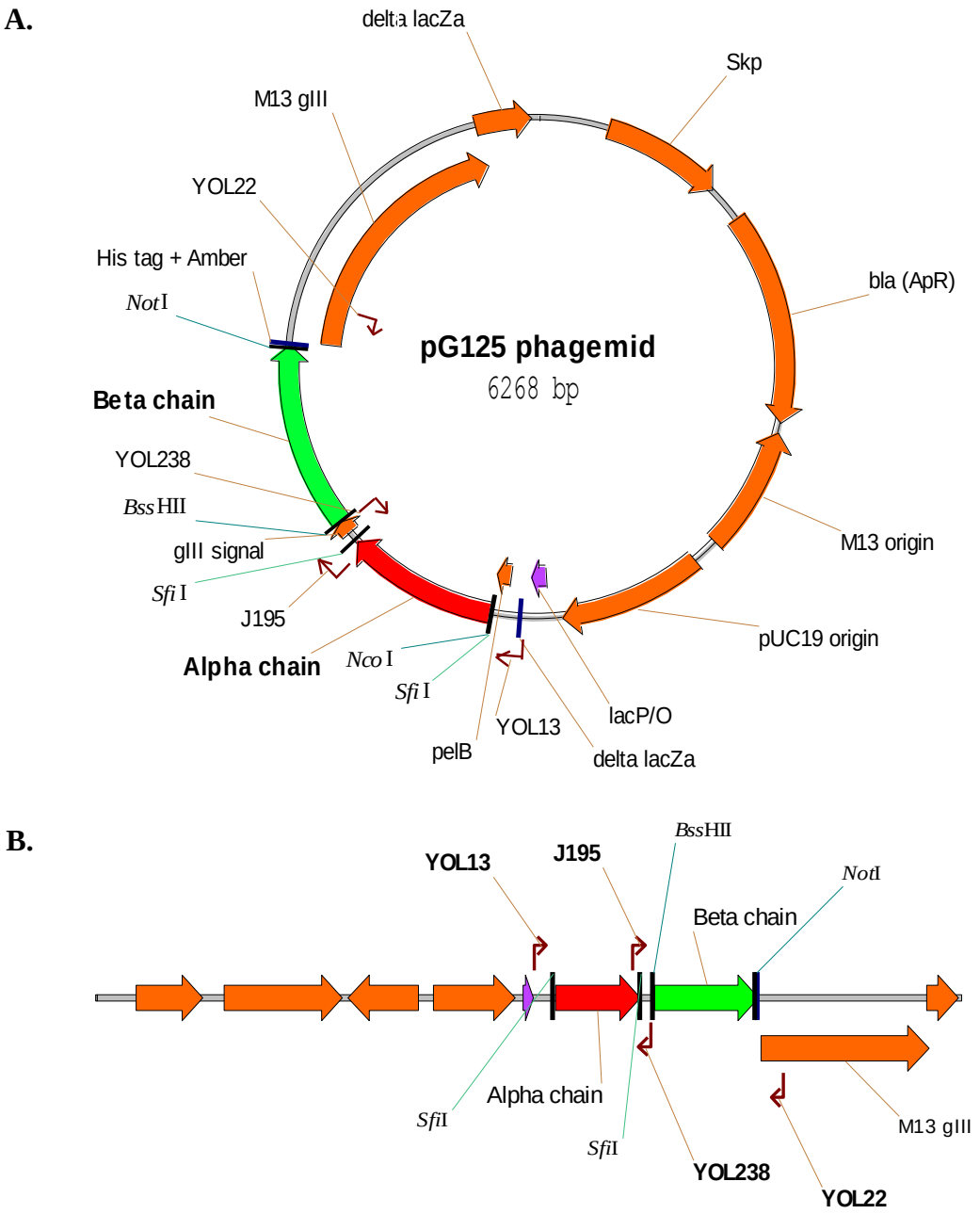

Figure 3.4. Map of phagemid vector pG125, for the construction of Mel-5 TCR phage display libraries. (A). Circular display. The vector encodes the Mel-5 TCR α and β chains (VαCα/VβCβ). The C-terminal end of the β chain is fused to the N-terminus of bacteriophage protein III (pIII). Transcription is under the control of the *lacZ* promoter. The vector includes both an *E. coli* (pUC19) and bacteriophage (M13) origin of replication to allow amplification in *E. coli* and phage. Other features include an ampicillin resistance gene, used for selection and maintenance of the plasmid and the gene encoding folding assistance chaperone Skp. The pelB and geneIII signal peptides direct the α and β chain-gIII fusion to the periplasm (respectively). The TCR genes are cloned between SfiI and NotI for display on the phage coat protein, pIII. **(B).** Linear display. The location of the oligonucleotides YOL13, YOL238, J195 and YOL22 used for construction of the alpha and beta chain libraries are highlighted. An amber codon is located between the His-tag and geneIII. The vector maps were constructed with Vector NTI Advance 11.

3.2.2 Generating library PCR fragments

Libraries were assembled in which each of the six CDRs were individually targeted for mutagenesis producing TCRs with one wild-type and one mutated chain. The PCR strategy that outlines the construction of the Mel-5 TCR libraries is shown in Figure 2.1 of Materials and Methods. Using pG125 as the template, PCR fragments were generated to flank each of the CDR regions to be mutated. A mutagenic primer was then designed which had four (for the CDR1 and CDR2 loops) and five codons (for the CDR3 loops) mutated with the NNK motif but also containing overlapping regions to allow stitching to the two flanking PCR fragments.

Although the crystal structure of the Mel-5 TCR in complex with HLA-A*0201-Melan-A/MART-$1_{(26-35)}$ has since become available (Cole, Yuan et al. 2009), this information was not available at the time of library construction. Therefore, overlapping mutagenic primers were designed to span the entire length of each CDR. For the CDR3 loops, the NNK motif was shifted every two residues to ensure complete coverage. The number of mutagenic primers was determined by the length of the CDR. The primers used for mutagenising the TCR chains are shown in Section 2.4.1 of Materials and Methods. Following PCR amplification of the 24 initial fragments, 20 Units of *Dpn*I endonuclease was added to digest methylated bacterial double-stranded DNA. This step reduced the level of bacterial template DNA, present in the PCR product, that could be co-purified with the PCR fragments. After a 2-hour incubation at 37 ºC, each fragment was analysed by agarose gel electrophoresis. In general, the α chain segments amplified equally, with the exception of PCRa5 which yielded substantially more product (Figure 3.5 A). The YOL22-amplified β chain segments produced a high yield of product, with PCRb15 being the exception (Figure 3.5 B). The yield of the J195-amplified product varied.

A.

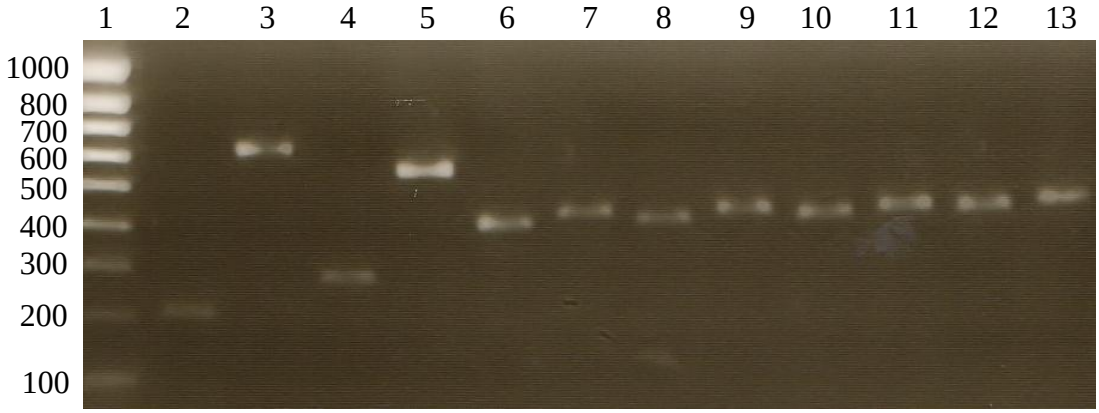

B.

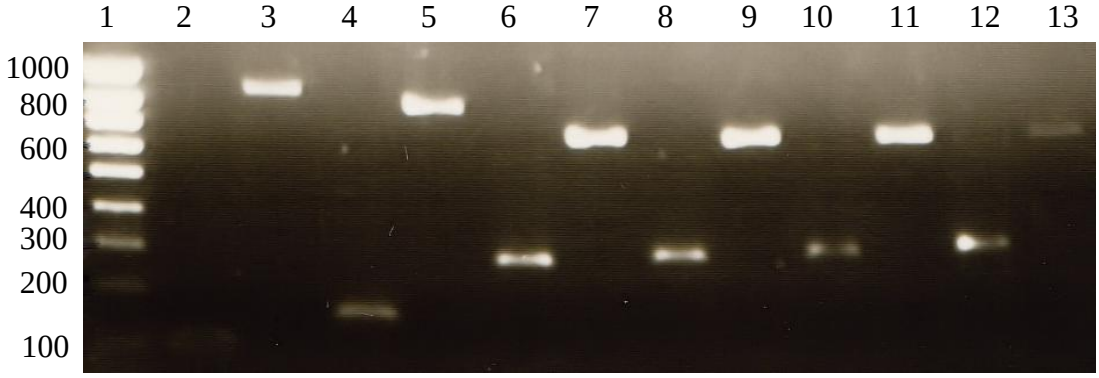

Figure 3.5. Agarose gel photo of gel-purified Mel-5 TCR PCR fragments. (A). α chain PCR fragments (1 μl of each). Lane 1, HYP IV; lane 2, PCR a1; lane 3, PCR a2; lane 4, PCR a4; lane 5, PCR a5; lane 6, PCR a7; lane 7, PCR a8; lane 8, PCR a10; lane 9, PCR a11; lane 10, PCR a13; lane 11, PCR a14; lane 12, PCR a16; lane 13, PCR a17. **(B).** β chain PCR fragments (1 μl of each). Lane 1, HYP IV; lane 2, PCR b1; lane 3, PCR b2; lane 4, PCR b4; lane 5, PCR b5; lane 6, PCR b7; lane 7, PCR b8; lane 8, PCR b10; lane 9, PCR b11; lane 10, PCR b13; lane 11, PCR b14; lane 12, PCR b16; lane 13, PCR b17.

3.2.3 Generating full-length α and β chain library PCR fragments

The gel-purified PCR fragments (10-12 ng total DNA) (Figure 3.5 A and 3.5 B) and the mutagenic NNK primer (1 pM) were assembled into a three-way PCR stitch reaction which generated a full length PCR fragment suitable for cloning into the phage display in vector (Section 3.4.1.2 of Materials and Methods). The 3' ends of the black fragment is complimentary to the 5' ends of the NNK primer and the 3' ends of this DNA linker was complimentary to the 5' ends of the red fragment (Figure 2.1 of Materials and Methods).

Whilst a single 4-NNK mutagenic primer was sufficient to randomise all positions of the CDR1 and CDR2 loops, four 5-NNK primers were required to randomise the CDR3 loops of both α and β chains. In addition to the test PCRs, PCRs were also set up to control for non-mutagenised background amplification of the template vector in which the NNK primer was omitted from the PCR mix. This meant for each SOE-PCR, an additional (control) PCR was also prepared; this was identical except for the omission of the NNK primer. To assess amplification of parental DNA, 5 μl of each PCR was resolved on a 1% (w/v) agarose gel (Figure 3.6 A and 3.6 B). Amplification of mutagenised α chain segments with primers YOL13 and YOL238 (Section 2.3.1 in Materials and Methods) yielded a product of ~850 bp. Amplification of mutagenised β chain segments with primers J195 and YOL22 produced a product of ~1100 bp. Amplification of full-length α and β gene segments yielded a significant amount of product compared to the control reactions. The remainder of each test PCR was analysed by agarose gel electrophoresis and DNA bands of the desired size were gel-purified (Figure 3.6 C).

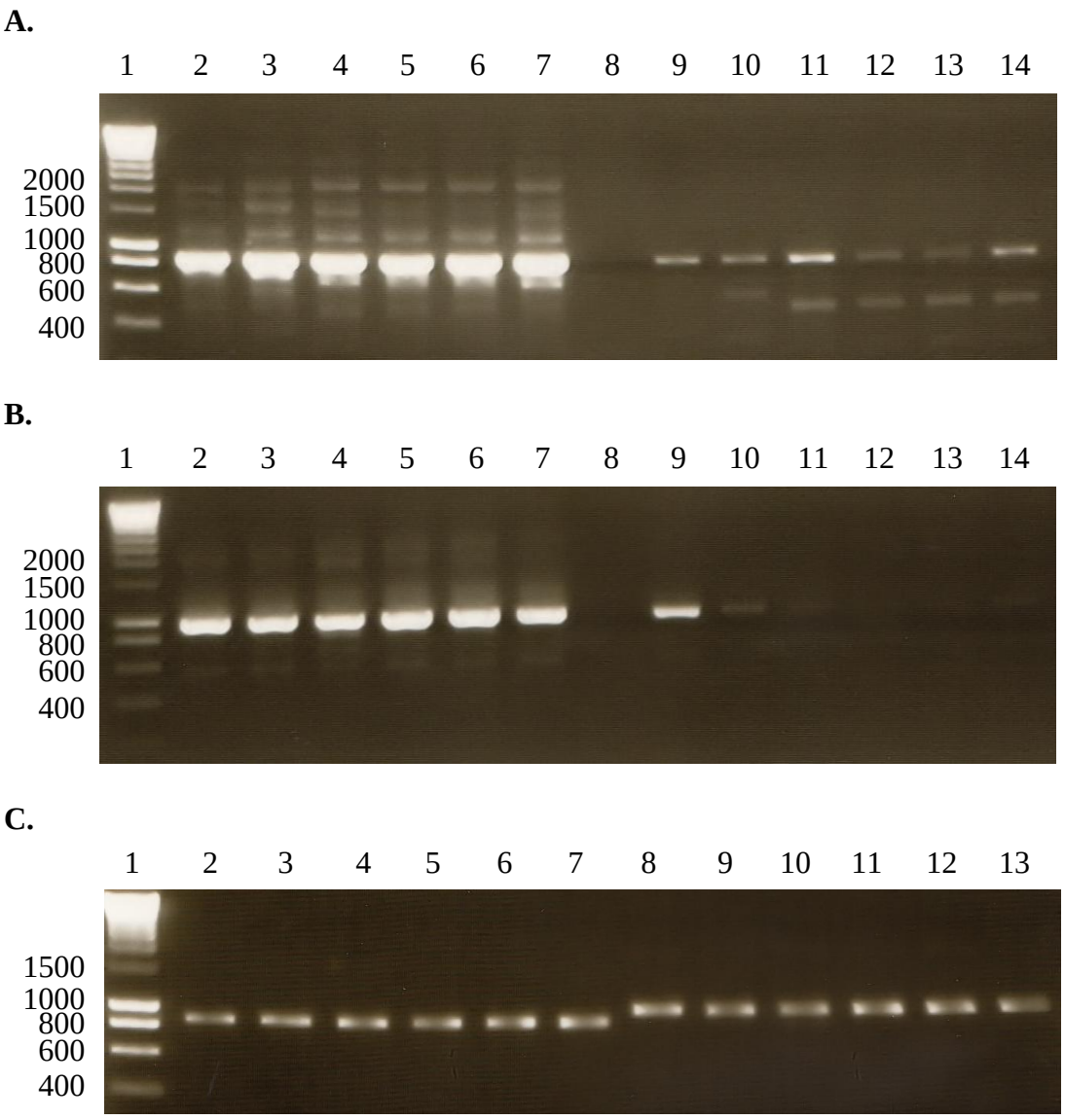

Figure 3.6. Agarose gel photos of overlapping stitch Mel-5 TCR library PCR fragments. (A). α chain PCR test and control reactions. Lane 1, HYP I; lane 2, PCR a1 + a2 + NNK primer; lane 3, PCR a4 + a5 + NNK primer; lane 4, PCR a7 + a8 + NNK primer; lane 5, PCR a10 + a11 + NNK primer; lane 6, PCR a13 + a14 + NNK primer; lane 7, PCR a16 + a17 + NNK primer; lane 8, no sample; lane 9, PCR a1 + a2 - NNK primer; lane 3, PCR a4 + a5 - NNK primer; lane 4, PCR a7 + a8 - NNK primer; lane 5, PCR a10 + a11 - NNK primer; lane 6, PCR a13 + a14 - NNK primer; lane 7, PCR a16 + a17 - NNK primer. **(B).** β chain PCR test and control reactions. Lane 1, HYP I; lane 2, PCR b1 + b2 + NNK primer; lane 3, PCR b4 + b5 + NNK primer; lane 4, PCR b7 + b8 + NNK primer; lane 5, PCR b10 + b11 + NNK primer; lane 6, PCR b13 + b14 + NNK primer; lane 7, PCR b16 + b17 + NNK primer; lane 8, no sample; lane 9, PCR b1 + b2 - NNK primer; lane 3, PCR b4 + b5 - NNK primer; lane 4, PCR b7 + b8 - NNK primer; lane 5, PCR b10 + b11 - NNK primer; lane 6, PCR b13 + b14 - NNK primer; lane 7, PCR b16 + b17 - NNK primer. **(C).** Gel-purified α and β chain stitch library PCR fragments. Lane 1, HYP I; lane 2, PCR a3; lane 3, PCR a6; lane 4, PCR a9; lane 5, PCR a12; lane 6, PCR a15; lane 7, PCR a18; lane 8, PCR b3; lane 9, PCR b6; lane 10, PCR b9; lane 11, PCR b12; lane 12, PCR b15; lane 13, PCR b18.

3.2.4 Generating bacterial libraries

The gel-purified library SOE-PCR products were subsequently digested with *Sfi*I for the six α chain segments (PCR a3, a6, a9, a12, a15 and a18) and *Bss*HII-*Not*I for the six β chain segments (PCR b3, b6, b9, b12, b15 and b18) (Section 2.4.1.3 of Materials and Methods). To reduce the level of background of non-recombinant clones, the vector and insert fragments were over-digested with five times the recommended amount of restriction enzymes. Gel-purified digested PCR fragments were analysed by agarose gel electrophoresis (Figure 3.7). Digesting the stitch PCRs removed ~200 bp from the α fragments and ~350 bp from the β fragments to yield fragments of the expected size; ~650 bp for the α chains and ~750 bp for the β chains.

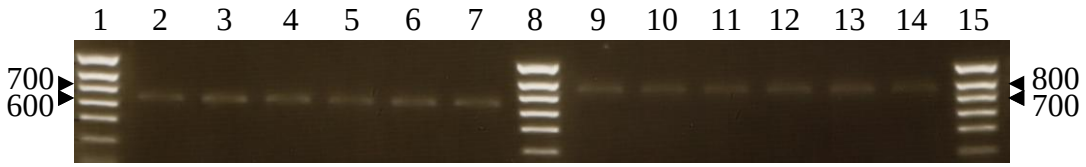

Figure 3.7. Agarose gel photo of gel-purified digested stitch Mel-5 TCR library PCRs. Lane 1, HYP IV; lane 2, PCR a3; lane 3, PCR a6; lane 4, PCR a9; lane 5, PCR a12; lane 6, PCR a15; lane 7, PCR a18; lane 8, Hyperladder IV; lane 9, PCR b3; lane 10, PCR b6; lane 11, PCR b9; lane 12, PCR b12; lane 13, PCR b15; lane 14, PCR b18; lane 15, Hyperladder IV.

To monitor the efficiency of vector and insert digests, a pilot ligation was set up for each of the twelve SOE-PCR library products using a scaled down amount of DNA (~80 ng total DNA) (Section 2.4.1.4 Materials and Methods). Transformation of *E. coli* XL1-blue cells yielded an acceptably low level of background for the vector

only control (1-20%) and so, large scale ligations were prepared (5-7 μg total DNA per ligation). Each of the twelve SOE-PCR products were ligated separately into pG125 (with T4 DNA ligase) as *Sfi*I fragments for the TCR CDRα mutated libraries and as *Bss*HII-*Not*I digested fragments for the CDRβ mutated libraries (Section 2.4.1.4 of Materials and Methods). This generated libraries in which only one of the two TCR chains was mutated in a single construct; mutated TCR α chain libraries were spliced with the wild-type TCR β chain and, conversely, mutated TCR β chain libraries were spliced with the wild-type TCR α chain.

NNK degeneracy allows for the substitution of all 20 amino acids encoded by 32 codons. The theoretical protein diversity of a library with four residues fully randomised (as in the CDR1 and CDR2 libraries) is 20^4 = 1.6 x 10^5 and for five residues it is 20^5 = 3.2 x 10^6. The CDR3 loops are mutated by four 5-NNK oligonucleotides and so the theoretical protein diversity is 4 x (20^5) = 1.28 x 10^7. TG1 electrocompetent *E. coli* cells were transformed with 200-300 ng of each of the twelve ligated DNA products to generate libraries of approximately 0.4 to 1 x 10^8 clones (Section 2.4.1.4 of Materials and Methods). Libraries having this diversity are therefore theoretically sufficient to encompass the entire repertoire of potential mutations.

Library integrity was assessed by DNA sequence analysis. Randomly selected colonies were PCR amplified with primers YOL13 and YOL22; four colonies were analysed for the CDR1α and CDR2α libraries and ten colonies analysed for the CDR3α library. Similarly, four colonies were analysed for the CDR1β (although one of the sequences was of poor quality and is not shown) and CDR2β libraries and ten colonies analysed for the CDR3β library. Sequence analysis of each library revealed a broad diversity of mutations spanning each of the targeted CDRs (Table 3.1 A and 3.1

B). Additionally, but equally important, the TCR fragments were all in-frame. A number of the clones (CDR2α-1, CDR3α-4 and CDR3α-7) contained an amber codon and were translated as Gln in suppressor strains of *E. coli* (such as TG1). As a result the library size and diversity was not compromised by their inclusion. Amber codons probably occur when a higher expression level of certain TCRs is toxic for bacteria.

A.

	CDR1α$_{(R28\text{-}Q31)}$
CDR1α_wt	R G S Q cgaggttcccag
CDR1α_1	**N I H G** aatattcatggt
CDR1α_2	**S R Y G** tcgcgttatggg
CDR1α_3	**W X A H** tggnaggctcat
CDR1α_4	**S** G S **S** tctggttcgtct

	CDR2α$_{(I50\text{-}N53)}$
CDR2α_wt	I Y S N atatactccaat
CDR2α_1	**W T *Q* C** tggacgtagtgt
CDR2α_2	**G P G L** ggtcctggtttg
CDR2α_3	**A G L E** gctggtctggag
CDR2α_4	**G G N L** gggggtaatctg

	CDR3α$_{(A90\text{-}T98)}$
CDR3α_wt	A V N V A G K S T gccgtgaacgttgcaggcaaatcaacc
CDR3α_1	**G T G I W** G K S T gggacgggtatttggggcaaatcaacc
CDR3α_2	**S L K G G** G K S T tctttgaagggtgggggcaaatcaacc
CDR3α_3	A **P G R L** G K S T gcgccgggggggcttggcaaatcaacc
CDR3α_4	**V T T G *Q*** G K S T gttactactgggtagggcaaatcaacc
CDR3α_5	A **W P G G** G K S T gccactgctgggtagggcaaatcaacc
CDR3α_6	A **F A C C P** K S T gcctgtgcgtgttgtcctaaatcaacc
CDR3α_7	A **H I N L *Q*** K S T gcccatgttcatctttagaaatcaacc
CDR3α_8	A V N **P D I G V** T gccgtgaacccngatattggggttacc
CDR3α_9	A V N V **R K M I V** gccgtgaacgttcggaagatgattgtg
CDR3α_10	A V N V **I V G R P** gccgtgaacgttattgtgggtaggcct

B.

	CDR1β$_{(T28\text{-}P31)}$
CDR1β_wt	T S N P
	acatcaaacccc
CDR1β_1	**G A A G**
	ggtgctgcgggt
CDR1β_2	**W V G G**
	tgggttgggggg
CDR1β_3	T **Y F** P
	acttattttcct

	CDR2β$_{(V51\text{-}G54)}$
CDR2β_wt	V G I G
	gttggtattggc
CDR2β_1	**H A S L**
	catgcttcgttg
CDR2β_2	**T L W V**
	actttgtgggtg
CDR2β_3	**I T A F**
	attactgctttt
CDR2β_4	**S A K F**
	agtgcgaagttt

	CDR3β$_{(A92\text{-}L103)}$
CDR3β_wt	A W S E T G L G T G E L
	gcctggtccgagacagggttaggcaccggggagctg
CDR3β_1	***Q*** **V** ***Q*** **A V** G L G T G E L
	taggtgtaggcggttgggttaggcaccggggagctg
CDR3β_2	**G H V R R** G L G T G E L
	gggcatgtgaggaggggttaggcaccggggagctg
CDR3β_3	A W **W F A P C** G T G E L
	gcctggtggtttgctccgtgtggcaccggggagctg
CDR3β_4	A W **N L F L** L G T G E L
	gcctggaatctttttctttgggcaccggggagctg
CDR3β_5	A W S E **N T V V** T G E L
	gcctggtccgagaatactgttgttactggggagctg
CDR3β_6	A W S E **F N R E R** G E L
	gcctggtccgagtttaatcgggagcgggggagctg
CDR3β_7	A W S E **L R A L F** G E L
	gcctggtccgagctgagggcgctgttcggggagctg
CDR3β_8	A W S E T G L **W D S G S**
	gcctggtccgagacagggttatgggattcggggtcg
CDR3β_9	A W S E T G L **S M Q Y N**
	gcctggtccgagacagggttaagtatgcagtataat
CDR3β_10	A W S E T G L **F H V I C**
	gcctggtccgagacagggttatttcatgttatttgt

Table 3.1. Sequence analysis of Mel-5 TCR phage display NNK libraries. (A). Alpha chain libraries: CDR1α, CDR2α and CDR3α. **(B).** Beta chain libraries: CDR1β, CDR2β and CDR3β. Nucleotides marked with an "n" and amino acid residue marked with an "X" are undefined because the DNA sample is mixed and contains more than one DNA template. Amino acids that differ from wild-type are highlighted in red. Nucleotides that differ from wild-type are highlighted in blue. *Q*, Amber codon. wt, wild-type. International Immunogenetics (IMGT) nomenclature (Lefranc, Giudicelli et al. 1999).

3.3 Phage selections and screening

Phage was separately prepared from each of the twelve *E. coli* TG1 transformations as described in Section 2.5.1 and 2.5.2 of Materials and Methods and then pooled into four libraries for panning: (1) CDR1α (SOE-PCR 3a) + CDR2α (6a); (2) CDR3α (9a + 12a + 15a + 18a); (3) CDR1β (3b) + CDR2β (9a); (4) CDR3β (9b + 12b + 15b + 18b) (Table 3.1). Briefly, 50 mL of 2xYT growth media supplemented with ampicillin (100 μg/ml final concentration) and 2% glucose (w/v) was inoculated separately with each of the twelve *E. coli* TG1 bacterial glycerol stocks to an OD_{600} of 0.05-0.08. The 12 cultures were incubated at 37°C with shaking until an of OD_{600} 0.3-0.5 was reached. Phage was rescued by infection with helper phage and grown in kanamycin-containing media overnight at 26°C with shaking. The following day, the 12 cultures were pelleted and the phage supernatant was precipitated twice with polyethylene glycol (PEG)/NaCl (Section 2.5.2 of Materials and Methods). After resuspending each precipitated phage pellet in 1 mL PBS, the phage was divided into the four libraries described above for panning.

Panning was performed against the TAA, Melan-A/MART-$1_{(26-35)}$, bound in the context of biotinylated HLA-A*0201. The quality and stability of the antigen is critical to the success of affinity maturation. A limitation of many antigenic peptides derived from TAAs is that they are not always optimal for binding to HLA in that they do not contain the dominant anchor residues. This results in a low binding affinity of these peptides in the groove of the HLA molecule. Modification of the anchor residues to generate heteroclitic peptides enhances the binding affinity of the peptide in the HLA groove stabilising the complex. The wild-type peptide binds weakly to the HLA-A*0201 heavy chain and so forms relatively unstable complexes (Valmori, Fonteneau et al. 1998). A heteroclitic version of the Melan-A/MART-$1_{(26-}$

$_{35)}$ peptide was used in all panning and ELISA screening experiments. The variant peptide contains an Ala27Leu substitution at position 2 from the N-terminus (ELAGIGILTV). Soluble HLA-A*0201-Melan-A/MART-$1_{(26-35)}$ was prepared from *E. coli* expressed inclusion bodies and synthetic peptide (Garboczi, Hung et al. 1992) and biotinylated with the BirA enzyme (O'Callaghan C, Byford et al. 1999).

Three cycles of panning were performed as described in Section 2.5.4 of Materials and Methods. Phage (100 µl) was pre-blocked with 3% Marvel-PBS and then incubated with 100 nM biotinylated HLA-A*0201-Melan-A/MART-$1_{(26-35)}$. The phage:HLA-A*0201-Melan-A/MART-$1_{(26-35)}$ complexes were rescued with 100 µl streptavidin-coated paramagnetic beads. The beads were washed two times with PBS containing 3% Marvel (w/v) (MPBS), five times with PBS containing 0.1% Tween-20 (v/v) (PBST) and further two times with PBS to remove non-binding or weakly binding variants. Phage displayed TCRs were eluted with 0.1 M Triethylamine and then neutralised with 1 M Tris (pH 7.4). Eluted phage was used to infect early log phase *E. coli* TG1 cells prior to plating on ampicillin-containing agar plates supplemented with 2% glucose (v/v). Overnight incubation at 30°C completed one round of selection. A total of three cycles of panning were performed under identical conditions.

3.3.1 Monoclonal phage ELISA

The output titre for each round of selection was determined and, following the third round, a ten-fold increase was observed for each of the four libraries. To screen monoclonal phage TCRs, individual clones were rescued by transferring ninety-five ampicillin-resistant *E. coli* TG1 colonies from each of the four libraries to the wells of sterile 96-well microtitre plates. Glycerol stocks of each of the 96-well libraries were prepared (master-plate) for storage at -80°C. Fresh 96-well cultures were grown from

the master-plates and phage was rescued by infection with helper phage and grown in kanamycin-containing media overnight at 26°C with shaking as described in Section 2.5.1 of Materials and Methods. The following day, the cultures were pelleted and the supernatant containing monoclonal phage TCRs were screened for binding to immobilised biotinylated HLA-A*0201-Melan-A/MART-$1_{(26-35)}$ in an ELISA assay as described in Section 2.5.5 of Materials and Methods. Antigen-binding phage were detected with an anti-M13 antibody and a phosphatase-labelled anti-rabbit IgG monoclonal antibody. The phage were scored as ELISA positive if the absorbance at 650 nm was at least two-times higher than the background absorbance value at 650 nm.

The only library to yield antigen-binding phage was the CDR3α library (Figure 3.8). From this population, thirty-three positive clones (a frequency of ~35%) showed binding to HLA-A*0201-Melan-A/MART-$1_{(26-35)}$. Considerable variation in the level of expression of the positive-binding TCRs was observed with differences in the ELISA signal between the clones. Six out of the thirty-three clones (23, 28, 40, 59, 60 and 83) failed to satisfy the antigen-binding absorbance criteria, but were deemed ELISA positive based on visual appearance of the developed ELISA plate.

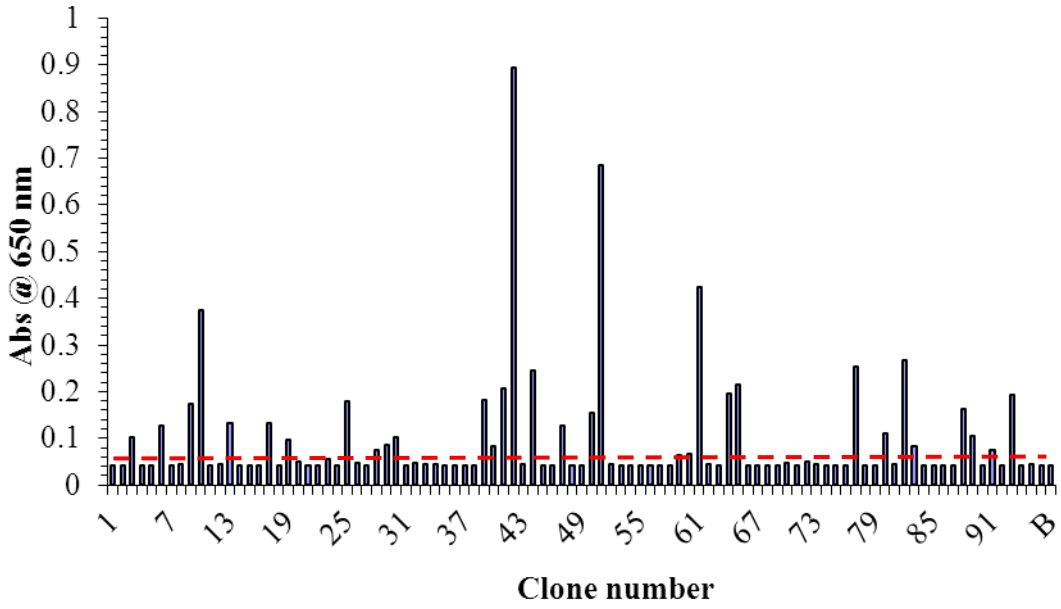

Figure 3.8. Monoclonal phage ELISA screen of Mel-5 TCR CDR3α library Pan 3 output. Following the third round of selection, ninety-five random colonies were screened by ELISA for binding to immobilised HLA-A*0201-Melan-A/MART-$1_{(26-35)}$ (ELAGIGILTV). The cut-off for defining positive binding is indicated with a red dotted line. B, background.

3.3.2 Inhibition phage ELISA at 100 nM inhibitor

The thirty-three positive HLA-A*0201-Melan-A/MART-$1_{(26-35)}$ binders selected from the CDR3α library were further characterised in an inhibition phage ELISA at 100 nM HLA-A*0201-Melan-A/MART-$1_{(26-35)}$ to determine if any of the TCRs demonstrated competitive inhibition (Section 2.5.5 of Materials and Methods). The phage supernatant (as used in Figure 3.8) was incubated with 100 nM non-biotinylated-HLA-A*0201-Melan-A/MART-$1_{(26-35)}$ for 1 h prior to adding to ELISA plates immobilised with HLA-A*0201-Melan-A/MART-$1_{(26-35)}$. High affinity binding phages are removed from the solution giving a reduction in ELISA signal. Inhibition was measured as a percentage reduction in signal and was calculated using the following formula: 100 - (Abs 650 nm sample with inhibitor ÷ Abs 650 nm sample without inhibitor x 100).

The inhibition values for the thirty-three clones are shown in Table 3.2. Of the 33 clones tested, inhibition values for 19 were calculated: 7/19 demonstrated >90% inhibition; 9/19 60-90% inhibition and 3/19 28-60% inhibition. It was noticeable that there was an overall reduction in the ELISA signal for each of the thirty-three clones compared to the values recorded in Figure 3.8. Overnight storage of the phage supernatant prior to this assay may have resulted in proteolysis of the phage displayed TCRs, reducing the amount of functional TCR in each well. Several of the clones showed almost no detectable binding to HLA-A*0201-Melan-A/MART-$1_{(26-35)}$ and so the inhibition levels could not be calculated.

Clone number	Abs @ 650 nm + 0 nM inhib.	Abs @ 650 nm + 100 nM inhib.	% Inhib. @ 100 nM
3	0.069	0.000	99
6	0.021	0.003	nd
9	0.071	0.010	86
10	0.268	0.057	79
13	0.031	0.001	nd
17	0.119	0.022	82
19	0.034	0.007	nd
23	0.002	0.023	nd
25	0.283	0.026	91
28	0.014	0.000	nd
29	0.015	-0.006	nd
30	0.030	0.008	nd
39	0.109	0.067	39
40	0.020	0.003	nd
41	0.142	0.079	44
42	0.798	0.063	92
44	0.143	0.018	87
47	0.012	0.002	nd
50	0.040	1.0101*	nd
51	0.362	0.092	75
59	0.015	0.008	42
60	0.015	-0.001	nd
61	0.359	0.257	28
64	0.149	0.022	85
65	0.160	0.040	75
77	0.186	0.017	91
80	0.117	0.006	95
82	0.149	0.025	84
83	0.031	0.004	nd
88	0.082	0.007	91
89	0.107	0.008	93
91	0.040	0.001	nd
93	0.164	0.026	84

Table 3.2. Inhibition phage ELISA of Mel-5 TCR CDR3α variants at a concentration of 100 nM inhibitor. The phage supernatant was incubated with 100 nM non-biotinylated-HLA-A*0201-Melan-A/MART-$1_{(26-35)}$ (ELAGIGILTV) for 1 h prior to adding to ELISA plates immobilised with HLA-A*0201-Melan-A/MART-$1_{(26-35)}$ (ELAGIGILTV). Absorbance (Abs) was measured at 650 nm. Percentage inhibition (% Inhib.) is measured as the percentage reduction in ELISA signal. The background absorbance value was subtracted from all readings before % Inhib. was calculated. *The Abs reading at 650 nm + 100 nM inhib. for clone is an outlier and probably due to a pipetting error. nd, not determined.

3.3.3 Sequencing analysis of the Pan 3 output

The 33 CDR3α mutated clones were sequenced with primers YOL13 and YOL22 (Table 3.3). One failed to produce sequence of sufficient quality and so was excluded from the analysis. Of the rest, 16 unique TCRs were identified. With the exception of clone 51, in which a Met at residue 48 in framework 2 was substituted for lle, no other mutations were observed outside of the targeted CDR3 region. Analysis of the variants showed a selection towards consensus sequences. It was apparent that certain residues were preferred at particular positions: Val^{93} was frequently substituted for Ser, Asp or Pro; Ala^{94} was changed to Gly in almost all of the mutated TCRs (in 26 of 32 clones); the wild-type residue at position Gly^{95} was retained in 50 % of the sequenced clones; some variation was observed at position Lys^{96}, which was substituted equally for a hydrophilic (His or Arg) or a hydrophobic (Leu or Tyr) residue; Leu was predominantly found at residue Ser^{97} (in 21 of 32 clones); Thr^{98} was commonly substituted for Leu. Several common motifs were seen; a central Gly^{94}-Gly^{95} motif was found in almost half of the sequenced clones and a $G^{94}X^{95}X^{96}L^{97}$ motif was found in 18 of 32 sequenced clones.

Multiple codon usage provides an indication of library diversity. For example, in the $D^{93}G^{94}G^{95}R^{96}L^{97}$ motif, Gly^{94} is encoded by codons ggt or ggg, Arg^{96} is encoded by cgg or cgt and Leu^{97} is encoded by ttg or ctt. A second example, in the $P^{93}G^{94}G^{95}L^{96}L^{97}$ motif, Gly^{94} is encoded by codons ggt or ggg, the wild-type residue Gly^{95} is encoded by codons ggt or ggc (as in the parental DNA template) and Leu^{97} is encoded by ttg or ctt. A third example, in the $L^{93}S^{94}P^{95}G^{96}L^{97}$ motif, Ser^{94} is encoded by agt or tcg and Pro^{95} is encoded by ccg or cct.

Clone Number	CDR3α$_{(V91\text{-}T98)}$	Frequency
wt	V N V A G K S T gtgaacgttgcaggcaaatcaacc	
17	V N **S G N H M** T gtgaactctggtaatcatatgacc	5
19	V N **S G N H M** T gtgaactctggtaatcatatgacc	
83	V N **S G N H M** T gtgaactctggtaatcatatgacc	
64	V N **S G N H M** T gtgaactctggtaatcatatgacc	
39	X N **S G X H M** T gngaactctggtnatcatatgacc	
25	V N **D G** G **R L** T gtgaacgatggtggtcggttgacc	5
42	V N **D G** G **R L** T gtgaacgatgggggtcgtcttacc	
77	V N **D G** G **R L** T gtgaacgatgggggtcgtcttacc	
44	V N **D G** G **R L** T gtgaacgatgggggtcgtcttacc	
50	V N **D G** G **R L** T gtgaacgatgggggtcgtcttacc	
9	V N **P G** G **L L** T gtgaacccgggtggtttgttgacc	3
47	V N **P G** G **L L** T gtgaacccgggggggcttcttacc	
13	V N **P G** G **L L** T gtgaacccgggggggcttcttacc	
3	V N **L S P G L** T gtgaacctgagtccgggtttgacc	3
28	V N **L S P G L** T gtgaacctgagtccgggtttgacc	
60	V N **L S P G L** T gtgaacctgtcgcctggtttgacc	
51	V N V **G** G **Y L L** gtgaacgttggtgggtatttgttg	3
82	V N V **G** G **Y L L** gtgaacgttggtgggtatttgttg	
65	V N V **G** G **Y L L** gtgaacgttggtgggtatttgttg	
29	V N **P G** G **V L** T gtgaacccggggggggtgttgacc	2
89	V N **P G** G **F L** T gtgaacccgggtggttttctgacc	
59	V N **N G M P** S T gtgaacaatggtatgccgtctacc	2
80	V N **N G M P** S T gtgaacaatggtatgccgtctacc	
10	V N V **G** G **Y L S** gtgaacgttgggggttatttgtcg	1
61	V N V **G** G **L L R** gtgaacgttggtgggttgttgagg	1
41	V N **N P T L A** T gtgaacaatcctacgctggctacc	1
40	V N **N G L P Q** T gtgaacaatggtctgcctcagacc	1
6	V N V A **M H I L**	1

	gtgaacgttgcgatgcatattttg	
88	V N V **G V I L R** gtgaacgttggggtgattctgcgt	1
23	**S G Y L** G K S T gtcngggtatcttggnaaatcaacc	1
30	V N **P G L I L** T gtgaaccctgggctgattttgacc	1
91	V N V **G L I L L** gtgaacgttggtttgattctgctg	1

Table 3.3. Mel-5 TCR variants selected from the CDR3α libraries. Sequences are grouped according to frequency. Nucleotides marked with an "n" and the corresponding amino acid residue marked with an "X" are unknown because the DNA sample is mixed and contains more than one DNA template. Amino acids that differ from wild-type are highlighted in red. Blue lettering indicates alternative codon usage compared to the parental sequence. International Immunogenetics (IMGT) nomenclature (Lefranc, Giudicelli et al. 1999).

3.3.4 Inhibition and specificity phage ELISA

Sequence analysis of the 33 Mel-5 TCR CDR3α variants guided the selection of ten unique clones to further characterise in an inhibition ELISA at two concentrations of inhibitor (5 nM and 50 nM) (Table 3.4). A new batch of phage was produced for each of the 10 clones from the *E. coli* TG1 glycerol stock master-plate prepared in section 3.3.1.

Of the ten clones analysed, only clone 89 failed to show any detectable binding to HLA-A*0201-Melan-A/MART-$1_{(26-35)}$ (ELAGIGILTV) despite having demonstrated binding in the previous ELISA (Table 3.3).

Whilst several of the clones demonstrated a high level of inhibition at both concentrations of inhibitor, the clones could not be accurately ranked according by affinity because the level of displayed TCR varied amongst the clones. For example, the % inhibition values would imply that clone 59 was the highest affinity clone and clone 51 the lowest. However, this assumption would be erroneous because the level of TCR display for clone 51 (inferred from absorbance 650 nm values) is ~8-fold higher than for clone 59.

In the same experiment, the ten clones were analysed for specificity against a panel of three non-cognate peptide HLA-A*0201 complexes: MUC-$1_{(167-175)}$ (ALGSTAPPV), HIV $GAG_{(77-85)}$ (SLYNTVATL) and NY-$ESO_{(157-165)}$ (SLLMWITQC) (Figure 3.9). All clones maintained specificity for HLA-A*0201-Melan-A/MART-$1_{(26-35)}$ (ELAGIGILTV); no detectable binding to the three non-cognate peptide HLA-A*0201 molecules was observed.

Clone number	Abs @ 650 nm + 0 nM inhib.	Abs @ 650 nm + 50 nM inhib.	% Inhib. @ 50 nM	Abs @ 650 nm + 5 nM inhib.	% Inhib. @ 5 nM
3	0.286	0.036	87	0.215	25
9	0.172	0.039	77	0.108	37
17	1.050	0.317	70	0.878	16
29	0.176	0.056	68	0.131	26
42	0.859	0.291	66	0.775	10
51	0.969	0.355	63	0.789	19
59	0.127	0.012	91	0.058	54
88	0.295	0.050	83	0.258	13
89	-0.002	0.003	nd	0.001	nd
91	0.123	0.021	83	0.114	7

Table 3.4. Inhibition phage ELISA of Mel-5 TCR CDR3α variants at a concentration of 50 nM and 5 nM inhibitor. The phage supernatant was incubated with the appropriate concentration of non-biotinylated-HLA-A*0201-Melan-A/MART-$1_{(26-35)}$ (ELAGIGILTV) prior to adding to ELISA plates immobilised with HLA-A*0201-Melan-A/MART-$1_{(26-35)}$ (ELAGIGILTV). % Inhib. is measured as the percentage reduction in ELISA signal. The background absorbance value was subtracted from all readings before % Inhib. calculated. nd, not determined.

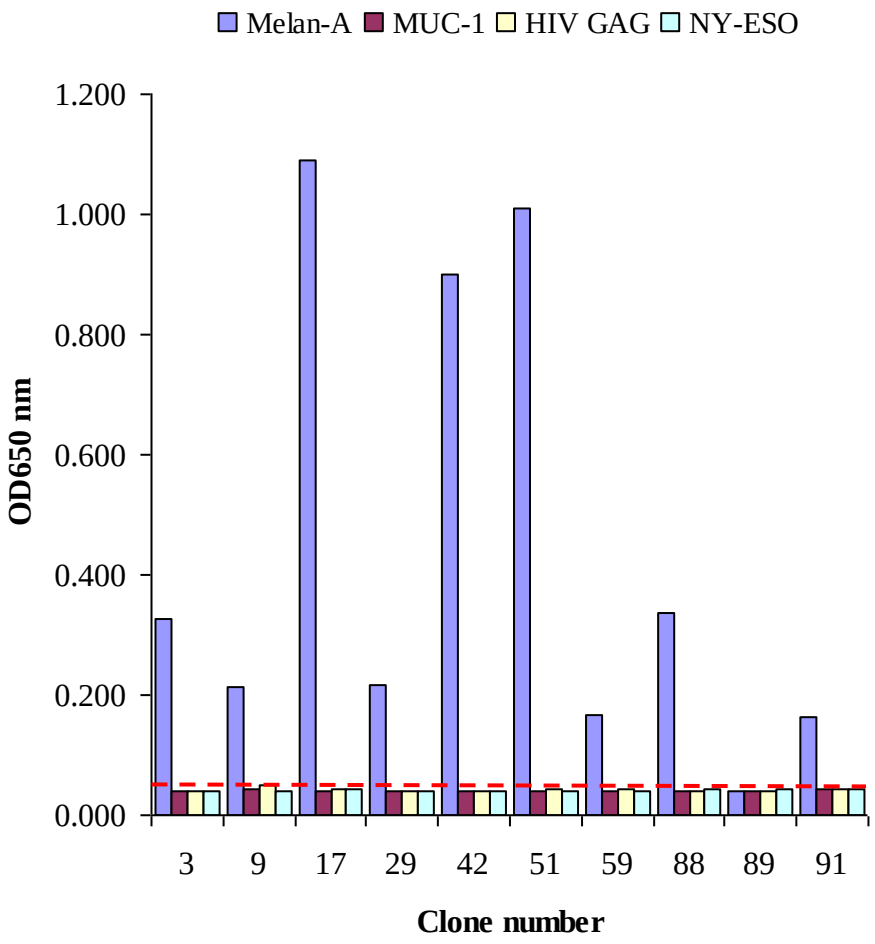

Figure 3.9. Specificity phage ELISA screen of Mel-5 TCR CDR3α variants. Specificity analysis against cognate pHLA: HLA-A*0201-Melan-A/MART-$1_{(26-35)}$ (ELAGIGILTV) and non-cognate pHLA: HLA-A*0201-MUC-$1_{(167-175)}$ (ALGSTAPPV), HLA-A*0201-HIV $GAG_{(77-85)}$ (SLYNTVATL) and HLA-A*0201-NY-$ESO_{(157-165)}$ (SLLMWITQC). The background value is indicated with a red dotted line.

3.4 Characterisation of first generation Mel-5 TCRs

3.4.1 Soluble expression of Mel-5 TCRs

The nine Mel-5 CDR3α mutated TCRs that showed specific binding to HLA-A*0201-Melan-A/MART-$1_{(26-35)}$ (ELAGIGILTV) (Figure 3.9) were cloned into the expression plasmid pGMT7 for expression in *E. coli* strain BL21 (DE3) pLysS as described in Section 3.6.3 of Materials and Methods. The nine TCR mutants were renamed for the subsequent *E. coli* expression work: clone 42 = MELa1; clone 51 = MELa2; clone 29 = MELa3; clone 9 = MELa4; clone 17 = MELa5; clone 3 = MELa6; clone 88 = MELa7; clone 59 = MELa8; clone 91 = MELa9.

The *E. coli* TG1 glycerol stock 96-well master-plate for the Mel-5 TCR CDR3α Pan 3 output (from Section 3.3.1) was used as the template to PCR amplify the nine mutated Vα domains. The primers TRAV12-2 and SalI Rev (Section 2.6.3 of Materials and Methods) were used to amplify the complete TCR Vα domain together with the first 20 amino acid residues of the TCR Cα (TRAC*01) domain. All PCR products were resolved on a 1.5% (w/v) agarose gel. The desired ~380 bp fragment was gel-purified and digested with restriction enzymes *Cla*I and *Sal*I. Digested Vα domains were ligated into a modified version of pGMT7 (pEX954) containing a complete ds-bond engineered TCR Cα (TRAC*01) domain. Following transformation of chemically-competent *E. coli* XL1-Blue cells, DNA from three ampicillin-resistant colonies was isolated and the DNA sequenced with the T7 primer (Section 2.6.3 of Materials and Methods).

A sequence-verified clone for each of MEL1a-MEL9a, containing a full-length Vα/Cα TCR chain, was transformed into chemically-competent *E. coli* BL21 (DE3) pLysS cells. The wild-type Mel-5 TCR β chain containing a ds-bond engineered TCR Cβ (TRBC*01) domain was cloned separately into pGMT7 (pG176) and transformed

into *E. coli* BL21 (DE3) pLysS cells. One litre cultures were set up for each of the nine mutated Mel-5 TCR α chains and the Mel-5 wild-type TCR β chain (bwt) (Section 2.6.4 of Materials and Methods). Following induction with IPTG, the cultures were pelleted and inclusion bodies (IBs) were prepared as described in Section 2.6.5 of Materials and Methods. Soluble TCR was refolded by rapid dilution in a refold buffer containing 5 M urea and 0.4 M L-arginine and a redox pair (Section 2.6.8 of Materials and Methods). After dialysing against deionised water and then 10 mM Tris pH 8.1, samples were loaded onto a POROS 50HQ column. A salt gradient was applied to the column to elute the TCR. Refolded TCR was further purified by gel-filtration on a Superdex 75PG 26/60 column (Section 2.6.8 of Materials and Methods). Purified Mel-5 TCR was analysed by Coomassie stained SDS PAGE under reducing and non-reducing conditions.

3.4.2 Kinetic analysis of Mel-5 TCRs

Surface plasmon resonance (SPR) studies with BIAcore provided quantitative measures of TCR-pHLA binding and dissociation kinetics as described in Section 2.7 of Materials and Methods. Table 3.5 provides the kinetic values of parental and affinity-matured TCRs. Briefly, biotinylated pHLA-A*0201-Melan-A/MART-$1_{(26-35)}$ monomer was immobilised onto streptavidin-coupled CM-5 sensor chips up to 200 response units (RU) and biotin-blocked. TCRs were analysed using a single injection of TCR (in kinetic conditions) at a concentration ten-fold higher than the predicted K_D as described in Section 2.7 of Materials and Methods.

Each of the Mel-5 TCR CDR3α mutants was improved in affinity for HLA-A*0201-Melan-A/MART-$1_{(26-35)}$ (ELAGIGILTV) (Table 3.5 A). The K_D values for the mutants ranged from 6.4 nM to 120 nM with half-life values of between 1.8 and

4.9 minutes. The highest affinity clone, MELa1bwt was improved ~2800-fold in affinity above the wild-type TCR (MELawtbwt). Retention of the wild-type Gly at position 95 in the highest affinity clones may be required to allow the CDR3α loop to adopt a conformation necessary for improved binding to cognate pHLA.

Having selected on the common heteroclitic 10mer Melan-A/MART-$1_{(26-35)}$ peptide (ELAGIGILTV), I next tested whether binding to the wild-type peptide was maintained. Although the heteroclitic 10mer peptide was used in phage selections, a wild-type 9mer Melan-A/MART-$1_{(27-35)}$ peptide (AAGIGILTV), demonstrated that the binding affinity of the high affinity TCR (MELa1bwt) was largely unaffected; the calculated K_D was 6.4 nM for the heteroclitic peptide versus 7.8 nM for the wild-type peptide (Table 3.5 B).

A.

Clone ID	TCRαF2	CDR3α$_{(V93-T98)}$	Freq	K_{on} (M^{-1} s^{-1})	K_{off} (s^{-1})	K_D (nM)	$T_{1/2}$ (min)	$\frac{K_D\ (parent)}{K_D\ (mutant)}$
MELawtbwt	IMF	VAGKST	-	nd	nd	18000	nd	1
MELa1bwt	I**I**F	**DG**G**RL**T	5	5.08 x 10^5	3.26 x 10^{-3}	6.4	3.5	2812.5
MELa2bwt	IMF	V**G**G**YLL**	3	5.01 x 10^5	6.07 x 10^{-3}	12	1.9	1500
MELa3bwt	IMF	**PG**G**VL**T	1	3.18 x 10^5	6.58 x 10^{-3}	21	1.8	857.1
MELa4bwt	IMF	**PG**G**LL**T	3	2.58 x 10^5	5.72 x 10^{-3}	22	2.0	818.2
MELa5bwt	IMF	**SGNHM**T	5	2.20 x 10^5	5.08 x 10^{-3}	23	2.3	782.6
MELa6bwt	IMF	**LSPGL**T	3	1.05 x 10^5	2.38 x 10^{-3}	23	4.9	782.6
MELa7bwt	IMF	V**GVILR**	1	1.66 x 10^5	4.49 x 10^{-3}	27	2.6	666.7
MELa8bwt	IMF	**NGMP**ST	2	5.61 x 10^5	4.36 x 10^{-3}	77	2.6	233.8
MELa9bwt	IMF	V**GLILL**	1	3.82 x 10^4	4.57 x 10^{-3}	120	2.5	150

B.

	Melan-A/MART-1$_{(26-35)}$ (AAGIGILTV)				Melan-A/MART-1$_{(27-35)}$ (ELAGIGILTV)			
	K_{on} (M^{-1} s^{-1})	K_{off} (s^{-1})	K_D (nM)	$T_{1/2}$ (sec)	K_{on} (M^{-1} s^{-1})	K_{off} (s^{-1})	K_D (nM)	$T_{1/2}$ (sec)
MELa1bwt	4.68 x 10^5	3.65 x 10^{-3}	7.8	190	7.31 x 10^4	1.16 x 10^{-2}	6.4	59

Table 3.5. Binding kinetics of Mel-5 TCR CDR3α mutants from first generation affinity enhancement. (A). Binding kinetics of MELa1bwt-MELa9bwt TCRs were measured by SPR on a BIAcore T100. HLA-A*0201-Melan-A/MART-1$_{(26-35)}$ (ELAGIGILTV) was immobilised on the biosensor chip. Control response values to a non-cognate pHLA: HLA-A*0201-hTERT$_{(540-548)}$ were subtracted from each reading prior to analysis. The ratio of K_D values indicates the fold increase in binding affinity as compared to the wild-type (parent), Mel-5 TCR. Red lettering indicates residues mutated from the parental sequence. TCRαF2, = TCR α framework 2. Freq, = number of repeated sequences within the population of clones analysed. nd, not determined. **(B).** Binding affinity of MELa1bwt to the 10mer heteroclitic Melan-A/MART-1$_{(26-35)}$ (ELAGIGILTV) peptide was compared to the 9mer wild-type Melan-A/MART-1$_{(27-35)}$ (AAGIGILTV) peptide by SPR. International Immunogenetics (IMGT) nomenclature (Lefranc, Giudicelli et al. 1999). (Data kindly provided by Dr. E. Baston).

3.5 Generating Mel-5 TCR template for second generation libraries

Mel-5 TCR CDR3α clones with affinities up to 6.4 nM (MELa1bwt) were isolated from the first round selection libraries. In an effort to generate Mel-5 TCR mutants with sub-nanomolar affinity, additional mutated TCR libraries required construction. Engineering antibodies for high affinity through a CDR-walking approach has proved highly successful (Yang, Green et al. 1995; Schier, McCall et al. 1996; Pavoni, Flego et al. 2006). It was therefore hypothesised that whilst only CDR3α mutated clones were isolated using the wild-type Mel-5 TCR as template, building libraries on an enhanced-affinity clone might lead to the isolation of mutations in other CDR loops.

The highest affinity clone (MELa1) from the first generation libraries was chosen as one of the two templates on which to introduce further mutations. Because it was unknown which would be the optimal affinity clone to use as a framework on which to build further mutagenic libraries, a clone exhibiting a K_D in the high nanomolar range was sought. Unfortunately, such a clone was not isolated from the CDR3α library Pan 3 output.

To identify a clone possessing optimal binding kinetics, a panel of four templates were generated by back-mutating, to wild-type, each residue in the MELa1 CDR3α motif that differed from the parent clone. In this way, it was possible to examine the role that the individual CDR3α residues play in the interactions with HLA-A*0201-Melan-A/MART-$1_{(26-35)}$. The MELa1 motif is: DGGRL and the panel of back-mutants include: MELa1a, <u>V</u>GGRL; MELa1b, D<u>A</u>GRL; MELa1c, DGG<u>K</u>L and MELa1d, DGGR<u>S</u> (the back-mutated wild-type residue is underlined).

3.5.1 Cloning and refolding of back-mutated MELa1 TCRs

Using the pGMT7:MELa1 *E. coli* expression plasmid (Section 3.5) as template and four pairs of complimentary primers (Section 2.6.3 of Materials and Methods) to reintroduce the desired wild-type residue, the four *E. coli* expression plasmids MELa1a, MELa1b, MELa1c and MELa1d were generated. Sequence analysis confirmed the desired CDR3α motif of each clone.

E. coli BL21 (DE3) pLysS cells were transformed with each of the four CDR3α back-mutated constructs, protein expression was induced with IPTG and inclusion bodies purified as described in Section 2.6.4 and 2.6.5 of Materials and Methods. Purified IBs were analysed by SDS-PAGE as described in Section 2.6.6 of Materials and Methods (Figure 3.10). An over-expressed protein corresponding to the Mel-5 TCR α chain (MELa1a-MELa1d) was seen at the expected molecular weight of ~23 kilodaltons (kDa).

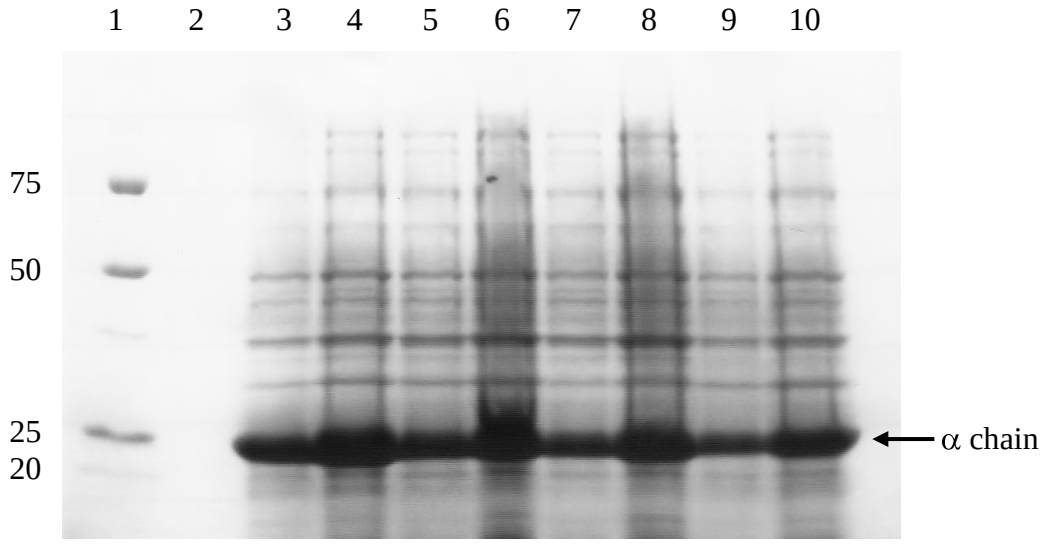

Figure 3.10. Coomassie-stained reducing SDS PAGE analysis of MELa1 back-mutated inclusion bodies. Lane 1, Bio-Rad Molecular Weight Marker (MWM) kilodaltons; lane 2, no sample; lane 3, MELa1a 5 μl; lane 4, MELa1a 10 μl; lane 5, MELa1b 5 μl; lane 6, MELa1b 10 μl; lane 7, MELa1c 5 μl; lane 8, MELa1c 10 μl; lane 9, MELa1d 5 μl; lane 10, MELa1d 10 μl.

Each of the back-mutated α chains was refolded with the wild-type Mel-5 TCR β chain as described in Section 2.6.8 of Materials and Methods and each of the four TCR refolds was subjected to anion exchange chromatography followed by gel-filtration chromatography. The chromatography profiles for each of the TCRs followed a similar pattern (data not shown). Purification of the four TCRs is exemplified by TCR MELa1abwt. MELa1abwt was purified by anion exchange chromatography on a POROS 50HQ column (Figure 3.11 A). A salt gradient was applied to the column to elute the TCR in 1 ml fractions. Three peaks of eluted protein were collected (P1, P2 and P3). The disulphide-linked TCR (dsTCR) elutes at a known conductivity and it was therefore predicted that peak 3 (P3) contained the refolded TCR. Three eluted fractions from P3 (fraction, Fr. 1, 2 and 3) were analysed by Coomassie stained SDS PAGE under non-reducing (Figure 3.11 B) and reducing conditions (Figure 3.11 C). A single band of ~45 kDa corresponding to the dsTCR can be seen (Figure 3.11 B) which upon reduction runs as separate α and β chains of ~23 kDa and ~28 kDa respectively (Figure 3.11 C). The fraction containing the most protein (Fr. 2) was further purified by gel-filtration on a Superdex 75PG 26/60 (S75) column equilibrated with HEPES-buffered-saline-EP (HBS-EP) solution. A slight shoulder of aggregated protein can be seen at an elution volume between 8 and 10 ml. Four 0.5 ml peak fractions (Fr. 1, 2, 3 and 4) were collected (Figure 3.12 A). Each fraction was analysed by Coomassie stained SDS PAGE under non-reducing (Figure 3.12 B) and reducing conditions (Figure 3.12 C) revealing high purity of TCR.

A.

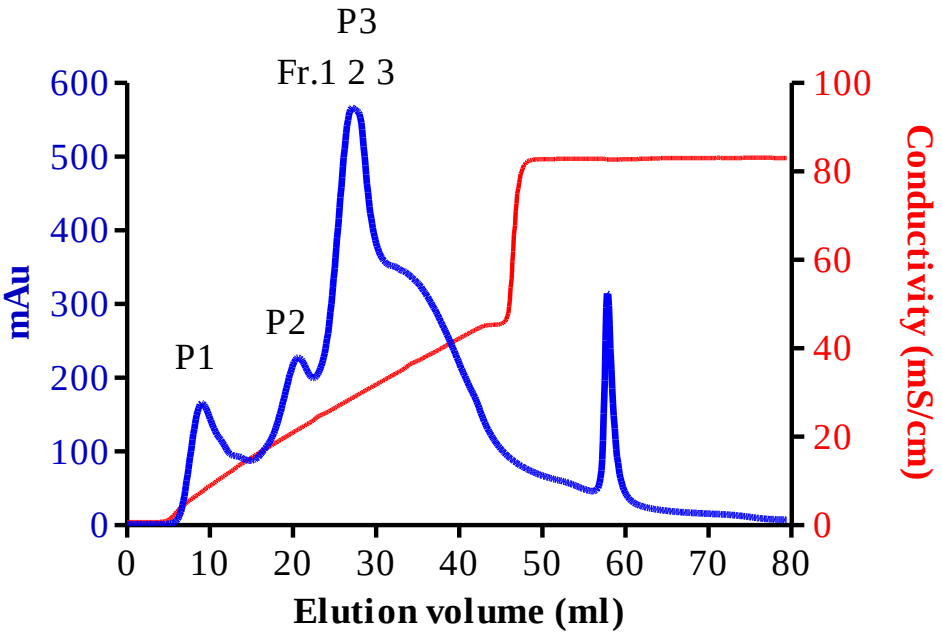

B.

C.

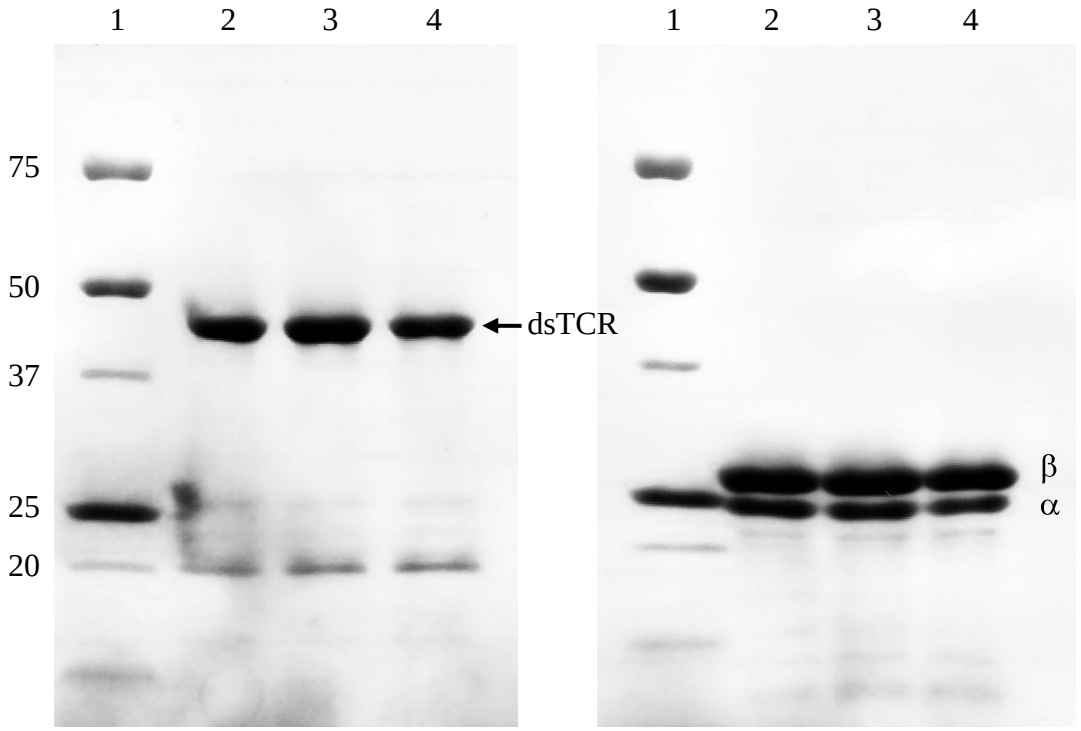

Figure 3.11. Purification of MELa1a by anion exchange chromatography. (A). Elution profile of MELa1abwt from Poros HQ column (highlighted in blue). Salt gradient shown in red. Absorbance at 280 nm converted into mAu (left Y-axis). Salt gradient converted into conductivity, mS/cm (right Y-axis). **(B).** Coomassie-stained SDS PAGE analysis of peak 3 (P3) fractions (Fr.) 1, 2 and 3 non-reducing. **(C).** Reducing. The lane order is the same for both gels. Lane 1, BioRad MWM (kDa); lane 2, fraction 1; lane 3, fraction 2; lane 4, fraction 3. α and β chains are highlighted. dsTCR, disulphide-linked TCR.

A.

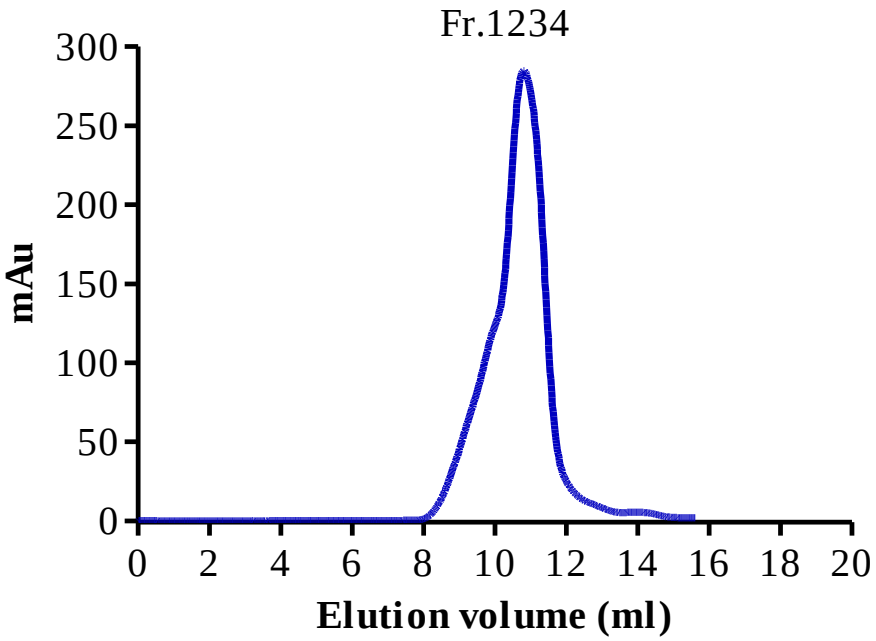

B. **C.**

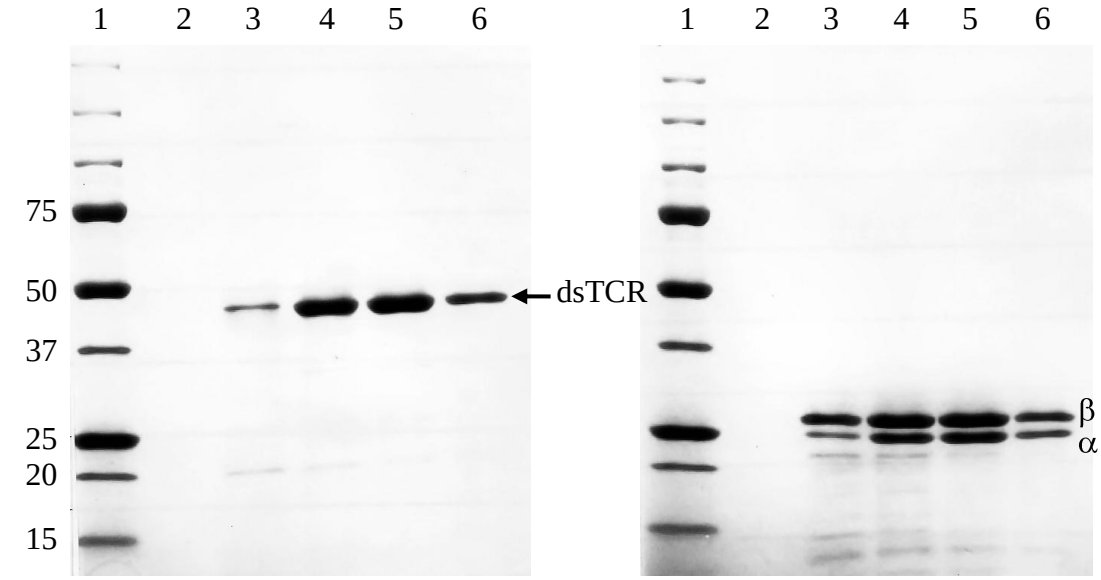

Figure 3.12. Purification of MELa1abwt by gel-filtration chromatography. (A). Superdex 75 profile. Collected fractions 1-4 are highlighted. Absorbance at 280 nm converted into mAu. **(B).** Coomassie-stained SDS PAGE analysis fractions (Fr.) 1, 2, 3 and 4 under non-reducing conditions. **(C).** Coomassie-stained SDS PAGE analysis fractions 1, 2, 3 and 4 under reducing conditions. The lane order is the same for both gels. Lane 1, BioRad MWM (kDa); lane 2, no sample; lane 3, fraction 1; lane 4, fraction 2; lane 5, fraction 3; lane 6, fraction 4. α and β chains are highlighted. dsTCR, disulphide-linked TCR.

3.5.2 Kinetic analysis of back-mutated MELa1 TCRs

Dissociation rate (K_D) constants for the four MELa1 back-mutated TCRs binding to HLA-A*0201-Melan-A/MART-$1_{(26-35)}$ (ELAGIGILTV) were determined by SPR analysis on a BIAcore 3000 as outlined in Section 2.7 of Materials and Methods. Briefly, a separate streptavidin-coupled flow cells of a CM-5 sensor chip were coated with up to 1000 RU of HLA-A*0201-Melan-A/MART-$1_{(26-35)}$ (ELAGIGILTV) and HLA-A*0201-$PSCA_{(14-22)}$ (ALQPGTALL). The non-cognate antigen, HLA-A*0201-$PSCA_{(14-22)}$, was used to control for non-specific binding. S75 fractions 2, 3 and 4 were pooled (~1.5 ml volume) for each TCR and concentrated to ~0.1 ml in a YM-10 spin column. The concentration of each TCR was calculated: MELa1abwt, 1.93 mg/ml (58.88 μM); MELa1bbwt, 2.65 mg/ml (80.85 μM); MELa1cbwt, 2.87 mg/ml (87.56 μM) and MELa1dbwt, 1.90 mg/ml (57.97 μM). A ten-point serial dilution of each TCR was flowed over both pHLA complexes and the RU value at each concentration was measured. RU values for non-specific binding to HLA-A*0201-$PSCA_{(14-22)}$ were subtracted from RU values for specific binding to HLA-A*0201-Melan-A/MART-$1_{(26-35)}$. Equilibrium binding constants were calculated by plotting the RU values for specific binding against the protein concentrations using a least-squares fit to the Langmuir equation, assuming a 1:1 interaction (Figure 3.13).

Substituting each of the mutated residues in the MELa1 clone for the corresponding wild-type residue in the parent clone had a dramatic effect on the binding affinity for HLA-A*0201-Melan-A/MART-$1_{(26-35)}$ (ELAGIGILTV). The binding affinity of MELa1 was reduced up to ~900-fold. By serendipity, the panel of back-mutated TCRs exhibited the desired binding kinetics suitable to use as templates for second generation libraries: MELa1a, 2.36 μM; MELa1b, 5.9 μM; MELa1c, 0.45 μM and MELa1d, 1.5 μM.

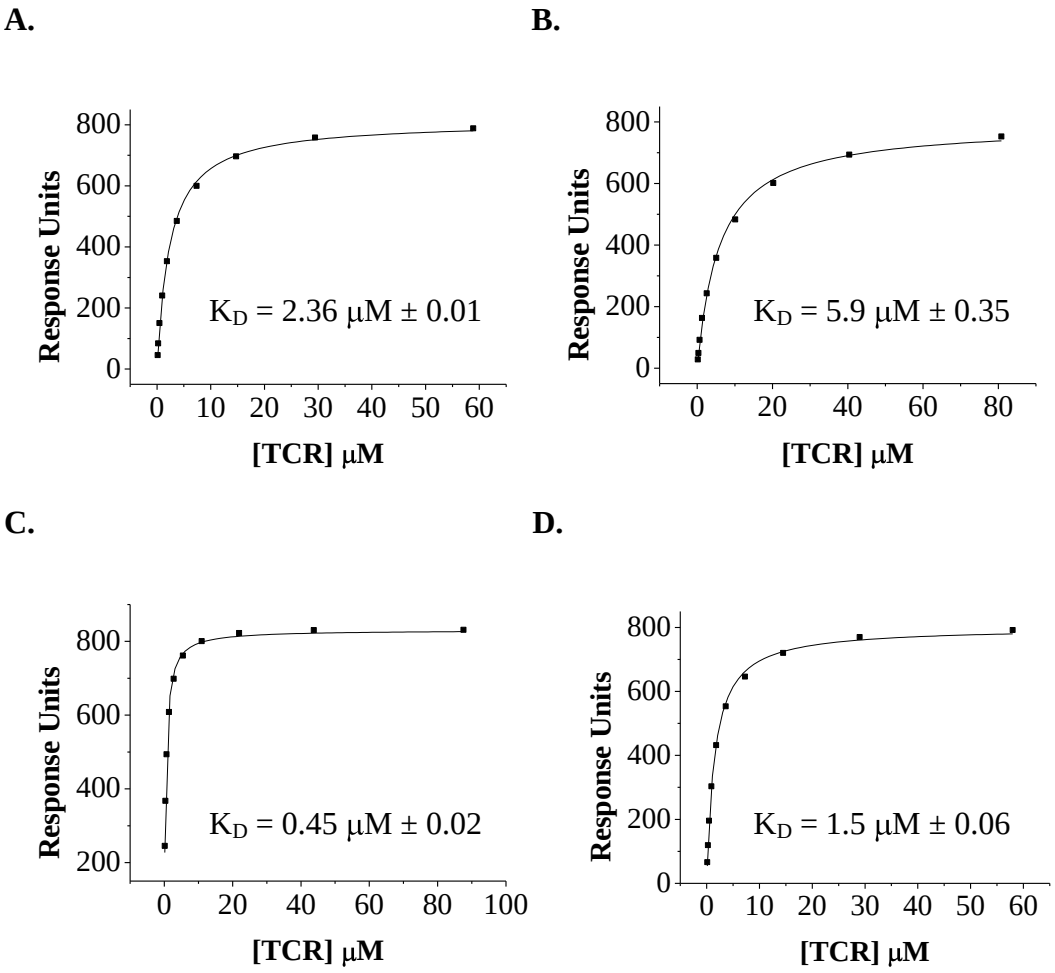

Figure 3.13. Equilibrium-binding analysis of MELa1 back-mutants at 25°C. Serial dilutions of soluble TCR were flowed over CM-5 biosensor chips coated with ~1000 RUs of cognate and non-cognate pHLA complexes. RU values at each TCR concentration were measured. Using a non-linear curve fitting equation the equilibrium K_D of each TCR for HLA-A*0201-Melan-A/MART-$1_{(26-35)}$ (ELAGIGILTV) was calculated. **(A).** MELa1abwt (VGGRL). **(B).** MELa1bbwt (DAGRL). **(C).** MELa1cbwt (DGGKL). **(D).** MELa1dbwt (DGGRS).

3.6 Design and construction of second generation libraries

Two clones were chosen as templates for further mutagenesis: one isolated directly from the first generation libraries (MELa1) and the second, a modified version of this clone (MELa1c), which exhibited binding affinities against HLA-A*0201-Melan-A/MART-$1_{(26-35)}$ (ELAGIGILTV) of 6.4 nM and 450 nM respectively.

3.6.1 Cloning the Mela1c TCR into the phagemid vector

The phagemid vector encoding the MELa1 CDR3α mutant already existed in the phagemid vector and was designated pG396. The MELa1c mutant was cloned into the phagemid vector, pG125, by SOE-PCR as described in Section 2.3.1 of Materials and Methods. Fragment A, encoding the mutated MELa1c CDR3α motif was amplified from the *E. coli* expression plasmid, pG246 (pGMT7 containing the MELa1c α chain) with primers Nat22 and YOL237. Fragments B, C and D were prepared previously for cloning the Mel-5 wild-type TCR (Section 3.2). The final SOE-PCR product was ligated into pG125 and designated pG397.

3.6.2 Generating DNA libraries

Second generation libraries were constructed by SOE-PCR following the strategy used to build the first generation libraries (Section 2.4.1 of Materials and Methods). Several of the primers used to construct the first generation libraries were used to build second generation libraries. However, additional NNK oligonucleotides were designed to ensure more comprehensive coverage across particular CDRs; one more for each of CDR1α, CDR1β and CDR2β and two extra for CDR3β (Figure 2.2 of Materials and Methods). The NNK-mutagenised CDRs were cloned onto both the MELa1 (pG396, K_D 6.4 nM) and MELa1c (pG397, K_D 450 nM) frameworks. The CDR1α and CDR2α libraries were constructed by SOE-PCR using either phagemid

vector pG396 or pG397 as template to introduce the mutated CDR3α motif (MELa1 or MELa1c) into the PCR splice product and were cloned as *Sfi*I fragments into pG125. The CDR1β, CDR2β and CDR3β libraries were built by SOE-PCR using pG125 as template and were cloned as *BssH*II-*Not*I fragments into both pG396 and pG397.

The gel-purified digested α and β chain fragments used in the ligation reactions are shown in Figure 3.14. In Figure 3.14 A, a single band of ~650 bp can be observed that corresponds to the *Sfi*I digested α chain fragments. PCR fragments amplified from pG396 are distinguished from fragments amplified from pG397 using the designated nomenclature a or à respectively. Additionally, a single band (~6.2 kbp) can be seen for the linearised phagemid vector pG125. In Figure 3.14 B and 3.14 C, a single band of ~750 bp can be observed corresponding to the *BssH*II-*Not*I digested β chain fragments together with digested phagemid vectors pG396 (Figure 3.14 B) and pG397 (Figure 3.14 C).

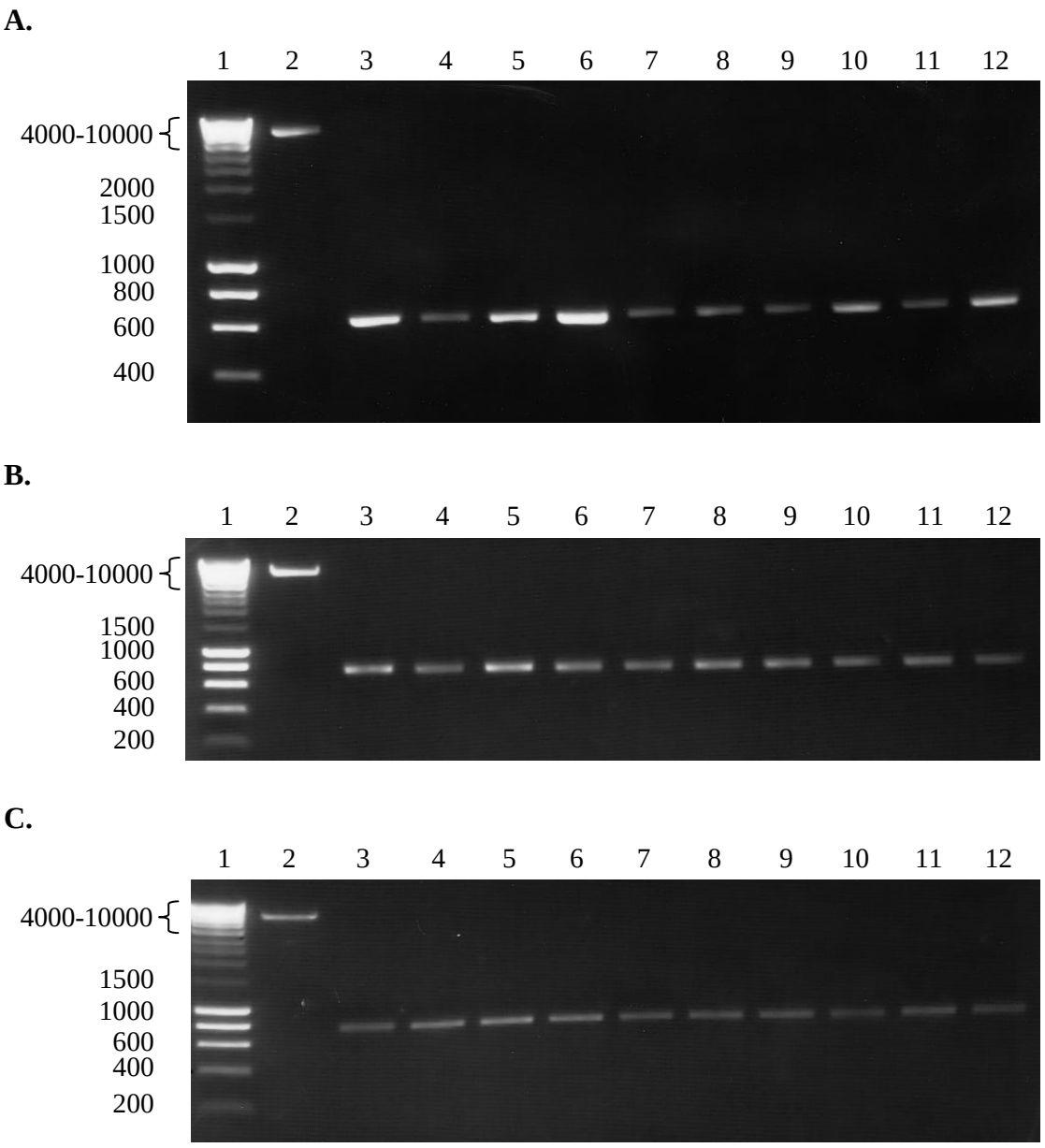

Figure 3.14. Agarose gel photo of gel-purified digested Mel-5 TCR SOE-PCR second generation library fragments and phagemid vectors. (A). α chain library PCRs digested with *Sfi*I. Lane 1, HYP I; lane 2, phagemid vector pG125; lane 3, PCR a3; lane 4, PCR a6; lane 5, PCR a6; lane 6, PCR à3; lane 7, PCR à6; lane 8, PCR à6; lane 9, a9; lane 10, PCR a9; lane 11, PCR à9; lane 12, PCR à9. Fragments generated using pG396 as template are shown as "a" and fragments generated using pG397 as template are shown as "à". **(B).** β chain library PCRs digested with *BssH*II-NotI. Lane 1, HYP I; lane 2, phagemid vector pG396; lane 3, PCR b3; lane 4, PCR b6; lane 5, PCR b9; lane 6, PCR b12; lane 7, PCR b15; lane 8, PCR b18; lane 9, b21; lane 10, PCR b24; lane 11, PCR b27; lane 12, PCR b30. **(C).** β chain library PCRs digested with *BssH*II-NotI. Lane 1, HYP I; lane 2, phagemid vector pG397; lane 3, PCR b3; lane 4, PCR b6; lane 5, PCR b9; lane 6, PCR b12; lane 7, PCR b15; lane 8, PCR b18; lane 9, b21; lane 10, PCR b24; lane 11, PCR b27; lane 12, PCR b30.

3.6.3 Generating bacterial libraries

Electrocompetent *E. coli* TG1 cells were transformed with 200-300 ng of each of the ten ligated DNA products (Section 2.4.1.4 of Materials and Methods) to yield libraries containing 1 to 3 x 10^8 TCR clones. Sequence analysis of random clones from each electroporation revealed that ligations 5, 6 and 9 (β chain libraries built on the MELa1 framework) contained a high level of MELa1 template contamination (sequence data not shown). Isolation of high affinity clone MELa1 from the first generation libraries indicates the fitness of this TCR in terms of its ability to be displayed on the surface of phage. Library contamination with such a clone could compromise the enrichment for higher affinity clones. Libraries comprising ligations 5, 6 and 9 were therefore discarded.

The potential for contamination of phage display libraries with parental template DNA requires consideration. Contamination can originate from a variety of sources. First, bacterial plasmid DNA can be co-purified with the initial PCR fragments and provide a source of template for PCR amplification. This source of contamination can be reduced by using *Dpn*I endonuclease to specifically digest methylated bacterial double-stranded DNA. Second, excessive PCR extension times in the cycling reaction. In the Mel-5 TCR library strategy, the initial two PCR fragments are generated with one of the two stitch flanking primers. If the PCR extension times are too long, the PCR product will be extended to include the second stitch flanking priming site. In the subsequent stitch reaction, that includes both external primers, amplification of parental DNA is possible.

The four libraries taken forward into the panning experiments are shown in Section 2.4.1.4 of Materials and Methods. Each of these libraries contained sufficient diversity across each of the CDRs, as assessed by sequence analysis (data not shown).

3.7 Phage selections and screening

The methods used for the selection and screening of high affinity binders were based on those described in Section 3.3 with several modifications. In an effort to isolate mutants with improved affinity exceeding that of the first generation clone, more stringent selection conditions were adopted.

Following one cycle of panning with 100 nM HLA-A*0201-Melan-A/MART-$1_{(26-35)}$ complexes, the concentration of HLA antigen was lowered 2-fold (50 nM) for Pan 2 and a further 5-fold (10 nM) for Pan 3. For the affinity maturation of antibodies it has been demonstrated that reduction of the antigen concentration helps ensure that selection for higher affinity scFv occurs, rather than selection for scFv that express well on phage or are less toxic to *E. coli* (Hawkins, Russell et al. 1992; Schier, McCall et al. 1996).

Additionally, off-rate selection was performed during the final two cycles of panning as described in Section 2.5.4 of Materials and Methods. In off-rate selection clones with lower affinity will dissociate from the bead:pHLA complexes quicker than clones with a reduced off-rate. Thus lower affinity clones will be sequestered by the excess of non-biotinylated pHLA in solution enriching for higher affinity clones retained bound to the beads. The off-rate method involved incubating the phage clones with biotinylated pHLA under equilibrium conditions, followed by washing and incubation with a 10-fold (in Pan 2) or 100-fold (in Pan 3) excess of non-biotinylated pHLA.

The phage:pHLA complexes were rescued with 50 μl of streptavidin-coated paramagnetic beads. The washing and elution conditions were as described in section 3.4. Eluted phage was used to infect early log phase TG1 cells prior to plating on YTE agar containing 100 μg/ml ampicillin and 2% glucose. Overnight incubation at 30°C

completed one cycle of selection. A total of three cycles of panning against biotinylated HLA-A*0201-Melan-A/MART-$1_{(26-35)}$ complexes were performed.

3.7.1 Characterisation of phage clones: phage ELISA and sequencing

Following the third cycle of panning, ninety-three monoclonal phage TCRs from each of the four libraries were screened for binding to immobilised biotinylated HLA-A*0201-Melan-A/MART-$1_{(26-35)}$ complexes. Affinity ranking of the binders was determined by incubating the phage supernatant with 5 nM (for library 1) or 10 nM (for library 2, 3 and 4) non-biotinylated-HLA-A*0201-Melan-A/MART-$1_{(26-35)}$ complexes at room temperature for 1 h prior to adding to HLA-A*0201-Melan-A-coated plates. Figure 3.15 provides an example inhibition phage ELISA plate from the Pan 3 output for library 4 (CDR3β built on MELa1c). Monoclonal phage TCRs for both MELa1bwt (K_D 6.4 nM) and MELa1cbwt (K_D 450 nM) were prepared in the same 96-well format to allow direct comparison of improvements in affinity over these clones (Figure 3.15). The % inhibition value at 10 nM inhibitor was ~90% and ~40% for MELa1bwt and MELa1cbwt respectively. The % inhibition value at 5 nM inhibitor was ~50-60% for MELa1bwt (MELa1c was not tested at 5 nM inhibitor).

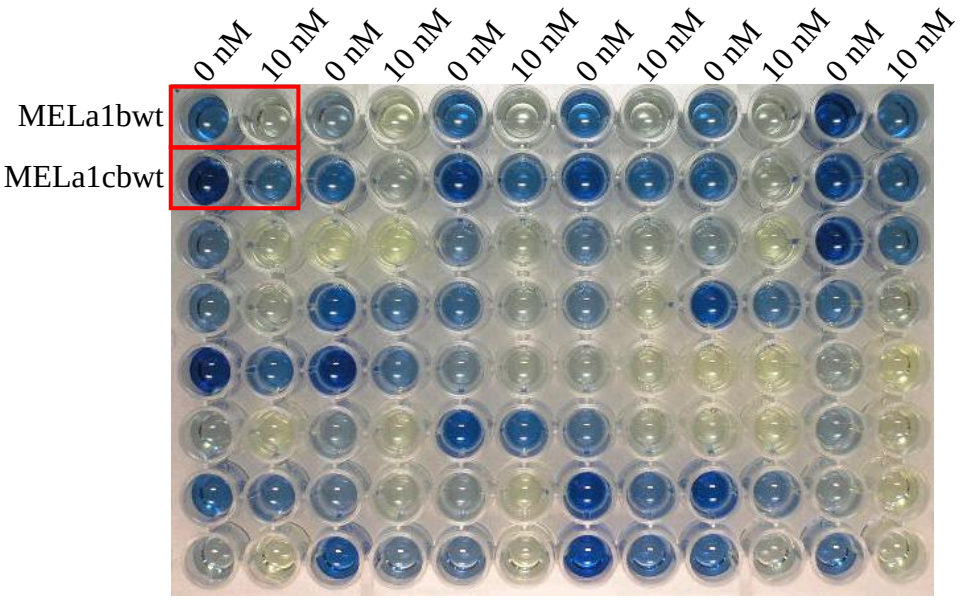

Figure 3.15. Representative inhibition phage ELISA at a concentration of 10 nM inhibitor. Data shown is for 46 individual clones from library 4 (CDR3β built on MELa1c). The remaining 47 phage-TCR clones were assayed on a second ELISA plate (data not shown). The phage supernatant was incubated with 10 nM non-biotinylated-HLA-A*0201-Melan-A/MART-$1_{(26-35)}$ (ELAGIGILTV) for 1 h prior to adding to ELISA plates immobilised with HLA-A*0201-Melan-A/MART-$1_{(26-35)}$ (ELAGIGILTV). The ELISA signal for MELa1bwt and MELa1cbwt TCRs are highlighted in red. The % inhibition value at 10 nM inhibitor for these TCRs was ~90% and ~40% respectively.

A selection of antigen-binding clones were further analysed by DNA sequencing of the CDR genes (Table 3.6). It should be noted that binders from library 2 showed no inhibition at 5 nM inhibitor and were therefore not sequenced. Sequence analysis of twenty-two binders from library 1 that gave the highest % inhibition in ELISA signal showed that 36% (8 out of 22) was the parental clone (MELa1) (Table 3.6 A). Enrichment for this clone that had been isolated from the first generation libraries, clearly illustrated an inherent fitness in terms of affinity and expression. As such, it was not surprising to see this level of background binding in the Pan 3 output. Despite these concerns, however, a number of unique sequences were isolated. Library 1 (a mixture of mutated CDR1α and CDR2α segments) was dominated by CDR1α mutants; 11 sequenced clones converged to 8 variants. Residues at particular positions were preferred: Asp^{27} was frequently substituted for a hydrophobic aromatic residue, predominantly Phe; the wild-type residues at position Gly^{29}, Ser^{30} and Gln^{31} were frequently retained (~92%, ~70% and 100% of the sequenced clones). Of the 14 sequenced clones 9 contained an amber stop codon, suppressible to Gln. A single CDR2α variant was isolated from library 1 which retained a wild-type residue at position Tyr^{51}. Clone MELa23 contains a non-targeted mutation, Tyr to His in alpha framework 3. From the % inhibition data it was difficult to assess any improvement in affinity over the background clone (MELa1); % inhibition for all variants was in a similar range and compared closely to MELa1. Without BIAcore data it was not possible to discriminate between the mutants and the parental clone.

Sequence analysis of the library 3 output (Table 3.6 B) revealed a dramatic enrichment for a consensus CDR2β motif: a central Gly-Pro couplet flanked by a hydrophobic aromatic pair (Tyr, Phe or Trp). All selected clones contain a Leu to Pro substitution in beta framework 2. Clone MELb3 also contains a non-targeted

mutation, Val to Ala in beta framework 3. The % inhibition at 10 nM was greater for each of the mutants compared to the framework clone: 85-90% versus 60% for MELa1c. Although a single sequence dominated the output (MELb1), the % inhibition for all CDR2β mutants was measured within a narrow range (85-90%). If this comparable level of inhibition translates to similar binding affinities, it would indicate that enrichment for clone MELb1 is likely the result of improvements in expression in addition to affinity.

Sequence analysis of twenty ELISA positive clones from library 4 (Table 3.6 C) showed that the output was comprised of mutants derived from two overlapping oligonucleotides (Nat241 and Nat36; Figure 2.2 of Materials and Methods) displaced by one codon: Group A, MELb10-MELb14 mutated at residue positions $Gly^{99}Leu^{103}$ and Group B, MELb5-MELb9 mutated at residue positions $Thr^{100}Phe^{104}$. Common to both groups a clear preference for a consensus motif can be observed: $Glu^{102}Leu^{103}$ were substituted for a Gly-Trp pair in all sequenced clones. The wild-type residue at position Gly^{101} was retained in over half of the sequenced clones. In Group A, Thr^{100} was substituted equally for a Met or Val. Position Phe^{104} was more permissive; five different residues were observed in this position. In Group B, Gly^{99} was substituted for Asn in all of the clones; Thr^{100} was substituted for a Thr, Leu or Val. Excluding clones MELb8 and MELb10 which contain non-targeted mutations in beta framework 2 and beta framework 3 respectively, the % inhibition at 10 nM inhibitor is in the range of 70-80% compared to 60% for the parental clone (MELa1c). It is probable that the conserved central Gly-Trp pair is responsible for the apparent improvement in affinity over the base clone, MELa1c.

A.

Clone Number	CDR1α$_{(D27-Q31)}$	CDR2α$_{(I50-N53)}$	TCRαF3	Freq	% Inhib. @ 5 nM
wt	DRGSQ	IYSN	QYV	–	–
MELa1	DRGSQ	IYSN	QYV	8	51-61
MELa15	**FQ**GSQ	IYSN	QYV	5	54-66
MELa16	**FL**GSQ	IYSN	QYV	2	60
MELa17	**FQ**G**A**Q	IYSN	QYV	1	51
MELa18	**YQ**G**A**Q	IYSN	QYV	1	50
MELa19	**FQ**GS***Q***	IYSN	QYV	1	47
MELa20	**SIHA**Q	IYSN	QYV	1	59
MELa21	**NL**GSQ	IYSN	QYV	1	55
MELa22	**DF**G**A*Q***	IYSN	QYV	1	51
MELa23	DRGSQ	**T**Y**RE**	Q**H**V	1	63

B.

Clone Number	TCRβF2	CDR2β$_{(S50-I53)}$	TCRβF3	Freq	% Inhib. @ 10 nM
wt	GLQ	SVGI	EVP	–	–
MELa1c	GLQ	SVGI	EVP	–	60
MELb1	G**P**Q	**YGPF**	EVP	16	85-90
MELb2	G**P**Q	**FGPF**	EVP	3	85-90
MELb3	G**P**Q	**FGPY**	E**A**P	4	85-90
MELb4	G**P**Q	**WGPF**	EVP	1	85-90

C.

Clone Number	TCRβF2	CDR3β$_{(G99-F104)}$	TCRβF3	Freq	% Inhib. @ 10 nM
wt	GLQ	GTGELF	FIL	–	–
MELa1c	GLQ	GTGELF	FIL	–	60
MELb5	GLQ	G**M**G**GWQ**	FIL	3	80
MELb6	GLQ	G**M**G**GWS**	FIL	1	78
MELb7	GLQ	G**M**G**GWA**	FIL	1	79
MELb8	G**P**Q	G**V**G**GWD**	FIL	1	82
MELb9	GLQ	G**V**G**GWE**	FIL	3	80
MELb10	GLQ	**NTSGW**F	F**V**L	2	83
MELb11	GLQ	**NTNGW**F	FIL	1	83
MELb12	GLQ	**NL**G**GW**F	FIL	3	79
MELb13	GLQ	**NVSGW**F	FIL	4	75
MELb14	GLQ	**NTTGW**F	FIL	1	73

Table 3.6. Output clones obtained following three rounds of panning against biotinylated-HLA-A*0201-Melan-A/MART-1$_{(26-35)}$ complexes (100 nM in round 1, followed by two subsequent cycles against 10 nM HLA). (A). Library 1: CDR1α and CDR2α mutants on the MELa1bwt background. Clone MELa15 contains an amber codon (*Q*). Clone MELa23bwt has acquired a mutation in alpha framework 3 (tyrosine to histidine). From soluble inhibition ELISA Library 1 clones showed 60-63% inhibition compared to 56% for the background clone (MELa1) at 5 nM HLA-A*0201-Melan-A/MART-1$_{(26-35)}$ complexes. **(B).** Library 3: CDR2β mutants on the MELa1cbwt background. All selected clones contain a leucine (L) to proline (P)

substitution in the beta framework 2. Clone MELb3 also contains a non-targeted mutation, valine (V) to alanine (A) in beta framework 3. **(C).** Library 4: CDR3β mutants on the MELa1cbwt background. Clone MELb8 contains a non-targeted mutation, leucine (L) to proline (P) in beta framework 2. Clone MELb10 contains a non-targeted mutation, isoleucine (I) to valine (V) in beta framework 3. From soluble inhibition ELISA library 3 and library 4 clones showed 75-89% inhibition compared to ~60% for the background clone (MELa1c) at 10 nM HLA-A*0201-Melan-A/MART-$1_{(26-35)}$ complexes. Red lettering indicates residues mutated from the parental sequence. International Immunogenetics (IMGT) nomenclature (Lefranc, Giudicelli et al. 1999).

3.8 Characterisation of the second generation Mel-5 TCRs

3.8.1 Soluble expression of Mel-5 TCRs

PCR construction and ligation into the expression plasmid pGMT7 for expression in *E. coli* strain Rosetta (DE3) pLysS of 2 α and 8 β chain Mel-5 TCR mutants described in Table 3.9 was performed by Dr. A. Vuidepot and Dr. T. Mahon. The *E. coli* TG1 glycerol stock 96-well master-plates for the Mel-5 TCR Pan 3 output (Section 3.7.1) were used as the template to PCR amplify the two mutated Vα domains and eight mutated Vβ domains. Amber codons were replaced with Gln for TCR expression in the non-suppressor strain *E. coli* Rosetta (DE3) pLysS. The mutated Vα domains were amplified from the phagemid vector using primers TRAV12-2 and SalI Rev and cloned into pEX954 as *Cla*I-*Sal*I fragments. The mutated Vβ domains were amplified from the phagemid vector using primers TRBV30 and AgeI Rev and cloned as *Nde*I-*Age*I fragments into modified version of pGMT7 (pEX821) containing a complete wild-type TCR Cβ (TRBC*01) domain containing the introduced TCR chain stabilising mutation at position 57 (Ser to Cys substitution). To generate clone MELa24 the CDR1α segment from MELa16 was spliced onto the CDR2α region from MELa23 by SOE-PCR and cloned as a *Cla*I-*Sal*I fragment into pEX954. To generate clone MELb15 the CDR2β segment from MELb1 was spliced onto the CDR3β region from MELb5 by SOE-PCR and cloned as a *Cla*I-*Sal*I fragment into pEX954. Similarly, MELb16 was generated by splicing the CDR2β segment from MELb4 onto the CDR3β region of MELb5 by SOE-PCR and cloned as an *Nde*I-*Age*I fragment into pEX821. TCRs were refolded from purified inclusion bodies and purified as described in Section 2.6.4-2.6.8 of Materials and Methods. The goal of the affinity maturation of the Mel-5 TCR was to achieve the highest affinity clones from the pool of mutated CDR segments isolated from the

various phage libraries. Therefore, rather than refold the mutated β segments in the context of the chain with which they were isolated (MELa1c), mutated β chain CDR segments were refolded with the highest affinity α chain mutant (MELa1).

3.8.2 Kinetic analysis of second generation Mel-5 TCRs

Equilibrium binding constants were calculated from kinetic data following the methods outlined in Section 2.7 of Materials and Methods.

Recruitment of CDR1α segments, MELa15 and MELa16 into the MELa1 clone yielded a modest 0.7 and 2-fold increase in affinity respectively (Table 3.7 A). This moderate improvement in affinity agreed with the phage inhibition ELISA data (Table 3.8 A) that showed little if any difference in the % inhibition values between the mutants and MELa1. Whilst the affinity remained largely unchanged, up to a 5-fold reduction in off-rate was observed. Although addition of a CDR2α segment into the MELa1 clone resulted in a reduction in affinity (1.7-fold), the half-life of dissociation ($T_{1/2}$) was increased by ~2-fold (Table 3.7 A) as a consequence of a reduced off-rate. This slight improvement in $T_{1/2}$ may contribute to further increases in affinity when combined with other CDR segments.

Recruitment of CDR2β segments into the MELa1 clone resulted in increases in affinity of between ~8 and 15-fold (Table 3.7 B). The highly conserved sequence of the mutants was reflected in almost identical binding kinetics. The mutated CDR2β segment, MELb1, dominated the Pan 3 phage output (67% of sequenced clones) (Table 3.6 B) and although this enrichment conferred the highest affinity of all the mutants from this library, the difference was marginal (up to 2.5-fold). Selection of this clone is probably a consequence of affinity and more importantly, favourable expression. Addition of the CDR3β segments conferred similar improvements in

affinity to that of the CDR2β regions. The CDR3β mutations reside in two groups separated by a single residue: Group A, targeted positions G99-L103 and Group B, positions T100-F104. Mutations within the Group B region of the CDR loop conferred greater increases in affinity (up to 4.8-fold increase).

Combining the CDR1α region from MELa16 with the CDR2α region from MELa23 yielded clone MELa24 with a 4.9-fold and 13,846-fold improvement in affinity compared to MELa1 and the wild-type TCR respectively (Table 3.7 C). Combining the most optimal CDR segments isolated from first and second generation phage libraries into a single clone generated a TCR with significantly enhanced affinity compared to the wild-type molecule; 1.8 million-fold increase in affinity (Table 3.7 C).

CDRs were independently optimised and then combined in a single clone. This step-wise approach proved highly successful in generating ultra-high affinity TCRs with extremely long half-lives (Figure 3.16 A and 3.16 B). Additivity of the CDR segments was demonstrated and is most clearly illustrated by $T_{1/2}$ values calculated for alpha chain mutants (Figure 3.16 B). Combining the alpha chain CDRs incrementally increased the $T_{1/2}$. The mean fold increase in $T_{1/2}$ for the addition of two mutated CDRs was 2.85-fold and for the addition of a third CDR segment was 8.6-fold. Inclusion of beta chain CDR segments in a combination of five mutated CDRs increased the $T_{1/2}$ by 1423-fold (setting the $T_{1/2}$ value for MELa1 at 1). The on-rates remained largely unchanged; up to 14-fold variation (Figure 3.16 D).

Improvements in affinity are dominated by decreases in off-rate; up to 1000-fold slower off-rate for the highest affinity clone compared to MELa1 (Figure 3.16 C; 3α = MELa1 and the highest affinity clones are labelled 1α2α3α2β3β).

A.

Clone ID	CDR1α	CDR2α	CDR3α	CDR2β	CDR3β	K_{on} (M^{-1} s^{-1})	K_{off} (s^{-1})	K_D (nM)	$T_{1/2}$ (min)	K_D (MELa1bwt) / K_D (mutant)	K_D (parent) / K_D (mutant)
MELawtbwt	DRGSQ	IYSNG	VAGKS	SVGI	GTGELF	nd	nd	18000	nd	-	1
MELa1bwt	DRGSQ	IYSNG	**DG**G**RL**	SVGI	GTGELF	5.08×10^{5}	3.26×10^{-3}	6.4	3.5	1	2813
MELa15bwt	**FQ**GSQ	IYSNG	**DG**G**RL**	SVGI	GTGELF	2.00×10^{5}	1.21×10^{-3}	6.1	9.5	0.7	2951
MELa16bwt	**FL**GSQ	IYSNG	**DG**G**RL**	SVGI	GTGELF	2.00×10^{5}	6.56×10^{-4}	3.2	17.5	2	5625
MELa23bwt	DRGSQ	**T**Y**RE**G	**DG**G**RL**	SVGI	GTGELF	1.70×10^{5}	1.80×10^{-3}	10.6	6.4	-1.7	1698

B.

Clone ID	CDR1α	CDR2α	CDR3α	CDR2β	CDR3β	K_{on} (M^{-1} s^{-1})	K_{off} (s^{-1})	K_D (nM)	$T_{1/2}$ (min)	K_D (MELa1bwt) / K_D (mutant)	K_D (parent) / K_D (mutant)
MELawtbwt	DRGSQ	IYSN	VAGKS	SVGI	GTGELF	nd	nd	18000	nd	-	1
MELa1bwt	DRGSQ	IYSN	**DG**G**RL**	SVGI	GTGELF	5.08×10^{5}	3.26×10^{-3}	6.4	3.5	1	2813
MELa1b1	DRGSQ	IYSN	**DG**G**RL**	**YGPF**	GTGELF	5.46×10^{5}	2.30×10^{-4}	0.42	50.2	15.2	42857
MELa1b2	DRGSQ	IYSN	**DG**G**RL**	**FGPF**	GTGELF	3.92×10^{5}	2.04×10^{-4}	0.52	57	12.3	34615
MELa1b3	DRGSQ	IYSN	**DG**G**RL**	**FGPY**	GTGELF	2.69×10^{5}	2.20×10^{-4}	0.82	52.5	7.8	21951
MELa1b4	DRGSQ	IYSN	**DG**G**RL**	**WGPF**	GTGELF	2.83×10^{5}	1.73×10^{-4}	0.61	66.7	10.5	29508
MELa1b5	DRGSQ	IYSN	**DG**G**RL**	SVGI	G**M**G**GWQ**	3.87×10^{5}	1.55×10^{-4}	0.4	74	16	45000
MELa1b9	DRGSQ	IYSN	**DG**G**RL**	SVGI	G**V**G**GWE**	3.63×10^{5}	2.06×10^{-4}	0.57	56	11.2	31579
MELa1b12	DRGSQ	IYSN	**DG**G**RL**	SVGI	**NL**G**GW**F	1.14×10^{5}	1.14×10^{-4}	1	101	6.4	18000
MELa1b13	DRGSQ	IYSN	**DG**G**RL**	SVGI	**NVSGW**F	8.40×10^{4}	1.62×10^{-4}	1.9	71	3.4	9474

C.

Clone ID	CDR1α	CDR2α	CDR3α	CDR2β	CDR3β	K_{on} (M^{-1} s^{-1})	K_{off} (s^{-1})	K_D (nM)	$T_{1/2}$ (min)	K_D (MELa1bwt) / K_D (mutant)	K_D (parent) / K_D (mutant)
MELawtbwt	DRGSQ	IYSN	VAGKS	SVGI	GTGELF	nd	nd	18000	nd	-	1
MELa1bwt	DRGSQ	IYSN	**DG**G**RL**	SVGI	GTGELF	5.08×10^{5}	3.26×10^{-3}	6.4	3.5	1	2813
MELa24bwt	**FL**GSQ	**T**Y**RE**	**DG**G**RL**	SVGI	GTGELF	2.99×10^{5}	3.85×10^{-4}	1.3	30	4.9	13846
MELa24b15	**FL**GSQ	**T**Y**RE**	**DG**G**RL**	**YGPF**	G**M**G**GWQ**	2.85×10^{5}	2.86×10^{-6}	0.01	4020	640	1800000
MELa24b16	**FL**GSQ	**T**Y**RE**	**DG**G**RL**	**WGPF**	G**M**G**GWQ**	6.87×10^{4}	1.94×10^{-6}	0.028	5940	228.6	642857

Table 3.7. Affinities and binding kinetics of Mel-5 TCR mutants isolated from second generation libraries. (A). Mutants isolated from CDR1α and CDR2α libraries built on the MELa1 framework. **(B).** Mutants isolated from CDR2β and CDR3β libraries built on the MELa1c framework were refolded with the highest affinity α chain MELa1. **(C).** Combination of the most optimal α and β chain CDR segments. The ratio of K_D parent and mutant K_D gives the overall improvement in affinity from the starting Mel-5 wild-type TCR. K_{on} and K_{off} were determined by SPR in a BIAcore using purified refolded TCR and K_D calculated. nd, not determined. *Q*, Amber codon. (Data kindly provided by Dr. A. Vuidepot and Dr. T. Mahon).

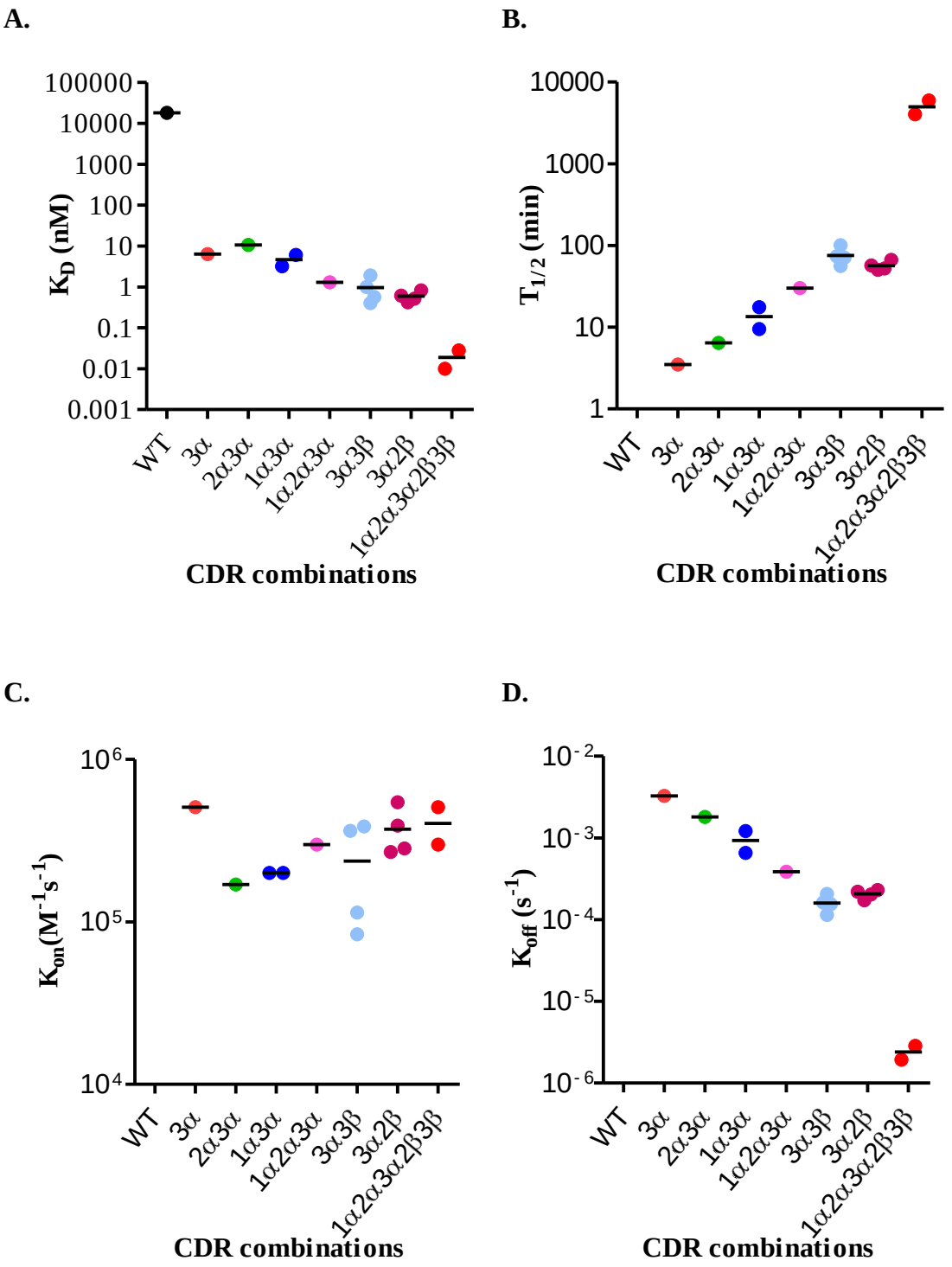

Figure 3.16. Affinities and binding kinetics of Mel-5 TCR CDR segments isolated from first and second generation libraries. Mutated CDR regions were combined in a step-wise manner to enhance the binding affinity of the engineered Mel-5 TCR for HLA-A*0201-Melan-A/MART-$1_{(26-35)}$. **(A).** Equilibrium dissociation constant (K_D). **(B).** Dissociation half-life ($T_{1/2}$). **(C).** Association rate constant (K_{on}). **(D).** Dissociation rate constant (K_{off}).

ENGINEERING FOR HIGH AFFINITY A CLASS I HLA-A2 RESTRICTED T CELL RECEPTOR AGAINST THE GP100$_{(280-288)}$ TUMOUR ASSOCIATED ANTIGEN BY PHAGE DISPLAY

4.1 Introduction

This chapter further explores the sequential optimisation strategy that was successfully employed to affinity mature the Mel-5 TCR (Chapter 3). This type of CDR walking strategy, in which CDR segments are independently optimised and then recombined, is based on the assumption that non-interacting mutations will be additive (Wells 1990). Although this optimisation method has proved successful in antibody affinity maturation, the additive effects of enhanced-affinity antibody CDR segments are often unpredictable (Yang, Green et al. 1995; Chen, Wiesmann et al. 1999). The aim of this chapter was to determine the generality of the CDR walking based method for the affinity maturation of TCRs.

The focus of this chapter is the affinity maturation of the gp100 TCR that recognises the melanoma-specific epitope derived from HLA-A*0201-gp100$_{280-288}$ (Cox, Skipper et al. 1994). The gp100 TCR was isolated from a gp100-specific human CD8$^+$ T-cell clone that recognizes the YLEPGPVTA peptide in complex with HLA-A*0201 and was kindly provided by Cassian Yee (Fred Hutchinson Cancer Research Centre, Seattle WA, USA). The wild-type TCR α and β chains were expressed separately in *E. coli* and the TCR was refolded from inclusion bodies. The affinity of interaction against the wild-type peptide (YLEPGPVTA) and heteroclitic variant peptide (YLEPGPVTV) was determined as 26 μM (Aleksic, Liddy et al. 2012; Liddy, Bossi et al. 2012) and 22 μM respectively (unpublished).

4.2 First-generation gp100 TCR affinity maturation phage libraries

First-generation libraries were kindly provided by Dr. N. Harwood. The phagemid vector pG159 for the phage display of the gp100 TCR (specific for HLA-A*0201 in complex with the gp100$_{(280-288)}$ peptide) was constructed as described in section 3.2 using Vα and Vβ specific primers to amplify the wild-type gp100 TCR α and β

chains. The templates used to generate the fragments were *E. coli* expression plasmids encoding the wild-type α and β chains. The gp100 TCR α chain V domain is encoded by TRAV17*01 and TRAJ29*01 gene segments. The α C region is encoded by TRAC*01 gene segment. The gp100 TCR β chain V domain is encoded by TRBV19*01, TRBJ2-7*01 and TRBD1*01 gene segments. The β C region is encoded by TRBC1*01 segments. In the final construct, the α and β chains contain the engineered ds cysteines (in the mTCR format). The 3' end of the TCR β chain is fused in frame to the 5' end of the bacteriophage M13 geneIII. The pelB and geneIII leader sequences are fused to the 5' end of the α and β chains respectively as illustrated in Figure 3.4. The sequence of the wild-type gp100 TCR *Nco*I-*Not*I phagemid fragment is shown in Figure 4.1.

NcoI

pelB leader gene

~~

M K Y L L P T A A A G L L L L A A Q P A

1 ATGAAATACC TATTGCCTAC GGCAGCCGCT GGATTGTTAT TACTCGCGGC CCAGCCGGCC
TACTTTATGG ATAACGGATG CCGTCGGCGA CCTAACAATA ATGAGCGCCG GGTCGGCCGG

NcoI

~~~~

M A S Q Q G E E D P Q A L S I Q E G E N

61 ATGGCCAGTC AACAAGGAGA AGAAGATCCT CAGGCCTTGA GCATCCAGGA GGGTGAAAAT
TACCGGTCAG TTGTTCCTCT TCTTCTAGGA GTCCGGAACT CGTAGGTCCT CCCACTTTTA

CDR1α

A T M N C S Y K **T S I N N** L Q W Y R Q N

121 GCCACCATGA ACTGCAGTTA CAAAACTAGT ATAAACAATT TACAGTGGTA TAGACAAAAT
CGGTGGTACT TGACGTCAAT GTTTTGATCA TATTTGTTAA ATGTCACCAT ATCTGTTTTA

CDR2α

S G R G L V H L I L **I R S N E R E** K H S

181 TCAGGTAGAG GCCTTGTCCA CCTAATTTTA ATACGTTCAA ATGAAAGAGA GAAACACAGT
AGTCCATCTC CGGAACAGGT GGATTAAAAT TATGCAAGTT TACTTTCTCT CTTTGTGTCA

G R L R V T L D T S K K S S S L L I T A

241 GGAAGATTAA GAGTCACGCT TGACACTTCC AAGAAAAGCA GTTCCTTGTT GATCACGGCT
CCTTCTAATT CTCAGTGCGA ACTGTGAAGG TTCTTTTCGT CAAGGAACAA CTAGTGCCGA

CDR3α

S R A A D T A S Y F **C A T D G D T P L V**

301 TCCCGGGCAG CAGACACTGC TTCTTACTTC TGTGCTACGG ACGGAGACAC ACCTCTTGTC
AGGGCCCGTC GTCTGTGACG AAGAATGAAG ACACGATGCC TGCCTCTGTG TGGAGAACAG

F G K G T R L S V I A N I Q **K** P D P A V

361 TTTGGAAAGG GCACAAGACT TTCTGTGATT GCAAATATCC AGAAGCCTGA CCCTGCCGTG
AAACCTTTCC CGTGTTCTGA AAGACACTAA CGTTTATAGG TCTTCGGACT GGGACGGCAC

Y Q L R D S K S S D K S V C L F T D F D

421 TACCAGCTGA GAGACTCTAA GTCGAGTGAC AAGTCTGTCT GCCTATTCAC CGATTTTGAT
ATGGTCGACT CTCTGAGATT CAGCTCACTG TTCAGACAGA CGGATAAGTG GCTAAAACTA

S Q T N V S Q S K D S D V Y I T D K **C** V

481 TCTCAAACAA ATGTGTCACA AAGTAAGGAT TCTGATGTGT ATATCACAGA CAAATGTGTG
AGAGTTTGTT TACACAGTGT TTCATTCCTA AGACTACACA TATAGTGTCT GTTTACACAC

L D M R S M D F K S N S A V A W S N K S

541 CTAGACATGA GGTCTATGGA CTTCAAGAGC AACAGTGCTG TGGCCTGGAG CAACAAATCT
GATCTGTACT CCAGATACCT GAAGTTCTCG TTGTCACGAC ACCGGACCTC GTTGTTTAGA

D F A C A N A F N N S I I P E D T F F P

601 GACTTTGCAT GTGCAAACGC CTTCAACAAC AGCATTATTC CAGAAGACAC CTTCTTCCCC
CTGAAACGTA CACGTTTGCG GAAGTTGTTG TCGTAATAAG GTCTTCTGTG GAAGAAGGGG

S P E S S * *

661 AGCCCAGAAA GTTCCTAATA ACCTAGGTTA ATTAAGAATT CTTTAAGAAG GGGATATACA
TCGGGTCTTT CAAGGATTAT TGGATCCAAT TAATTCTTAA GAAATTCTTC CCCTATATGT

gIII leader gene

M K K L L F A I P L V V P F Y S H S A Q

721 TATGAAAAAA TTATTATTCG CAATTCCTTT AGTTGTTCCT TTCTATTCTC ACAGCGCGCA
ATACTTTTTT AATAATAAGC GTTAAGGAAA TCAACAAGGA AAGATAAGAG TGTCGCGCGT

· D G G I T Q S P K Y L F R K E G Q N V T

781 GGATGGTGGA ATCACTCAGT CCCCAAAGTA CCTGTTCAGA AAGGAAGGAC AGAATGTGAC
CCTACCACCT TAGTGAGTCA GGGGTTTCAT GGACAAGTCT TTCCTTCCTG TCTTACACTG

CDR1β

· L S C E Q N **L N H D A** M Y W Y R Q D P G

841 CCTGAGTTGT GAACAGAATT TGAACCACGA TGCCATGTAC TGGTACCGAC AGGACCCAGG
GGACTCAACA CTTGTCTTAA ACTTGGTGCT ACGGTACATG ACCATGGCTG TCCTGGGTCC
~~~~

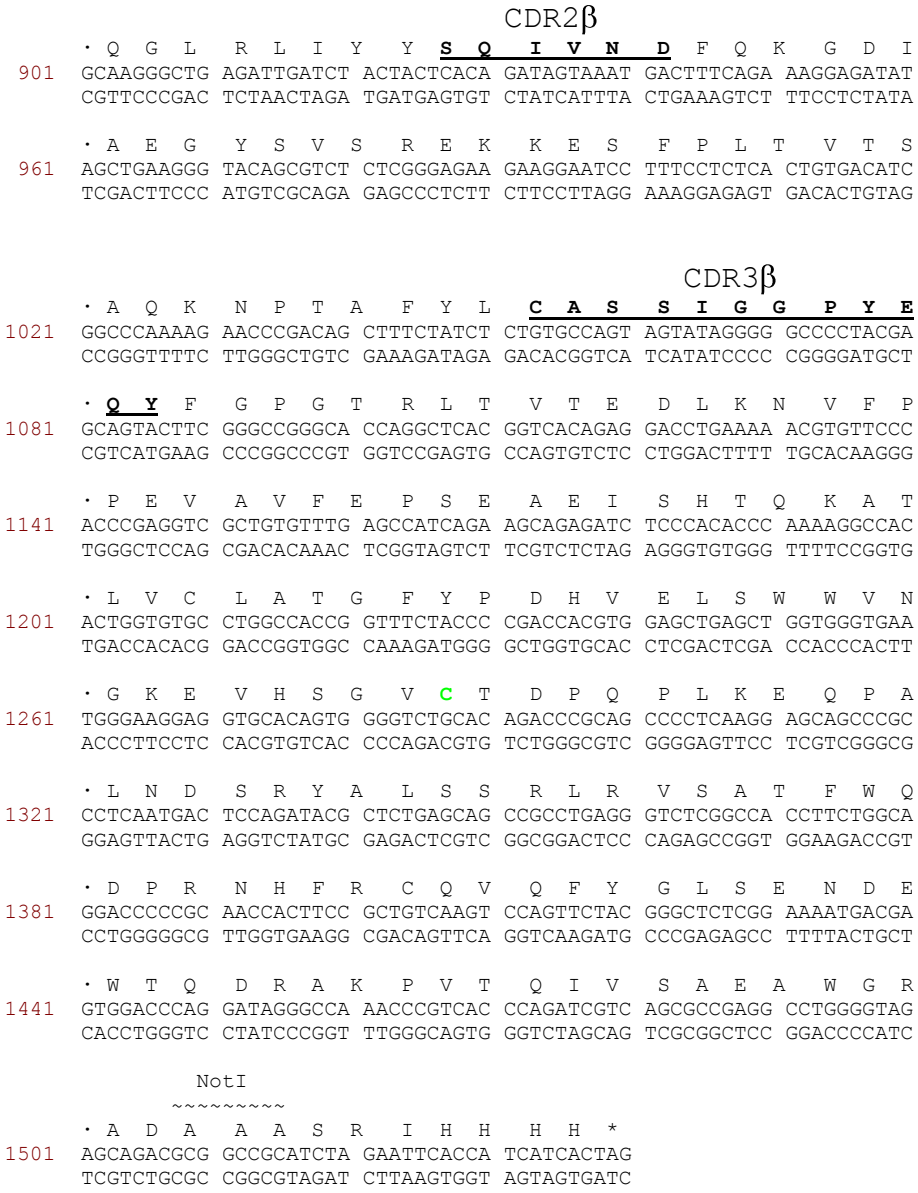

Figure 4.1. Sequence of gp100 wild-type TCR cloned into the phagemid vector pEX922. The amino acid residues encoding the pelB and bacteriophage M13 gene III leader genes are highlighted in red and blue respectively. The six CDR loops, designated by the International Immunogenetics (IMGT) database (Lefranc, Giudicelli et al. 1999), are in bold and underlined. The TCR membrane-proximal cysteines in both the α and β chains have been removed. The introduced TCR stabilising constant region cysteines (at positions TRAC threonine 48 and TRBC serine 57) are highlighted in bright green. An N4K mutation has been introduced into Cα by PCR error (shown in violet). The restriction enzyme sites used for molecular cloning purposes are highlighted (*Nco*I and *Not*I). Asterisks show the location of TAA and TAG (amber) stop codons. The sequence was analysed with Vector NTI Advance 11.

Libraries were assembled in which each of the six CDRs were individually targeted for mutagenesis resulting in TCRs with one wild-type and one mutant chain as described in section 3.3. Panning was performed against the TAA, $gp100_{(280-288)}$, bound in the context of biotinylated HLA-A*0201. To increase the stability of the pHLA complex, a heteroclitic version of the $gp100_{(280-288)}$ peptide was used in all panning and ELISA screening experiments. The variant peptide contains an Ala288Val substitution (YLEPGPVTV). Three cycles of panning were performed against HLA-A*0201-$gp100_{(280-288)}$ peptide. Antigen binding clones were exclusively isolated from the CDR2β library.

Seven CDR2β variants were expressed in *E. coli* Rosetta (DE3) pLysS cells and refolded with the gp100 TCR wild-type α chain. Purified refolded TCR was subjected to SPR on a BIAcore instrument. Equilibrium binding constants were calculated from kinetic data following the methods outlined in Section 2.7 of Materials and Methods. The affinity of interaction between the CDR2β mutants and the wild-type (YLEPGPVTA) and variant peptide (YLEPGPVTV) was substantially improved compared to the parental TCR; ~5000-fold and ~3800-fold improvement for clone GPawtb1 respectively (Table 4.1). The affinities were in the range of ~5-39 nM (wild-type peptide) and ~6-45 nM (heteroclitic peptide) compared to 26 μM (wild-type peptide) and 22 μM (heteroclitic peptide) for the wild-type TCR. The $T_{1/2}$ values were in the range of ~1-5 minutes. Importantly, the affinity engineered gp100 TCRs bound both the wild-type and heteroclitic peptide ligands with comparable kinetics (Table 4.1) providing support for the use of the HLA-stabilising peptide variant for all further experiments.

Clone ID	Peptide	CDR2β	K_{on} (M^{-1} s^{-1})	K_{off} (s^{-1})	K_D (nM)	$T_{1/2}$ (min)	$\frac{K_D \text{ (parent)}}{K_D \text{ (mutant)}}$
GPawtbwt	wt	SQIVND	nd	nd	26000	nd	1
	het		nd	nd	22000	nd	1
GPawtb1	wt	S**WAQG**D	4.77×10^5	2.47×10^{-3}	5.18	4.6	5019
	het		4×10^5	2.33×10^{-3}	5.83	4.9	3773.6
GPawtb2	wt	S**WGVG**D	2.88×10^5	1.09×10^{-2}	37.8	1.1	687.8
	het		3.05×10^5	1.02×10^{-2}	33.4	1.13	658.7
GPawtb3	wt	S**WAQGH**	3.2×10^5	4.71×10^{-3}	14.7	2.44	1768.7
	het		3.71×10^5	4.47×10^{-3}	12	2.57	1833.3
GPawtb4	wt	S**WAYGH**	2.84×10^5	3.13×10^{-3}	19.5	3.67	1333.3
	het		3.16×10^5	3.02×10^{-3}	9.5	3.8	2736.8
GPawtb5	wt	S**WA**V**GN**	2.99×10^5	5.82×10^{-3}	19.5	1.97	1333.3
	het		2.32×10^5	5.81×10^{-3}	25	1.98	880
GPawtb6	wt	S**WAQF**D	1.25×10^5	3.41×10^{-3}	27.2	3.3	955.9
	het		3.53×10^5	3.33×10^{-3}	9.44	3.4	2330.6
GPawtb7	wt	S**WGTG**D	3.44×10^5	1.33×10^{-2}	38.7	0.87	671.8
	het		2.78×10^5	1.24×10^{-2}	44.6	0.9	493.3

Table 4.1. Affinities and binding kinetics of gp100 TCR mutants isolated from first-generation libraries. Mutants isolated from CDR2β libraries built on the wild-type framework. K_{on} and K_{off} were determined by SPR in a BIAcore using purified refolded TCR and K_D calculated. Binding against HLA-A*0201-gp100$_{(280\text{-}288)}$ wild-type (wt) peptide (YLEPGPVTA) and heteroclitic (het) peptide (YLEPGPVTV). nd, not determined. (Data kindly provided by J. Gaverret).

As had been observed with the Mel-5 TCR, mutants isolated from the first-generation affinity maturation libraries did not possess the required binding kinetics for suitability as protein therapeutics. Using an enhanced affinity mutant as the template for second-generation mutagenesis had proved a successful strategy for isolating high affinity Mel-5 TCRs. The aim was to establish whether this was a generic method to increase the affinity of TCRs using a stepwise strategy. Here, clone

GPb7 (having the weakest affinity from the first-generation phage output) was used as the template to build further CDR-targeted phage libraries.

4.3 Design and construction of second-generation gp100 TCR libraries

Following on from the affinity maturation of the Mel-5 TCR, a number of modifications to the method for generating and cloning mutagenised gp100 TCR fragments were implemented. First, the SOE-PCR strategy was adapted; rather than introducing mutations into the CDR loop using a linking NNK oligonucleotide as illustrated in Figure 5, here the NNK primer was used to amplify one of the two PCR fragments. This modification simplified the assembly step by reducing the number of fragments from three to two. Second, instead of cloning a mutagenised α or β chain segment into a phagemid bearing the corresponding wild-type chain, here a mutagenised α or β chain fragment was spliced onto the corresponding wild-type chain by SOE-PCR. In this way, the final pull-through PCR could be performed with two primers (YOL13 and YOL22) compatible to the 5' *Nco*I or 3' *Not*I segments of the amplified TCR gene fragments. Therefore each could be conveniently cloned into the phagemid vector as *Nco*I-*Not*I fragments. Third, in an attempt to reduce further the potential contamination of library PCRs with parent DNA (in addition to the *Dpn*I-treatment of the PCR fragments), the phagemid vector template was linearised separately with *Nco*I and *Not*I. Fourth, SOE-PCR fragments were sequenced before progressing to the digestion and ligation steps to assess quality and to monitor for parental DNA contamination.

4.3.1 Generating library PCR fragments

Linearising the template DNA was performed to reduce the level of background amplification of parental DNA. Fragments generated with the YOL13 primer using

*Not*I cut template were not extended beyond the *Not*I site and so the YOL22 priming site was not present in the PCR product. Likewise, YOL22 fragments amplified from *Nco*I digested DNA were not extended past the *Nco*I site and so prevented the synthesis of the YOL13 priming site. This step reduced the amount of non-mutagenised parental DNA amplified in the SOE-PCR reaction with YOL13-YOL22. This is of particular importance when using an affinity-enhanced clone which could be enriched over other mutants if present at high levels in the library population.

The phagemid vector containing the wild-type gp100 α chain and the affinity-enhanced CDR2β mutant, GPb7, was linearised separately with *Nco*I and *Not*I and gel-purified. Purified plasmids were quantitated by agarose gel electrophoresis (Figure 4.2) and diluted to ~2 ng/μl for PCR. The *Not*I linearised plasmid was used as the template for PCRs set up with the YOL13 forward primer and *Nco*I linearised plasmid was used as the template for PCRs set up with the YOL22 reverse primer.

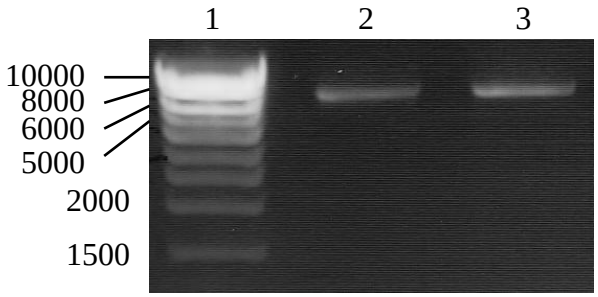

Figure 4.2. Ethidium bromide stained agarose gel photo of gel-purified linearised phagemid vector pEX922:GPawtb7. Lane 1, Hyperladder I size of bands in bp; lane 2, pEX922:gp100awtb12 digested with *Nco*I; lane 3, pEX922:gp100awtb7 digested with *Not*I. 1% (w/v) agarose gel.

Three independent libraries were constructed within the context of clone GPb7 CDR2β mutant. The CDR loops targeted for NNK mutagenesis were CDR2α, CDR3α and CDR3β. For each library overlapping 5-NNK oligonucleotides were designed to span the entire CDR: two for CDR2α, three for CDR3α and four for CDR3β. The number of NNK primers was dictated by the CDR length. Using the strategy depicted in Figure 2.3 of Materials and Methods as a guide and the primer set in Section 2.4.2 of Materials and Methods, eighteen PCR fragments were generated. As can be seen from Figure 2.3 of Materials and Methods there is no fragment a4. Instead the fragment amplified with YOL13-Nat53 (a1) was used in the SOE-PCR with fragments a2 and a5. The primer that had been designed specifically for amplification with YOL13 to generate fragment a4 failed to yield a product and so PCR a1 was used as a substitute. Fragments a2 and a5 generated with NNK primers Nat54 and Nat55 respectively only differ by a 3 bp shift at the 5' end and so fragment a1 would anneal to both with comparable efficiency. PCR fragments of the expected size were gel-purified and 1 μl of each was resolved on a 1% (w/v) agarose gel (Figure 4.3). The PCR fragments were all of the desired size and could be quanititated using the Hyperladder I DNA ladder as a guide.

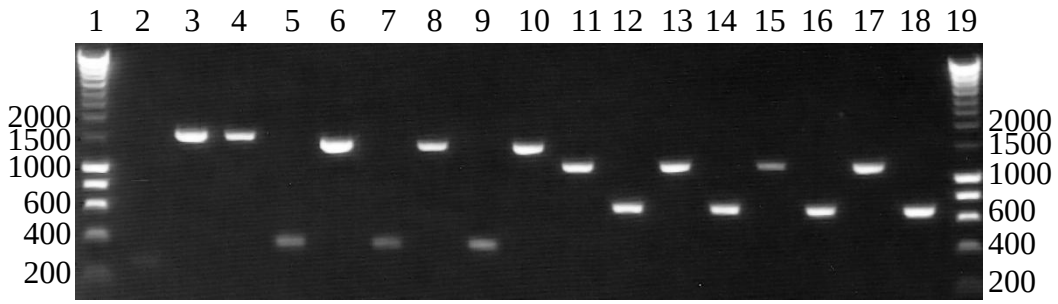

Figure 4.3. Ethidium bromide stained agarose gel photo of gel-purified gp100 TCR library PCR fragments. Lane 1, HYP I; lane 2, PCR fragment a1; lane 3, PCR a2; lane 4, PCR a5; lane 5, PCR a7; lane 6, PCR a8; lane 7, PCR a10; lane 8, PCR a11; lane 9, PCR a13; lane 10, PCR a14; lane 11, PCR b1; lane 12, PCR b2; lane 13, PCR fragment b4; lane 14, PCR b5; lane 15, PCR b7; lane 16, PCR b8; lane 17, PCR b10; lane 18, PCR b11; lane 19, HYP I. 1% (w/v) agarose gel.

4.3.2 Generating full-length α and β chain library PCR fragments

TCR fragments containing mutagenised CDR segments were assembled by SOE-PCR: equimolar amounts of each of the two PCR fragments (~10-12 ng total DNA) were added together with the external primers YOL13 and YOL22 and amplified through 30 cycles of PCR with Expand polymerase (Roche) (Section 2.4.2.1 of Materials and Methods). Amplification of background parental template was assessed by setting up control PCRs with YOL13 and YOL22 in which one or other of the two fragments was excluded. An equal volume of each PCR was resolved on a 1% (w/v) agarose gel (Figure 4.4 A and 4.4 B). A dominant band of the desired size (~1800 bp) was observed for each of the SOE-PCR reactions. Background amplification of template DNA was almost undetectable. A faint band was seen at ~600-700 bp for each of the stitch PCRs but was eliminated following gel-purification of the ~1800 bp product (Figure 4.4 C).

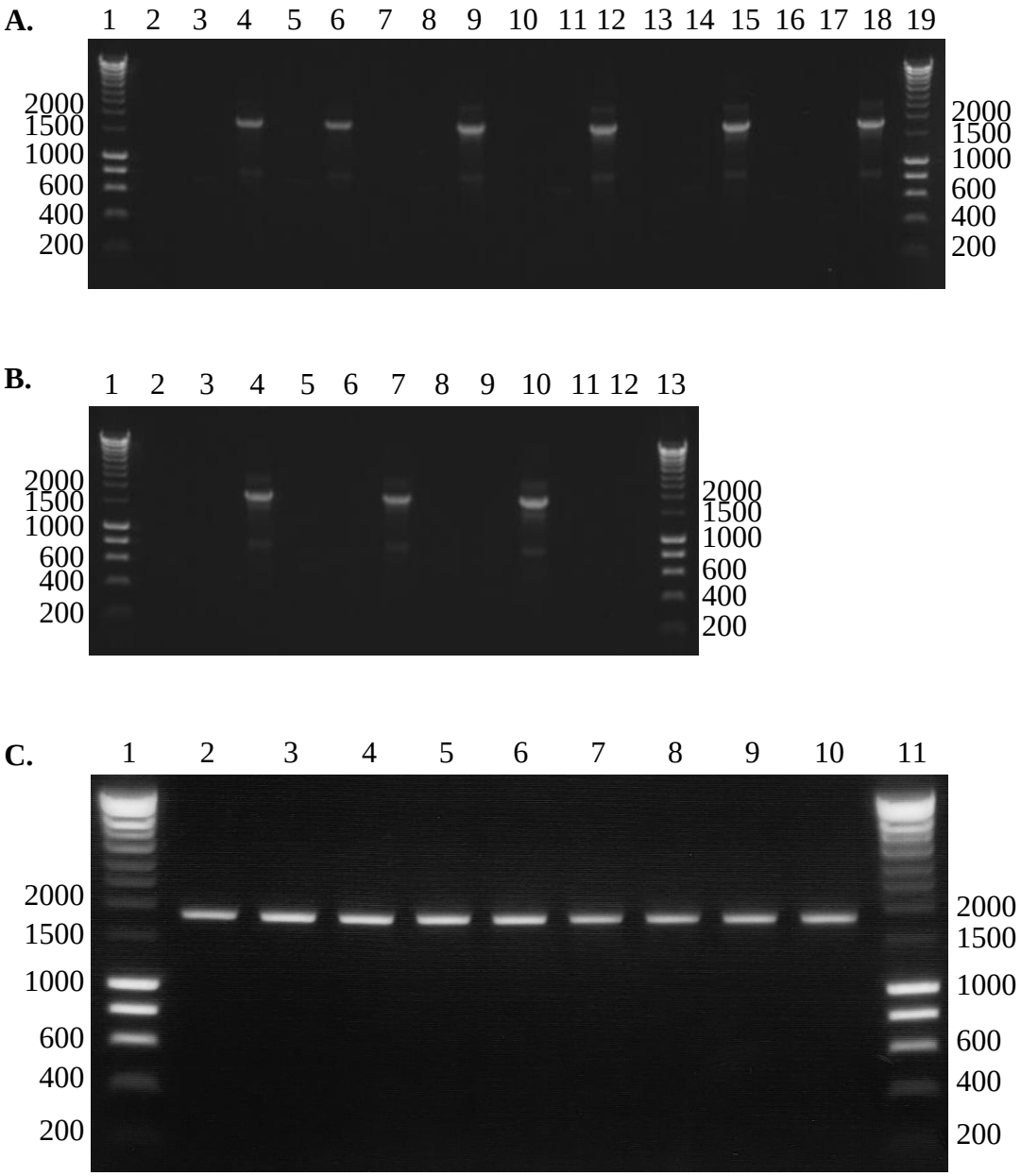

Figure 4.4. Photo of ethidium bromide agarose gel of overlapping stitch gp100 TCR library PCR fragments. (A). Lane 1, HYP I; lane 2, PCR a1 only; lane 3, PCR a2 only; lane 4, PCR a1 + a2; lane 5, PCR a5 only; lane 6, PCR a1 + a5; lane 7, PCR a7 only; lane 8, PCR a8 only; lane 9, PCR a7 + a8; lane 10, PCR a10 only; lane 11, PCR a11 only; lane 12, PCR a10 + a11; lane 13, PCR a13 only; lane 14, PCR a14 only; lane 15, PCR a13 + a14; lane 16, b1 only; lane 17, b2 only; lane 18 PCR b1 + b2; lane19, HYP I. **(B).** Lane 1, HYP I; lane 2, PCR b4 only; lane 3, PCR a5 only; lane 4, PCR b4 + b5; lane 5, PCR b7 only; lane 6, PCR b8 only; lane 7, PCR b7 + b8; lane 8, PCR b10 only; lane 9, PCR b11; lane 10, PCR b10 + b11; lane 11, no template control; lane 12, no sample; lane 13, HYP I. **(C).** Agarose gel photo of gel-purified alpha and beta chain stitch library PCR fragments. Lane 1, HYP I; lane 2, PCR a3; lane 3, PCR a6; lane 4, PCR a9; lane 5, PCR a12; lane 6, PCR a15; lane 7, PCR b3; lane 8, PCR b6; lane 9, PCR b9; lane 10, PCR b12; lane 11, HYP I. 1% (w/v) agarose gel.

4.3.3 Polyclonal sequencing of library PCR fragments

Contamination of the library population, as monitored by sequence analysis, had proved to be a concern during the Mel-5 TCR second-generation library construction (Section 3.7.1). As a result, two of the libraries were discarded from the panning experiments. In this example, library integrity was not assessed until after the electroporation step. In the affinity maturation of the gp100 TCR, we used polyclonal sequencing of the undigested stitch products to assess, far earlier in the process, the quality of each library.

Figure 4.5 illustrates the polyclonal sequencing of two individual 5-NNK stitch products: PCR fragment a3 (Figure 4.5 A) and PCR fragment a15 (Figure 4.5 B). The chromatogram shows a central mutated region that is flanked by parental sequence. The targeted region is mutated with a 5-NNK motif where N represents each of the four nucleotides and K represents nucleotides G or T. At position N each of the four nucleotide traces can be seen and at position K only G and T are present. Multiple nucleotides at a single position results in a reduction in the chromatogram signal at that position. Both chromatogram traces shown in Figure 24 depict polyclonal library sequence that was considered of sufficient quality to progress to the next stage of library construction. Polyclonal sequences showing either the NNK trace overlapping into the parental sequence or parental sequence overlapping the mutated region would be discarded. Polyclonal sequencing of the nine stitched library fragments showed no detectable parental contamination and each was of sufficient quality to proceed to the next stage of the library build.

A.

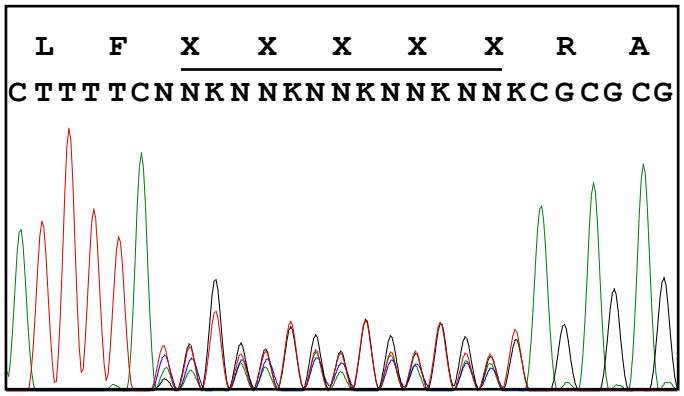

B.

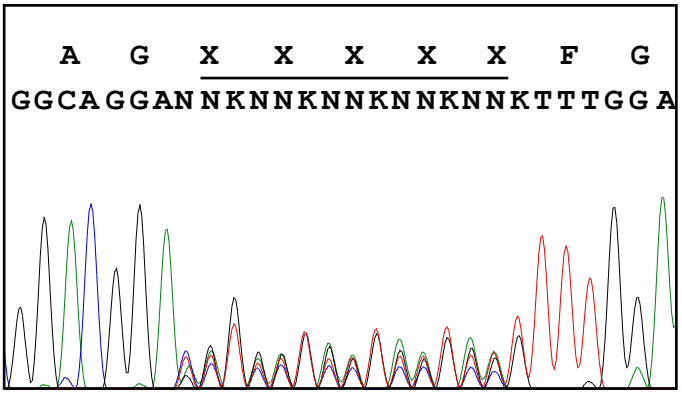

Figure 4.5. Examples of polyclonal sequencing of mutagenised gp100 TCR CDR loops using NNK oligonucleotides. SOE-PCR fragments amplified with YOL13-YOL22 were sequenced. NNK mutagenised regions are flanked by monoclonal non-mutagenised template DNA. **(A).** PCR a3 (CDR2α segment). **(B).** PCR a15 (CDR3α segment).

4.3.4 Generating bacterial libraries

Libraries targeting CDR2α (library 1), CDR3α (library 2) and CDR3β (library 3) were cloned into the phagemid vector pEX922 as *Nco*I-*Not*I fragments as described in Section 2.4.2 of Materials and Methods. Figure 4.6 illustrates the purity of the digested vector and library fragments used in the ligation reactions. A single sharp band can be observed for the phagemid vector pEX922 and for each of the ten library fragments. Electrocompetent *E. coli* TG1 cells were transformed separately with each of the three libraries to yield individual CDR libraries containing between 10^8 and 10^9 independent transformants. Ten randomly selected colonies from each of the three libraries were PCR amplified with primers YOL13 and YOL22. The integrity and diversity of the gp100 TCR libraries was confirmed by DNA sequencing to reveal a broad diversity of mutations spanning each of the targeted CDRs (data not shown).

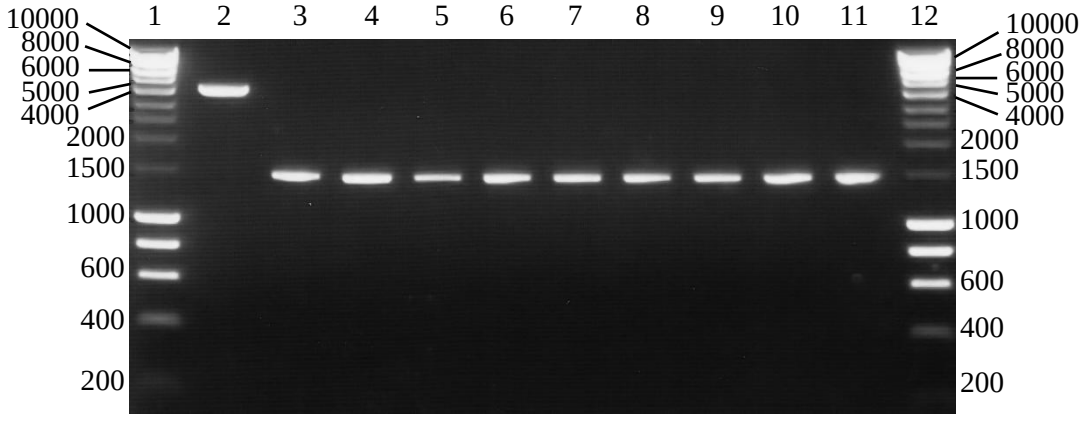

Figure 4.6. Ethidium bromide stained agarose gel photo of gp100 TCR gel-purified *Nco*I-*Not*I digested stitch library PCRs and pEX922 phagemid vector. Lane 1, HYP I; lane 2, pEX922; lane 3, PCR a3; lane 4, PCR a6; lane 5, PCR a9; lane 6, PCR a12; lane 7, PCR a15; lane 8, PCR b3; lane 9, PCR b6; lane 10, PCR b9; lane 11, PCR b12; lane 12, HYP I. 1% (w/v) agarose gel.

4.4 Phage selections and screening

The GPawtb7 mutant that was used as the framework on which to introduce mutations into the CDR2α, CDR3α and CDR3β loops binds to HLA-A*0201-gp100$_{(280-288)}$ with a K_D value of 44.6 nM. The concentration of antigen used in panning was chosen on the basis of this affinity. Three cycles of panning against 10 nM biotinylated HLA-A*0201-gp100$_{(280-288)}$ variant peptide (YLEPGPVTV) were performed with increased number of washes at each round (Section 3.5.4 of Materials and Methods). The output titre for each round of selection was estimated and following the third round of panning a significant increase was observed for each library: a 10-fold for library 1, a 14-fold for library 2 and a 30-fold for library 3.

Individual ampicillin-resistant *E. coli* TG1 colonies were picked from each of the library outputs and grown in a sterile 96-well tissue culture plate containing 100 μl growth media supplemented with ampicillin and 2% glucose (master-plates). As a control, a single *E. coli* TG1 colony bearing the GPawtb7 clone was grown in each of the three plates. Phage was rescued by infection with helper phage and grown in kanamycin-containing media overnight at 26°C with shaking as outlined in Section 2.5.1 of Materials and Methods. The following day, the cultures were pelleted and the supernatant containing monoclonal-phage-TCRs were screened in an inhibition phage ELISA at 5 nM HLA-A*0201-gp100$_{(280-288)}$ variant peptide (YLEPGPVTV) to determine if any of the TCRs demonstrated competitive inhibition. Antigen-binding phage clones were obtained from all three libraries.

4.4.1 ELISA screening of crude phage supernatant

Twenty clones from each library demonstrating the highest % inhibition at 5 nM inhibitor were sequenced. Sequence analysis of library 1 revealed mutations in CDR3α rather than in the region intentionally mutated (CDR2α). Of the 20

sequenced clones, 10 contained a single point mutation within CDR3α (data not shown). Enrichment of the CDR3α single point mutant resulted from contamination of library 1 with library 2 during library construction. Contamination was at a low level since sequencing of ten unselected variants revealed ten unique sequences (data not shown). The remaining library 1 sequenced clones were clone GPb7.

Of the sequenced library 2 output (Table 4.2 A), 50% was enriched for clone GPb7 and 50% for five unique clones. Clones GPa1 and GPa2 were represented by multiple copies (four and two copies respectively). Each of the clones retained at least two wild-type residues. In all cases wild-type residues at positions Thr^{95} and Pro^{96} were retained through alternative codon usage compared to the parental sequence. With the exception of clone GPa6, in which an Asp at residue 6 in Cα was substituted for Gly, no other mutations were observed outside of the targeted CDR3 region. The % inhibition at 5 nM was greater for each of the mutants compared to the framework clone (GPb7): 55-74% for the mutants versus 30% for GPb7.

Dramatic sequence convergence was observed in library 3 (Table 4.2 B). Of the twenty sequenced clones, nineteen contained the motif $G^{96}A^{97}P^{98}Y^{99}$ in which Ala^{97} was the only residue mutated from wild-type. Introduction of a Tyr at position Ile^{95} produced a significant increase in the % inhibition in clone GPb13; 90% compared to 38% of the framework clone. Addition of the Ala^{97} substitution further enhanced the apparent affinity demonstrated by clone GPb12; from 90% for GPb13 to 100% for GPb12. Thus highlighting the importance of the G97A substitution for affinity enhancement. Clone GPb8 which contained an Ala at position 97 and a Pro at position 100 dominated the library 3 output (55% of sequenced clones).

A.

Clone Number	CDR3α$_{(D94\text{-}G102)}$	Cα	Freq	% Inhib. @ 5 nM
GPb7	D T P L V F G K G gacacacctcttgtctttggaaagggc	K P D aagcctgac	10	30
GPa1	**S** T P L **M** F G K G tcgactcctttgatgtttggaaagggc	K P D aagcctgac	4	55
GPa2	D T P L **A** F G K G gacacacctcttgcctttggaaagggc	K P D aagcctgac	2	55
GPa3	**S** T P **M** **Q** F G K G tcgactccgatgcagtttggaaagggc	K P D aagcctgac	1	59
GPa4	**R** T P **M** **S** F G K G cggactcctatgagttttggaaagggc	K P D aagcctgac	1	57
GPa5	**T** T P L **G** F G K **D** acgacgccgcttggttttggaaaggac	K P D aagcctgac	1	74
GPa6	D T P L V F G K G gacacacctcttgtctttggaaagggc	K P **G** aagcctggc	1	58

B.

Clone Number	CDR3β$_{(S94\text{-}E100)}$	Freq	% Inhib. @ 5 nM
GPb7	S I G G P Y E agtataggggggcccctacgag	-	38
GPb8	S I G **A** P Y **P** agtataggtgcgccgtatccg	11	83
GPb9	S **H** G **A** P Y E tctcatggggctccgtacgag	3	87
GPb10	S I G **A** P Y **Q** agtataggtgctccgtatcag	2	83
GPb11	S **S** G **A** P Y E tcgtcgggggcgccgtacgag	1	80
GPb12	S **W** G **A** P Y E agttggggtgctccttacgag	1	100
GPb13	S **Y** G G P Y E agttatgggggccgtacgag	1	90
GPb14	S **V** G **A** P Y E agtgtgggggcgccgtacgag	1	76

Table 4.2. Output clones obtained following three rounds of panning against 10 nM biotinylated-HLA-A*0201-gp100$_{(280\text{-}288)}$ complexes. (A). Library 2: CDR3α mutants on the GPb7 background. Clone GPa6 has acquired a mutation in Cα (Asp to Gly). From soluble inhibition ELISA library 2 clones showed 55-74% inhibition compared to 30% for the background clone (GPb7) at 5 nM HLA-A*0201-gp100$_{(280\text{-}288)}$ complexes. **(B).** Library 3: CDR3β mutants on the GPb7 background. From soluble inhibition ELISA library 3 showed 76-100% inhibition compared to 38% for the background clone (GPb7) at 5 nM HLA-A*0201-gp100$_{(280\text{-}288)}$ complexes. Red lettering indicates residues mutated from the parental sequence. Blue lettering indicates alternative codon usage compared to the parental sequence. The α and β chain fragments are denoted by the letter a or b respectively. International Immunogenetics (IMGT) nomenclature (Lefranc, Giudicelli et al. 1999).

4.4.2 ELISA screening of purified phage supernatant

To more accurately characterise the Pan 3 output, phage supernatant was purified for a selection of clones. Fifty ml of growth media containing 100 μg/ml ampicillin and 2% glucose (w/v) was inoculated with clones GPa1, GPa2, GPa3, GPa4, GPb8 and the framework clone GPb7 from the *E. coli* TG1 glycerol master-plates (Section 4.4). Phage was rescued by infection with helper phage and grown in kanamycin-containing media overnight at 26°C with shaking. The following day, the cultures were pelleted and the supernatant containing monoclonal phage TCRs was twice precipitated with PEG/NaCl as described in Section 2.5.2 of Materials and Methods. The phage pellet was resuspended in a final volume of 1 ml PBS. To control for variation in the TCR display levels, a preliminary antigen binding phage ELISA was performed as outlined in Section 2.5.5 of Materials and Methods. A 7-point doubling dilution series of each phage sample was prepared in PBS (from 1:4 to 1:256). The purpose of the ELISA was to determine a phage dilution that produced an absorbance 650 nm reading of ~1.0. In the subsequent inhibition ELISA the amount of TCR-displaying phage could be normalised and so the % inhibition values could be more accurately compared independent of expression levels. One salient point from Figure 4.7 is the variation of TCR display levels between the clones. It can be surmised that the dominance of clone GPb8 in the Pan 3 output is due to the fitness of this clone in terms of both expression and affinity. The ELISA signal at each of the dilution points is >2-fold higher than the other clones. The ELISA is designed to measure the display of functional correctly folded TCR and so it can be concluded that a greater proportion of phage particles are displaying this TCR variant compared to the other clones. The sample dilution that produced an absorbance value at 650 nm of ~1.0 were: 1:4 (GPb7 and GPa4); 1:8 (GPa2 and GPa3); 1:16 (GPa1) and 1:64 (GPb8).

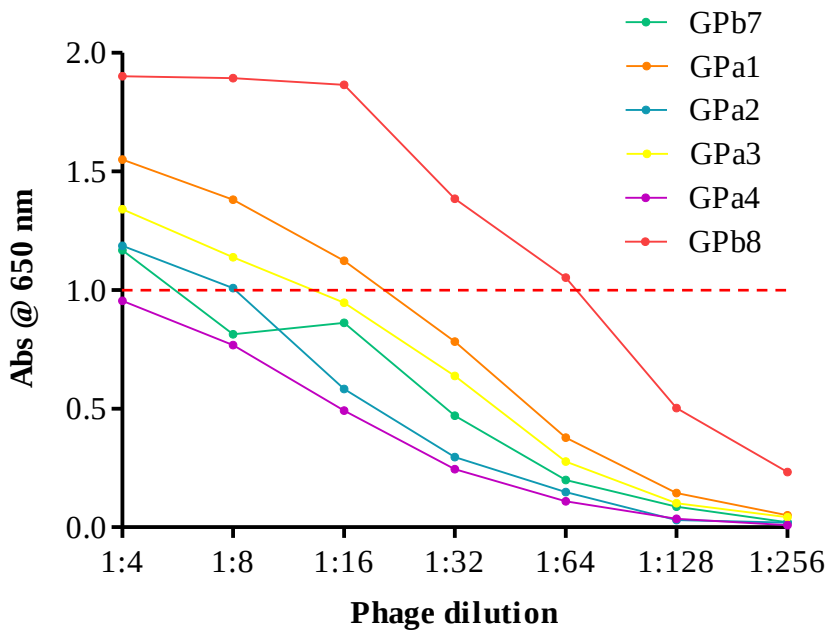

Figure 4.7. Titration of gp100 TCR purified phage samples in a antigen-binding ELISA. Streptavidin-coated Nunc-Maxisorp plates were immobilised with 0.5 μg biotinylated HLA-A*0201-gp100$_{(280\text{-}288)}$ (YLEPGPVTV). A doubling dilution series of PEG-precipitated phage was prepared in 6% MPBS. Antigen-binding phage were detected with an anti-M13 antibody and a phosphatase-labelled anti-rabbit IgG monoclonal antibody. ELISA signals were measured as an absorbance at 650 nm. The dotted line indicates an absorbance at 650 nm of 1. The background absorbance value was subtracted from all readings before % Inhib. was calculated. The α and β chain fragments are denoted by the letter a or b respectively.

An inhibition ELISA was performed at 5, 10, 25 and 50 nM inhibitor using a phage dilution that gave an absorbance of ~1.0 (Figure 4.8). Normalising the level of TCR-displaying phage in each of the samples made it now possible to assess improvements in affinity by comparison with the inhibition profile of the framework clone GPb7. The inhibition profiles of each of the mutants provided evidence for improvements in affinity over the framework clone GPb7. Inclusion of the CDR3α segments (GPa1, GPa2, GPa3 and GPa4) into the GPb7 clone produced a similar increase in apparent antigen-binding affinity as judged by % inhibition. The improvement in relative affinity over clone GPb7 is illustrated by comparing the average % inhibition value (at 10 nM inhibitor) for the mutated α chains against the framework clone: ~70% versus 45% respectively. The recruitment of a CDR3β (GPb8) segment into clone GPb7 produced a more significant improvement in the apparent affinity; ~90% inhibition at 10 nM inhibitor compared to 45% for clone GPb7. The dilution curve for clone GPb8 (Figure 4.7) and the inhibition profile (Figure 4.8) supported the hypothesis that GPb8 was selected for both expression and affinity.

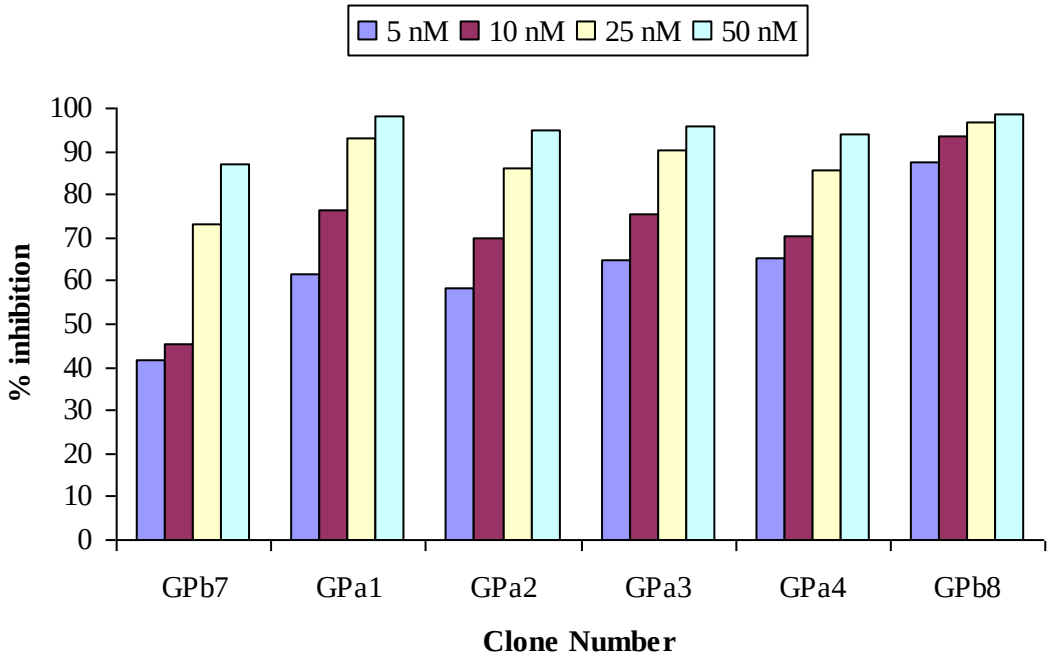

Figure 4.8. Inhibition phage ELISA of gp100 TCR CDR3α and CDR3β variants at a concentration of 50, 25, 10 and 5 nM inhibitor. All phage samples were diluted to give an absorbance at 650 nm of ~1 in an antigen binding phage ELISA. GPb7 is the first-generation enhanced affinity CDR2β mutant upon which second-generation mutants were built. The PEG-precipitated phage samples were incubated with the appropriate concentration of non-biotinylated HLA-A*0201-gp100$_{(280-288)}$ (YLEPGPVTV) prior to adding to ELISA plates immobilised with HLA-A*0201-gp100$_{(280-288)}$ (YLEPGPVTV). % Inhib. is measured as the percentage reduction in ELISA signal. The background absorbance value was subtracted from all readings before % Inhib. was calculated. The α and β chain fragments are denoted by the letter a or b respectively.

4.5 Characterisation of the second-generation gp100 TCRs

4.5.1 Soluble expression of gp100 TCRs

Three mutated α (GPa1, GPa3 and GPa5) and three mutated β (GPb8, GPb9 and GPb12) CDR segments were selected for kinetic analysis by SPR. The CDR3β segments were cloned both in combination with the CDR2β segment from GPb7 (as selected from library 3) and also in combination with the highest affinity CDR2β segment (GPb1) from the first-generation affinity maturation libraries (Table 4.1). All chains were cloned into the expression plasmid pGMT7 (pEX954 for the α chain and pEX821 for the β chain) for expression in *E. coli* strain Rosetta (DE3) pLysS. TCRs were refolded from inclusion bodies and purified by anion exchange chromatography followed by size exclusion chromatography as outlined in Section 2.6.4-2.6.8 of Materials and Methods.

4.5.2 Kinetic analysis of gp100 TCRs

Purified refolded TCR was subjected to SPR on a BIAcore instrument. Equilibrium binding constants were calculated from kinetic data following the methods outlined in Section 2.7 of Materials and Methods.

Recruitment of CDR3α segments into TCR clone GPawtb7 increased the affinity up to 8-fold (Table 4.3 A). Inclusion of the CDR3β segments GPb8 and GPb9 into clone GPb7 had a greater effect on the binding affinity; increasing the K_D by 10 and 26-fold respectively. However, recruitment of CDR3β segment GPb10 into clone GPawtb7 had a more striking effect on the affinity; increasing it by ~200-fold. This represents a 10-fold increase in affinity compared to clone GPb9. Clones GPb9 and GPb12 differ by only a single residue; an Ile at position 95 is substituted for His in GPb9 and for Trp in GPb12. Addition of a large bulky hydrophobic side chain at this

position is likely to be responsible for the dramatic affinity enhancement observed with this clone.

Combining the most optimal α and β chain segments isolated from first and second-generation libraries further improved the binding affinity in an additive manner (Table 4.3 B). The CDR3α clone with the longest $T_{1/2}$, GPa3, was refolded with three β chain double mutants, GPb15, GP16 and GPb17. To generate the β chain mutants each of the CDR3β variants (GPb8, GPb9 and GPb12) were combined with the highest affinity CDR segment from the first-generation libraries, GPb1 (CDR2β). Although the increase in affinity between GPb1 and GPb7 was only moderate (~8-fold), we have shown that even minor CDR-derived improvements can enhance binding affinity in a step-wise manner. Generating TCR clone GPa3b17, comprising only three engineered CDRs, resulted in a ~1.7 million-fold increase in binding affinity compared to the wild-type (parental) TCR.

Mutagenesis of individual CDR segments has proved a successful strategy to improve the binding affinity of the gp100 TCR for its cognate pHLA. Engineering of separate CDRs has enhanced the affinity and half-life by incremental steps (Figure 4.9 A and 4.9 B). Combination of affinity enhanced CDRs has generated TCRs with significantly improved binding affinities. Improvements in affinity are almost exclusively driven by decreases in off-rates rather than alterations to on-rates which remain largely unchanged (Figure 4.9 C and 4.9 D). A comparison of the weakest affinity first-generation mutant, GPb7 with the highest affinity combined mutant, GPa3b17 illustrates this point. Only a two-fold variation in on-rate was observed compared to a 1850-fold variation in off-rate (Table 4.3) between the two mutants.

A.

Clone ID	CDR3α	CDR2β	CDR3β	K_{on} (M^{-1} s^{-1})	K_{off} (s^{-1})	K_D (nM)	$T_{1/2}$ (min)	$\frac{K_D\ (GPawtb7)}{K_D\ (mutant)}$	$\frac{K_D\ (parent)}{K_D\ (mutant)}$
GPawtbwt	DTPLVFGKG	SQIVND	IGGPYE	nd	nd	22000	nd	-	1
GPawtb7	DTPLVFGKG	S**WGTG**D	IGGPYE	2.78 x 10^5	1.24 x 10^{-2}	44.6	0.9	1	493.3
GPa1b7	**S**TPL**M**FGKG	S**WGTG**D	IGGPYE	4.55 x 10^5	2.85 x 10^{-3}	6.26	4	7.1	3514.4
GPa3b7	**S**TP**MQ**FGKG	S**WGTG**D	IGGPYE	4.36 x 10^5	2.49 x 10^{-3}	5.71	4.6	7.8	3852.9
GPa5b7	**T**TPL**G**FGK**D**	S**WGTG**D	IGGPYE	5.33 x 10^5	2.82 x 10^{-3}	5.3	4	8.4	4150.9
GPawtb8	DTPLVFGKG	S**WGTG**D	IG**A**PY**P**	1.72 x 10^5	7.05 x 10^{-4}	4.11	16.3	10.9	5352.8
GPawtb9	DTPLVFGKG	S**WGTG**D	**H**G**A**PYE	3.28 x 10^5	5.6 x 10^{-4}	1.71	20.5	26.1	12865.4
GPawtb12	DTPLVFGKG	S**WGTG**D	**W**G**A**PYE	4.87 x 10^5	9.93 x 10^{-5}	0.2	115	223	110000

B.

Clone ID	CDR3α	CDR2β	CDR3β	K_{on} (M^{-1} s^{-1})	K_{off} (s^{-1})	K_D (nM)	$T_{1/2}$ (min)	$\frac{K_D\ (parent)}{K_D\ (mutant)}$
GPawtbwt	DTPLVFGKG	SQIVND	IGGPYE	nd	nd	22000	nd	1
GPawtb1	DTPLVFGKG	S**WAQG**D	IGGPYE	4 x 10^5	2.33 x 10^{-3}	5.83	4.9	3773.6
GPa3b15	**S**TP**MQ**FGKG	S**WAQG**D	IG**A**PY**P**	6.21 x 10^5	2.35 x 10^{-5}	0.038	486	578947.4
GPa3b16	**S**TP**MQ**FGKG	S**WAQG**D	**H**G**A**PYE	4.47 x 10^5	3.75 x 10^{-5}	0.084	306	261904.8
GPa3b17	**S**TP**MQ**FGKG	S**WAQG**D	**W**G**A**PYE	5.31 x 10^5	6.7 x 10^{-6}	0.013	1716	1692307.7

Table 4.3. Affinities and binding kinetics of gp100 TCR mutants isolated from second-generation libraries. (A). Second-generation phage output. Mutants isolated from CDR3α, CDR2β and CDR3β libraries built on the GPb7 framework. **(B).** Combination of the most optimal alpha and beta chain CDR segments obtained from both first and second-generation phage libraries. GPb1 was the highest affinity clone isolated from the first-generation library selections. The ratio of K_D parent and mutant K_D gives the overall improvement in affinity from the starting gp100 wild-type TCR. K_{on} and K_{off} were determined by SPR in a BIAcore using purified refolded TCR and K_D calculated. Binding was measured against the HLA-A*0201-gp100$_{(280\text{-}288)}$ (YLEPGPVTV) ligand. nd, not determined. (Data kindly provided by J. Gavarret).

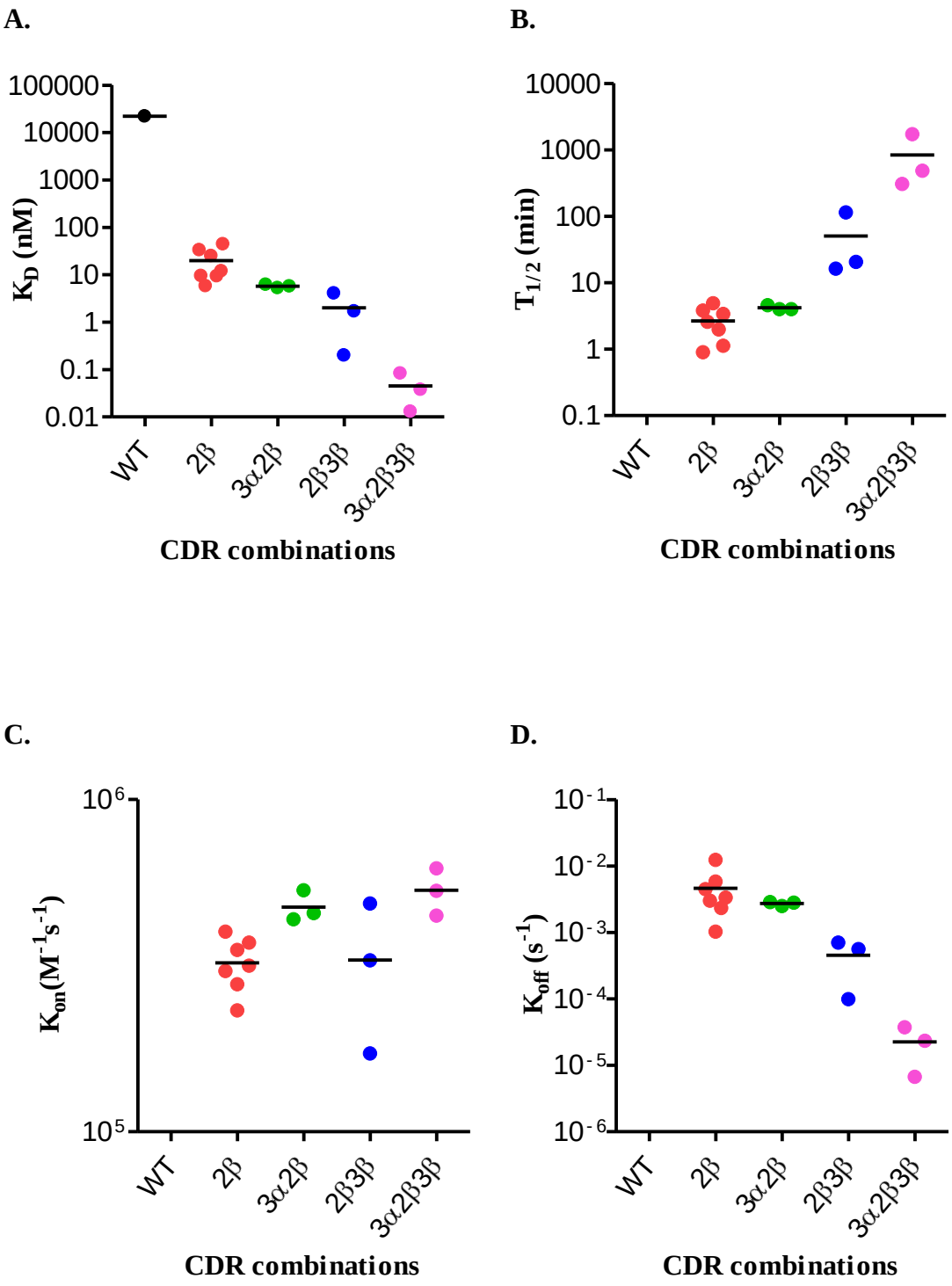

Figure 4.9. Affinities and binding kinetics of gp100 TCR CDR segments isolated from first and second-generation libraries. Mutated CDR regions were combined in a step-wise manner to enhance the binding affinity of the engineered gp100 TCR for HLA-A*0201-gp100$_{(280\text{-}288)}$ (YLEPGPVTV). **(A).** Equilibrium dissociation constant (K_D). **(B).** Dissociation half-life ($T_{1/2}$). **(C).** Association rate constant (K_{on}). **(D).** Dissociation rate constant (K_{off}).

EXPLORING PHAGE DISPLAY METHODOLOGIES TO ISOLATE AN HLA-A1-RESTRICTED HIGH AFFINITY T CELL RECEPTOR AGAINST THE MAGE-A3$_{168-176}$ TUMOUR ASSOCIATED ANTIGEN

5.1 Introduction

The MAGE-A3-EB81-103 T-cell clone was kindly supplied by Pierre Coulie (University of Louvian, Brussels, Belgium) (Karanikas, Lurquin et al. 2003). The MAGE-A3-EB81-103 T-cell clone recognises the TAA epitope derived from MAGE-$A3_{(168-176)}$ (EVDPIGHLY) presented in the context of the HLA-A*0101 complex.

Of the TCRs described in this thesis, the MAGE-A3-EB81-103 TCR (hereafter referred to as the MAGE-A3 TCR) exhibits the lowest affinity for its cognate pHLA with a K_D of 248 μM. The affinity is 14-fold and 9.5-fold weaker than the wild-type Mel-5 (K_D of 18 μM) and gp100 (K_D of 26 μM) TCRs, respectively.

In this chapter, the affinity-maturation of the MAGE-A3 TCR will be described. Moreover, the off-target activity of the first-generation MAGE-A3 TCR mutants will be addressed through exploring various features of the phage display system. This will include investigating the format of the TCR (native versus mTCR), the number of consecutive CDR residues randomised (5-NNK versus 6-NNK) and the use of subtractive panning of phage libraries on mammalian cells to remove off-target binders and enrich for target-specific binders.

The Mel-5 and gp100 TCRs were displayed on the bacteriophage surface in the engineered mTCR format in which the membrane-proximal Cα and Cβ cysteines (native) were removed and a C-region cysteine pair was introduced (Boulter, Glick et al. 2003). Whilst, intuitively it was believed that the engineered disulphide (ds)-format would favour the display on the bacteriophage surface, by stabilising the interaction between the α and β chains, the opposite was demonstrated. We have shown, using a (limited) panel of TCRs containing the native C-region cysteine pair, that the display is enhanced over the ds-engineered equivalent. Since a greater proportion of the phage population display a TCR available for interaction with pHLA

ligand, it was hypothesised that increasing the efficiency of display using the native ds-format would increase the likelihood of isolating high affinity MAGE-A3 TCR mutants.

5.2 Design and construction of MAGE-A3 TCR libraries

5.2.1 Cloning the MAGE-A3 wild-type TCR into the phagemid vector

The phagemid vector pIM160 for the phage display of the MAGE-A3 TCR (specific for HLA-A*0101 in complex with the MAGE-A3$_{(168\text{-}176)}$ peptide) was constructed as described in Section 2.3 of Materials and Methods using Vα and Vβ specific primers (primers J135 and J155) to amplify the wild-type MAGE-A3 TCR α and β chains. The template used to amplify the variable fragments was cDNA isolated from the MAGE-A3-EB81-103 T-cell clone (cDNA was provided by Dr. B. Cameron). The Cα and Cβ domains were amplified from the phagemid vector pG484 encoding TCR C-regions in the native format; in which the engineered ds-cysteines were replaced with wild-type residues and the native membrane-proximal cysteines were introduced. The MAGE-A3 TCR α chain V domain is encoded by TRAV21*01 and TRAJ28*01 gene segments. The α C region is encoded by TRAC*01. The MAGE-A3 TCR β chain V domain is encoded by TRBV5-1*01, TRBJ2-7*01 and TRBD1*01 gene segments. The β C region is encoded by TRBC1*01. The sequence of the wild-type MAGE-A3 TCR *Nco*I-*Not*I phagemid fragment is shown in Figure 5.1.

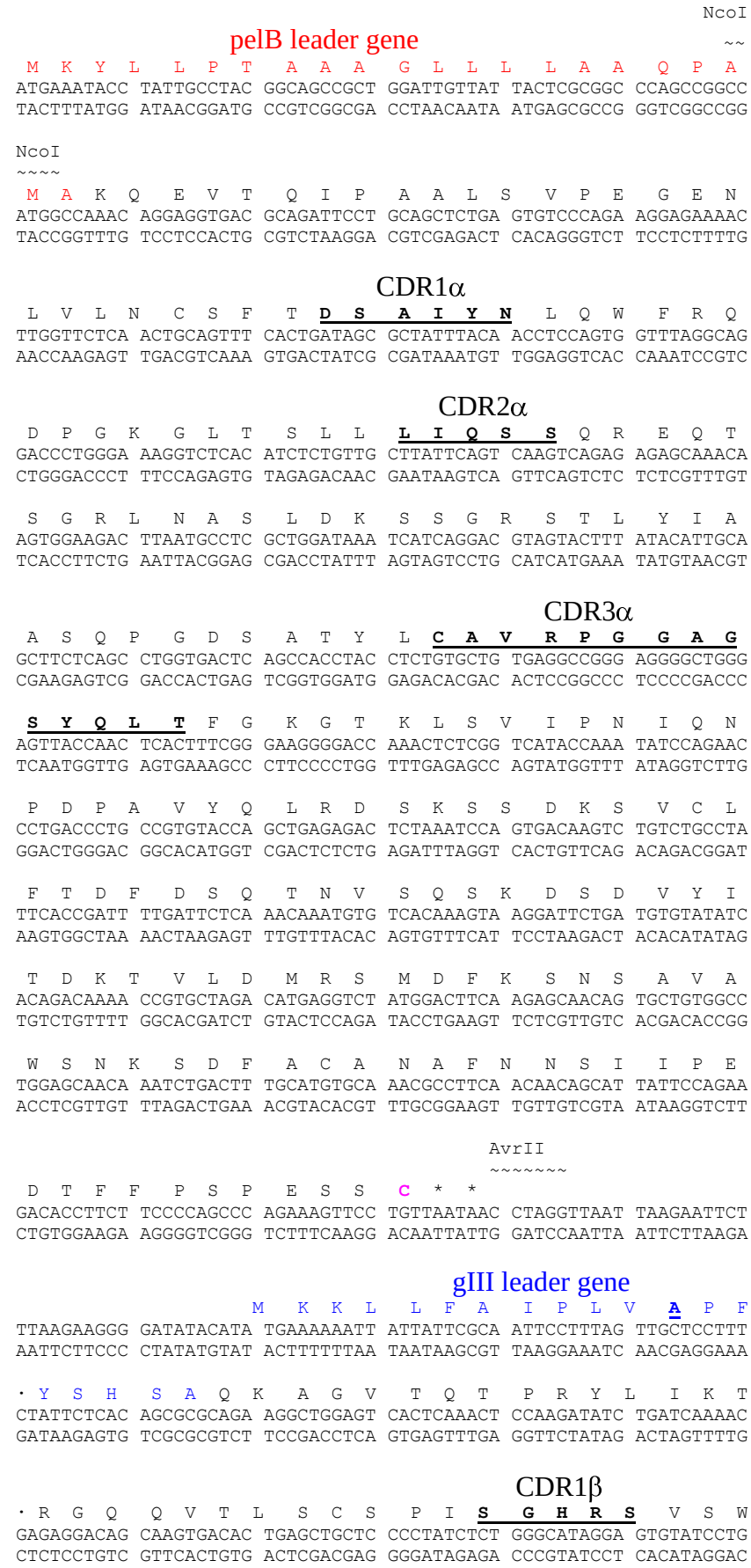
NcoI
pelB leader gene
M K Y L L P T A A A G L L L L A A Q P A
1 ATGAAATACC TATTGCCTAC GGCAGCCGCT GGATTGTTAT TACTCGCGGC CCAGCCGGCC
TACTTTATGG ATAACGGATG CCGTCGGCGA CCTAACAATA ATGAGCGCCG GGTCGGCCGG
NcoI
M A K Q E V T Q I P A A L S V P E G E N
61 ATGGCCAAAC AGGAGGTGAC GCAGATTCCT GCAGCTCTGA GTGTCCCAGA AGGAGAAAAC
TACCGGTTTG TCCTCCACTG CGTCTAAGGA CGTCGAGACT CACAGGGTCT TCCTCTTTTG
CDR1α
L V L N C S F T D S A I Y N L Q W F R Q
121 TTGGTTCTCA ACTGCAGTTT CACTGATAGC GCTATTTACA ACCTCCAGTG GTTTAGGCAG
AACCAAGAGT TGACGTCAAA GTGACTATCG CGATAAATGT TGGAGGTCAC CAAATCCGTC
CDR2α
D P G K G L T S L L L I Q S S Q R E Q T
181 GACCCTGGGA AAGGTCTCAC ATCTCTGTTG CTTATTCAGT CAAGTCAGAG AGAGCAAACA
CTGGGACCCT TTCCAGAGTG TAGAGACAAC GAATAAGTCA GTTCAGTCTC TCTCGTTTGT
S G R L N A S L D K S S G R S T L Y I A
241 AGTGGAAGAC TTAATGCCTC GCTGGATAAA TCATCAGGAC GTAGTACTTT ATACATTGCA
TCACCTTCTG AATTACGGAG CGACCTATTT AGTAGTCCTG CATCATGAAA TATGTAACGT
CDR3α
A S Q P G D S A T Y L C A V R P G G A G
301 GCTTCTCAGC CTGGTGACTC AGCCACCTAC CTCTGTGCTG TGAGGCCGGG AGGGGCTGGG
CGAAGAGTCG GACCACTGAG TCGGTGGATG GAGACACGAC ACTCCGGCCC TCCCCGACCC
S Y Q L T F G K G T K L S V I P N I Q N
361 AGTTACCAAC TCACTTTCGG GAAGGGGACC AAACTCTCGG TCATACCAAA TATCCAGAAC
TCAATGGTTG AGTGAAAGCC CTTCCCCTGG TTTGAGAGCC AGTATGGTTT ATAGGTCTTG
P D P A V Y Q L R D S K S S D K S V C L
421 CCTGACCCTG CCGTGTACCA GCTGAGAGAC TCTAAATCCA GTGACAAGTC TGTCTGCCTA
GGACTGGGAC GGCACATGGT CGACTCTCTG AGATTTAGGT CACTGTTCAG ACAGACGGAT
F T D F D S Q T N V S Q S K D S D V Y I
481 TTCACCGATT TTGATTCTCA AACAAATGTG TCACAAAGTA AGGATTCTGA TGTGTATATC
AAGTGGCTAA AACTAAGAGT TTGTTTACAC AGTGTTTCAT TCCTAAGACT ACACATATAG
T D K T V L D M R S M D F K S N S A V A
541 ACAGACAAAA CCGTGCTAGA CATGAGGTCT ATGGACTTCA AGAGCAACAG TGCTGTGGCC
TGTCTGTTTT GGCACGATCT GTACTCCAGA TACCTGAAGT TCTCGTTGTC ACGACACCGG
W S N K S D F A C A N A F N N S I I P E
601 TGGAGCAACA AATCTGACTT TGCATGTGCA AACGCCTTCA ACAACAGCAT TATTCCAGAA
ACCTCGTTGT TTAGACTGAA ACGTACACGT TTGCGGAAGT TGTTGTCGTA ATAAGGTCTT
AvrII
D T F F P S P E S S C * *
661 GACACCTTCT TCCCCAGCCC AGAAAGTTCC TGTTAATAAC CTAGGTTAAT TAAGAATTCT
CTGTGGAAGA AGGGGTCGGG TCTTTCAAGG ACAATTATTG GATCCAATTA ATTCTTAAGA
gIII leader gene
M K K L L F A I P L V A P F
721 TTAAGAAGGG GATATACATA TGAAAAAATT ATTATTCGCA ATTCCTTTAG TTGCTCCTTT
AATTCTTCCC CTATATGTAT ACTTTTTTAA TAATAAGCGT TAAGGAAATC AACGAGGAAA
· Y S H S A Q K A G V T Q T P R Y L I K T
781 CTATTCTCAC AGCGCGCAGA AGGCTGGAGT CACTCAAACT CCAAGATATC TGATCAAAAC
GATAAGAGTG TCGCGCGTCT TCCGACCTCA GTGAGTTTGA GGTTCTATAG ACTAGTTTTG
CDR1β
· R G Q Q V T L S C S P I S G H R S V S W
841 GAGAGGACAG CAAGTGACAC TGAGCTGCTC CCCTATCTCT GGGCATAGGA GTGTATCCTG
CTCTCCTGTC GTTCACTGTG ACTCGACGAG GGGATAGAGA CCCGTATCCT CACATAGGAC

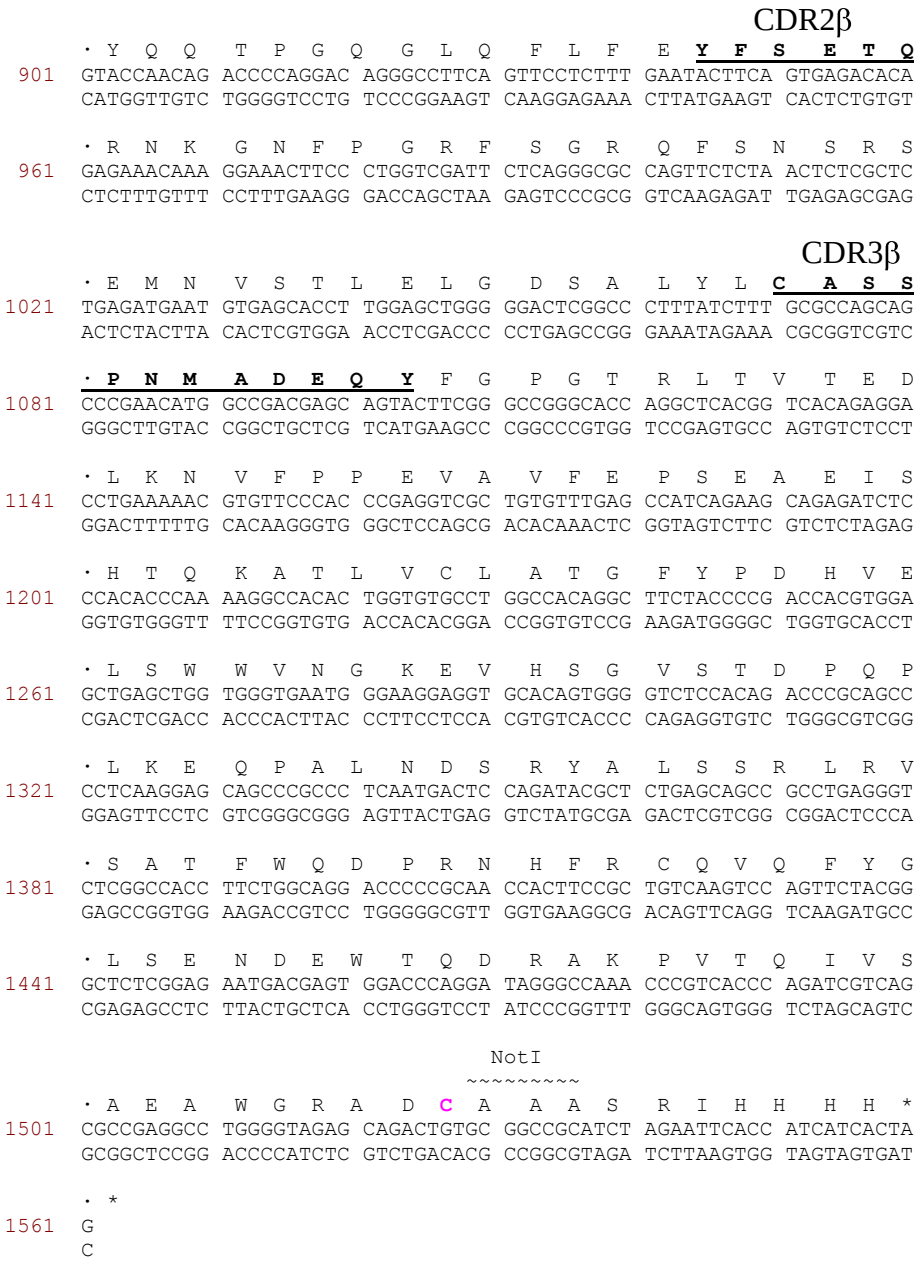

Figure 5.1. Sequence of wild-type MAGE TCR (recognising the epitope derived from the MAGE-A3$_{168-176}$) cloned into the phagemid vector pEX922. The amino acid residues encoding the pelB and bacteriophage M13 geneIII leader genes are highlighted in red and blue respectively. The six CDR loops, designated by the International Immunogenetics (IMGT) database (Lefranc, Giudicelli et al. 1999), are in bold and underlined. The TCR membrane-proximal cysteines in both the α and β chains are highlighted in bold purple. The restriction enzyme sites used for molecular cloning purposes are highlighted (*Nco*I, *Avr*II and *Not*I). Asterisks show the location of stop codons including an amber codon (TAG) at the C-terminus of the beta chain. A V12A mutation has been introduced into the geneIII leader sequence by PCR error (shown in bold and underlined). The sequence was analysed with Vector NTI Advance 11 (Invitrogen).

5.2.2 Generating DNA and bacterial libraries

Libraries were assembled in which each of the six CDRs were individually targeted for mutagenesis producing TCRs with one wild-type and one mutant chain as described in Section 2.4.3 Materials and Methods. The PCR strategy is outlined in Figure 2.4 of Materials and Methods. The phagemid vector pIM160 was linearised separately with *Nco*I and *Not*I and gel-purified. Purified plasmids were quantitated by agarose gel electrophoresis and diluted to ~2 ng/μl for PCR. The *Not*I linearised plasmid was used as the template for YOL13 PCRs and *Nco*I linearised plasmid was used as the template for YOL22 PCRs.

The DNA fragments used to generate the MAGE-A3 TCR libraries are shown in Figure 5.2. For each library, overlapping 5-NNK oligonucleotides were designed to span the entire CDR: two for CDR1α, one for CDR2α, five for CDR3α, one for CDR1β, two for CDR2β and four for CDR3β. Following the strategy depicted in Figure 2.4 of Materials and Methods and the primer set and methods outlined in Section 2.4.3 of Materials and Methods PCR fragments were generated. PCR fragments of the expected size were gel-purified and 1 μl of each was resolved on a 1% (w/v) agarose gel (Figure 5.2 A and 5.2 B).

TCR fragments containing mutagenised CDR segments were assembled by SOE-PCR: equimolar amounts of each of the two PCR fragments (~13 ng total DNA) were added together with the external primers YOL13 and YOL22 and amplified through 30 cycles of PCR with Expand polymerase. Amplification of background parental template was assessed by setting up control PCRs with YOL13 and YOL22 in which one or other of the two fragments was excluded. An equal volume of each PCR was resolved on a 1% (w/v) agarose gel (Figure 5.2 C and 5.2 D). A dominant band of the expected size (~1800 bp) was observed for each of the SOE-PCR reactions.

Background amplification of template DNA was almost undetectable. The fifteen SOE-PCR fragments (~1800 bp) were excised from the gel, purified and analysed by agarose gel electrophoresis (Figure 5.2 E). Each of the purified stitch PCRs were sequenced with primers YOL13 and YOL22. Polyclonal sequencing (data not shown) demonstrated sufficient integrity of the libraries to proceed to the next stages of library construction. Each library fragment was digested with *Nco*I-*Not*I to generate a ~1500 bp product; gel-purified fragments were analysed by agarose gel electrophoresis (Figure 5.2 F).

Libraries targeting each of the six CDRs were cloned into the phagemid vector pEX922 as *Nco*I-*Not*I fragments as described in Section 2.4.3.1 of Materials and Methods. Electrocompetent *E. coli* TG1 cells were transformed separately with each of the six libraries. Multiple electroporations were performed for each of the libraries (ten CDR1α, six CDR2α, twenty CDR3α, six CDR1β, ten CDR2β and twenty CDR3β) to yield individual CDR libraries containing between 10^8 and 10^9 independent transformants. Eight randomly selected colonies from each of the six libraries were PCR amplified with primers YOL13 and YOL22. The integrity and diversity of the MAGE-A3 TCR libraries was confirmed by DNA sequencing to reveal a broad diversity of mutations spanning each of the targeted CDRs (data not shown).

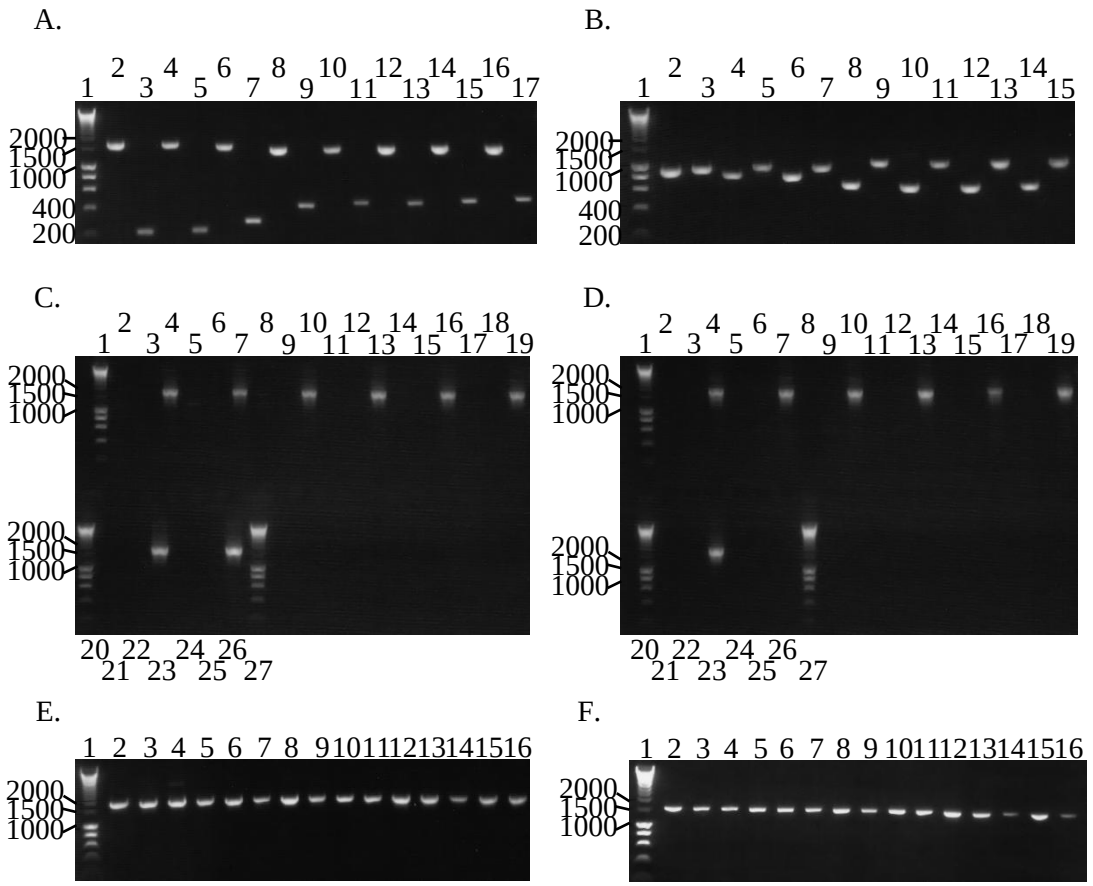

Figure 5.2. Ethidium bromide stained agarose gel photos of MAGE TCR library construction. (A). Gel-purified α chain library PCR fragments. Lane 1, HYP I; lane 2, PCR fragment a1; lane 3, a2; lane 4, a4; lane 5, a5; lane 6, a7; lane 7, a8; lane 8, a10; lane 9, a11; lane 10, a13; lane 11, a14; lane 12, a16 ; lane 13, a17; lane 14, a19; lane 15, a20; lane 16, a22; lane 17, a23. **(B).** Gel-purified β chain library PCR fragments. Lane 1, HYP I; lane 2, PCR fragment b1; lane 3, b2; lane 4, b4; lane 5, b5; lane 6, b7; lane 7, b8; lane 8, b10; lane 9, b11; lane 10, b13; lane 11, b14; lane 12, b16 ; lane 13, b17; lane 14, b19; lane 15, b20. **(C).** Overlapping stitch α chain library PCR fragments. Lane 1, HYP I; lane 2, PCR fragment a1 only; lane 3, PCR a2 only; lane 4, PCR a1 + a2; lane 5, a4 only; lane 6, a5 only; lane 7, a4 + a5; lane 8, a7 only; lane 9, a8 only; lane 10, a7 + a8; lane 11, a10 only; lane 12, a11 only; lane 13, a10 + a11; lane 14, a13 only; lane 15, a14 only; lane 16, a13 + a14; lane 17, a16 only; lane 18 a17 only; lane 19, a16 + a17; lane 20, HYP I; lane 21, a19 only; lane 22, a20 only; lane 23, a19 + a20; lane 24, a22 only; lane 25, a23 only; lane 26, a22 + a23; lane 27, HYP I. **(D).** Overlapping stitch β chain library PCR fragments. Lane 1, HYP I; lane 2, PCR b1 only; lane 3, PCR b2 only; lane 4, PCR b1 + b2; lane 5, b4 only; lane 6, b5 only; lane 7, b4 + b5; lane 8, b7 only; lane 9, b8 only; lane 10, b7 + b8; lane 11, b10 only; lane 12, b11 only; lane 13, b10 + b11; lane 14, b13 only; lane 15, b14 only; lane 16, b13 + b14; lane 17, b16 only; lane 18, b17 only; lane 19, b16 + b17; lane 20, HYP I; lane 21, b19 only; lane 22, b20 only; lane 23, b19 + b20; lane 24, blank; lane 25, blank; lane 26, blank; lane 27, HYP I. **(E).** Gel-purified α and β chain SOE-PCR fragments. Lane 1, HYP I; lane 2, PCR a3; lane 3, a6; lane 4, a9; lane 5, a12; lane 6, a15; lane 7, a18; lane 8, a21; lane 9, a24; lane 10, b3; lane 11, b6; lane 12, b9; lane 13, b12; lane 14, b15; lane 15, b18; lane 16, b21. **(F).** Gel-purified *Nco*I-*Not*I digested α and β chain SOE-PCR fragments. Lane order the same as for gel **(E)**.

5.3 Phage selections and screening

Phage was separately prepared from each of the six libraries as outlined in Section 2.5.1 and 2.5.2 of Materials and Methods. Panning was performed against the TAA, MAGE-A3$_{(168-176)}$, bound in the context of biotinylated HLA-A*0101. Rather than using an HLA-stabilising peptide as employed in the Mel-5 and gp100 TCR affinity maturation projects, the wild-type MAGE-A3$_{(168-176)}$ peptide bound in the HLA-A*0101 was sufficiently stable for panning and screening experiments. A total of three cycles of panning on 100 nM HLA-A*0101-MAGE-A3$_{(168-176)}$ complexes were performed under identical conditions as described in Section 2.5.4 of Materials and Methods.

The output titre for each round of selection was estimated and following the third round of panning a significant increase was observed for library 2 (CDR2α) and library 5 (CDR2β): ~100-fold for library 2 and 17-fold for library 5. The output titre for each of the other four libraries remained unchanged from the previous selection cycle and so were not analysed.

Phage was rescued from ninety-three individual ampicillin-resistant *E. coli* TG1 colonies from both the CDR2α and CDR2β library outputs as described in Section 2.5.1 of Materials and Methods. A single *E. coli* TG1 colony bearing the MAGE-A3 wild-type clone was grown in each of the two plates. Monoclonal-phage-TCRs were screened in an inhibition phage ELISA at 200 nM HLA-A*0101-MAGE-A3$_{(168-176)}$ (EVDPIGHLY) to determine if any of the TCRs demonstrated competitive inhibition.

5.3.1 Inhibition phage ELISA

From the population of CDR2α clones picked, 82 ELISA-positive clones were obtained, representing a hit frequency of ~88%. Even more striking was the 100%

ELISA-positive hit frequency observed for the CDR2β library clones. Unsurprisingly, the wild-type MAGE-A3 TCR failed to produce a signal reflecting the low affinity pHLA interaction. A total of eighteen clones from library 2 and nineteen clones from library 5 that gave the highest % inhibition readings were sequenced with primers YOL13 and J195. A clear convergence to particular mutations was evident in both library outputs (Table 5.1). The CDR2α output clones had converged exclusively to the following motif: $Y^{49}X^{50}R^{51}P^{52}Y/F^{53}$. Similarly, the CDR2β clones showed remarkable convergence to the following mutations: $T^{50}D^{51}X^{52}L^{53}L^{54}$ in all sequenced clones. The average % inhibition value at 200 nM inhibitor for the CDR2α mutants was ~30% and for the CDR2β mutants ~40%.

A.

Clone Number	CDR2α$_{(L49\text{-}S53)}$	Freq.	% Inhib. @ 200 nM
wt	L I Q S S cttattcagtcaagt	-	-
MAGEa1	**Y F R P F** tattttcggccgttt	6	28
MAGEa2	**Y M R P F** tatatgcggccgttt	3	29
MAGEa3	**Y** I **R P Y** tatattcggccgtat	2	31
MAGEa4	**Y L R P Y** tatctgcggccgtat	1	33
MAGEa5	**Y L R P F** tatttgcggccgttt	1	25
MAGEa6	**Y V R P Y** tatgttaggccttat	1	26
MAGEa7	**Y H R P Y** tatcataggccttat	1	31

B.

Clone Number	CDR2β$_{(F50\text{-}Q54)}$	Freq.	% Inhib. @ 200 nM
wt	F S E T Q ttcagtgagacacag	-	-
MAGEb1	**T D L L L** acggatctttgttg	4	38
MAGEb2	**T D M L L** acggatatgttgttg	1	86*
MAGEb3	**T D S L L** acggatagtttgttg	3	34
MAGEb4	**T D G L L** acggatggtctgctg	3	41
MAGEb5	**T D T L L** acggatactttgttg	2	24
MAGEb6	**T D R L L** actgataggttgttg	1	37
MAGEb7	**T D H L L** acggatcatttgttg	1	49
MAGEb8	**T D A L L** actgatgcgcttttg	1	44

Table 5.1. Output clones obtained following three rounds of panning against biotinylated-HLA-A*0101-MAGE$_{(168\text{-}176)}$ (EVDPIGHLY) complexes. (A). Library 2: CDR2α mutants. Eighteen clones were sequenced; 3 contained mixed templates and are not included in the analysis. **(B).** Library 5: CDR2β mutants. Red lettering indicates residues mutated from the parental sequence. Nineteen clones were sequenced; 3 contained mixed templates and are not included in the analysis. Freq., the number of copies in the sequenced pool. For repeated sequences, the % inhib. represents the average value between the repeats. *The Abs reading for MAGEb2 was significantly lower than the readings for the other clones.

5.4 Constructing CDR2α:CDR2β crossing library

A crossing library is assembled by splicing two independent libraries (CDR2α and CDR2β) so that a new library of TCRs is generated in which two CDRs are mutated within the same molecule (CDR2α:CDR2β). Crossing libraries were constructed (as described in Section 2.4.3.2 of Materials and Methods) firstly to identify an improved-affinity clone on which to construct second -generation libraries and secondly to ascertain if the mutations in the two CDR segments were additive.

Although it is difficult to accurately predict the affinity of a TCR mutant based on phage inhibition ELISA data alone, in combination with BIAcore data of previous TCRs, such assays do provide an affinity window for a panel of novel clones. The phage inhibition ELISA data and BIAcore measurements, compiled for the Mel-5 and gp100 TCRs provided a guide against which to compare the MAGE-A3 TCR mutants. Whilst the comparisons did not account for variation in TCR-display levels, quality and stability of pHLA antigen or HLA-restriction, they were informative nonetheless.

Mel-5 TCR clone MELa1bwt (K_D value of 6.4 nM) and gp100 TCR clone GPa1b7 (K_D value of 6.26 nM) exhibited inhibition values of 50-60% at 5 nM inhibitor. Mel-5 TCR clone MELa1cbwt (K_D value of 450 nM) gave an inhibition level of 60% at 10 nM inhibitor. Guided by this information, it was anticipated that the MAGE-A3 TCR single CDR mutants would exhibit K_D values in the low micromolar range. If these predications were confirmed by BIAcore analysis, TCRs demonstrating such a kinetic profile would be unsuitable for therapeutic application or as template for second maturation libraries. It was envisaged that recruiting two mutated CDR segments into the same molecule would provide the necessary improvement in affinity to satisfy these requirements.

DNA was isolated from the CDR2α and CDR2β Pan 3 bacterial glycerol stocks using the QIAprep spin miniprep kit (Qiagen) as described in Section 2.4.3.2 of Materials and Methods and 10 μg of each was digested with *Nco*I-*Avr*II to excise α chain library fragments from the CDR2α libraries and wild-type α chains from the CDR2β libraries (see Figure 5.1 for location of restriction enzyme sites). Digests were resolved on a 1% agarose gel. The *Nco*I-*Avr*II fragment (~640 bp) from the CDR2α library miniprep DNA was cloned into the *Nco*I-*Avr*II digested CDR2β library miniprep DNA (~6.2 kbp) to generate TCRs mutated in both CDR2α and CDR2β loops. The 5 μg ligation reaction was used to transform electrocompetent *E. coli* TG1 cells and yielded 10^8 discrete transformants.

5.4.1 Phage selection and screening

Since the Pan 3 output of both the CDR2α and CDR2β libraries was highly enriched as assessed by sequence analysis (Table 5.1) only a single cycle of selection at 100 nM biotinylated HLA-A*0101-MAGE-A3$_{(168-176)}$ was performed. Monoclonal-phage-TCRs were prepared from a representative set of ninety CDR2α:CDR2β transformants together with two separate *E. coli* TG1 colonies bearing single CDR mutated clones MAGEa1bwt (CDR2α) and MAGEawtb1 (CDR2β). Of the population of clones that were screened in an inhibition phage ELISA at 200 nM HLA-A*0101-MAGE-A3$_{(168-176)}$ (EVDPIGHLY), 84 ELISA-positive clones were obtained, representing a 93% hit-rate. Encouragingly, combining mutated CDR2α and CDR2β segments into the same TCR molecule increased the % inhibition compared to the single CDR mutated clones. Clones MAGEa1bwt and MAGEawtb1 exhibited inhibition values of 37% and 26% respectively, whereas the double-mutants displayed inhibition values in the range of 66-94% at the same concentration of inhibitor.

Twenty-four clones that demonstrated the highest % inhibition at 200 nM inhibitor were sequenced with primers YOL13 and J195 (Table 5.2). Sequence analysis of the double-CDR-mutated clones confirmed the strong selective enrichment of mutations present in the Pan 3 output shown in Table 5.1. Of the seven CDR2α mutants shown in Table 5.1 A, five were re-selected in combination with a mutated CDR2β segment (Table 5.2). Of the eight mutated CDR2β regions obtained from the individual CDR libraries (Table 5.1 B), six were re-isolated in association with a mutated CDR2α segment (Table 5.2). The α chain segments contained the consensus sequence $Y^{49}X^{50}R^{51}P^{52}Y/F^{53}$ with the exception of clones MAGEa8, MAGEa12 and MAGEa13 which varied in two, four or one of these conserved positions respectively. The β chain segments also maintained the consensus sequence $T^{50}D^{51}X^{52}L^{53}L^{54}$ shown in Table 18B with the exception of clones MAGEb12 and MAGEb13 which varied in one and three positions respectively.

Clone Number	CDR2α$_{(L49\text{-}S53)}$	CDR2β$_{(F50\text{-}Q54)}$	% Inhib. @ 200 nM
wt	L I Q S S	F S E T Q	-
MAGEa1bwt	Y F R P F	F S E T Q	37
MAGEawtb1	L I Q S S	T D L L L	26
MAGEa3b6	Y I R P Y	T D R L L	77
MAGEa4b6	Y L R P Y	T D R L L	83
MAGEa8b6	Y L G A Y	T D R L L	66
MAGEa9b3	Y **I** R P F	T D S L L	80
MAGEa10b3	Y F R P Y	T D S L L	69
MAGEa3b3	Y **I** R P Y	T D S L L	69
MAGEa4b4	Y L R P Y	T D G L L	69
MAGEa11b4	Y M R P Y	T D G L L	94
MAGEa11b1	Y M R P Y	T D L L L	70
MAGEa12b1	G F I N *Q*	T D L L L	97
MAGEa11b1	Y M R P Y	T D L L L	67
MAGEa13b9	Y Y L P Y	T D F L L	67
MAGEa6b9	Y V R P Y	T D F L L	88
MAGEa1b10	Y F R P F	T D D L L	72
MAGEa7b11	Y H R P Y	T D A L L	71
MAGEa9b7	Y **I** R P F	T D H L L	70
MAGEa9b12	Y **I** R P F	T **S** S L L	70
MAGEa6b9	Y V R P Y	T D F L L	70
MAGEa14b13	Y S R P Y	*Q* D G M L	68

Table 5.2. Output clones obtained from the crossed Pan 3 CDR2α:CDR2β libraries. The Pan 3 CDR2α library output was cloned as *Nco*I-*Avr*II fragments into the Pan 3 CDR2β output so that each phagemid vector construct encoded a TCR mutated in both CDR2α and CDR2β segments. Following one cycle of panning against biotinylated-HLA-A*0101-MAGE$_{(168\text{-}176)}$ complexes phage was prepared from 90 individual ampicillin-resistant clones and analysed in a phage inhibition ELISA with 200 nM non-biotinylated HLA-A*0101-MAGE$_{(168\text{-}176)}$ antigen. Twenty-four clones demonstrating the highest level of inhibition were sequenced of which five failed to yield readable sequence. Clones MAGEa1bwt and MAGEawtb1 were also analysed to provide inhibition values for single-mutated CDR mutants. Clones MAGEa12 and MAGEb13 contain an amber codon (*Q*). Red lettering indicates wild-type residues retained from the parental sequence. In the Clone Number heading, a = α chain and b = β chain.

5.5 Kinetic analysis of first-generation MAGE-A3 TCRs

Since the enrichment for particular CDR2α and CDR2β sequences was so dramatic, it was proposed that characterisation of a limited panel of mutants would provide sufficient information regarding the binding kinetics of the entire phage selection output. Three α chain (MAGEa1, MAGEa2 and MAGEa6) and three β chain (MAGEb1, MAGEb2 and MAGEb9) mutants were cloned into pEX954 for the α chains and pEX821 for the β chains for expression in *E. coli* strain Rosetta (DE3) pLysS. Soluble TCR was refolded from denatured inclusion bodies as described in Section 2.6 of Materials and Methods. BIAcore experiments were performed under kinetic conditions as described in Section 2.7 of Materials and Methods. Recruiting α and β chain segments into the MAGE-A3 TCR increased the affinity up to ~7000-fold (K_D of 35 nM) and ~4000-fold (K_D of 61 nM) respectively (Table 5.3 A). Clone MAGEa1bwt and clone MAGEa2bwt differ by a single residue in CDR2α; S51F and S51M respectively. Since single residue differences within the CDR motif accounted for only minor variation in affinity the importance of the conserved residues in affinity improvements were therefore highlighted. Combining mutated CDR2α and CDR2β segments to generate clone MAGEa6b9 yielded a significant improvement in the affinity; >3.5 million-fold increase over the wild-type TCR. Such a dramatic improvement in affinity was not anticipated from the phage inhibition ELISA results (Table 5.1 and 5.2) or from the affinity maturation of the Mel-5 and gp100 TCRs. The highest affinity TCR generated by the combination of two mutated CDR segments was 400 pM for the Mel-5 TCR, 200 pM for the gp100 TCR and was 67 pM for the MAGE-A3 TCR (Table 5.3 B). This represented affinity improvements over the wild-type TCR of 45,000-fold, 415,000-fold and 3,701,492-fold respectively.

A.

Clone ID	CDR2α	CDR2β	K_{on} (M^{-1} s^{-1})	K_{off} (s^{-1})	K_D (nM)	$T_{1/2}$ (min)	$\frac{K_D \text{ (parent)}}{K_D \text{ (mutant)}}$
MAGEawtbwt	LIQSS	FSETQ	nd	nd	248000	nd	1
MAGEa1bwt	**YFRPF**	FSETQ	2.75×10^5	9.60×10^{-3}	35	1.2	7085.7
MAGEa2bwt	**YMRPF**	FSETQ	2.43×10^5	1.51×10^{-2}	62	0.77	4000
MAGEa6bwt	**YVRPY**	FSETQ	5.49×10^5	1.04×10^{-2}	190	1.1	1305.3
MAGEawtb1	LIQSS	**TDLLL**	4.24×10^5	2.58×10^{-3}	60.8	4.4	4079
MAGEawtb2	LIQSS	**TDMLL**	3.29×10^5	5.55×10^{-2}	169	2	1467.5
MAGEawtb9	LIQSS	**TDFLL**	4.47×10^5	3.87×10^{-2}	86.5	2.9	2867.1

B.

Clone ID	CDR2α	CDR2β	K_{on} (M^{-1} s^{-1})	K_{off} (s^{-1})	K_D (nM)	$T_{1/2}$ (min)	$\frac{K_D \text{ (parent)}}{K_D \text{ (mutant)}}$
MAGEawtbwt	LIQSS	FSETQ	nd	nd	248000	nd	1
MAGEa1b1	**YFRPF**	**TDLLL**	2.81×10^5	2.83×10^{-5}	0.1005	417	2467661.7
MAGEa6b9	**YVRPY**	**TDFLL**	3.38×10^5	2.17×10^{-5}	0.067	546	3701492.5

Table 5.3. Affinities and binding kinetics of MAGE TCR mutants isolated from first-generation libraries. (A). Phage output. Mutants isolated from CDR2α and CDR2β libraries. **(B).** Combination of the most optimal alpha and beta chain CDR segments. K_{on} and K_{off} were determined by SPR in a BIAcore using purified refolded TCR and K_D calculated. nd, not determined. In the Clone Number, a = alpha chain, b = beta chain and wt = wild-type. HLA-A*0101-MAGE$_{(168\text{-}176)}$ (EVDPIGHLY) and HLA-A*0101-M1$_{(58\text{-}66)}$ (GILGFVFTL) were used as test and control antigen respectively. (Data kindly provided by J. Gavarret).

5.6 Cellular testing of clone MAGEa6b9 in T-cell redirection assays

Hitherto, the engineering of soluble TCRs to generate high affinity molecules against TAA targets has been described. To enable therapeutic utility an associated effector function is necessary since in a soluble form the TCR is uncoupled from the naturally-occurring function, i.e. the T-cell.

Clone MAGEa6b9 was reformatted into a bispecific molecule capable of targeting two distinct cell surface proteins by fusing a CD3-specific scFv to the high affinity TCR β chain. To evaluate the mechanism of action of MAGEa6b9-anti-CD3-scFv two components of the proteins intended function were examined; redirected T-cell activation and target cell lysis. Experiments were performed by Dr. N. Hassan. Activation of T-cells was investigated by measuring release of pro-inflammatory cytokines; target cell lysis was determined by assessing the release of metabolic enzymes or the triggering of apoptotic enzymes in dying cells. Utilising these assay systems it was shown that MAGEa6b9-anti-CD3-scFv potently redirected T-cells against MAGE antigen positive targets. However, a significant level of activity against MAGE antigen negative targets was also measured (Figure 5.3). This was deemed too high to be clinically acceptable.

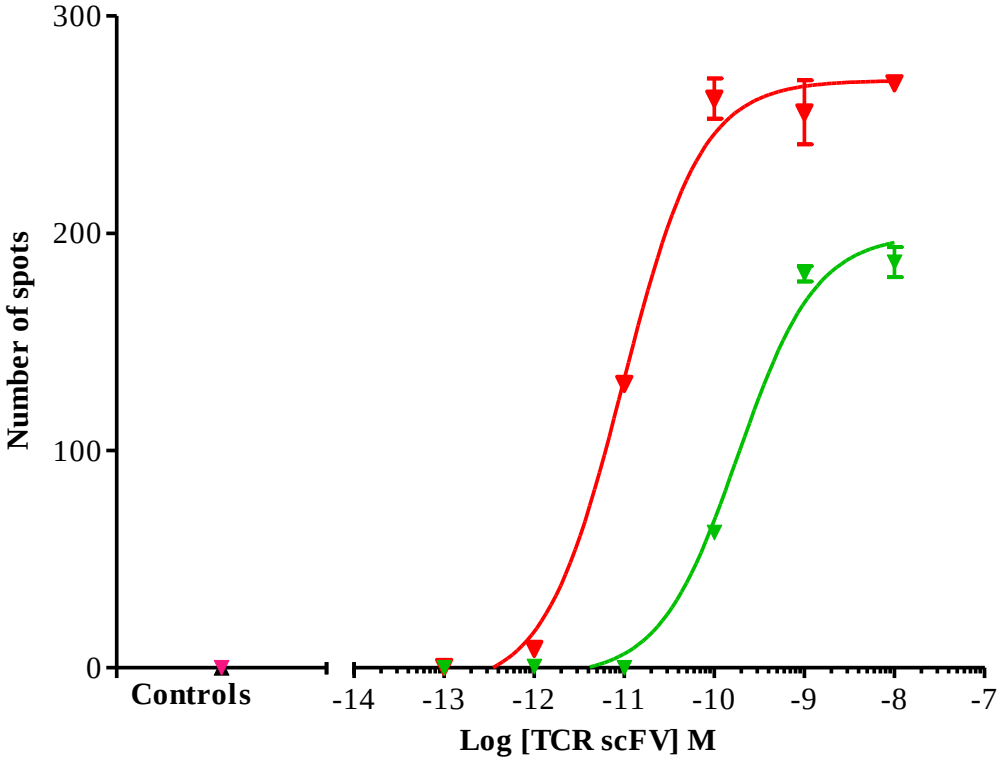

Figure 5.3. MAGEa6b9-anti-CD3-scFv redirected T-cell activation in the presence of MAGE-positive tumour cells. HLA-A*0101^{+}/MAGE-A3^{+} (▼ A375) and HLA-A*0101^{+}/MAGE-A3^{-} (▼ HEP2) cell-lines were incubated with CD8^{+} T-cells derived from normal donors and increasing concentrations of MAGEa6b9-anti-CD3-scFv in a granzyme B release ELISPOT assay. Controls included A375 cells + CD8^{+} T-cells (▼) and HEP2 cells + CD8^{+} T-cells (▲). Data points represent mean of triplicate values. Error bars are standard error of mean (SEM). Assays were performed overnight at 37^{o}C and 5% CO_2. (Data kindly provided by Dr. N. Hassan).

5.7 Second -generation MAGE-A3 TCR libraries

5.7.1 Addressing the off-target activity of clone MAGEa6b9

An overview of both the first and second -generation libraries is provided in Figure 5.4. It was hypothesised that increasing the affinity of the MAGE-A3 TCR through mutations exclusively within the germline-encoded CDR2 loops could enhance the affinity for the HLA-A*0101 heavy chain by increasing off-target binding in a peptide-independent manner. Although BIAcore experiments had indicated initial specificity of the MAGEa6b9 TCR with no detectable binding to HLA-A*0101-$M1_{(58\text{-}66)}$ (GILGFVFTL), such experiments are not representative of the complexity of the cellular milieu.

Selectively altering the amino acid residues of the CDR3 which interact with the peptide as it lies in the HLA groove, could redress the compromised specificity observed with clone MAGEa6b9. Three strategies were devised to target the CDR3 loops for mutagenesis (Table 5.4). These strategies addressed several features of the phage display process: (1) the format of the TCR (native or mTCR), (2) the number of consecutive residues mutated (5-NNK or 6-NNK) and (3) the selection conditions (subtractive panning on human primary cells followed by selection on soluble pHLA).

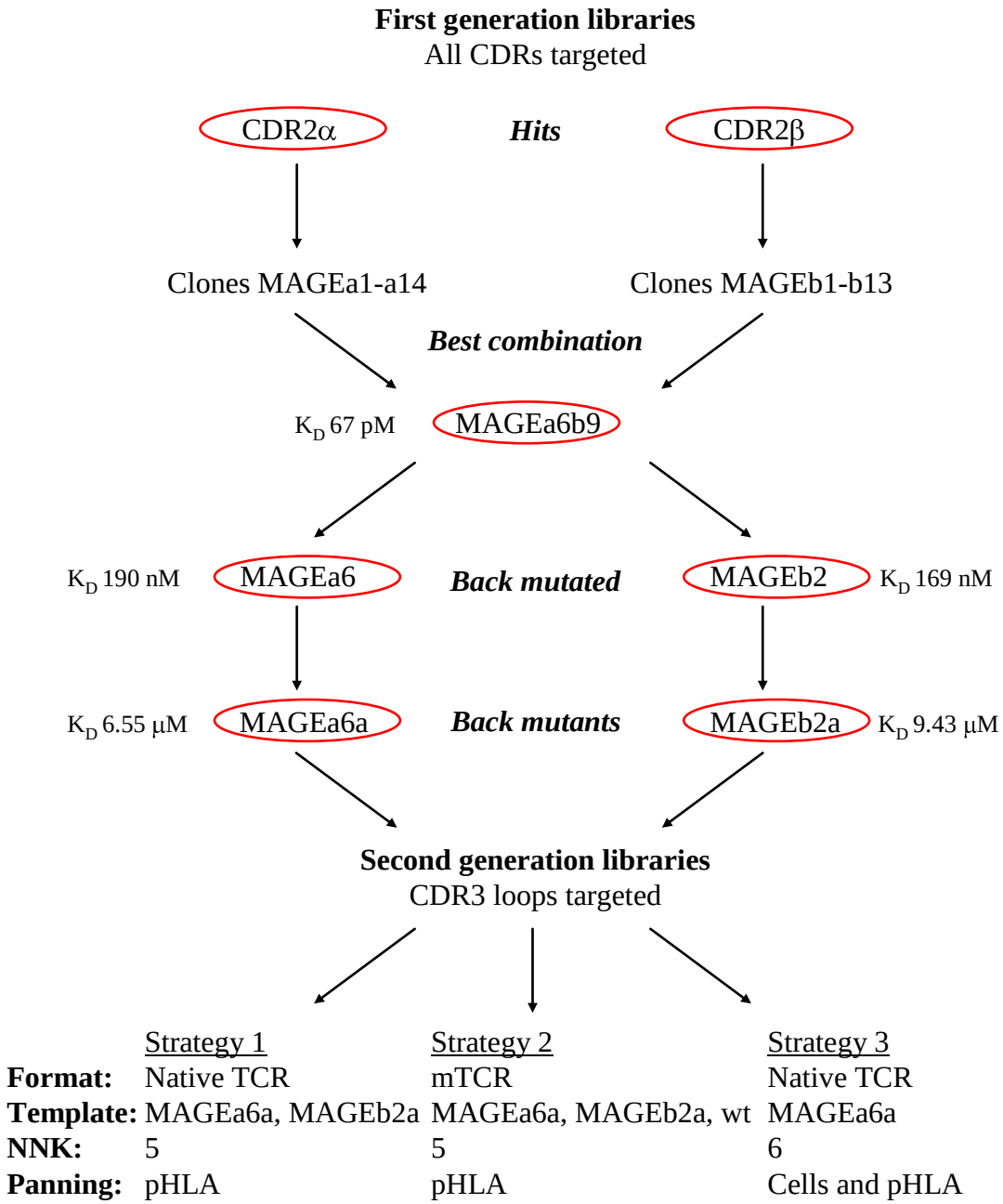

Figure 5.4. Schematic overview of the affinity maturation of the MAGE-A3 TCR. First-generation libraries targeted all six CDR loops with 5-NNK oligonucleotides using the wild-type MAGE-A3 TCR (native format) as template. Phage-ELISA screening identified mutations exclusively in the CDR2 loops of the α and β chains. Combination of the CDR2α and CDR2β segments produced clone MAGEa6b9 with a K_D of 67 pM and a $T_{1/2}$ of ~9 hours. The off-target binding activity of MAGEa6b9 was deemed unacceptable and required further engineering. Back mutation of clones MAGEa6 and MAGEb2 generated clones MAGEa6a and MAGEb2a with K_D values of 6.55 μM and 9.43 μM respectively suitable for use as second -generation templates. Three second -generation strategies were investigated to isolate CDR3 mutations; exploring the TCR format, the number of residues simultaneously mutated and the panning conditions.

Strategy	ds-format	Targeted CDR	Framework	NNK	Panning strategy	Sequence analysis
1	Native	CDR3α CDR3β	MAGEa6a MAGEb2a	5	3 cycles against HLA-A*0101-MAGE$_{(168-176)}$	Normal
2	mTCR	CDR3α CDR3β	wt MAGEa6a MAGEb2a	5	3 cycles against HLA-A*0101-MAGE$_{(168-176)}$	Deep sequencing of TCR β chain
3	Native	CDR3α CDR3β	MAGEa6a	6	(a) 3 cycles of subtractive panning on HLA-A1^{+} MAGE^{-} human primary cell lines followed by panning against HLA-A*0101-MAGE$_{(168-176)}$ (b) 3 cycles against HLA-A*0101-MAGE$_{(168-176)}$	Deep sequencing of TCR β chain

Table 5.4. Outline of selection strategies employed to isolate MAGE-A3 TCR CDR3 mutations. ds-format: TCR constant domains containing the membrane-proximal cysteine pair in the native format or TCR constant domains containing the engineered cysteine pair in the mTCR format. Targeted CDR: CDR3 domains exclusively targeted. Framework: mutated CDR3 libraries built in the context of the wt TCR chains, enhanced-affinity clone MAGEa6a (CDR2α mutant) or enhanced-affinity clone MAGEb2a (CDR2β mutant). NNK: 5 or 6 residues targeted with the NNK motif.

5.8 Strategy 1 - Exploring the native TCR format on enhanced-affinity framework

The first-generation MAGE-A3 TCR libraries built in the context of the wild-type framework had failed to yield high affinity CDR3 mutants. Using an enhanced-affinity clone from the first maturation libraries for further mutagenesis had proved a fruitful strategy in isolating mutations in further CDR loops for both the Mel-5 and gp100 TCRs. Mutations within the CDR2 loops had been identified from first maturation MAGE-A3 TCR libraries. Based on the engineering of the Mel-5 and gp100 TCRs, enhanced-affinity CDR2α and CDR2β MAGE-A3 TCRs were used as template to obtain mutations in the CDR3 loops. The enhanced-affinity MAGE TCR templates were first cloned in the native TCR format and the CDR3 loops were subsequently mutated using overlapping 5-NNK oligonucleotides.

5.8.1 Cloning the MAGEa6a and MAGEb2a TCRs into the phagemid vectors

The binding kinetics of MAGEa6 (K_D of 190 nM and $T_{1/2}$ of 66 seconds) and MAGEb2 (K_D of 170 nM and $T_{1/2}$ of 120 seconds) were deemed unsuitable to use as templates for further mutagenesis. Whilst it had proved difficult to isolate novel mutations in the Mel-5 TCR using the highest affinity clone MELa1 as template (K_D of 6.4 nM and $T_{1/2}$ of 210 s), using a back-mutated version (K_D of 450 nM), provided a more optimal framework to isolate further mutations.

Consequently, a panel of back-mutated TCRs, based on clones MAGEa6 (YVRPY) and MAGEb2 (TDMLL) was generated by Dr. A. Bennett. Each mutated residue in the CDR2 loop was sequentially reverted to wild-type to produce eight separate *E. coli* expression plasmids designated MAGEa6a-a6d and MAGEb2a-b2d. TCRs were refolded from denatured inclusion bodies and purified ds-linked TCRs

were subjected SPR analysis on a BIAcore3000. Equilibrium binding constants (K_D) of 6.55 μM for MAGEa6abwt and 9.43 μM for MAGEawtb2a were calculated.

Clones MAGEa6a (LVRPY) and MAGEb2a (TDMTL) did not exist in the phagemid format and required engineering. The phagemid vectors pIM194 and pIM195 encoding the back-mutated TCR segments MAGEa6a and MAGEb2a respectively, were constructed by SOE-PCR as described in Section 2.3.2 of Materials and Methods.

5.8.2 Design and construction of Strategy 1 libraries

Mutated CDR3α and CDR3β libraries were constructed on both the MAGEa6a and MAGEb2a frameworks (a total of four independent libraries) as described in Section 2.4.3 of Materials and Methods. *Nco*I and *Not*I digested pIM194 and pIM195 phagemid vectors were used as template and CDR3 segments were mutated using 5-NNK oligonucleotides listed in Section 2.4.3 of Materials and Methods and following the PCR strategy depicted in Figure 2.5 of Materials and Methods. In addition to the first-generation primers, an extra NNK primer was designed to increase coverage of both the CDR3α (primer Nat100) and CDR3β (primer Nat102) segments (Section 2.4.3 of Materials and Methods). SOE-PCR-generated library fragments (six CDR3α and five CDR3β) were cloned into pEX922 as *Nco*I-*Not*I fragments to yield libraries comprising 10^8-10^9 transformants. Sequencing of ten random clones showed diversity across each CDR (data not shown).

5.8.3 Phage selection and screening

Three cycles of panning against biotinylated HLA-A*0101-MAGE-$A3_{(168-176)}$ were performed as described in Section 2.5.4 of Materials and Methods. The stringency of selection was increased with each round: decreased antigen concentration, decreased

phage input and increased number of washes (Table 5.5). The output titre for each round of selection was estimated and following the third round of panning up to a 10-fold increase was observed for libraries 1, 2 and 4 (Table 5.5).

Pan 3 phage from individual ampicillin-resistant *E. coli* TG1 colonies was rescued together with a single *E. coli* TG1 colony bearing enhanced-affinity clones MAGEa6, MAGEa6a and MAGEb2a (grown in each of the four plates). Monoclonal phage TCRs were screened in an inhibition phage ELISA at 200 nM biotinylated HLA-A*0101-MAGE-A3$_{(168-176)}$ to determine if any of the TCRs demonstrated competitive inhibition. Antigen-binding phage clones were obtained from all four libraries.

Library	Targeted CDR:Template	Pan 1 100 nM pHLA 7 washes		Pan 2 80 nM pHLA 9 washes		Pan 3 50 nM pHLA 9 washes	
		Input phage ml^{-1}	Output cfu ml^{-1}	Input phage ml^{-1}	Output cfu ml^{-1}	Input phage ml^{-1}	Output cfu ml^{-1}
1	CDR3α:MAGEa6a	6×10^{11}	5×10^{5}	2×10^{11}	1.5×10^{6}	1×10^{11}	1.5×10^{7}
2	CDR3α:MAGEb2a	6×10^{11}	5×10^{5}	2×10^{11}	4×10^{7}	1×10^{11}	3.6×10^{8}
3	CDR3β:MAGEa6a	6×10^{11}	5×10^{5}	2×10^{11}	9×10^{6}	1×10^{11}	1.3×10^{7}
4	CDR3α:MAGEb2a	6×10^{11}	3×10^{5}	2×10^{11}	7×10^{6}	1×10^{11}	6×10^{7}

Table 5.5. MAGE-A3 TCR CDR3 Strategy 1 library selections. Three cycles of selection against biotinylated HLA-A*0101-$MAGE_{(168\text{-}176)}$ antigen were performed. The stringency of the panning conditions was increased with each round; pHLA concentration was decreased and the number of washes increased. To estimate the phage titre, the input phage preparation was diluted 50-fold in PBS and the absorption at 260 nm was measured. The phage titres were estimated according to the following empirical formula: phage ml^{-1} = Abs_{260} x phage dilution x 22.14 x 10^{10} (Lee, Iorno et al. 2007). The output phage titres were estimated by infecting log-phase *E. coli* TG1 cells with eluted phage and plating onto agar plates supplemented with ampicillin and 2% glucose and incubated overnight at 30 ºC as described in Section 2.5.4 of Materials and Methods. The estimation of phage titre determined using either method correlated closely (data not shown). In order to reduce potential proteolysis of the display TCR, the input phage was titred using the Abs_{260} method to allow a cycle of selection to be performed on the day of phage precipitation. Thus reducing potential proteolysis of the displayed TCR.

5.8.4 Primary screening of crude phage supernatant

Twenty clones from each library demonstrating the highest % inhibition at 200 nM inhibitor were sequenced (Table 5.6). The Pan 3 output for library 2 (Table 5.6 B) and library 4 (Table 5.6 D) built on MAGEb2a were enriched for a non-designed αβ TCR combination; clone MAGEa6b2a (19 out of 20 and 3 out of 20 sequenced clones respectively). The presence of this clone in the two libraries was the result of a PCR-splice reaction between the MAGEa6 α chain and the MAGEb2a β chain that occurred during library construction. The MAGEa6b2a clone was not seen in the sequencing of either pre-selected libraries. Such a degree of enrichment for this clone in library 2 (95%) indicated a lack of CDR3α mutants in the context of MAGEb2a with improved binding kinetics compared to clone MAGEa6b2a. Assuming that library 4 (built on the same template as library 2) contained a similar level of MAGEa6b2a contamination, the presence of 85% unique CDR3β clones in the Pan 3 output suggested an improved fitness over the contaminating splice variant.

Of the 20 sequenced clones from library 1 (Table 5.6 A), one was of poor quality and so was not included in the analysis. The remaining sequences converged to 7 unique clones with several being represented by multiple copies. Fourteen sequenced clones shared a common motif: P-F-X^{101}-V-X^{103}, where X^{101} was mutated to a Tyr or Phe and X^{103} mutated to a Val, Lys or Arg. In clone MAGEa21, the wild-type Ser^{99} was retained but also included the Y^{100} to Phe and L^{102} to Val substitutions common to all clones. Although an S99P substitution was seen in 14 out of 19 sequenced clones, S^{99} was also substituted for an Ala in several clones. The % inhibition values at 200 nM inhibitor for the selected library 1 clones were in a similar range (86-91%) to that observed for clone MAGEa6 (86%). This relatedness in phage inhibition ELISA would imply that they also shared similar affinity values. The back mutated

TCRs MAGEa6a and MAGEb2a failed to produce a signal reflecting the low affinity pHLA interaction. The nucleotides highlighted in blue (Table 5.6) indicate alternative codon usage; multiple codon usage provides confidence of library diversity. The single unique clone from library 2 (Table 5.6 B), MAGEa22 demonstrated an inhibition value higher than the reference clone, MAGEa6. As the output was dominated by the contaminant clone MAGEa6b2a, it was likely that this mutant was selected based on improvements in affinity. Of the 20 sequenced clones from library 3, 11 shared the consensus *Q*VS motif (residues 97-99). All variants conferred an increase in the level of inhibition compared to clone MAGEa6 reflecting a potential improvement in affinity over the parental clone. The affinity of clone MAGEa6a is too weak to exhibit a signal in this system indicating that the ELISA positive clones were of higher affinity. A second group of mutants, derived from a separate NNK primer was isolated yielding inhibition values in excess of that registered for clone MAGEa6. In this collection, five individual sequences had converged to three clones. This subset showed a strong preference for particular substitutions: S94G and M97E. In all cases, the wild-type Asn^{96} was retained. The 17 sequenced clones from library 4 (Table 5.6 D), excluding the 3 non-designed MAGEa6b2a sequences, converged to 9 unique mutants. Second -generation libraries were built on more than one framework with the aim to satisfy two objectives: (1) to increase the opportunity of isolating improved-affinity mutants and (2) to identify clones with varied sequence. The CDR3β libraries were constructed on the MAGEa6a (Table 5.6 C) and MAGEb2a (Table 5.6 D) templates. Although common to both outputs was a $Q^{97}V^{98}$ motif, a diverse sequence output was obtained from overlapping mutations covering as total of 8 residues. Clone MAGEb30 (containing the $Q^{97}V^{98}$ motif) dominated the output (45 % of sequenced clones). All clones contained an amber codon.

A.

Clone Number	CDR3α$_{(S99\text{-}T103)}$	Freq.	% Inhib. @ 200 nM
wt	S Y Q L T agttaccaactcact	-	-
MAGEa6	S Y Q L T agttaccaactcact	-	86
MAGEa15*	**P F Y V V** ccttttatgtggtg	6	89
MAGEa16*	**P F Y V K** ccttttatgtgaag	3	91
MAGEa17	**P F Y V R** ccgttttatgttcgg	5	90
MAGEa18*	**P F F V V** cctttttttgtggtt	3	90
MAGEa19	**A F Y V R** gcttttatgttagg	1	89
MAGEa20	**A F Y V V** gcgttttatgtggtt	1	88
MAGEa21	S **F A V V** gtctttgctgtggtt	1	86

B.

Clone Number	CDR3α$_{(G95\text{-}S99)}$	Freq.	% Inhib. @ 200 nM
wt	G G A G S ggaggggctgggagt	-	-
MAGEa6	G G A G S ggaggggctgggagt	-	86
MAGEa22*	**S Q S** G **R** agtcagtcgggtagg	1	97

C.

Clone Number	CDR3β$_{(S94\text{-}E100)}$	Freq.	% Inhib. @ 200 nM
wt	S P N M A D E agcccgaacatggccgacgag	-	-
MAGEa6	S P N M A D E agcccgaacatggccgacgag	-	86
MAGEb14*	**G R** N **E** A D E ggtaggaatgaggccgacgag	2	94
MAGEb15	**G L** N M A D E ggtcttaatatggccgacgag	2	92
MAGEb16	**G L** N **E** A D E ggtttgaatgaggccgacgag	1	97
MAGEb17	**G I** N **E** A D E gggattaatgaggccgacgag	1	94
MAGEb18	S **E W Q V S** E agcgagtggcaggtgtctgag	1	98
MAGEb19	S **E W *Q* V S** E	1	98

	agcgagtggtaggtgtctgag		
MAGEb20	S **E** **H** ***Q*** **V** **S** E agcgagcattaggtgtcggag	2	99
MAGEb21	S **K** **Y** ***Q*** **V** **S** E agcaagtattaggtgagtgag	1	92
MAGEb22*	S **K** **H** ***Q*** **V** **S** E agcaagcattaggtgtctgag	1	97
MAGEb23	S **R** **Y** ***Q*** **V** **S** E agcaggtattaggtgagtgag	1	99
MAGEb24	S **L** **G** ***Q*** **V** **S** E agcttggggtaggtttcggag	1	97
MAGEb25	S **Q** **Y** **Q** **V** **S** E agccagtatcaggtttcggag	1	99
MAGEb26*	S **Y** N **L** A **S** E agctataatcttgcgtctgag	1	96
MAGEb27	S **V** **G** **Q** **V** **S** E agcgttggtcaggtgtcggag	1	93
MAGEb28*	S **M** **Y** ***Q*** **V** **S** E agcatgtattaggtgagtgag	1	99
MAGEb29*	S P **H** ***Q*** **V** **G** **R** agcccgcattaggttggtcgt	1	98

D.

Clone Number	CDR3β$_{(S93\text{-}E100)}$	Freq.	% Inhib. @ 200 nM
wt	S S P N M A D E agcagcccgaacatggccgacgag	-	-
MAGEa6	S S P N M A D E agcagcccgaacatggccgacgag	-	86
MAGEb30	S S P N ***Q*** **V** D **G** agcagcccgaattaggttgatggg	9	98
MAGEb31	S S P N **Q** **V** D **G** agcagcccgaaccaggtggatggt	1	96
MAGEb32*	S S **Y** **V** **L** A **M** E agcagctatgttttggcgatggag	1	100
MAGEb33*	S S **Y** **V** **L** **V** **A** E agcagctatgttttggttgcggag	1	97
MAGEb34*	S S **Y** **V** **L** A D E agcagctatgtgcttgctgatgag	1	92
MAGEb35	**G** S **Y** **V** **L** A D E gggtcgtatgtgttggccgacgag	1	100
MAGEb36*	**G** S **Y** **T** **L** A D E gggtcgtatacgttggccgacgag	1	98
MAGEb37*	S **N** **L** N **G** A D E tcgaatcttaatggtgccgacgag	1	97
MAGEb38*	S **N** **R** N **G** A D E tcgaatcggaatggggccgacgag	1	75

Table 5.6. Output clones obtained after three cycles of panning against biotinylated HLA-A*0101-MAGE$_{(168\text{-}176)}$ antigen. A phage inhibition ELISA was performed at 200 nM non-biotinylated HLA-A*0101-MAGE$_{(168\text{-}176)}$ antigen. Twenty clones showing the highest % inhibition level were sequenced from each library. **(A).** Library 1: MAGE-A3 TCR CDR3α library built on clone MAGEa6a (CDR2α mutant; KD of 6.55 μM). **(B).** Library 2: MAGE-A3 TCR CDR3α library built on

clone MAGEb2a (CDR2β mutant; KD of 9.43 μM). Library 2 was contaminated with the high affinity clone MAGEa6b2a. Of the 20 sequenced clones, only one clone contained mutations in the targeted CDR3α region. **(C).** Library 3: MAGE-A3 TCR CDR3β library built on clone MAGEa6a. One out of twenty sequenced clones was of poor quality and so was not included in the analysis. **(D).** Library 4: MAGE-A3 TCR CDR3β library built on clone MAGEb2a. Library 4 contained a low level contamination of high affinity clone MAGEa6b2a (3 out of 20). Amino acids that differ from wt are highlighted in bold and red. Nucleotides highlighted in blue indicate alternate codon usage between clones sharing the same amino acid sequence. *Q*, amber codon. wt, wild-type. * Clones selected for further analysis in secondary phage ELISA screen (section 5.8.5).

5.8.5 Secondary screening of purified phage supernatant

To more precisely establish affinity improvement over the parental clones, a phage ELISA was performed at three concentrations of inhibitor (200, 100 and 20 nM). Phage was PEG precipitated from 10 ml culture supernatant for the 16 clones highlighted in Table 5.6 (Section 2.5.1 and 2.5.2 of Materials and Methods): four CDR3α and twelve CDR3β mutants. Additionally, phage was prepared for clone MAGEa6 as a reference.

A preliminary ELISA was performed to determine the dilution of phage that would generate a similar level of signal between clones of Abs_{650} ~1.0 (data not shown). A subsequent inhibition ELISA was performed using the dilution of phage (1.75-fold) determined from the first ELISA that produced an Abs_{650} ~1.0. The % reduction in signal was measured at 200, 100 and 20 nM inhibitor (Figure 5.5). Using the inhibition profile measured for the reference clone MAGEa6 (with a K_D of 190 nM), it was possible to assess the relative affinity of each of the test mutants.

Several of the TCR variants (MAGEa22, MAGEb28, MAGE32 and MAGE36) registered inhibition values similar to or in excess of the reference clone MAGEa6. A number of clones (MAGEa15, MAGEa16, MAGEa18 and MAGEb38) failed to yield inhibition values similar to those measured in the primary screen (Table 5.6). This may reflect a discrepancy in the amount of displayed TCR assayed in the primary screen compared to the secondary screen. Having normalised the TCR display level in the secondary screen the inhibition profiles are more informative (Figure 5.5).

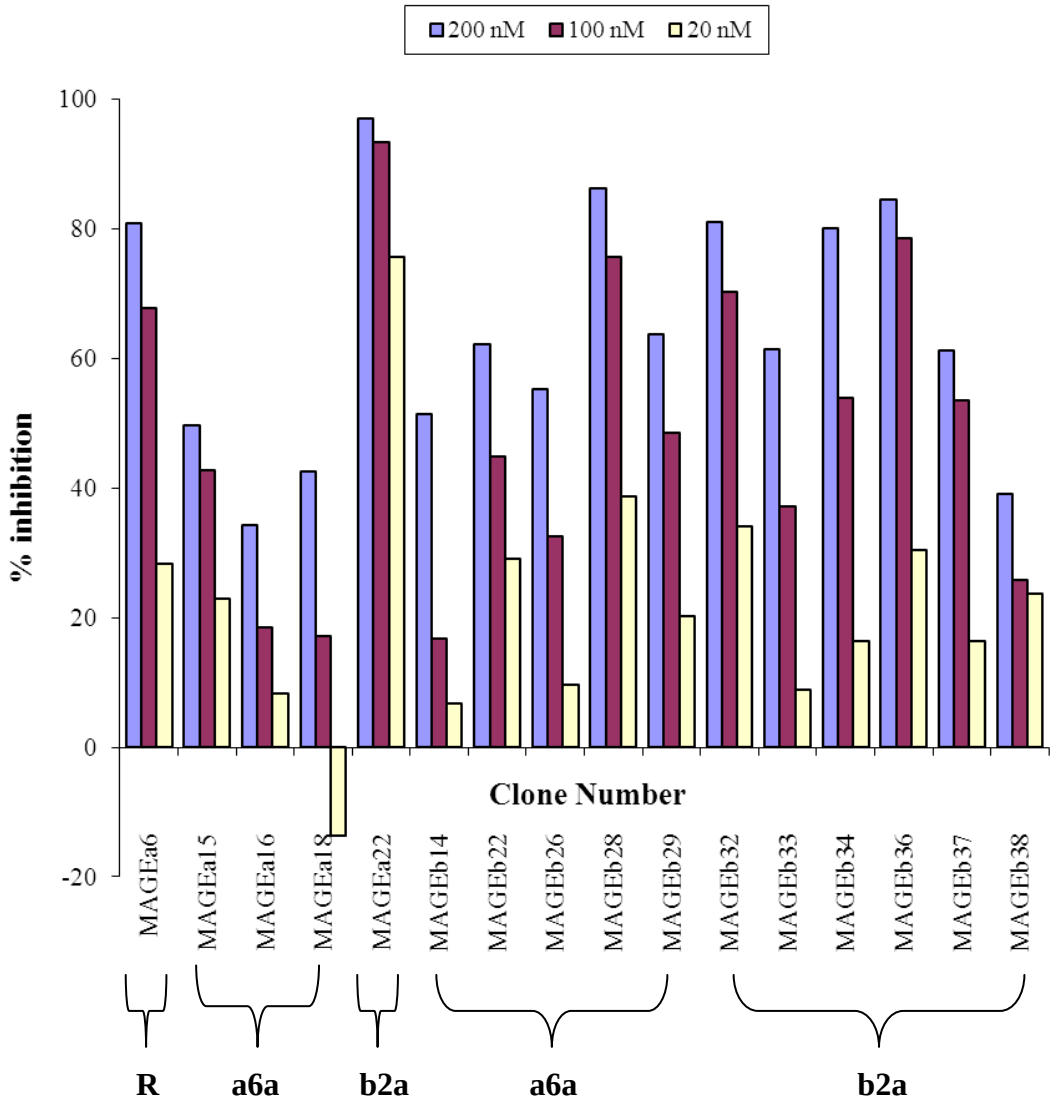

Figure 5.5. Inhibition phage ELISA of MAGE-A3 TCR CDR3α and CDR3β variants at a concentration of 200, 100 and 20 nM inhibitor. The CDR3 libraries were built in the context of enhanced-affinity clones MAGEa6a (a6a) and MAGEb2a (b2a); clones are grouped accordingly. High affinity clone MAGEa6 was included in the ELISA as the reference (R). The PEG-precipitated phage samples were incubated with the appropriate concentration of non-biotinylated HLA-A*0101-MAGE$_{(168-176)}$ antigen prior to adding to ELISA plates immobilised with HLA-A*0101-MAGE$_{(168-176)}$ antigen. % Inhib. is measured as the percentage reduction in ELISA signal. The background absorbance value was subtracted from all readings before % Inhib. was calculated.

5.8.6 Kinetic analysis of Strategy 1 TCRs

To assess the contribution of the CDR3 segments to improvements in affinity, four α chain (three isolated in the context of MAGEa6a and one in the context of MAGEb2a) and eleven β chain (five selected in the context of MAGEa6a and six in the context of MAGEb2a) mutants were cloned onto the wild-type MAGE-A3 TCR framework and named MAGEa' or MAGEb' (Table 5.7 A-D). One α chain (MAGEa22) and one β chain (MAGEb28) mutant were also cloned in the context of the enhanced-affinity mutant on which they were isolated (Table 5.7 E). PCR fragments were ligated into pEX954 for the α chains and pEX821 for the β chains for expression in *E. coli* strain Rosetta (DE3) pLysS. Soluble TCR was refolded from denatured inclusion bodies as described in Section 2.6.4 and 2.6.5 of Materials and Methods and binding affinity analysis was performed on a BIAcore3000 as described in Section of Materials and Methods. Based on the kinetic data obtained from BIAcore experiments, the most optimal CDR3α and CDR3β segments were combined (Table 5.7 F).

For libraries 1, 2 and 3 the hierarchy of mutants determined by phage inhibition ELISA was largely maintained when affinities were determined by SPR. Comparison of phage ELISA data and BIAcore data was not possible for the library 4 output as 4 out of 6 clones aggregated during refolding or failed to show any detectable binding as measured by BIAcore.

A selection of the mutants (highlighted in Table 5.7) was refolded firstly in the context of the wild-type MAGE-A3 TCR. The CDR3α segments isolated in the context of MAGEa6a (library 1) increased the affinity of the wild-type MAGE-A3 TCR up to ~1000-fold (Table 5.7 A). However, the soluble protein produced from this clone (MAGEa18') aggregated and so binding kinetic data was not accurate. Proteins from the other two clones that were tested (MAGEa15' and MAGEa16') shared

similar binding kinetics; with improvements in affinity of ~40-fold and ~60-fold respectively.

Although the library 2 output (built on the MAGEb2a framework) was enriched for the non-designed mutant MAGEa6b2a, the single unique CDR3α variant isolated (MAGEa22') improved the affinity of the wild-type MAGE-A3 TCR; up to ~1000-fold (Table 5.7 B).

The CDR3β segments isolated in the context of MAGEa6a (library 3) increased the affinity of the wild-type MAGE-A3 TCR up to ~145-fold (Table 5.7 C). The three clones that gave the greatest improvement in affinity shared a QV motif highlighting the importance of these residues to the binding.

Of the six CDR3β segments isolated in the context of MAGEb2a (library 4) only two produced measurable kinetics; although one (MAGEb38') aggregated upon purification (Table 5.7 D). Whilst each of the four remaining mutants (MAGEb32', MAGEb34', MAGEb36' and MAGEb37') had registered a positive signal in the phage ELISA in the context of the MAGEb2a segment (Table 5.6 D), they failed to show any detectable binding when refolded on the wild-type framework (Table 5.7 D).

Two of the mutants were subsequently refolded in the context of the enhanced-affinity TCR on which they were isolated: MAGEa18 (built on MAGEa6a) and MAGEb28 (built on MAGEb2a). Improvements in affinity of ~25-fold and ~15-fold were observed over the parental clones MAGEa6a and MAGEb2a respectively (Table 5.7 E). Although additivity of CDR segments was demonstrated for clone MAGEb28 (K_D of 1.7 μM on wild-type TCR and 0.6 μM on MAGEb2a), this was not observed for clone MAGEa18. Clone MAGEa18 on the wild-type TCR framework gave a K_D of 230 nM and 257 nM on MAGEa6a. One explanation for this unexpected result was

that MAGEa18 refolded in the context of the wild-type TCR yielded aggregated protein leading to an inaccurate K_D of 257 nM.

The most optimal CDR3 segments were combined; a representative mutant was chosen from each of the four libraries (Table 5.7 F). Combining the highest affinity CDR3α clone from library 2 (MAGEa22') with the highest affinity CDR3β clones from library 3, increased the affinity up to a further 100-fold over MAGEa22'. However, cooperative association of enhanced-affinity CDR segments was not always observed. Combining MAGEa22' with MAGEb38' reduced the affinity ~100-fold over MAGEa22'. Combining MAGEa18' and MAGEb38' resulted in loss of detectable binding. Clone MAGEa38' refolded with the wild-type β chain formed aggregates upon purification and as such does not represent an optimal β chain folding partner.

Strategy 1 successfully identified mutations in the CDR3 domains that increased the affinity over the wild-type TCR. Combining CDR3α and CDR3β mutated segments further improved the affinity up to ~100,000-fold. The aim of the second - generation libraries was not only to identify high affinity CDR3 mutations, but moreover, to isolate a variety of CDR3 mutations. As such, further strategies were pursued in order to realise these objectives.

Based on the binding kinetic data obtained for the CDR3 mutants refolded in the context of the wild-type TCR, it is not surprising that the first maturation libraries (built on the wild-type framework), failed to yield mutations in the CDR3 loops. The design of the phage ELISA allows detection of TCR/pHLA interactions with dissociation rate constant K_D <1 μM.

A.

Clone ID	CDR3α	K_D (nM)	$T_{1/2}$ (min)	K_D (parent) / K_D (mutant)
MAGEawtbwt	SYQLT	248000	nd	1
MAGEa15'bwt	**PFYVV**	5800	0.15	42.8
MAGEa16'bwt	**PFYVK**	3800	0.15	65.3
MAGEa18'bwt	**PFFVV**	230	12.6[a]	1078.3

B.

Clone ID	CDR3α	K_D (nM)	$T_{1/2}$ (min)	K_D (parent) / K_D (mutant)
MAGEawtbwt	GGAGS	248000	nd	1
MAGEa22'bwt	**SQS**G**R**	230	0.9	1078.3

C.

Clone ID	CDR3β	K_D (nM)	$T_{1/2}$ (min)	K_D (parent) / K_D (mutant)
MAGEawtbwt	SPNMADE	248000	nd	1
MAGEawtb14'	**GR**N**E**ADE	21000	nd	11.8
MAGEawtb22'	S**KH*Q*VS**E	2000	0.11	124
MAGEawtb26'	S**Y**N**L**A**S**E	21000	nd	11.8
MAGEawtb28'	S**MY*Q*VS**E	1700	0.1	145.9
MAGEawtb29'	SP**H*Q*VGR**	2500	4	99.2

D.

Clone ID	CDR3β	K_D (nM)	$T_{1/2}$ (min)	K_D (parent) / K_D (mutant)
MAGEawtbwt	SSPNMAD	248000	nd	1
MAGEawtb32'	SS**YVL**A**M**	[b]	-	-
MAGEawtb33'	SS**YVLVA**	35000	nd	7.1
MAGEawtb34'	SS**YVL**AD	nb	-	-
MAGEawtb36'	**G**S**YTL**AD	nb	-	-
MAGEawtb37'	S**NL**N**G**AD	nb	-	-
MAGEawtb38'	S**NR**N**G**AD	5500	10.6[a]	45.1

E.

Clone ID	CDR2α	CDR3α	CDR2β	CDR3β	K_D (nM)	$T_{1/2}$ (min)	K_D (parent) / K_D (mutant)
MAGEa6abwt	L**VRPY**	SYQLT	FSETQ	PNMAD	6550	nd	1
MAGEa18bwt	L**VRPY**	**PFFVV**	FSETQ	PNMAD	257	1.8	24.5
MAGEawtb2a	LIQSS	SYQLT	**TDMTL**	PNMAD	9430	nd	1
MAGEawtb28	LIQSS	SYQLT	**TDMTL**	**MYQVS**	626	0.7	15.1

F.

Clone ID	CDR3α	CDR3β	K_D (nM)	$T_{1/2}$ (min)	K_D (parent) / K_D (mutant)
MAGEawtbwt	GGAGSSYQLT	SSPNMADE	248000	nd	-
MAGEa22'b22'	**SQS**G**R**SYQLT	SS**KH*Q*VS**E	3.4	15.7	72941.2
MAGEa22'b28'	**SQS**G**R**SYQLT	SS**MY*Q*VS**E	3.4	13.5	72941.2
MAGEa22'b29'	**SQS**G**R**SYQLT	SSP**H*Q*VGR**	2.3	12.5	107826.1
MAGEa18'b38'	GGAGS**PFFVV**	S**NR**N**G**ADE	nb	-	-
MAGEa22'b38'	**SQS**G**R**SYQLT	S**NR**N**G**ADE	22500	1.2	11

Table 5.7. Binding affinities of MAGE-A3 TCR mutants isolated from Strategy 1 CDR3 libraries. (A). Library 1 (MAGEa6a) mutated CDR3α segments refolded with wt β chain. **(B).** Library 2 (MAGEb2a) mutated CDR3α segments refolded with wt β chain. **(C).** Library 3 (MAGEa6a) mutated CDR3β segments refolded with wt α chain. **(D).** Library 4 (MAGEb2a) mutated CDR3β segments refolded with wt α chain. **(E).** Mutated CDR3 segments refolded in the context of the enhanced-affinity clones MAGEa6a and MAGEb2a on which they were selected. **(F).** Combination of the most optimal α and β chain CDR3 segments. *Q*, amber codon. wt, wild-type. K_D values were determined by SPR in a BIAcore using purified refolded TCR. nd, not determined. 'Indicates mutated CDR3 segment cloned in the context of the wt framework and not the enhanced-affinity CDR2 mutant on which they were isolated. [a]Aggregation of refolded TCR. [b]Instability of refolded TCR. nb, no binding observed. (Data kindly provided by Dr. A. Powlesland and Dr. A. Legg).

5.9 Strategy 2 - Exploring the mTCR format on enhanced-affinity framework

Up until this point the MAGE-A3 TCR mutagenic libraries had been constructed on the native disulphide bond TCR framework. It was unclear how the positioning of the inter-chain disulphide cysteines would influence the composition of the phage display selection output. Whereas the mTCR cysteines fix the TCR α and β chains in a more rigid structure, the native TCR retains a degree of conformational flexibility possibly contributing to increased promiscuity. Strategy 2 aimed to explore the impact of the TCR format on the variation of mutants isolated.

5.9.1 Cloning the wild-type MAGE-A3 TCR (mTCR format) into the phagemid vector

The phagemid vector pLAS0282 for the display of the MAGE-A3 TCR in the mTCR format was constructed as described in Section 2.3 of Materials and Methods. MAGE-A3 TCR PCR fragments A (Vα), B (Vβ), C (Cα containing mTCR cysteine) and D (Cβ containing mTCR cysteine) (all fragments from Section 2.3 of Materials and Methods) were amplified by SOE-PCR with primers J135 and YOL22. The full-length VαCα/VβCβ product was cloned into pEX922 as an *Nco*I-*Not*I fragment. A sequence-verified clone was used for library construction. Fragment C containing a wild-type geneIII leader sequence was used in the construction of pLA0282; the geneIII leader sequence from phagemid pIM160 contained a point mutation (Figure 5.1).

5.9.2 Design and construction of Strategy 2 libraries

In this strategy, an alternative method for generating mutagenised TCR libraries was adopted. In the normal approach, two PCR fragments are generated for each overlapping NNK oligonucleotide which are subsequently stitched by SOE-PCR. To

construct MAGE-A3 TCR CDR3α and CDR3β libraries on two separate frameworks using this method would require 24 individual and 12 SOE-PCRs for each CDR; a total of 72 PCRs. As CDR3α and CDR3β libraries had already been built, albeit in the native format (Section 5.3 and Section 5.9.3), this material could be used as template to generate Strategy 2 libraries.

A PCR approach was designed to convert CDR3α and CDR3β libraries from the native format into the mTCR format (Figure 2.6 of Materials and Methods). The CDR3α libraries to be reformatted were library 3 (built on the wild-type framework; Section 5.3) and library 1 (on the MAGEa6a framework; Section 5.9.3). The CDR3α libraries built in the context of MAGEb2a were contaminated with the non-designed clone MAGEa3b2a and so were excluded from further libraries (Table 5.6 B). The CDR3β libraries to be reformatted were library 6 (built on the wild-type framework; Section 5.3) and library 4 (on the MAGEb2a framework; Section 5.9.3). Whilst the CDR3β library built in the context of MAGEa6a had yielded several high affinity clones that refolded with a high degree of efficiency, the CDR3β library built on MAGEb2a had not. Therefore it was of interest to mine this library further for potential high affinity mutants. A total of two CDR3α and two CDR3β libraries were reformatted. The schematic diagram in Figure 2.6 of Materials and Methods and the design outlined in Section 2.4.3.3 of Materials and Methods describe the strategy employed. In brief, the Vα and Vβ library fragments were amplified from the appropriate CDR3α and CDR3β library *E. coli* TG1 glycerol stocks using a reverse Cα or Cβ primer located upstream of the native constant region cysteine. Full-length VαCα and VβCβ domains were assembled by splicing onto the variable domain library fragment, a Cα or Cβ region containing the mTCR cysteines. The two CDR3α

and two CDR3β library SOE-PCR products were cloned into pLAS0282 as *Nco*I-*Avr*II and *Avr*II-*Not*I fragments respectively to yield libraries containing 10^9 independent transformants. Five randomly selected colonies from each of the four libraries were PCR amplified with primers YOL13 and YOL22. The integrity and diversity of the MAGE-A3 TCR libraries was confirmed by DNA sequencing to reveal a broad diversity of mutations spanning each of the targeted CDRs (data not shown).

5.9.3 Phage selection and screening

The libraries were affinity-selected three times against biotinylated HLA-A*0101-MAGE-$A3_{(168-176)}$; the antigen concentration was decreased and the number of washes were increased with each round (Table 5.8). The output titre for each round of selection was estimated. Following the third round of panning the output increased 10-fold for library 1, 20-fold for library 2 and 100-fold for library 4. The output of library 3 decreased by ~2-fold indicating a failure to enrich for high affinity clones (Table 5.8). Phage was prepared from individual ampicillin-resistant colonies as described in Section 2.5.1 and 2.5.2 of Materials and Methods. Monoclonal-phage-TCRs were screened in an inhibition phage ELISA at 100 nM biotinylated HLA-A*0101-MAGE-$A3_{(168-176)}$ to determine if any of the TCRs demonstrated competitive inhibition.

Library	Targeted CDR	Framework	Pan 1 100 nM pHLA 7 washes Input phage ml^{-1}	Pan 1 100 nM pHLA 7 washes Output cfu ml^{-1}	Pan 2 50 nM pHLA 7 washes Input phage ml^{-1}	Pan 2 50 nM pHLA 7 washes Output cfu ml^{-1}	Pan 3 50 nM pHLA 9 washes Input phage ml^{-1}	Pan 3 50 nM pHLA 9 washes Output cfu ml^{-1}
1	CDR3α	wt	1.5×10^{11}	1×10^{6}	1×10^{11}	5×10^{4}	1×10^{11}	5×10^{5}
2	CDR3α	a6a	1.5×10^{11}	1×10^{6}	1×10^{11}	1×10^{6}	1×10^{11}	2×10^{7}
3	CDR3β	wt	1.5×10^{11}	4×10^{5}	1×10^{11}	1×10^{5}	1×10^{11}	4×10^{4}
4	CDR3β	b2a	1.5×10^{11}	4×10^{5}	1×10^{11}	5×10^{5}	1×10^{11}	5×10^{7}

Table 5.8. MAGE-A3 TCR CDR3 Strategy 2 library selections. CDR3α and CDR3β libraries were built on either wt, MAGEa6a or MAGEb2a frameworks. Three cycles of selection against biotinylated HLA-A*0101-$MAGE_{(168\text{-}176)}$ antigen were performed. The stringency of the panning conditions was increased with each round; pHLA concentration was decreased and the number of washes increased.

5.9.4 Phage inhibition ELISA

ELISA positive clones were obtained from all libraries except library 3, as expected from the decreasing output (Table 5.8) Twenty clones from library 1, 2 and 4 demonstrating the highest % inhibition at 100 nM inhibitor were sequenced (Table 5.9). Sequencing of the library 1 output showed a contamination with high affinity CDR2α library clones (from the first-generation libraries) and so the data is not shown. The sequencing data illustrated in Table 5.9 A shows that four of the mutants that were isolated in the native TCR format (Strategy 1 Table 5.6 A) were also identified in the mTCR format. Common to both the re-selected and unique library 2 clones was a $P^{99}F^{100}$ motif. Selection of this motif encoded by two overlapping 5-NNK oligonucleotides (residues A^{97}-Q^{101} or S^{99}-T^{103}) illustrated the importance of this combination to improvements in affinity.

The sequencing data shown in Table 5.9 B shows that three of the mutants that were isolated in the native TCR format (Strategy 1 Table 5.6 D) were also identified in the mTCR format (MAGEb30, MAGEb34 and MAGEb37). Clones MAGEb37, MAGEb39, MAGEb40 and MAGEb41 showed a preference for an Asn at positions 94 and 96 and a Gly at position 97. Of these four clones only MAGEb37 was isolated from Strategy 1 selections.

Although converting the CDR3α and CDR3β libraries from the native into the mTCR format identified a number of unique mutants, the clear overlap between the clones isolated from the two strategies indicated minimal influence of the TCR format on the selection of MAGE-A3 TCR mutants.

A.

Clone Number	CDR3α$_{(A97\text{-}T103)}$	Freq.	% Inhib. @ 100 nM	Isolated from Strategy 1
wt	A G S Y Q L T gctgggagttaccaactcact	-	-	
MAGEa15	A G **P F Y V V** gctgggcctttttatgtggtt	6	82	✓
MAGEa23	A G **P F Y V Q** gctgggccttttttatgttcag	1	57	×
MAGEa17	A G **P F Y V R** gctgggccttttttatgtgcgt	2	83	✓
MAGEa18	A G **P F F V V** gctgggccttttttttgttgtg	1	82	✓
MAGEa21	A G S **F A V V** gctgggagttttgctgttgtt	3	71	✓
MAGEa24	A G S **F A T K** gctgggagttttgcgactaag	1	39	×
MAGEa25	**V** G **P F N** L T gttggtccgtttaatctcact	1	58	×
MAGEa26	A G **P F F V R** gctgggccttttttttgttcgt	1	78	×
MAGEa27	**V** G **P F P** L T ttggtccttttcctctcact	1	85	×
MAGEa28	**V** G **S F E** L T gtggggagttttgagctcact	1	78	×
MAGEa29	A G **P F Y V K** gctgggccgttttatgtgaag	1	74	×

B.

Clone Number	CDR3β$_{(S93\text{-}E100)}$	Freq.	% Inhib. @ 100 nM	Isolated from Strategy 1
wt	S S P N M A D E agcagcccgaacatggccgacgag	-	-	
MAGEb39	**T N L** N **G** A D E acgaatttgaatggggccgacgag	6	66	×
MAGEb37	S **N L** N **G** A D E tcgaatctgaatggggccgacgag	4	92	✓
MAGEb40	S **N M** N **G** A D E tctaatatgaatggtgccgacgag	1	91	×
MAGEb41	**G N L** N **G** A D E ggtaatttgaatggtgccgacgag	1	68	×
MAGEb30	S S P N ***Q*** **V** D **G** agcagcccgaattaggtggatgga	4	95	✓
MAGEb34	S S **Y V L** A D E agttcttatgtgttggccgacgag	3	80	✓
MAGEb42	S S **Y V L S M** E agcagctatgttcttagtatggag	1	86	×

Table 5.9. Strategy 2 output clones obtained after three cycles of panning against biotinylated HLA-A*0101-MAGE$_{(168\text{-}176)}$ antigen. A phage inhibition ELISA was performed at 100 nM non-biotinylated HLA-A*0101-MAGE$_{(168\text{-}176)}$ antigen. Twenty clones showing the highest % inhibition were sequenced from each library. **(A).** Library 2: MAGE-A3 TCR CDR3α library built on clone MAGEa6a. One sequence contained a mixture of templates and so was not included in the analysis. **(B).** Library

4: MAGE-A3 TCR CDR3β library built on clone MAGEb2a. Library 1 pan 3 output was contaminated with CDR2α library mutants from the first-generation libraries. Library 3 yielded no ELISA positive clones. Amino acids that differ from wt are highlighted in bold and red. Nucleotides highlighted in blue indicate alternate codon usage between clones sharing the same amino acid sequence. *Q*, amber codon. wt, wild-type. Clones isolated from Strategy 1 library selections are indicated.

5.9.5 Deep sequencing of library 4 Pan 0 and Pan 3 outputs

Whilst high affinity TCR mutants had been successfully isolated from sequencing a relatively small number of clones, in order to capture a more complete picture of the enrichment of mutated CDR3β segments, a deep sequencing approach was explored. Using the high throughput sequencing services of Adaptive Biotechnologies on the Illumina GAII System (Robins, Campregher et al. 2009), ~90,000 Pan 0 and ~360,000 Pan 3 CDR3β sequences were obtained. The top 24 most enriched clones are shown in Table 5.10. Although three of the five most enriched clones were also identified by phage ELISA (Table 5.9), an additional collection of novel mutants were sequenced. Clones MAGEb34 and MAGEb39 dominated the Pan 3 output; ~60% of sequenced clones (~1500-fold and ~800-fold enrichment respectively).

Whilst the 24 clones shown in Table 5.10, derived from 4 out of the 5 overlapping 5-NNK primers used to generate the CDR3β libraries, suggests a paucity of mutational hot-spots, remarkably, there was a clear preference for certain residues at some positions: P^{95} was frequently substituted for Tyr or Leu; N^{96} was changed to Val or Tyr; M^{97} was substituted for Gln, Phe or Leu (collectively represented in 75% of sequences); A^{97} was substituted for Val in half of the sequenced clones; D^{99} was changed to Gly, Ser or Leu. Two motifs were also frequently isolated: Q^{97} V^{98} (~33% of sequenced clones) and Y^{95} V^{96} (~17% of sequenced clones).

Clone Number	CDR3β$_{(C91\text{-}E100)}$	Pan 0 % of total	Pan 3 % of total	Fold increase	Identified by ELISA
wt	CASSPNMADE	3.83443	0.12149	0.03	-
MAGEb34	CASS**YVL**ADE	0.01143	17.09598	1495.76	✓
MAGEb42	CAS**NFGQV**DE	0.00085	0.84545	998.60	×
MAGEb39	CA**TNL**N**G**ADE	0.05630	45.64693	810.76	✓
MAGEb43	CAS**TVHQVG**E	0.00212	0.89267	421.75	×
MAGEb18	CASS**EWQVS**E	0.00085	0.25181	297.43	✓
MAGEb44	CASS**WQPPY**E	0.00339	0.96714	285.58	×
MAGEb45	CASSP**YPDLS**	0.00127	0.29922	235.61	×
MAGEb46	CASS**MWQVS**E	0.00127	0.25546	201.16	×
MAGEb47	CASS**YVL**A**S**E	0.00339	0.39883	117.77	×
MAGEb48	CASSPN**QV**D**A**	0.00127	0.10479	82.52	×
MAGEb49	CASSP**YPILS**	0.00085	0.05988	70.73	×
MAGEb50	CASS**LLSVV**ADE	0.00085	0.05911	69.82	×
MAGEb51	CASS**VQDPL**E	0.00085	0.04299	50.78	×
MAGEb52	CASS**FVL**ADE	0.00169	0.07447	43.98	×
MAGEb53	CAS**NVGQVG**E	0.00381	0.14472	37.98	×
MAGEb54	CASS**YVL**A**N**E	0.00381	0.07313	19.19	×
MAGEb55	CASS**SSIVS**E	0.00085	0.01516	17.91	×
MAGEb56	CASSP**YPNLG**	0.00085	0.01497	17.68	×
MAGEb57	CASS**Y**N**LVG**E	0.00085	0.01132	13.38	×
MAGEb58	CASS**SMEVS**E	0.00212	0.02764	13.06	×
MAGEb59	CASS**LLQVS**E	0.00085	0.00960	11.33	×
MAGEb60	CASS**YVL**AD**D**	0.00085	0.00844	9.97	×
MAGEb61	CASS**MFQVS**E	0.00127	0.00902	7.10	×
MAGEb37	CAS**NLNG**ADE	0.00423	0.01209	2.86	✓

Table 5.10. MAGE-A3 TCR Strategy 2 deep sequencing of library 4 Pan 0 and Pan 3 outputs. 10 µg DNA was isolated from Pan 0 and Pan 3 library 4 (CDR3β) *E. coli* TG1 glycerol stocks. Sequencing of the Pan 0 and Pan 3 outputs on the Illumina GAII System generated 93,903 and 365,309 sequences respectively. The frequency of each sequence has been converted into a % of the total number of sequences. Enrichment of sequences is shown as the fold-increase at Pan 3. Identification of clones based on phage inhibition ELISA data (Table 5.9 B) is shown (✓ or ×**)**. Data kindly provided by Adaptive Biotechnologies (Seattle, USA).

5.9.6 Kinetic analysis of Strategy 2 TCRs

A subset of CDR3 mutants identified from the Strategy 2 output were refolded and TCR-pHLA binding analysed by BIAcore (Table 5.11). The clones were chosen based on isolation frequency or uniqueness of sequence compared to Strategy 1. Two CDR3α mutants (containing the MAGEa6a mutated segment) were refolded with the wild-type β chain. A single CDR3β mutant (containing the MAGEb2a mutated segment) was refolded with the wild-type α chain. Recruiting the CDR3α segments (unique to Strategy 2) into the MAGEa6a clone increased the K_D by ~30-fold; representing ~1000-fold improvement over the wild-type TCR. Recruiting the CDR3β segment MAGEb30 (highly represented in the Strategy 1 and 2 outputs) into the MAGEb2a clone increased the K_D by ~850-fold; representing ~22500-fold improvement over the wild-type TCR. However, clone MAGEb34 (muated CDR3β) refolded in the context of the wild-type TCR, failed to exhibit detectable binding to HLA-A*0101-$MAGE_{(168-176)}$ (data not shown). This CDR3β segment had yielded an ELISA positive signal in the context of MAGEb2a (Table 5.9 B), indicating co-operative binding between the mutated CDR2β and CDR3β segments. However, a lack of cooperativity between the wild-type CDR2β and mutated CDR3β culminated in abolished binding.

A.

Clone ID	CDR3α	K_{on} (M^{-1} s^{-1})	K_{off} (s^{-1})	K_D (nM)	$T_{1/2}$ (min)	$\frac{K_D \text{ (parent)}}{K_D \text{ (mutant)}}$	$\frac{K_D \text{ (MAGEa6a)}}{K_D \text{ (mutant)}}$
MAGEawtbwt	AGSYQLT	nd	nd	248000	nd	1	-
MAGEa6abwt	AGSYQLT	nd	nd	6550	nd	37.9	1
MAGEa24bwt	AGS**FATK**	1.19×10^{5}	2.69×10^{-2}	226	0.43	1097.3	29
MAGEa25bwt	**V**G**PFN**LT	3.93×10^{5}	9.03×10^{-3}	230	1.3	1078.3	28.5

B.

Clone ID	CDR3β	K_{on} (M^{-1} s^{-1})	K_{off} (s^{-1})	K_D (nM)	$T_{1/2}$ (min)	$\frac{K_D \text{ (parent)}}{K_D \text{ (mutant)}}$	$\frac{K_D \text{ (MAGEb2a)}}{K_D \text{ (mutant)}}$
MAGEawtbwt	PNMADE	nd	nd	248000	nd	1	-
MAGEawtb2a	PNMADE	nd	nd	9430	nd	26.3	1
MAGEawtb30	PN**QV**D**G**	5.43×10^{4}	5.84×10^{-4}	11	19.8	22545.5	857.3

Table 5.11. Binding affinities of MAGE-A3 TCR mutants isolated from Strategy 2 CDR3 libraries. (A). Library 2: MAGE-A3 TCR CDR3α mutant segments cloned in the context of MAGEa6a and refolded with wt β chain. **(B).** Library 4: MAGE-A3 TCR CDR3β mutant segment cloned in the context of MAGEb2a and refolded with wt α chain. *Q*, amber codon. wt, wild-type. K_D values were determined by SPR in a BIAcore using purified refolded TCR. nd, not determined. nb, no binding observed. (Data kindly provided by Dr. A. Legg).

5.10 Strategy 3 - Exploring subtractive panning on human primary cell lines

The MAGE-A3 TCR mutants isolated from the first-generation libraries (Section 5.7) demonstrated off-target activity against several human primary cell lines including HEP2 (human hepatocyte) and HDMEC3 (human microvascular endothelial cells) cell lines. The cell lines are HLA-A*0101 positive but MAGE antigen negative. In this context, identification of the exact antigen target on the cell surface is of little importance.

Selection of phage displayed antigens against cell surface receptors performed on adherent mammalian cells has proven successful (Liu, Teng et al. 2005; Wang, Liu et al. 2011). Panning on whole cells such as against primary cell suspensions of organs and tissues or selections against immortalised cell lines is reviewed in (Molek, Strukelj et al. 2011). It was hypothesised that preselecting the phage library against one or both of HEP2 and HDMEC3 cell lines at each cycle of panning would deplete the pool of cross-reactive phage-TCRs. Completing one cycle of panning against biotinylated HLA-A*0101-$MAGE_{(168\text{-}176)}$ should enrich for specific binders. The schematic shown in Figure 5.6 illustrates the strategy employed to deplete the phage library population of cross-reactive MAGE-A3 TCRs. Each cycle of panning is divided into two parallel selection approaches: (A). Pre-selection of phage libraries on human primary cell lines followed by selection on biotinylated HLA-A*0101-$MAGE_{(168\text{-}176)}$ (designated subtractive panning) or (B). Selection exclusively on biotinylated HLA-A*0101-$MAGE_{(168\text{-}176)}$ (designated normal panning).

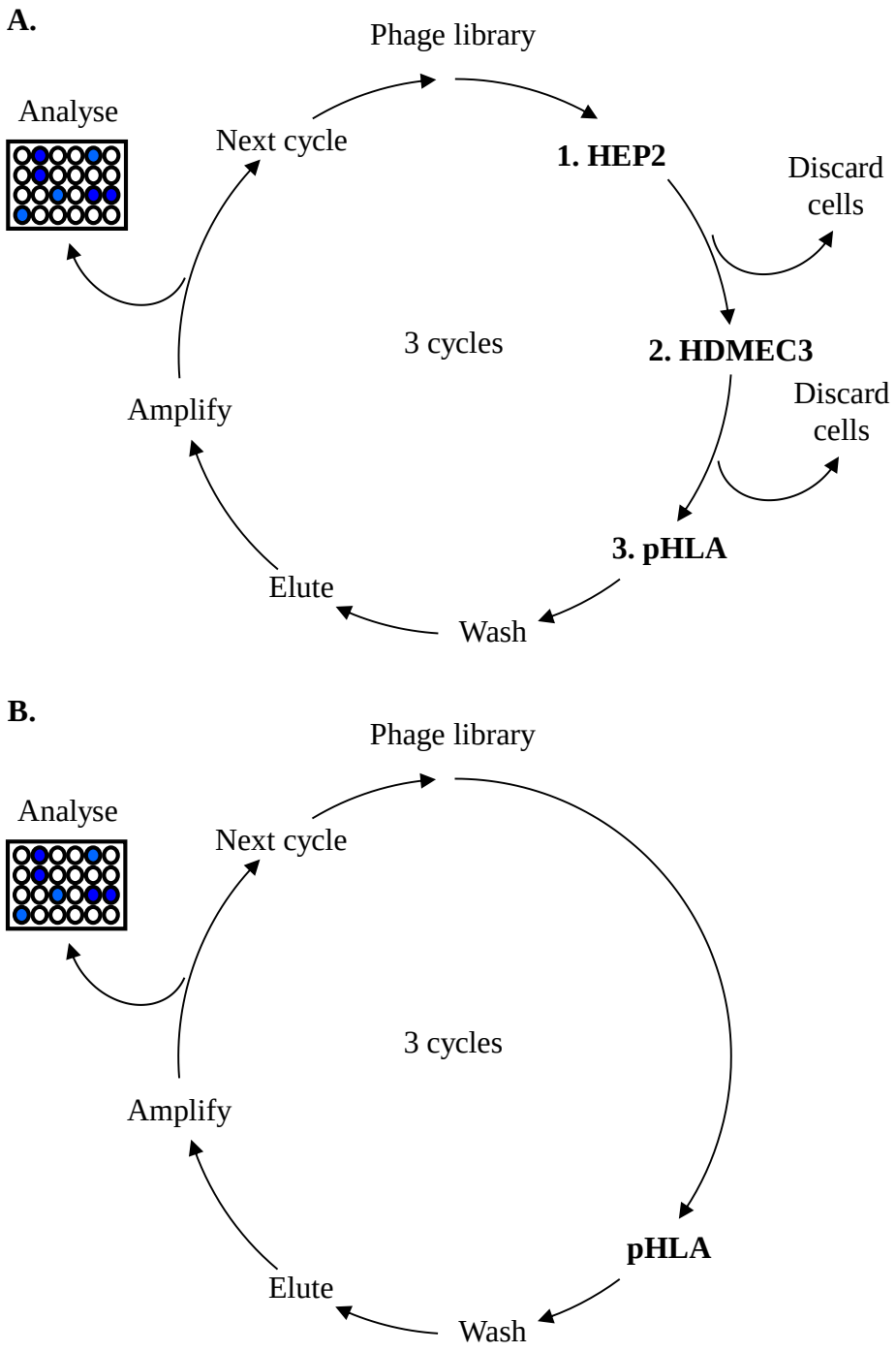

Figure 5.6. Schematic diagram of MAGE-A3 TCR Strategy 3 panning strategies. (A). Subtractive panning against human primary cell lines (HLA-A1^{+} MAGE^{-}). 1. Pre-blocked phage (1 x 10^{11}) was incubated with the HEP2 (human hepatocyte) cell line (~2 x 10^{6}) for 1 h at room temperature (RT). 2. Cells were pelleted at 4,000 rpm (RT) and phage supernatant (pSN) incubated with the HDMEC3 (human microvascular endothelial cells) cell line (~2 x 10^{6}) for 1 h at RT (only for Pan 1). 3. Cells were pelleted at 4,000 rpm (RT) and pSN was panned against biotinylated HLA-A*0101-MAGE$_{(168\text{-}176)}$ (pHLA-MAGE-bio). **(B).** Normal panning against pHLA-MAGE-bio. Three cycles of both selection strategies were performed in parallel.

5.10.1 Design and construction of Strategy 3 libraries

The CDR3α and CDR3β loops were mutated using overlapping 6-NNK oligonucleotides and phagemid vector pIM194 (MAGEa6a) as template. Libraries were kindly provided by Dr. Y. Li. Library fragments were assembled by SOE-PCR as described in Section 2.4.2 and 2.4.3 of Materials and Methods. Transformation of electrocompetent *E. coli* TG1 cells with each library ligation mixture yielded libraries with a complexity of ~10^{10} TCR members.

5.10.2 Phage selection and screening

Phage was subjected to three cycles of subtractive or normal panning as shown in Figure 5.6 following the methods described in Section 2.5.4 of Materials and Methods. In the subtractive panning, 1 x 10^{11} phage was incubated with 2 x 10^6 HEP2 cells for 1 hour at room temperature. Following centrifugation to pellet the cells, phage was incubated for a further hour with 2 x 10^6 HDMEC3 cells. In Pan 2 and 3, phage was incubated with only HEP2 cells. The cells were pelleted and the depleted phage population was panned against biotinylated HLA-A*0101-$MAGE_{(168-176)}$. In parallel, the phage was also treated to the normal conditions of panning against biotinylated HLA-A*0101-$MAGE_{(168-176)}$.

The output titre for each round of selection was estimated. Following the third round of panning the output increased between 20 and 30-fold for each library (Table 5.12). The outputs consistently were lower for the subtractive panning compared to the normal panning reflecting the more stringent conditions of selection. Phage was prepared from 96-individual ampicillin-resistant colonies as described in Section 2.5.1 and 2.5.2 of Materials and Methods. Monoclonal phage TCRs were screened in an inhibition phage ELISA at 100 nM biotinylated HLA-A*0101-MAGE-$A3_{(168-176)}$ to determine if any of the TCRs demonstrated competitive inhibition.

			Pan 1		Pan 2		Pan 3	
Library	Targeted CDR	Panning	Input phage ml^{-1}	Output cfu ml^{-1}	Input phage ml^{-1}	Output cfu ml^{-1}	Input phage ml^{-1}	Output cfu ml^{-1}
1	CDR3α	Subtractive	1×10^{11}	8×10^{4}	1×10^{11}	1.7×10^{6}	5×10^{10}	3×10^{7}
2	CDR3α	Normal	1×10^{11}	1×10^{5}	1×10^{11}	3.2×10^{6}	5×10^{10}	1×10^{8}
3	CDR3β	Subtractive	1×10^{11}	1×10^{5}	1×10^{11}	1.5×10^{6}	5×10^{10}	4×10^{7}
4	CDR3β	Normal	1×10^{11}	3×10^{5}	1×10^{11}	2.1×10^{6}	5×10^{10}	5×10^{7}

Table 5.12. MAGE-A3 TCR CDR3 Strategy 3 library selections. CDR3α and CDR3β libraries were built on the MAGEa6a framework. For the subtractive panning, a pre-selection step against HEP2 cells and HDMEC3 cells (in Pan 1 only) was included in each of three cycles of panning against biotinylated HLA-A*0101-$MAGE_{(168\text{-}176)}$ antigen. In parallel, three cycles of panning against biotinylated HLA-A*0101-$MAGE_{(168\text{-}176)}$ antigen was also performed.

5.10.3 Phage inhibition ELISA

ELISA positive clones were obtained from each of the four libraries. Sequencing of library 1 and 2 (CDR3α), however, showed complete enrichment for a non-designed clone MAGEa6ab2a (data not shown). Sequencing of library 3 and 4 (CDR3β) also showed enrichment for clone MAGEa6ab2a but at a lower frequency (~50% of total sequences) (Table 5.13). Significant convergence was observed for both the subtractive and normal panning outputs. M^{97} N^{98} was frequently substituted for Gln-Val in the subtractive (~67% of sequenced clones) and normal panning (50%) outputs. Furthermore, a Q-V-S/G motif at positions 97-99 was observed in both outputs (~60% subtractive and ~70% normal). The QV and QVS/G mutations derived from up to three overlapping 6-NNK primers illustrated the importance of these changes to the fitness of the phage-TCR clone. Positions surrounding this motif were more permissive. The QV motif was also identified using 5-NNK oligonucleotides in both Strategy 1 and 2 further highlighting the value of these substitutions to the selection of this clone. Clone MAGEb18 (Table 5.13 B) was also isolated from Strategy 2 libraries using 5-NNK primers (Table 5.10). Selection of this clone from both the 5-NNK and 6-NNK libraries (irrespective of the TCR format) reflects the influence of these mutations on expression and affinity.

A.

Clone Number	CDR3β$_{(S94\text{-}Y102)}$	Freq.	% Inhib. @ 100 nM
wt	SPNMADEQY	-	-
MAGEa6ab2a	SPNMADEQY	14	74
MAGEb62	**AAG*Q*VS**EQY	1	77
MAGEb63	**ARYQVS**EQY	1	80
MAGEb64	**GEMLVT**EQY	1	71
MAGEb65	S**RYEVGR**QY	1	87
MAGEb66	S**VGQVTG**QY	1	79
MAGEb67	S**VF*Q*VS**EQY	1	88
MAGEb68	S**MTQVGR**QY	1	83
MAGEb69	S**VG*Q*VSR**QY	1	86
MAGEb70	S**RD*Q*VSQ**QY	1	53
MAGEb71	S**WG*Q*VSR**QY	1	83
MAGEb72	S**KD*Q*VGR**QY	1	80
MAGEb73	S**RA*Q*VGR**QY	1	86
MAGEb74	S**KE*Q*VS**EQY	1	88
MAGEb75	SPN***Q*VGWSQ**	1	95
MAGEb76	SPN***Q*VGLSH**	1	86
MAGEb77	SPN**LASGID**	1	66
MAGEb78	SPN**QVGRA*Q***	1	83
MAGEb79	SPN**LA**D**GVT**	1	24

B.

Clone Number	CDR3β$_{(S94\text{-}Y102)}$	Freq.	% Inhib. @ 100 nM
wt	SPNMADEQY	-	-
MAGEa6ab2a	SPNMADEQY	18	74
MAGEb80	**ARF*Q*VS**EQY	1	87
MAGEb81	**GI**N**E**A**S**EQY	1	68
MAGEb82	S**RE*Q*VSS**QY	1	74
MAGEb83	S**KE*Q*VGR**QY	1	83
MAGEb84	S**Y**N**L**A**SG**QY	1	69
MAGEb18	S**EWQVS**EQY	1	83
MAGEb85	S**QDQVGR**QY	1	83
MAGEb86	S**KF*Q*V**D**QQY	1	81
MAGEb87	S**YGQVGR**QY	1	84
MAGEb88	S**EH*Q*VSR**QY	1	91
MAGEb89	S**QG*Q*V**D**R**QY	1	85
MAGEb90	SPN***Q*VGLSV**	1	67
MAGEb91	SPN**QVGLAQ**	1	84
MAGEb92	SPN***Q*VGLSV**	1	78

Table 5.13. MAGE-A3 TCR Strategy 3 output clones obtained after three cycles of panning. A phage inhibition ELISA was performed at 100 nM non-biotinylated HLA-A*0101-MAGE$_{(168\text{-}176)}$ antigen. Thirty-two clones showing the highest % inhibition were sequenced from each library. **(A).** Library 3: subtractive panning; 44% non-designed PCR splice clone MAGEa6ab2a. **(B).** Library 4: normal panning; 56% non-designed PCR splice clone MAGEa6ab2a. Library 1 and library 2 were contaminated with the non-designed PCR splice clone MAGEa6ab2a; no CDR3α mutants were identified. Amino acids that differ from wild-type are highlighted in bold and red. *Q*, amber codon. wt, wild-type.

5.10.4 Deep sequencing of library 3 and library 4 Pan 3 outputs

Sequencing of 32 ELISA positive clones from the subtractive and normal panning Pan 3 outputs (Table 5.13) failed to uncover any significant differences between the selection strategies. Through deep sequencing a considerably larger pool of clones, it was hoped to identify variants unique to the subtractive panning output. In total, ~140,000 CDR3β sequences from the subtractive panning (library 3) and ~170,000 sequences from the normal panning (library 4) were obtained.

The frequency of each clone was converted into a % of the total number of sequences (Figure 5.7). There were three groups of clones: those isolated exclusively in the subtractive panning output (x-axis, blue triangles), those isolated exclusively in the normal panning output (y-axis, green triangles) and those isolated in both outputs (red dots). Representing the Pan 3 outputs in this way helped guide the choice of mutants to further characterise. An example of the mutants identified solely in the subtractive panning output are listed in Figure 5.7. A single outlier sequence is also depicted which represents the non-designed clone MAGEa6ab2a.

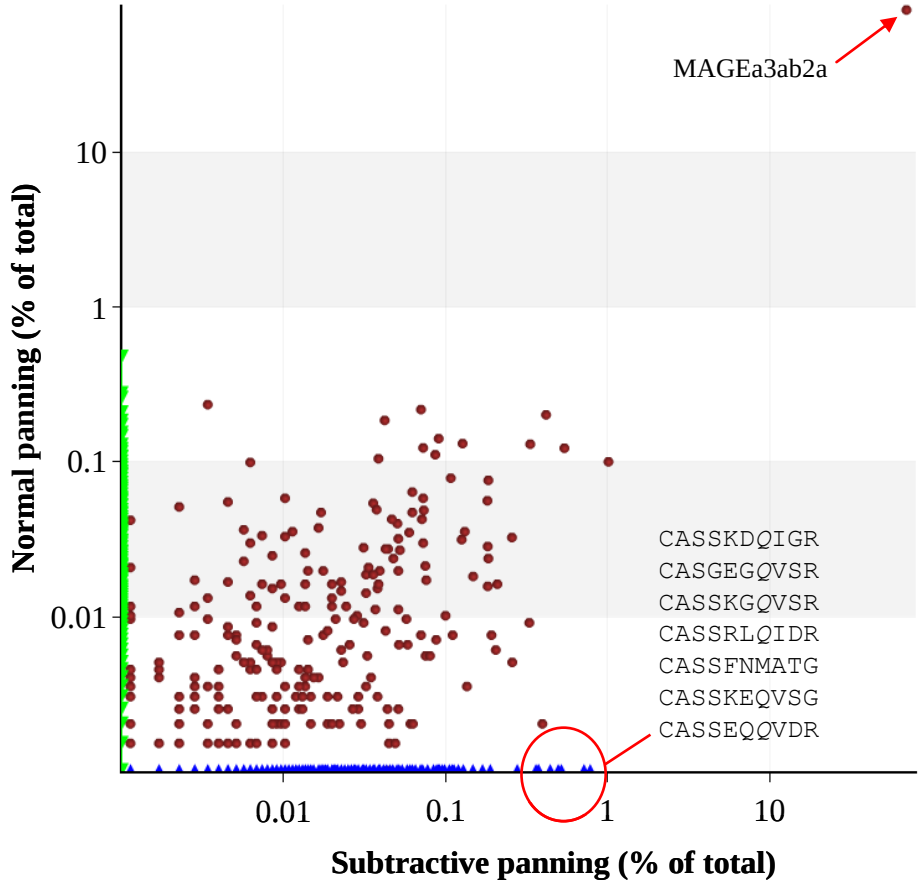

Figure 5.7. MAGE-A3 TCR Strategy 3 deep sequencing comparison of the Pan 3 outputs of library 3 (subtractive panning) and library 4 (normal panning). 10 μg of DNA was isolated from *E. coli* TG1 glycerol stocks of the Pan 3 outputs of library 3 (subtractive) and library 4 (normal). Sequencing of the pan 3 outputs of library 3 and library 4 on the Illumina GAII System generated 142,881 and 174,324 sequences respectively. The frequency of each sequence has been converted into a % of the total number of sequences. The sequences along the x-axis (blue triangles) represent mutants identified exclusively in the subtractive panning output. The sequences along the y-axis (green triangles) represent mutants identified exclusively in the normal panning output. Those sequences along the diagonal (red dots) represent mutants identified in both pan 3 library outputs. Of the clones circled along the x-axis three were characterised further by BIAcore. The clone indicated with an arrow is MAGEa6ab2a (non-designed PCR splice product). Data kindly provided by Adaptive Biotechnologies (Seattle, USA).

5.10.5 Kinetic analysis of Strategy 3 TCRs

A comprehensive number of CDR3β mutants identified by phage ELISA and a select group of CDR3β mutants identified from deep sequencing were refolded and analysed by SPR on a BIAcore3000 as described in Section 2.7 of Materials and Methods (Table 5.14). Eleven CDR3β segments isolated from the subtractive panning were refolded with MAGEa6a and yielded improvements of up to ~10,000-fold over MAGEa6a and ~370,000-fold over the wild-type TCR (Table 5.14 A). Seven CDR3β segments isolated from the normal panning were refolded with MAGEa6a and yielded improvements of up to ~13,500-fold over MAGEa6a and ~510,000-fold over the wild-type TCR (Table 5.14 B). The range of affinity was comparable between the two selection approaches; K_D of 0.663-29.4 nM for clones from the subtractive panning and K_D of 0.486-39.5 nM for clones from the normal panning.

In an attempt to generate the highest affinity MAGE-A3 TCR (including a CDR3β segment), MAGEb18 and MAGEb79 were refolded with the highest affinity α chain segment MAGEa26 (a combination of MAGEa6 and MAGEa18). In addition, the most abundant CDR3β clones identified from deep sequencing of the subtractive panning output were also refolded with MAGEa26. Whilst combining MAGEb18 and MAGEa26 was favourable in terms of a half-life gain (5-fold increase), recruiting MAGEb79 was not. A lack of cooperativity between the MAGEb79 and MAGEa26 resulted in a ~13-fold decrease in half-life. Combining MAGEb93, MAGEb96 and MAGEb97 with MAGEa26 yielded increases in affinity over the wild-type TCR of ~110,000-fold, ~177,000-fold and ~59,000-fold respectively.

A.

Clone ID	CDR3β	K_{on} (M^{-1} s^{-1})	K_{off} (s^{-1})	K_D (nM)	$T_{1/2}$ (min)	K_D (parent) / K_D (mutant)	K_D (MAGEa6a) / K_D (mutant)
MAGEawtbwt	SPNMADEQY	nd	nd	248000	nd	1	-
MAGEa6abwt	SPNMADEQY	nd	nd	6550	nd	37.9	1
MAGEb62	**AAGQVS**EQY	3.08×10^{5}	2.35×10^{-3}	7.63	4.9	33972.6	897.3
MAGEb63	**ARYQVS**EQY	2.35×10^{5}	8.1×10^{-4}	3.45	14.3	71884.1	1927.5
MAGEb64	**GEMLVT**EQY	2.86×10^{5}	2.2×10^{-3}	7.7	5.3	32207.8	850.6
MAGEb65	S**RYEVGR**QY	9.18×10^{5}	3.55×10^{-3}	3.9	3.3	63589.7	1679.5
MAGEb66	S**VGQVTG**QY	2.97×10^{5}	1.16×10^{-3}	3.9	10	63589.7	1679.5
MAGEb67	S**VFQVS**EQY	3.58×10^{5}	2.37×10^{-3}	6.62	4.9	37462.2	989.4
MAGEb68	S**MTQVGR**QY	3.27×10^{5}	1.47×10^{-3}	4.5	7.9	55111.1	1455.6
MAGEb71	S**WGQVSR**QY	1.15×10^{5}	7.61×10^{-4}	0.663	15.2	374057.3	9879.3
MAGEb73	SPN**QVGWSQ**	3.64×10^{5}	1.89×10^{-3}	5.19	6.1	47784.2	1262
MAGEb75	SPN**L**A**SGID**	1.53×10^{5}	4.49×10^{-3}	29.4	2.6	8435.4	222.8
MAGEb77	SPN**LA**D**GVT**	1.32×10^{5}	2.84×10^{-3}	21.6	4	11481.5	303.2

B.

Clone ID	CDR3β	K_{on} (M^{-1} s^{-1})	K_{off} (s^{-1})	K_D (nM)	$T_{1/2}$ (min)	K_D (parent) / K_D (mutant)	K_D (MAGEa6a) / K_D (mutant)
MAGEawtbwt	PNMADEQY	nd	nd	248000	nd	1	-
MAGEa6abwt	PNMADEQY	nd	nd	6550	nd	37.9	1
MAGEb78	**ARFQVS**EQ	3.43×10^{5}	1.06×10^{-3}	3.09	10.9	80258.9	2119.7
MAGEb79	**GI**N**E**A**S**EQ	1.88×10^{5}	9.15×10^{-5}	0.486	126	510288.1	13477.4
MAGEb82	**Y**N**L**A**SG**QY	3.01×10^{5}	3.92×10^{-3}	13	2.9	19076.9	503.8
MAGEb18	**EWQVS**EQY	2.3×10^{5}	4.79×10^{-4}	2.1	24	118095.2	3119
MAGEb85	**KFQV**D**Q**QY	2.52×10^{5}	1.3×10^{-3}	5.2	8.9	47692.3	1259.6
MAGEb88	**QGQV**D**R**QY	3.77×10^{5}	1.01×10^{-3}	2.7	11.4	91851.9	2425.9
MAGEb89	PN**QVGLSV**	1.7×10^{5}	6.72×10^{-3}	39.5	1.7	6278.5	165.8

C.

Clone ID	CDR2α	CDR3α	CDR3β	K_{on} (M^{-1} s^{-1})	K_{off} (s^{-1})	K_D (nM)	$T_{1/2}$ (min)	K_D (parent) / K_D (mutant)
MAGEawtbwt	LIQSS	SYQLT	PNMADEQY	nd	nd	248000	nd	1
MAGEa26b79	**YVRPY**	**PFFVV**	**GI**N**E**A**S**EQ	8.23 x 10^4	1.15 x 10^{-3}	14	10.1	17714.3
MAGEa26b18	**YVRPY**	**PFFVV**	**EWQVS**EQY	6.11 x 10^4	9.37 x 10^{-5}	1.5	122.4	161039
MAGEa26b93*	**YVRPY**	**PFFVV**	**F**NMA**TG**QY	8.87 x 10^4	3.77 x 10^{-4}	2.2	30.6	110714.3
MAGEa26b94*	**YVRPY**	**PFFVV**	**RLQI**D**R**QY	1 x 10^5	1.4 x 10^{-4}	1.4	81.6	177142.9
MAGEa26b95*	**YVRPY**	**PFFVV**	**KDQIGR**QY	7.6 x 10^4	3.18 x 10^{-4}	4.2	36.1	59047.6

Table 5.14. Binding affinities of MAGE-A3 TCR mutants isolated from Strategy 3 CDR3β libraries. (A). Library 3 (subtractive): MAGE-A3 TCR CDR3β mutant segments refolded in the context of MAGEa6a on which they were selected. **(B).** Library 4 (normal): MAGE-A3 TCR CDR3β mutant segments refolded in the context of MAGEa6a on which they were selected. **(C).** Most optimal α chain segments (MAGEa6/MAGEa18) combined with the most optimal CDR3β chain segments identified either by phage inhibition ELISA or through deep sequencing (*). *Q*, amber codon. wt, wild-type. K_D values were determined by SPR in a BIAcore using purified refolded TCR. nd, not determined. nb, no binding observed. (Data kindly provided by Dr. P. Todorov, Dr. A. Legg and Dr. A. Powlesland).

5.11 MAGE-A3 TCR clinical candidates

Mutated TCRs were reformatted as fusion molecules to an anti-CD3-scFv and tested in T-cell redirection assays. Five MAGE-A3 TCR clones (in addition to MAGEa6b9) (Table 5.15), selected through a combination of binding affinity and potency (initial T-cell redirection experiments), were taken forward for more detailed *in vitro* cellular testing. Mutated CDR segments identified from the first-generation libraries and from the three second-generation libraries are represented in at least one of the fusion molecules.

Clone Number	CDR1α	CDR2α	CDR3α	CDR1β	CDR2β	CDR3β
wt	DSAIYN	LIQSS	SYQLT	SGHRS	FSETQ	SPNMADE
MAGEa6b9	DSAIYN	**YVRPY**[a]	SYQLT	SGHRS	**TDFLL**[a]	SPNMADE
MAGEa26b7	DSAIYN	**YVRPY**[a]	**PFFVV**[bc]	SGHRS	**TDFLL**[a]	SPNMADE
MAGEa26b96	DSAIYN	**YVRPY**[a]	**PFFVV**[bc]	SGHRS	FS**FLL**[a]	SPNMADE
MAGEa26b97	DSAIYN	**YVRPY**[a]	**PFFVV**[bc]	SGHRS	**TDF**TQ[a]	SPNMADE
MAGEa26b93	DSAIYN	**YVRPY**[a]	**PFFVV**[bc]	SGHRS	FSETQ	S**F**NMA**TG**[d]
MAGEa26b79	DSAIYN	**YVRPY**[a]	**PFFVV**[bc]	SGHRS	FSETQ	**GI**N**E**A**S**E[d]

Table 5.15. List of potential MAGE-A3 TCR clinical candidates. [a]Segments isolated from first-generation libraries; [b]Segments isolated from Strategy 1 libraries; [c]Segments isolated from Strategy 2 libraries; [d]Segments isolated from Strategy 3 libraries.

DISCUSSION

6.1 TCRs, a suitable protein scaffold?

A protein scaffold is a polypeptide fold comprising surface exposed loops that form a sizeable target binding interface that is permissive to sequence variation within a geometrically constrained structure (Skerra 2000). Scaffold proteins can be divided into two distinct groups: (1) scaffolds with α-helical frameworks and (2) scaffolds with β-sheet frameworks (Hosse, Rothe et al. 2006). Whilst numerous examples of α-helical secondary structural scaffolds are reported in the literature, including affibodies and ankyrin domain repeats reviewed in (Hosse, Rothe et al. 2006; Nuttall and Walsh 2008; Gebauer and Skerra 2009), the β-sheet framework is the most prevalent scaffold used for library construction. Since the magic bullet theory was proposed over a century ago (Ehrlich 1906), antibodies have been the paradigm of binding proteins with desired specificities. Antibodies, for the most part, fulfil the criteria required for a suitable molecular scaffold; most significantly they possess an inherently prescribed binding function. The constant (C) and variable (V) domains are barrel-shaped structures consisting of two antiparallel β-sheets packed tightly against each other. In the C domains, each sheet consists of 4-strands and 3-strands respectively. The V domains consist of a total of 9 strands of 4 and 5-strands respectively. The characteristic β-sheet secondary structure is known as the Ig fold (Janeway, Travers et al. 2001). Six hypervariable loops (CDRs), one set of three loops from each variable domain of light and heavy chain, supported by the β-barrel structure, come together in close spatial proximity, to form an extended contiguous combining site. The ability of antibodies to recognise a nearly infinite array of antigenic determinants is due to their capacity to tolerate huge sequence heterogeneity within the antigen-binding loops, most notably within the third CDR. The well conserved structurally stable β-sheet Ig fold that supports the CDR loops provides an

ideal scaffold on which to introduce sequence variation for the purpose of affinity engineering or reshaping target specificity.

The other receptor arm of the adaptive immune response is the T-cell receptor. The overall structure of the TCR is remarkably similar to the Fab fragment. Three of the four domains comprise β-sheet secondary structure, typical to the Ig fold organisation; the Cα domain, however, forms a non-classical Ig fold due to the loss of a top β-sheet. Akin to the antigen-binding loops of antibodies, the CDR loops of TCR molecules can also accommodate significant sequence diversity. Since TCRs and antibodies share structurally similar architecture, related to a common antigen-binding function, there is a good rationale for applying the same engineering methodologies employed successfully to antibodies. However, the production of soluble TCRs has proven challenging. In contrast to antibodies, TCRs are not naturally expressed as soluble proteins and the ectodomains are highly unstable in the absence of the natural inter-chain disulphide bond. Several strategies have been explored to stabilise the α and β chains including single-chain TCRs (Chung, Wucherpfennig et al. 1994; Schodin, Schlueter et al. 1996) or fusions to the fos/jun leucine zipper domains (Willcox, Gao et al. 1999). More recently, a TCR format has been designed in which a non-native cysteine pair is introduced at the interface between the TCR constant domains (Boulter, Glick et al. 2003) and has proven a generic method for producing extremely stable TCRs in high yields.

6.2 Technical parameters affecting TCR phage display

Phage display is a powerful tool for isolating proteins with desirable target binding characteristics from libraries with diversities of millions or billions of variants. Although phage display follows a well-established method (Smith 1985), there

remains scope within the system for extensive fine tuning in order to tailor the parameters towards different binding partners. The process is defined by four principal steps: first, generating molecular diversity; second, applying a selective pressure; third, amplifying the enriched phage population; fourth, analysis of the selective output.

6.2.1 Library quality

The simplest method to introduce random mutations is to use an NNN oligonucleotide primer that encodes an equal mixture of the four nucleotides at each position of the codon. This strategy, however, suffers from a biased representation of certain amino acids since out of the 64 possible codon combinations, Leu, Arg or Ser use 18 and one each for Trp or Met. In addition, the 3 nonsense (stop) codons will result in chain termination in ~5% of sequences. These issues are to a large extent alleviated by using two degenerative mixes of nucleotides N, at codon position one and two and K at position three (where N represents a 25% mix each of A, C, G or T and K represents a 50% mix each of G or T). The benefit to library quality by using NNK oligonucleotides is two-fold: first, it reduces the number of codons from 64 to 32 (whilst still encoding all 20 amino acids) giving each amino acid a more even chance to incorporate into the library; second, it eliminates 2 of 3 stop codons thus reducing the amount of truncated protein within the library; the remaining stop codon TAG is translated as Gln in suppressor strains of *E. coli*. However, this approach still causes an uneven distribution of amino acids in the constructed library. Whilst this type of oligonucleotide directed mutagenesis was sufficient to isolate high affinity binders described for the Mel-5, gp100 and MAGE-A3 TCRs (Chapters 1, 2 and 3 respectively), the most efficient method of incorporating an equal distribution of mutations is to use trinucleotide phosphoramidites (Virnekas, Ge et al. 1994;

Knappik, Ge et al. 2000). Trinucleotide building-blocks allow greater control over sequence variation so that stop codons, frame-shift mutations and codon bias are all eliminated. However, in the case of TCRs, removal of amber codons from the library pool may in fact be deleterious to the isolation of tighter binding clones, since their enrichment in several libraries suggests an inherent toxicity of the TCR molecule to *E.coli*. The advent of presynthesised trinucleotide triplets provides a means to augment library quality by minimising codon redundancy and eliminating codon bias. However, in the absence of the appropriate experiments it is not certain what additional benefit this would confer on the engineering of the TCRs described here.

The chief objective in constructing a phage display library is to maximise diversity whilst minimising background parental template contamination. Several procedures were modified during the engineering of the three TCRs so that the lessons learnt from the Mel-5 TCR affinity maturation (Chapter 3) were implemented during the gp100 (Chapter 4) and MAGE-A3 (Chapter 5) TCR library builds. For example, in addition to *Dpn*I treating the initial PCR products to reduce the amount of bacterially propagated plasmid DNA, the DNA template was linearised with either *Nco*I or *Not*I restriction endonuclease. This step was designed to prevent PCR extension beyond either the *Nco*I or *Not*I restriction site that would result in synthesis of the SOE-PCR flanking primer sites YOL13 or YOL22 respectively. In effect, the parental DNA template would be synthesised including both YOL13 and YOL22 stitching primer sites available to act as template during the SOE-PCR reaction. In spite of these modifications, parental TCR was enriched during the second-generation affinity maturation of the gp100 TCR (Chapter 4; Table 4.2) and thus the benefit to the library integrity is unclear. Moreover, it illustrates the challenge of isolating high affinity TCRs from an already improved affinity framework.

Furthermore, a number of additional steps were implemented to standardise and thus simplify the process of library construction. The number of fragments spliced together by SOE-PCR was reduced from 3 to 2 in both the gp100 and MAGE-A3 TCR library builds to increase the efficiency of amplification. Moreover, the strategy of assembling and digesting the PCR fragments was redesigned for the gp100 and MAGE-A3 TCRs. The SOE-PCRs were performed using the same flanking primers (YOL13 and YOL22) to permit digestion of the PCR products with the same restriction endonucleases (*Nco*I and *Not*I) irrespective of CDR or TCR identity. Additionally, a quality control check point was introduced by sequencing the SOE-PCR products before restriction digests were performed (as exemplified in Chapter 4; Figure 4.5). Hence, DNA of poor quality could be resynthesised rather than blindly proceeding with restriction digests, ligations and transformations.

Background binding between target and display system is inherent to all molecular display strategies and can lead to a propensity of false-positives and confusing outputs. In the phage panning experiments described in Chapter 2; Section 2.5, the helper phage M13K07 was used to rescue the phagemid pEX922 encoding heterodimeric TCR molecules. In this system, phage-TCR:pHLA complexes were eluted from the streptavidin-coated magnetic beads under alkaline conditions using triethylamine (TEA). Bearing in mind that the majority of phage particles express only wild-type pIII proteins derived from the helper phage, indiscriminate elution (with TEA) of both wild-type and recombinant pIII proteins contributes to the background binding of bald phage that do not express recombinant fusions. Whilst the engineering of the TCRs in this work did not appear to suffer from this phenomenon, consideration must be given to alternative strategies with the potential to improve the system. One approach is to use a protease-cleavable helper phage (called KM13) that

has a trypsin cleavage sequence introduced between the D2 and D3 domains of the pIII protein in conjunction with an engineered phagemid that has a trypsin cleavage site interposed between the gene of interest and gIII (Kristensen and Winter 1998). Wild-type pIII proteins derived from the helper phage KM13 are susceptible to protease cleavage rendering phage that do not express a recombinant fusion protein non-infective since all three domains of the pIII protein (D1, D2 and D3) are required for infection. Therefore, the role of trypsin protease is two-fold: first, it elutes phage by cleaving the trypsin site between the protein of interest and the pIII protein and, second, it reduces the background infectivity of trypsin-sensitive KM13 helper phage (Lee, Iorno et al. 2007; Schofield, Pope et al. 2007; Pansri, Jaruseranee et al. 2009).

6.2.2 Size of library

The affinity of antibodies isolated from naïve libraries generally correlates to the size of the library. Whilst a small phage library with 3×10^7 clones built by the group of Greg Winter yielded antibodies with affinities of 10^{6-7} M^{-1} (Marks, Hoogenboom et al. 1991; Griffiths, Malmqvist et al. 1993), Vaughan et al. (Vaughan, Williams et al. 1996) isolated antibodies with affinities of 10^{8-10} M^{-1} from a very large library of 10^{10} members. In terms of lead optimisation, however, constructing libraries of this size may not be imperative to a successful outcome. Naïve antibody libraries comprise multiple chains from the natural repertoire of which a significant proportion will be redundant or incompatible. By comparison, manipulating the sequence of a well characterised single TCR α and β chain framework, as in affinity maturation, leads to more frequent productive combinations thus negating the demand for very large libraries. It is notable that although the Mel-5 TCR libraries (Chapter 3; Section 3.2.4) were 10-fold smaller than the gp100 (Chapter 4; Section 4.3.4) and MAGE-A3

(Chapter 5; Section 5.2.2) TCR libraries, clones with comparable affinities (in the low nanomolar range) were isolated. Strikingly, from a small yeast display TCR CDR3α library (10^5 mutants) built using a single 5-NNS degenerative oligonucleotide, clones with up to a 100-fold improvement in affinity over the parent molecule were obtained (Holler, Holman et al. 2000). In affinity maturation, the library size required to ensure coverage of the potential mutated sequence space is dictated by the number of consecutive amino acids mutated. Typically, the CDR3 is randomised using five overlapping 5-NNK degenerative oligonucleotides. The theoretical diversity of such a library is 1.7 x 10^8 (32^5 x 5) and a library size of 10^9 should be sufficient to represent the library. Wu et al. (Wu, Beuerlein et al. 1998) used a more reductionist approach to isolate high affinity binders. By separately introducing all 20 amino acids at each position across all CDRs a far smaller library was required. This strategy identified mutations from a library of only 2,592 sequences that individually conferred up to a 13-fold gain in affinity. Whilst small libraries can yield affinity-enhancing mutations, a limitation of this method, however, is the potential lack of cooperativity between mutations that have been isolated individually. This is overcome by mutating multiple consecutive residues within the same molecule (a strategy used for engineering the TCRs in this thesis) and allowing the process of Darwinian selection to identify molecules with the most optimised combination of residues.

6.2.3 Display levels

The low affinity interaction of TCR and pHLA prevents the detection of wild-type TCR on the surface of phage using a pHLA binding ELISA since a positive readout is limited to interactions with affinity values of <1 μM. Despite efforts to monitor TCR display by Western blot using a pIII-specific antibody (data not shown); these

analyses remain unreliable and inconclusive. As a consequence, engineering studies are often initiated in the absence of confirmed display.

Bothmann and Pluckthun (Bothmann and Pluckthun 1998) demonstrated that the *E. coli* periplasmic chaperone Skp improved the amount of correctly folded scFv protein (most notably aggregation prone and toxic fragments) on the phage surface. Encouraged by their finding together with supporting results from our lab that demonstrated an increased level of surface display (data not shown), the gene encoding for Skp was coexpressed on the same phagemid as the TCR. Having observed no significant effect on the productive phage surface display of a murine scTCR through coexpression of Skp, Loset et al. (Loset, Lunde et al. 2007) turned their attention to the role played by a second *E. coli* periplasmic factor, FkpA (Bothmann and Pluckthun 2000) in the display of TCRs. In the absence of specific soluble pMHC antigen, Loset et al. (Loset, Lunde et al. 2007) used a panel of anti-TCR mAbs, predominantly β-chain specific to detect TCR surface expression. Whilst coexpression of FkpA on the same phagemid as the αβ-dsTCR (analogous to the mTCR format) increased mAb reactivity, intact αβ TCR assembly was ambiguous since the antibodies were directed towards the β chain only. Although these results do not provide irrevocable evidence for a role played by FkpA in improving periplasmic folding of αβ TCR heterodimers, the clear benefit to the expression of scTCRs advocates further evaluation in our system with access to specific pHLA ligands.

The TCR format, whether native or engineered (mTCR), had little effect on the MAGE-A3 TCR selective output (Chapter 5; Section 5.9). However, a direct comparison between the two formats is not possible since the phagemid pG484 (encoding the wild-type MAGE-A3 TCR in the native format) contained a valine to alanine substitution in the geneIII leader sequence (Chapter 5; Figure 5.1) that was

corrected in phagemid pLAS0282 (encoding the wild-type MAGE-A3 TCR in the mTCR format). Western blot and phage ELISA analysis of the display of the MAGE-A3 TCR clone MAGEawtb1 (Chapter 5; Table 5.3) in the native versus the mTCR format with and without the geneIII mutation, demonstrates a clear hierarchy of expression levels (data not shown). The native TCR format in combination with a wild-type geneIII leader sequence supports the highest level of display whereas, the mTCR format in conjunction with a mutated gIII leader sequence supports the lowest. Inclusion of a mutated geneIII leader sequence in partnership with the native TCR format (Chapter 5; Section 5.8; Strategy 1) reduces the expression level in line with that observed for the wild-type geneIII leader sequence and mTCR format (Chapter 5; Section 5.9; Strategy 2). In effect, the wild-type geneIII leader sequence compensates for the reduced TCR display level conferred by the mTCR format. For the engineering of the libraries described in Section 5.9, it would have been more instructive to have retained the alanine geneIII leader sequence mutation. What effect would reducing the level of display have on the selective output? Conversely, what effect would increasing the level of display through correcting the geneIII leader mutation have on the selective output in either the first-generation libraries (Chapter 5; Section 5.2) or Strategy 1 libraries (Chapter 5; Section 5.8)? The introduction of the non-designed geneIII leader sequence mutation may have been fortuitous, since high levels of TCR expression are not well tolerated in *E. coli* which may well have been detrimental to the selective output.

6.2.4 Quality of the pHLA antigen

The outcome of a TCR affinity engineering project is largely, but not exclusively influenced by the efficiency of the wild-type TCR refold and the quality and stability of the pHLA complex. Whilst optimisation of TCR refolding represents a significant

obstacle, modification of the pHLA molecule to enhance stability is often a more fruitful exercise. It is well acknowledged that mutations in the peptide sequence at so-called anchor positions can stabilise the complex by fastening the peptide into the HLA binding groove (Hunt, Henderson et al. 1992; Parker, Bednarek et al. 1992; Parkhurst, Salgaller et al. 1996; Valmori, Fonteneau et al. 1998). For the affinity maturation of the Mel-5 (Chapter 3) and gp100 (Chapter 4) TCRs, a heteroclitic peptide variant was used, whereas for the MAGE-A3 (Chapter 5) TCR engineering, the wild-type peptide was employed because it folded with high efficiency into a stable molecule. Indeed, a first attempt at isolating high affinity gp100 TCR mutants failed in selections performed with the wild-type peptide (data not shown). The preferred peptide binding motif for HLA-A*0201 is xLxxxxxxV/L and for HLA-A*0101 is xxD/G xxxxxY. Whilst the wild-type MAGE-A3$_{(168-176)}$ peptide satisfies both the preferred anchor residues at P3 and P9 (EVDPIGHLY), the wild-type Melan-A/MART-1$_{(26-35)}$ and gp100$_{(280-288)}$ peptides do not (at P2 and PC); only containing one of the two preferred residues (EAAGIGILTV and YLEPGPVTA respectively). Accordingly, heteroclitic variants of both the Melan-A/MART-1$_{(26-35)}$ and gp100$_{(280-288)}$ peptides were designed; ELAGIGILTV and YLEPGPVTV respectively. It is important that modification of the peptide to improve binding to the HLA molecule is not deleterious to recognition by the TCR. It is noteworthy that the wild-type and improved affinity gp100 TCRs bind to the wild-type and heteroclitic variant peptides with comparable affinity (Chapter 4; Table 4.1).

6.2.5 Library selection - specificity

Having established the off-target activity of the highest affinity MAGE-A3 TCR clone (MAGEa6b9) against human primary cells (HEP2 and HDMEC3) (Chapter 5; Figure 5.3), three protein engineering strategies were designed to identify novel

mutations harnessed with adequate potency yet devoid of the cross-reactivity profile attributed to MAGEa6b9. It was hypothesised that the binding specificity could be augmented by preselecting the CDR3 libraries against an undesired target. In the third strategy (Chapter 5; Section 5.10) each cycle of panning started with a depletion (or subtractive) step in which the phage was incubated with 2 x 10^6 human primary cells (HEP2 or HDMEC3). Whilst the cell surface antigenic component responsible for MAGEa6b9 binding was unknown, the HEP2 and HDMEC3 cells provided a suitable target (Chapter 5; Figure 5.3). The effectiveness of this type of strategy hinges on a number of factors. Consideration must be given to the level and accessibility of antigen expressed at the cell surface, since the density of antigen may well be lower than the K_D of any of the off-target binders in the library. Moreover, the antigen may be inaccessible to interaction due to steric hindrance caused by the presence of other cell surface molecules. The impact of the subtractive panning procedure on the CDR3β library output was scrutinised through deep sequencing of ~150,000 sequences from each selection method (Chapter 5; Section 5.10.3). The consequence of the modifications in the panning procedure is shown in Figure 5.7 which highlights a group of mutants in the subtractive output divergent from those selected through the normal panning method. Whilst this data does not provide unequivocal evidence for the success of this approach, it does at least provide a plethora of novel mutants for biophysical and cellular characterisation.

6.2.6 Why do some CDRs not yield high affinity? Second-generation libraries

Antibodies selected from natural repertoire libraries have already been through a process of affinity optimisation (somatic hypermutation) akin to the first round of *in vitro* affinity engineering described here for TCRs. The isolated antibody fragments

that act as scaffolds for *in vitro* affinity maturation are therefore of high affinity and require only moderate fine tuning to satisfy clinical development criteria. By comparison, the natural affinity of TCRs is much lower than for antibodies and therefore substantial improvement in affinity is required to bring TCRs into a similar affinity window from which antibodies enter the process of lead optimisation.

Isolation of mutations in more than one CDR generally requires the construction of second-generation libraries, in which an enhanced-affinity first-generation mutant is used as template for further CDR mutagenesis. Of the three TCRs described here and the three TCRs engineered previously in our group (Li, Moysey et al. 2005; Purbhoo, Li et al. 2007), only two yielded mutations in more than one CDR from first-generation libraries. Whilst the reasons for this are not fully understood there are several possible explanations.

One reasoning is that whilst not all CDR loops are conducive to accommodating mutations in the context of the wild-type structure, conformational adjustment of the loops that result from the mutation of a single CDR, repositions the loops so that new pHLA contacts are made. These novel contacts at the TCR-pHLA interface are now accessible to modification through site directed mutagenesis that were not available in the wild-type structure. The structure of the high affinity A6c134 TCR supports this hypothesis, which shows that mutations in the CDR3β loop increase the number of contacts between the α chain and the Tax peptide (D. K. Cole, manuscript in preparation). It is conceivable that α chain libraries built on a high affinity β chain framework would yield mutations in the α chain that were not identified in the context of the wild-type TCR (Li, Moysey et al. 2005).

A second explanation is that high affinity binders are not present in the starting library population. However, based on the deep sequencing analysis of one of the Pan

0 (preselected) MAGE-A3 TCR libraries (data not shown) which shows a wide distribution and high diversity of mutations, this is unlikely. A more plausible explanation is that a selective loss of low affinity binders occurs during the selection process (de Bruin, Spelt et al. 1999). The binding kinetics of the selective output of the MAGE-A3 TCR Strategy 1 libraries endorses this notion (Chapter 5; Table 5.7). Enrichment for consensus sequences in the context of an affinity enhanced clone was observed (Chapter 5; Table 5.6). Whilst the mutated CDR segments conferred considerable improvements in affinity over the wild-type TCR of between 7 and 145-fold (K_D of 35-1.7 μM; Chapter 5; Table 5.7) (excluding clone MAGEa22 with a K_D of 230 nM), affinities in this range are not permissive to TCR capture during a solution-based selection approach and justifies the absence of such phages in the output described in Chapter 5; Section 5.3. It is noteworthy that the cut-off for detection of specific binding of TCR with cognate pHLA in a phage ELISA assay is approximately 1 μM (data not shown) and therefore it is likely that the selection of TCR mutants during the panning process is limited by this affinity value, i.e. there is a diminished probability of capturing TCRs with K_D values >1 μM. Without a surgical examination of each mutated CDR segment it is not possible to assess whether the affinity of mutations obtained from second-generation selections, as a general rule, fall below this detection threshold. It would be intriguing, for example, to determine the affinity of the Mel-5 TCR CDR1α segment (as described in Chapter 3) that in combination with clone MELa1 (K_D value of 6.4 nM) contributes to an affinity of 3.2 nM attributed to clone MELa16 (Table 3.7). Likewise, it would be compelling to calculate the affinity of the gp100 TCR CDR3β segment (discussed in Chapter 4) that, when refolded in the context of clone GPb7 (K_D value of 44.6 nM), affords an affinity of 4.11 nM measured for clone GPb8 (Table 4.3). If, indeed, these biophysical

determinations indicated affinities unfavourable to capture from the first-generation libraries, the question is, what modifications could be implemented to the panning strategy to permit complete mining of the sequence space? Moreover, how can these low affinity binders be retained in the selective output? One possible solution would be to use an alternative helper phage to rescue the phage TCR libraries. The traditional helper phage, M13K07 (as used here), supplies all the necessary proteins required for phage assembly; in addition, it also provides a source of pIII protein. Since the phagemid also supplies pIII (as a recombinant fusion protein), a competition for incorporation into the assembling phage particle is set up between the wild-type pIII (helper phage) and recombinant pIII (phagemid). Because the wild-type pIII is incorporated more efficiently than the recombinant pIII, less than 10% of phages have a single fusion protein displayed on the phage surface with the overwhelming majority displaying only wild-type pIII. Whilst monovalent display is conducive to the isolation of high affinity binders, low affinity binders may slip through the net. To increase the display level of recombinant pIII fusions on the phage surface, Rondot et al. (Rondot, Koch et al. 2001) produced a modified helper phage, called Hyperphage, that has a partial deletion of the pIII gene so that the only supply of pIII protein is from the phagemid. The resulting phages have up to five copies of pIII carrying a fusion protein. The effect on the selection process is two-fold: first, it reduces the background of phage displaying only pIII from the helper phage; second, and more importantly, it increases the avidity effect that may lead to the capture of lower affinity binders.

It is curious that certain CDRs are resistant to affinity engineering, despite being selected in the context of an enhanced-affinity first-generation mutant. For example, three CDRs were targeted for the gp100 TCR (Chapter 4; Section 4.4), namely

CDR2α, CDR3α and CDR3β (built on GPb7; a CDR2β mutant) yet high affinity clones were recovered from only the CDR3α and CDR3β libraries. An inspection of the crystal structure of the TCR-pHLA complex may offer a possible explanation for this. Recent findings from our lab (Dr. A. Knox; unpublished observations) have demonstrated the importance of structural information to the rational design of phage display libraries. The cocrystal structure showed that two of the CDRs were spatially too distant from the pHLA surface to mediate contact. Guided by this information, two and three randomised NNK amino acid residues were inserted into the relevant CDR loops and subjected to several cycles of phage display panning. Remarkably, creating novel contacts through bridging the gap between the TCR and pHLA molecule, conferred substantial gains in affinity.

6.3 Phage output - Binding affinity

Protein-protein interactions are fundamental to most biological processes (Pawson and Nash 2000) and as consequence there is much interest in unravelling the molecular mechanisms underlying these interactions with the aim to exploit this knowledge to affinity engineer a number of these molecules for targeting purposes. T-cells express on their surface the αβ TCR which recognises antigen in association with MHC molecules. Differences in the CDR regions of the TCR domains, specifically variation in length and amino acid composition, account for the diversity of peptide specificity demonstrated by T-cells. Tumour associated antigens (TAAs), which are not expressed on normal tissue or expressed at a low level in a few tissues, constitute suitable targets for therapeutic agents. Peptides derived from TAAs, so-called tumour associated peptide antigens (TAPAs), are presented on the surface of tumour cells in the context of MHC class I complexes. Optimal binding of soluble

TCR therapeutics to extremely low numbers of pMHC, typically 1-100 pMHC complexes per target cell (Purbhoo, Irvine et al. 2004), requires engineering to overcome the inherently low affinity TCR-pMHC interaction (K_D = 0.1-500 μM) (Cole, Pumphrey et al. 2007; Aleksic, Liddy et al. 2012). The ability to generate very high affinity TCRs is essential for their use as soluble therapeutics as, naturally, their affinities are too low to be useful when applied as monovalent targeting agents.

In the work described in this thesis, site-directed mutagenesis has proven to be a successful strategy for targeting each of the six CDRs for engineering ultra-high affinity TCRs. The aim of this study was to generate high affinity TCRs that recognise the melanoma-specific epitopes, including peptides derived from Melan-A/MART-1_{26-35} (Chapter 3), $gp100_{280-288}$ (Chapter 4) and MAGE-$A3_{168-176}$ (Chapter 5). The TCRs specific for these epitopes were designated Mel-5, gp100 and MAGE-A3 respectively and as wild-type molecules demonstrated binding affinities (K_D values) for their cognate pHLA antigens of 18 μM, 26 μM and 248 μM respectively (Aleksic, Liddy et al. 2012; Liddy, Bossi et al. 2012).

Using an *in vitro* directed evolution strategy and phage display, TCRs containing mutagenised CDR loops were expressed on the surface of bacteriophage as fusions to the phage coat protein pIII. Following enrichment of antigen-binding molecules, in a process of biopanning, the selective output was analysed by phage-ELISA for binding to pHLA. This method successfully identified mutated TCRs with improved affinity for pHLA. TCRs with the best combinations of mutated CDRs were shown to bind their cognate pHLA antigens with significantly improved K_D values of 10 pM (Mel-5 TCR-Melan-A/MART-1_{26-35}) (Chapter 3; Section 3.8.3), 13 pM (gp100 TCR-$gp100_{280-288}$) (Chapter 4; Section 4.5.2) and 67 pM (MAGE-A3 TCR-MAGE-$A3_{168-}$

$_{176}$) (Chapter 5; Section 5.5). The TCRs displaying these affinities are now in the range of affinity matured antibodies and potentially can have therapeutic application.

Two biophysical properties of the affinity-enhanced TCRs emerge (Chapter 3; Figure 3.16, Chapter 4; Figure 4.9 and Chapter 5; Table 5.3). First, in agreement with the affinity maturation of antibodies (Hawkins, Russell et al. 1992; Yang, Green et al. 1995; Thompson, Pope et al. 1996), improvements in affinity are almost exclusively driven by decreases in off-rates and the affinity gains correlate well with extended $T_{1/2}$ values (several hours). This observation confirms the findings of the engineered 1G4 TCR in which $T_{1/2}$ values of up to ~17 hours were reported (Li, Moysey et al. 2005). Second, on-rates between the improved affinity mutants remain largely unchanged. There are two possible explanations for this. First, wild-type TCRs possess extremely fast on-rates and so engineering for improvements present a significant challenge. Second, the underlying principle of affinity maturation of proteins by phage display favours the selection of binders with slower dissociation rate constants. This is particularly apparent when using off-rate selection strategies (Hawkins, Russell et al. 1992; Yang, Green et al. 1995; Chen, Wiesmann et al. 1999) as employed in the engineering of the Mel-5 (Chapter 3, Section 3.7) and gp100 TCRs. In these experiments a large excess of non-biotinylated, and, therefore, soluble, antigen is added to the panning reaction. The non-biotinylated antigen acts as a competitor and captures any binding molecules that dissociate from the biotinylated antigen. The probability of a binder dissociating from antigen is largely determined by its dissociation rate constant. The excess of non-biotinylated antigen prevents molecules with fast off-rates re-binding to biotinylated antigen and so binders with the slowest off-rates in the pre-selected library pool are enriched (Hawkins, Russell et al. 1992).

Using a combinatorial strategy, individual mutated affinity-enhanced CDRs were spliced into the same TCR molecule in a stepwise manner to further increase binding affinity. As a general rule, combining mutated CDRs improved binding affinity in an additive fashion; a feature not always evident for antibodies (Yang, Green et al. 1995). Whilst the initial affinity gain conferred by a single CDR segment was significant (~2,000-fold; average value between the three TCRs) (Chapter 3; Table 3.7, Chapter 4; Table 4.3 and Chapter 5; Table 5.3), affinity gains at each subsequent step were generally in smaller increments, about 40-fold. An exception was clone MAGEa6b9, which produced a ~3.7 million-fold improvement over the parent MAGE-A3 TCR by inclusion of a second CDR segment (Chapter 5; Table 5.3). The cumulative effect on the affinity of the inclusion of up to five mutated CDR segments translated to astounding improvements over the wild-type TCR of approximately 1.8 million-fold, 1.7 million-fold and 3.7 million-fold respectively for the Mel-5 (Chapter 3; Table 3.7), gp100 (Chapter 4; Table 4.3) and MAGE-A3 (Chapter 5; Table 5.3) TCRs. The capacity of TCRs to accommodate affinity-enhancing mutations in multiple CDRs in the same molecule indicates that the geometry of interaction between TCR and pHLA is unaffected by these changes. Indeed, superimposition of the wild-type and high affinity 1G4 TCR (Dunn, Rizkallah et al. 2006; Sami, Rizkallah et al. 2007) in complex with cognate pHLA provides supporting evidence for this and moreover, indicates that the high affinity mutations have not driven the binding away from the peptide.

In view of experiences with antibody affinity engineering, such a dramatic gain in affinity through a combination of as few as two mutated CDRs was not predicted. Antibody engineering has yielded less striking improvements over the wild-type antibody of 228-fold (Lowe, Gerhardt et al. 2011), 420-fold (Yang, Green et al. 1995)

and 5,000-fold (Steidl, Ratsch et al. 2008). However, it must be remembered that the affinity of wild-type antibodies can be several orders of magnitude higher than TCRs and as such improvements in affinity from an already high affinity background is often more challenging. Engineering of the murine 2C scTCR generated up to a 750-fold improvement in affinity over the wild-type TCR for a single CDR2α segment. However, additive binding between different CDR mutants was not tested (Chlewicki, Holler et al. 2005).

The TCRs described in this thesis have been shown to be capable of detecting antigen expressed on the surface of human tumour cell lines following previously described methods (Purbhoo, Sutton et al. 2006) (Chapter 6; Figure 6.1). Briefly, cancer cells were incubated with biotinylated TCR followed by streptavidin-PE. Based on the assumption that a single PE fluorescence corresponds to a single TCR-peptide-HLA complex, the following epitope numbers were determined: Mel526 cell line expresses ~118 Melan-A/MART-$1_{(26-35)}$ (EAAGIGILTV) and ~33 $gp100_{(280-288)}$ (YLEPGPVTA) epitopes and A375 cell line expresses ~39 MAGE-$A3_{(168-176)}$ (EVDPIGHLY) epitopes. Soluble protein therapeutics have been designed which combine the tumour targeting capability shown in Figure 6.1 (Chapter 6) with an effector function by fusing the high affinity TCR to an anti-CD3 scFv moiety. The therapeutic mode of action of the high affinity TCR-anti-CD3 scFv fusions (so-called ImmTACs; immune-mobilising monoclonal TCRs against cancer) is described in our recent publication (Liddy, Bossi et al. 2012).

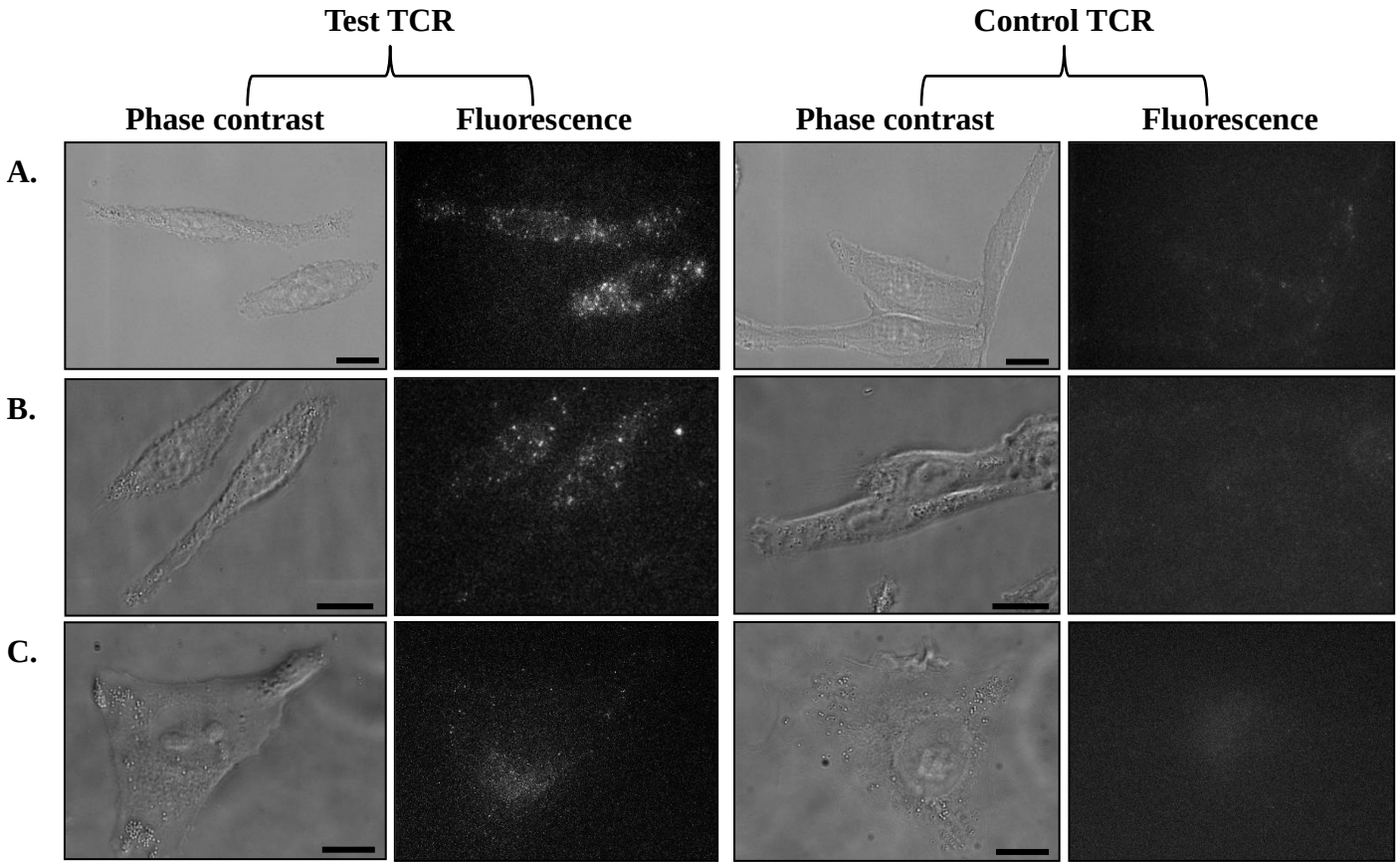

Figure 6.1. Imaging of individual peptide-HLA antigens on human tumour cell lines with high affinity TCRs. (A). Melan-A/MART-$1_{(26-35)}$ (EAAGIGILTV)/HLA-A2 antigens (Ags) on Mel 526 melanoma cell line using high affinity MELa24b15 TCR-biotinylated (bio) monomers and streptavidin-PE; **(B).** $gp100_{(280-288)}$ (YLEPGPVTA)/HLA-A2 Ags on Mel 526 cell line using high affinity GPa3b17 TCR-bio monomers and streptavidin- PE; **(C).** MAGE-$A3_{(168-176)}$ (EVDPIGHLY)/HLA-A1 Ags on A375 melanoma cell line using high affinity MAGEa6b9 TCR-bio monomers and streptavidin-PE. Each dot on the fluorescent images represents a single streptavidin-PE/TCR/Ag-HLA complex. Cells stained with control TCR-bio monomers and streptavidin-PE only are shown as controls. Cells shown are representative of the brightest 10% found among each staining condition. Bar, 10 μm. (Data kindly provided by Dr. G. Bossi).

6.4 Phage output - Sequence analysis

The sequence of antibody CDRs, although hypervariable, are biased towards certain amino acid residues. These include hydrophobic aromatic residues (tyrosine, tryptophan and phenylalanine), polar residues (arginine and histidine) and small residues (glycine, serine and alanine). The abundance of these residues at the binding interface may indicate an intrinsic suitability in forming antigen-binding sites, in which glycine and serine act as conformation residues and tyrosine, tryptophan and phenylalanine as the contact residues (Padlan 1994; Zemlin, Klinger et al. 2003; Fellouse, Wiesmann et al. 2004; Birtalan, Fisher et al. 2010). The structural similarity between antibodies and TCRs would imply that analogous patterns of protein-protein interactions may exist. However, the fact that T-cells are deselected during thymic education based on affinity parameters, argues against the desire for aromatic residues in the TCR antigen-binding loops since their inclusion may result in too strong interactions.

Subjecting the phage TCR libraries to three cycles of selective pressure was sufficient to obtain high affinity clones. Indeed, the selection output for each TCR revealed remarkable convergence to consensus sequences. Analysis of the Mel-5 TCR CDR3α output showed that 30 sequenced clones collapsed to 9 unique mutants (Chapter 3; Table 3.5). Likewise, the 22 sequenced CDR1α clones converged to 9 unique mutants and the CDR3β from 20 to 10 unique clones Table 3.6 (Chapter 3).

Notably, there was a prevalence of glycine residues in the CDR loops of both the engineered Mel-5 (Chapter 3; Table 3.3 and 3.6) and gp100 (Chapter 4; Table 4.1 and 4.2) TCRs. Enrichment for small residues such as glycine may indicate that flexibility is crucial to allow a conformation that is suitable for high affinity binding. For the Mel-5 TCR (Chapter 3), three of the four mutated CDRs that yielded enhanced-

affinity mutants contained at least one glycine residue (Chapter 3; Table 3.7). Glycine residues were either retained from the wild-type Mel-5 TCR or preferentially selected in place of the wild-type residue. For CDR1α, the wild-type glycine residue was retained in 7/8 clones (Chapter 3; Table 3.6). For CDR3α, a glycine residue was retained from the wild-type TCR in 4/9 clones and substituted for the wild-type residue in the remaining five mutants (Chapter 3; Table 3.5). The CDR2β clones were all selected with a glycine in place of the wild-type residue. The CDR3β clones all contained a glycine residue either retained from the wild-type clone (6/10) or introduced for the wild-type residue (4/10) (Chapter3; Table 3.6). Interestingly, in the fourth CDR loop that yielded improved affinity mutants, CDR2α, a wild-type glycine residue was located immediately adjacent to the targeted NNK region. In total, the CDR1α, CDR3α, CDR2β and CDR3β clones contain up to one, two, one and three glycine residues respectively.

A similar pattern emerged from the gp100 TCR affinity maturation (Chapter 4). Whilst the CDR3α selection output yielded only a single clone containing a glycine residue, both the CDR2β and CDR3β clones were substantially enriched for a glycine residue (86% and 100% of sequenced clones respectively) (Chapter 4; Table 4.2). The glycine residue was either retained from the wild-type parent TCR (CDR3β) or selected in preference to the wild-type residue (CDR2β) (Chapter 4; Table 4.3).

The pattern was not as evident in the MAGE-A3 TCR output (Chapter 5). Of the fifteen sequenced CDR2 clones, only three CDR2β clones contained a glycine residue (Chapter 5; Table 5.1). The selection of glycine-containing clones was more noticeable for the second-generation mutants, yet far less striking compared with the Mel-5 and gp100 TCRs. Although an average of ~20% CDR3α and ~50% CDR3β second-generation clones were enriched for glycine residues, a more rigorous

dissection of these mutants is required to determine the importance of glycine residues for the binding affinity.

Engineering of the 1G4 TCR for high affinity (Li, Moysey et al. 2005) identified glycine residues as key components of the CDR3α phage selection output. Indeed, at least one of the two wild-type glycine residues was retained in the centre of the mutated motif in all but one of the high affinity clones.

A propensity for glycine residues has also been observed in the CDR3α loop of the engineered yeast-displayed murine single-chain 2C TCR (Holler, Holman et al. 2000). Of the fifteen isolated mutants, nine contained a glycine residue in the centre of the mutated CDR3α motif which in combination with a stretch of four additional mutated residues conferred a 100-fold improvement in affinity compared with the parent 2C TCR. In agreement with these findings, Kranz and co-workers (Chlewicki, Holler et al. 2005) further demonstrated the importance of glycine residues to the binding affinity of the 2C TCR. They found that each of the CDR3β mutants isolated from engineering the 2C TCR retained two glycine residues. It is noteworthy that the wild-type CDR3β contains four adjacent glycine residues, possibly indicating a level of flexibility required for antigen-binding. The retention of two wild-type glycine residues provided sufficient loop flexibility to accommodate two residue substitutions that conferred a ~90-fold increase in affinity over the parent TCR.

The role of glycine residues in affording high affinity binding to the 2C TCR was further demonstrated by Kieke et al. (Kieke, Sundberg et al. 2001). The flexibility of the 2C TCR CDR2β loop due to two glycine residues was presumed critical for antigen-binding function since complete randomisation of the loop to increase the affinity for staphylococcal enterotoxin C3 (SEC3) generated mutants in which the two wild-type glycines were retained.

The contribution of the unique flexibility of glycine to the affinity of antibodies has also been widely explored (Fellouse, Esaki et al. 2007; Birtalan, Zhang et al. 2008). Sidhu and co-workers (Fellouse, Esaki et al. 2007) attributed a key role for glycine in the antigen-binding function of an anti-hVEGF Fab antibody. The HCDR3 loop was diversified using a spiked oligonucleotide strategy, in which the phage libraries were biased in favour of tyrosine, serine and glycine residues. Birtalan et al. (Birtalan, Zhang et al. 2008) also constructed anti-hVEGF Fab HCDR3 libraries in which diversity was added to the simplified binary tyrosine/serine background (Fellouse, Li et al. 2005) by introducing glycine, arginine or both. In each study, glycine residues were found in the majority of the selected antigen-binding clones in multiple positions. Taken together, these results suggest a critical role for glycine residues in providing conformational versatility that permits antigen recognition and high affinity binding. The prevalence of glycine residues in the HCDR3 loops of high affinity antibodies is supported by its high abundance in naïve antibodies in which it is the second most common residue after tyrosine (Zemlin, Klinger et al. 2003).

Accordingly, an alternative strategy to the blanket NNK mutagenesis approach, in which consecutive residues are mutated, would be to retain wild-type glycine residues and only target the adjacent amino acids. Whilst all 20 amino acids are encoded by degenerative NNK oligonucleotides, permitting the representation of wild-type residues in the initial phage library pool, limiting the library complexity by mutating fewer residues may offer benefits to library quality and composition. The only caveat to this strategy is that favourable substitutions of wild-type glycine residues would be overlooked, as illustrated in the case of the Mel-5 TCR CDR2β mutants (Chapter 3; Table 3.6).

The aromatic residues tyrosine, phenylalanine and tryptophan played a prominent role in mediating high affinity binding for each of the TCRs engineered in this thesis, most notably for the Mel-5 and gp100 TCRs (Chapter 6; Table 6.1). For the Mel-5 TCR, there was a dramatic enrichment for CDR3β clones containing a tryptophan residue (90% of sequenced clones). Interestingly, all of the CDR2β clones contained at least one aromatic residue. Over half of the CDR1α clones contained a phenylalanine. Of note, enrichment of an aromatic residue was frequently accompanied by a glycine residue.

TCR	CDR	**Total clones**	Y	F	W	G/Y	G/F	G/W
Mel-5	1α	**8**	1	5	0	0	5	0
	2α	**1**	1	0	0	1	0	0
	3α	**9**	1	0	0	1	0	0
	2β	**4**	2	4	1	2	4	1
	3β	**10**	0	0	9	0	0	0
gp100	3α	**6**	0	6	0	0	6	0
	2β	**7**	1	1	7	1	0	6
	3β	**7**	7	0	1	7	0	1
MAGE-A3	2α	**7**	7	3	0	0	0	0
	3α	**15**	7	14	0	7	14	0
	2β	**8**	0	0	0	0	0	0
	3β	**61**	14	9	5	4	0	2

Table 6.1. Frequency of the aromatic amino acid residues in the Pan 3 selection output of the Mel-5, gp100 and MAGE-A3 TCRs. Single letter amino acid nomenclature used: Y, tyrosine; F, phenylalanine; W, tryptophan; G, glycine. G/Y, G/F or G/W: Frequency of G in combination with Y, F or W in the same CDR. The mutagenised CDR is indicated.

The frequency of aromatic residues in the gp100 TCR output was even more striking (Chapter 6; Table 6.1): all sequenced CDR3α clones contained a phenylalanine residue; all CDR2β clones were enriched for a tryptophan residue; all CDR3β clones contained a tyrosine residue in addition to a single clone that contained a tryptophan residue. With the exception of a single CDR2β clone, which contained a phenylalanine residue, the selection of an aromatic residue was in combination with a glycine residue.

Excluding the CDR2β output, the MAGE-A3 TCR clones from CDR2α, CDR3α and CDR3β, were preferentially selected to a lesser or greater extent for the presence of an aromatic residue (Chapter 6; Table 6.1). Most notably, >90% of CDR3α clones contained a phenylalanine in conjunction with a glycine residue, of which over half include a tyrosine residue. The presence of a glycine residue may provide conformational mobility that allows bulky residues, such as tyrosine, phenylalanine and tryptophan to achieve an optimal fit.

Interestingly, a prevalence of aromatic residues in the CDRs of affinity matured TCRs has previously been reported. The (~90-fold) improved affinity murine 2C scTCR described earlier (Chlewicki, Holler et al. 2005), contained a phenylalanine residue in combination with a pair of glycine residues in the CDR3β loop. Also, Dunn et al. (Dunn, Rizkallah et al. 2006) isolated high affinity 1G4 TCR clones that were greatly enriched for tryptophan residues in the CDR2α loop that were frequently found in combination with a glycine residue.

Notably, in antibody engineering, Sidhu and colleagues (Fellouse, Li et al. 2005) also demonstrated the importance of tyrosine residues in mediating high affinity antigen recognition by constructing an anti-hVEGF Fab framework phage library in which binary tyrosine/serine diversity was introduced into four CDRs. Remarkably,

antibodies with high affinity and specificity were isolated, revealing that a minimal number of contacts are sufficient for binding. A follow-up study reported from the same lab (Birtalan, Zhang et al. 2008) showed that introduction of glycine residues into the simplified diversity tyrosine/serine background combined successfully with tyrosine to mediate high affinity binding. Furthermore, tyrosine residues in the HCDR3 loop of the G8 Fab (Hulsmeyer, Chames et al. 2005) have been shown to play a pivotal role in the interaction with the HLA-A1-MAGE-A1 complex since the high affinity derivative Hyb3, retained four of the six tyrosine residues. Accordingly, structural analysis showed the tyrosine-rich HCDR3 loop (FHYYYY) formed a clamp over the HLA α1 helix.

Besides glycine, tyrosine, tryptophan and phenylalanine several other residues were selectively enriched following engineering of the Mel-5 (Chapter 3; Table 3.5 and 3.7), gp100 (Chapter 4; Table 4.3) and MAGE-A3 (Chapter 5; Table 5.1) TCRs commonly including proline and to a lesser extent leucine and arginine.

Interestingly, in the Mel-5 TCR maturation, a leucine to proline substitution was preferentially selected at position 44 (outside of the targeted CDR region) in all of the CDR2β clones and in a single clone from the CDR3β output (Chapter 3; Table 3.6). Because the two libraries were independently constructed using CDR2β or CDR3β specific primers, the L44P substitution would appear to be advantageous in terms of expression or binding affinity. Prevalence for a proline residue in the CDR loops was observed in all three TCRs. Mel-5 TCR: in addition to the L44P substitution in β framework 2, a proline residue was selected for in all of the CDR2β clones (Chapter 3; Table 3.6); gp100 TCR: a single proline residue was retained from the wild-type sequence in all of the CDR3α and CDR3β mutants (Chapter 4; Table 4.2); MAGE-A3 TCR: a proline residue was introduced into each of the selected CDR2α clones

(Chapter 5; Table 5.1) and highly enriched in the CDR3α mutants (Chapter 5; Table 5.6 and 5.9). The presence of a proline residue could have some effect on the geometry of these loops, yet without structural information its precise role in the antigen-binding domains is unclear.

Additionally, amber codons were frequently found in the CDR regions of the selective output of all three TCRs; a phenomenon that has been observed in both antibody (Shinohara and Fukuda 2002; Rinderknecht, Villa et al. 2010) and TCR affinity engineering (Dunn, Rizkallah et al. 2006). The amber stop codon is transcribed as a glutamine residue in suppressor strains of *E. coli* (such as TG1 cells used in this work) with an efficiency of 10-20%. Krebber et al. (Krebber, Burmester et al. 1996) demonstrated that inserting an amber stop codon between the gene of interest and geneIII in a phagemid vector reduced the amount of fusion protein produced thus limiting the negative effect on bacterial cell growth. Furthermore, Paschke and Hohne (Paschke and Hohne 2005) showed that introduction of an amber codon in the pelB leader sequence conferred elevated display levels of the protein of interest by reducing the expression of pIII. Enrichment for an amber codon in many of the TCRs described in this thesis and in TCRs engineered previously by our group (Dunn, Rizkallah et al. 2006) perhaps indicates the toxic character of the pIII-TCR fusion proteins or alternatively may demonstrate an improvement in affinity sufficient to compensate for reduced expression.

Dissection of the mutated CDR segments to assess the affinity gains attributable to particular residues would be highly informative. One method to achieve this would be to revert back to wild-type each of the mutated residues as described for the MELa1 CDR3α mutant (Chapter 3; Section 3.5). In this example, the importance of Gly^{92} to the affinity of the MELa1 clone was demonstrated by substituting for the wild-type

alanine residue at this position. The outcome of this mutation was a dramatic ~900-fold reduction in the affinity (Chapter 3; Figure 3.13) endorsing the role of glycine residues to the binding affinity as described above. By comparison, the contribution of Arg^{94} to the affinity of the MELa1 clone was far less significant since substitution for the wild-type lysine reduced the affinity by ~70-fold (Chapter 3; Figure 3.13).

Finally, it is interesting to note that Shiroishi et al. (Shiroishi, Tsumoto et al. 2007) suggest that the lower number of tyrosine residues participating at the TCR-pMHC interface compared with antibodies may account for the differences in binding affinity between these two structurally related molecules. The scattering of tyrosine residues in the high affinity TCRs described in this thesis provides some support to this notion.

6.5 What is the structural basis of high affinity?

Several factors, most likely working synergistically, contribute to the high affinity binding of the engineered Mel-5, gp100 and MAGE-A3 TCR mutants; these include improved shape complimentarity (SC), additional number of interfacial hydrogen bonds, van der Waals interactions, increased buried hydrophobic surface area and exclusion of water molecules (Lo Conte, Chothia et al. 1999).

Following the completion of the Mel-5 TCR affinity engineering project, the structure of the wild-type Mel-5 TCR in complex with HLA-A*0201-Melan-A/MART-1_{26-35}, (ELAGIGILTV) has been solved (Cole, Yuan et al. 2009). In the absence of a structure of at least one of the high affinity Mel-5 TCRs, it is difficult to assess which mutations directly contribute to the affinity improvements. However, the structure of the wild-type Mel-5 TCR provides a framework to identify key binding contacts between the TCR, the ELA peptide and the HLA surface which may assist in the interpretation of the high affinity interactions. The Mel-5 TCR binds to the N-terminus of the peptide as observed for the A6 TCR (in complex with HLA-A2-Tax)

which also uses the TRAV12-2 gene (Ding, Smith et al. 1998). Unusually, the Mel-5 TCR (Cole, Yuan et al. 2009) CDR3α makes a minimal contact with the peptide, with TCR residue Asn^{92} making only a single electrostatic interaction with ELA peptide residue Gly^{P4}. The CDR1α loop plays a more dominant role in contacting the ELA peptide, with TCR residue Gln^{31} making a significant network of contacts to ELA peptide residues Glu^{P1}, Leu^{P2}, Gly^{P4} and Ile^{P5}. More specifically, the CDR1α loop uses side chain atoms to contact the peptide. Cole et al. (Cole, Yuan et al. 2009) suggest that changes to the sequence of this loop would therefore not be well tolerated and may well abrogate TCR recognition of peptide. The results of the Mel-5 TCR affinity maturation (Chapter 3) lend credence to this hypothesis. The CDR1α mutations are predominantly at positions 27 and 28, whilst Gln^{31} remains invariant (except when replaced with an amber codon, suppressible to Gln) (Chapter 3; Table 3.6). Mutation of Gln^{31} likely results in loss of peptide binding and therefore such mutants were not selected during the panning process. Although residue Arg^{28} in the wild-type TCR makes four electrostatic interactions with the MHC surface, it is mutated in all CDR1α clones (Chapter 3; Table 3.6). The introduction of a phenylalanine or tyrosine residue at position 27 in over half of the clones may well compensate for the loss of these MHC contacts. Interestingly, the mutations isolated at positions 27 and 28 conferred only modest improvements in affinity (up to 2-fold) (Chapter 3; Table 3.7) and may have been selected on the basis of reduced expression mediated by an amber codon at position 28. Since the CDR3α loop makes minimal contact with the peptide it is surprising that affinity-enhancing mutations within this region were identified (Chapter 3; Table 3.3). Presumably, the mutated high affinity alpha chains make substantially more contacts with the peptide compared with the wild-type Mel-5 TCR. By contrast, the CDR3β loop makes a total of ten contacts

(five hydrogen bonds and five van de Waals interactions) between TCR residues Thr^{96}, Leu^{98} and Gly^{99} and ELA peptide residues Ala^{P3}, Gly^{P4}, Ile^{P5}, Gly^{P6}, Ile^{P7} and Thr^{P9}. Because the CDR3β loop largely makes contact with the ELA peptide main chain Cole et al. (Cole, Yuan et al. 2009) proposed the loop would be tolerant to changes to its sequence without the loss of peptide recognition. Accordingly, engineering of the CDR3β loop yielded mutants with significant changes from the wild-type sequence. Most notably, a leucine residue at position 103 was substituted for a tryptophan residue in all sequenced clones (Chapter 3; Table 3.6). Preference for a tryptophan residue conferred a substantial gain in affinity of up to 16-fold (Chapter 3; Table 3.7). The CDR2α loop makes no contact with the ELA peptide and only a single electrostatic interaction between TCR residue Tyr^{51} and the MHC residue His^{151}. Only a single CDR2α mutant was isolated and interestingly retained the residue Tyr^{51}.

The structures of the high affinity 1G4 TCR (Sami, Rizkallah et al. 2007) and the A6 TCR (D.K. Cole, manuscript in preparation) are now available and offer structural suggestions for the observed high affinity. Sami et al. (Sami, Rizkallah et al. 2007) showed that for the 1G4 TCR, increases in the shape complementarity (SC) index (Lawrence and Colman 1993) of TCR/pMHC, TCR/peptide and TCR/$Met^{P4}Tyr^{P5}$ peptide motif correlated well with increased affinity. Most strikingly were the observed increases in the SC index of the TCR/peptide, particularly when both CDR2 and CDR3 mutations occurred simultaneously. The improved number of peptide contacts made as a consequence of the increased SC index provides a likely explanation for the increases in binding affinity and is in agreement with observations for the high affinity A6 TCR (D. K. Cole, manuscript in preparation). Whilst the geometry of the A6 TCR/HLA-A2-Tax interaction was largely unchanged between

the wild-type and high affinity TCRs, the affinity gains were therefore the result of other interactions. Indeed, an extra 28 van de Waals interactions were made between the high affinity TCR and the Tax peptide compared with the wild-type TCR. Although it seems likely that increases in the number of contacts made between the TCR and peptide are chiefly responsible for the high affinity binding, it would be hugely ambitious to predict the location and nature of these mutations and this is exemplified by the high affinity A6 TCR CDR3β mutant, A6c134 ($M^{99}S^{100}A^{101}Q^{102}$). Interestingly, the R102Q mutation resulted in the loss of 8 peptide contacts, attributed to the loss of a potential salt bridge forming between the Ser^{100} and Arg^{102} side chains. Indeed, the A6c134R (MSAR) derivative displayed higher binding affinity compared with A6c134 probably due the opening of the CDR3β loop to accommodate the Tax peptide residue Tyr^{P5}. It is the combination of individual residues that generate high affinity binding and as such, the cooperativity between these residues, in the context of a multi-domain protein, cannot be predicted. It is also not possible to predict the effect mutations in one CDR loop will confer on the other non-targeted CDRs within the same or opposing chain. Although the A6c134 TCR α chain contained no mutations, the introduction of mutations in the β chain facilitated a number of additional contacts between the α chain and the Tax peptide compared with the wild-type TCR.

Kranz and colleagues have attempted to identify generic TCR mutations that are beneficial to protein expression (Richman, Aggen et al. 2009; Aggen, Chervin et al. 2011). Whilst their studies highlighted common V-region mutations that permitted yeast surface display, many with clear structural advantages, a large number of changes however, were more difficult to comprehend. This provides a further example, in addition to those described earlier, of the challenge in designing rational

mutagenesis strategies that target only a specific collection of residues. For this reason, a directed evolution approach, in which mutations are enriched based on the Darwinian principle of selection, is the most effective method of identifying affinity-enhancing mutations.

The prevalence of aromatic residues in the pMHC binding loops of the affinity matured TCRs described in this thesis has been alluded to earlier (Chapter 6; Section 6.4). Numerous studies have explored the unique properties of these residues that make them well suited for molecular recognition. Whilst most hydrophobic residues are mainly located in the interior of proteins, tyrosine and tryptophan are found in the interior and on the surface of proteins with similar frequency (Tsai, Lin et al. 1997). Studies of the amino acid composition of antibodies have highlighted the overabundance of aromatic residues, particularly tyrosine and tryptophan in the CDR loops that comprise the interface with the antigen (Padlan 1994; Bogan and Thorn 1998; Lo Conte, Chothia et al. 1999). The frequency of tyrosine and tryptophan residues in the contact area has been attributed to their capacity to mediate multiple types of intermolecular interactions, including aromatic π interactions, hydrogen bonding via the hydroxyl group, van der Waals interactions and hydrophobic interactions (Bogan and Thorn 1998).

The importance of aromatic residues in contributing to high affinity binding of the engineered 1G4 TCR has been demonstrated (Sami, Rizkallah et al. 2007). The role attributed to tyrosine residues in mediating key contacts between the TCR loops was two-fold. First, a V94L substitution in the high affinity CDR3β clone provided a more favourable contact with the aromatic ring of wild-type residue $Tyr^{100}\alpha$ to enable the CDR3 loops to lock around the central peptide residues $Met^{P4}Trp^{P5}$. Second, π ring stacking interactions between CDR1/CDR3α loops and peptide residue Trp^{P5} were

implicated in generating high affinity since a Y31Dα substitution, that abrogated aromatic stacking, dramatically reduced binding affinity.

More recently, a structure-based design was used to indentify affinity-enhancing mutations at the A6 TCR-HLA-Tax interface (Haidar, Pierce et al. 2009). Four mutations were identified that individually increased the affinity as much as 6-fold (for an αD26W substitution) and in combination by nearly 100-fold. The mutations that increased the binding affinity were hydrophobic substitutions that improved complementarity and hydrophobic packing. A drawback, however, of structure-based approaches is that cooperativity between residues, frequently seen in the mutants selected from a directed evolution strategy, may not be observed since a selective pressure has not been applied. Haider et al. (Haidar, Pierce et al. 2009) combined the highest binding five point mutations (α chain motif $W^{26}F^{27}T^{28}M^{51}T^{100}$) that individually improved the affinity for pMHC up to 6-fold. Surprisingly, the combination only yielded a ~9-fold gain in affinity over the wild-type TCR. Structure analysis suggested the side chains of W^{26} and T^{28} were incompatible. Accordingly, replacing the wild-type G^{28} produced a dramatic improvement in affinity of nearly 100-fold.

The nature of the antigenic peptide clearly plays an integral role in shaping the output of affinity selection strategies. In the case of the 1G4 TCR (Sami, Rizkallah et al. 2007), the CDR3 loops clamp around the central $Met^{P4}Tyr^{P5}$ peptide residues that protrude directly into the solvent. However, not all peptides present "interesting" residue side chains and instead present fairly flat antigenic surfaces as demonstrated by the HLA-A1-MAGE-A1 (EADPTGHSY) peptide complex recognised by the high affinity Fab-Hyb3 (Hulsmeyer, Chames et al. 2005). In this example, a lack of solvent-accessible peptide side chain contacts is alleviated by a density of water

molecules that mediate hydrogen bonding between Hyb3 CDR loops and the MAGE-A1 peptide. The antibody makes 8 contacts with the MAGE-A1 peptide; 4 direct hydrogen bonds and 4 water-bridged contacts. This may provide a possible mechanism for the MAGE-A3 TCR (Chapter 5) to engage the HLA-A1-MAGE-A3 (EVDPIGHLY) peptide complex in which six of the nine peptide residues are shared with MAGE-A1 epitope.

6.6 Specificity

A central feature underpinning T-cell function that appears implicitly paradoxical is, on the one hand, the capacity to discriminate between variant peptides with a high level of specificity, whilst on the other hand, the propensity to cross-react with a multitude of peptide ligands. A resolution to this incongruity is based on numerical considerations. Combinatorial rearrangement of TCR gene segments has the capacity to generate ~10^{15} unique TCRs. However, the final repertoire of TCRs that survive the culling process of thymic selection has been estimated to be around 25 million (Arstila, Casrouge et al. 1999). The total number of possible decamer peptides that can be generated from the 20 proteinogenic amino acids is >10^{13}. Assuming that 1% of these peptides bind to MHC (~10^{11}) and a single TCR can functionally recognise ~10^{6} decamer peptides, a cross-reactivity frequency of only 1:100,000 manifests (Mason 1998; Sewell 2012; Wooldridge, Ekeruche-Makinde et al. 2012). Therefore, in terms of the number of possible peptides recognised, TCRs appear considerably cross-reactive, yet in terms of the frequency of peptides recognised in the context of the vast peptide universe, TCRs appear highly specific (Donermeyer, Weber et al. 2006).

A further enigma in the study of T-cell antigen recognition is the high specificity-low affinity TCR-pMHC interaction. It is difficult to assign a generic definition to

specificity since there is no intrinsic unit of measurement. A determination of specificity is dependent on the design, conditions and stringency of the experimental model. In terms of three-dimensional (3D) biophysical analysis by surface plasmon resonance (SPR), binding affinities between TCR and variant pMHC ligands may indicate specificity based on defined kinetic parameters. Alternatively, in the context of a two-dimensional (2D) cellular environment, the interaction between a TCR and pMHC that is sufficient to induce productive intracellular signalling and activation provides a measure of T-cell responsiveness or specificity towards a given antigen. It is important to distinguish between TCR intrinsic affinity which is a measure of the strength of binding of monomeric interactions between one TCR molecule and the pMHC ligand and TCR avidity, which is the combined synergistic outcome of multiple TCR-pMHC interactions that occur at the T-cell-APC contact zone.

T-cell recognition is highly sensitive such that engagement with a single agonist pMHC ligand is sufficient for T-cell stimulation (Irvine, Purbhoo et al. 2002; Purbhoo, Irvine et al. 2004; Morris and Allen 2012). This level of sensitivity is all the more extraordinary considering the background of 10^5 or so irrelevant pMHC molecules on the surface of antigen presenting cells (Yewdell 2001). The binding affinity between soluble TCR and pMHC, as determined by SPR, which is typically in the low micromolar range (Davis, Boniface et al. 1998; Cole, Pumphrey et al. 2007; Stone, Chervin et al. 2009), seemingly is not consistent with this observation. The mechanisms that govern such remarkable T-cell sensitivity are not fully understood. However, the 3D biophysical measurements do not account for the complexity of the synaptic environment. For example, a clear role in enhancing T-cell sensitivity has been attributed to CD8 co-receptor molecules (Wooldridge, van den Berg et al. 2005; Laugel, van den Berg et al. 2007; Cole, Laugel et al. 2012) and to the formation of

microclusters of multivalent TCRs at the TCR-pMHC interface (Schamel, Arechaga et al. 2005; Lillemeier, Mortelmaier et al. 2009).

Measurements of the 2D TCR-pMHC interactions at the cell surface show that the kinetics differ markedly from the corresponding 3D (SPR) values (Huang, Zarnitsyna et al. 2010; Huppa, Axmann et al. 2010). These studies, which are seen by many researchers to more accurately reflect the T-cell-APC interaction, show the higher affinity TCR-pMHC kinetics are the result of significantly increased association rates. Huang et al. (Huang, Zarnitsyna et al. 2010) propose that the rapid kinetics allows the T-cell to sample a vast array of pMHC complexes with the sensitivity required to discriminate between variant ligands, since the fast off-rates associated with the breaking of bonds are recompensed by the rapid on-rates and the reforming of bonds. The resulting rapid serial engagement of the rare agonist pMHC molecules, against a background of self-pMHC, amplifies the binding signals that influence T-cell responsiveness.

In general, there is a good correlation with $T_{1/2}$ and the strength of T-cell activation (Davis, Boniface et al. 1998; Gascoigne, Zal et al. 2001; van der Merwe and Davis 2003). Several TCR triggering models have been proposed to reconcile the low affinity TCR-pMHC interactions with the exquisite sensitivity of T-cell activation (van der Merwe and Dushek 2011). Kinetic models (McKeithan 1995; Rabinowitz, Beeson et al. 1996) suggest that potent T-cell activation is dictated by the duration of the TCR-pMHC interaction since sufficient time is required to allow completion of the intracellular signalling cascade that involves the multistep phosphorylation of CD3 subunits (Kersh, Shaw et al. 1998). By contrast, the serial engagement model stipulates that the dissociation rates need to be sufficiently short to allow multiple TCRs to interact with the same pMHC (Valitutti, Muller et al. 1995; Valitutti and

Lanzavecchia 1997). Both models predict an optimal $T_{1/2}$ for the TCR-pMHC interaction and that above or below an 'affinity ceiling', T-cell sensitivity is impaired (Sewell 2002; Schmid, Irving et al. 2010). The 'affinity ceiling' hypothesis has been challenged by Kranz and colleagues (Holler and Kranz 2003) since T-cells transfected with high affinity TCRs ($T_{1/2}$ 100-fold slower than the wild-type TCR) were potently activated. However, a caveat to these findings is that the T-cells bearing TCRs engineered with supraphysiological affinities lost peptide fine-specificity (Holler, Chlewicki et al. 2003). Moreover, a trade-off between T-cell potency as the TCR affinity increased and the increased number of stimulatory peptides that the T-cell could recognise was observed (Donermeyer, Weber et al. 2006). These findings impact significantly on the design of T-cell gene therapy strategies; it is imperative that the engineered TCRs do not exceed an affinity threshold above which off target activity against self-pMHCs is mediated. Morgan and colleagues (Zhao, Bennett et al. 2007) in a recent study provided support for such a cautious approach. They demonstrated that increased off target activity correlated with increased TCR affinity, since $CD8^+$ T-cells transfected with high affinity TCRs (ranging from 84 nM to 26 pM) lysed T2 cells pulsed with noncognate peptide, whereas those transfected with a moderate affinity (4 μM) TCR only lysed T2 cells pulsed with cognate peptide and not control targets.

Despite these investigations into the effect of increasing TCR affinity on the potency of T-cell activation and antigen recognition have been made in the context of T-cell therapy, the observations provide clear support for the rationale behind engineering high affinity soluble TCRs as an efficient means to overcome the limitations of natural TCR-mediated antigen recognition. Whilst there are concerns regarding potential cross-reactivity of picomolar-affinity soluble TCR reagents to

non-target epitopes, our lab has recently demonstrated that target cell lysis is specific even at pMHC class I levels as low as 2-10 copies per cell and is restricted to cells presenting cognate pMHC complexes (Liddy, Bossi et al. 2012).

6.7 Closing remarks and future perspectives

The work presented here demonstrates that the phage display methodologies employed to increase antibody affinity can be successfully modified to the engineering of TCRs for high affinity. Importantly, picomolar affinity TCRs can be produced, commonly with $T_{1/2}$ values of many hours, by combining multiple mutated CDR segments into the same molecule. This general observation is imperative to the successful application of TCRs as immune therapeutics since the antigenic peptides recognised by TCRs are presented at extremely low levels at the surface of tumour cells.

Antibodies have become the benchmark for the targeted treatment of malignant cells. The membrane-bound targets for antibodies are intact proteins. By contrast, TCRs recognise the degradation products of intracellular proteins that are loaded onto MHC molecules and displayed at the cell surface for inspection by patrolling cytotoxic T-cells. This continuous process of peptide fragmentation and presentation which takes place in almost all cells generates an enormous repertoire of diverse TCR-accessible peptide targets that substantially exceeds the potential antibody targets. The development of high affinity TCR-based therapeutics provides the first tumour-targeting agent able to exploit this vast array of antigens inaccessible to any other naturally-occurring molecule. The first of these reagents is now being tested in clinical trials; if successful, the versatility of the TCR-pHLA platform potentially makes it relevant for virtually every form of cancer. High affinity bispecific TCRs have potential beyond targeted cancer therapy. A similar approach of enhancing a

targeted immune response, could be used to selectively lyse virally-infected cells or alternatively, to dampen autoimmunity by conjugation of a high affinity TCR molecule to an immunosuppressive effector.

Adams, G. P., J. E. McCartney, M. S. Tai, H. Oppermann, J. S. Huston, W. F. Stafford, 3rd, M. A. Bookman, I. Fand, L. L. Houston and L. M. Weiner (1993). "Highly specific in vivo tumor targeting by monovalent and divalent forms of 741F8 anti-c-erbB-2 single-chain Fv." *Cancer Res* 53(17): 4026-34.

Adams, G. P., R. Schier, K. Marshall, E. J. Wolf, A. M. McCall, J. D. Marks and L. M. Weiner (1998). "Increased affinity leads to improved selective tumor delivery of single-chain Fv antibodies." *Cancer Res* 58(3): 485-90.

Adams, G. P., R. Schier, A. M. McCall, H. H. Simmons, E. M. Horak, R. K. Alpaugh, J. D. Marks and L. M. Weiner (2001). "High affinity restricts the localization and tumor penetration of single-chain fv antibody molecules." *Cancer Res* 61(12): 4750-5.

Aggen, D. H., A. S. Chervin, F. K. Insaidoo, K. H. Piepenbrink, B. M. Baker and D. M. Kranz (2011). "Identification and engineering of human variable regions that allow expression of stable single-chain T cell receptors." *Protein Eng Des Sel*.

Aleksic, M., N. Liddy, P. E. Molloy, N. Pumphrey, A. Vuidepot, K. M. Chang and B. K. Jakobsen (2012). "Different affinity windows for virus and cancer-specific T-cell receptors - implications for therapeutic strategies." *Eur J Immunol*.

Alt, M., R. Muller and R. E. Kontermann (1999). "Novel tetravalent and bispecific IgG-like antibody molecules combining single-chain diabodies with the immunoglobulin gamma1 Fc or CH3 region." *FEBS Lett* 454(1-2): 90-4.

Anichini, A., C. Maccalli, R. Mortarini, S. Salvi, A. Mazzocchi, P. Squarcina, M. Herlyn and G. Parmiani (1993). "Melanoma cells and normal melanocytes share antigens recognized by HLA-A2-restricted cytotoxic T cell clones from melanoma patients." *J Exp Med* 177(4): 989-98.

Armstrong, K. M., K. H. Piepenbrink and B. M. Baker (2008). "Conformational changes and flexibility in T-cell receptor recognition of peptide-MHC complexes." *Biochem J* 415(2): 183-96.

Arndt, K. M., K. M. Muller and A. Pluckthun (1998). "Factors influencing the dimer to monomer transition of an antibody single-chain Fv fragment." *Biochemistry* 37(37): 12918-26.

Arstila, T. P., A. Casrouge, V. Baron, J. Even, J. Kanellopoulos and P. Kourilsky (1999). "A direct estimate of the human alphabeta T cell receptor diversity." *Science* 286(5441): 958-61.

Atanackovic, D., T. Luetkens, Y. Hildebrandt, J. Arfsten, K. Bartels, C. Horn, T. Stahl, Y. Cao, A. R. Zander, C. Bokemeyer and N. Kroger (2009). "Longitudinal analysis and prognostic effect of cancer-testis antigen expression in multiple myeloma." *Clin Cancer Res* 15(4): 1343-52.

Baeuerle, P. A., P. Kufer and R. Bargou (2009). "BiTE: Teaching antibodies to engage T-cells for cancer therapy." *Curr Opin Mol Ther* 11(1): 22-30.

Baeuerle, P. A. and C. Reinhardt (2009). "Bispecific T-cell engaging antibodies for cancer therapy." *Cancer Res* 69(12): 4941-4.

Bakker, A. B., M. W. Schreurs, A. J. de Boer, Y. Kawakami, S. A. Rosenberg, G. J. Adema and C. G. Figdor (1994). "Melanocyte lineage-specific antigen gp100 is recognized by melanoma-derived tumor-infiltrating lymphocytes." *J Exp Med* 179(3): 1005-9.

Barbas, C. F., 3rd, E. Bjorling, F. Chiodi, N. Dunlop, D. Cababa, T. M. Jones, S. L. Zebedee, M. A. Persson, P. L. Nara, E. Norrby and et al. (1992). "Recombinant human Fab fragments neutralize human type 1 immunodeficiency virus in vitro." *Proc Natl Acad Sci U S A* 89(19): 9339-43.

Barbas, C. F., 3rd, J. E. Crowe, Jr., D. Cababa, T. M. Jones, S. L. Zebedee, B. R. Murphy, R. M. Chanock and D. R. Burton (1992). "Human monoclonal Fab fragments derived from a combinatorial library bind to respiratory syncytial virus F glycoprotein and neutralize infectivity." *Proc Natl Acad Sci U S A* 89(21): 10164-8.

Beck, A., T. Wurch and J. M. Reichert (2011). "6th Annual European Antibody Congress 2010: November 29-December 1, 2010, Geneva, Switzerland." *MAbs* 3(2): 111-32.

Bentley, G. A., G. Boulot, K. Karjalainen and R. A. Mariuzza (1995). "Crystal structure of the beta chain of a T cell antigen receptor." *Science* 267(5206): 1984-7.

Better, M., C. P. Chang, R. R. Robinson and A. H. Horwitz (1988). "Escherichia coli secretion of an active chimeric antibody fragment." *Science* 240(4855): 1041-3.

Bindea, G., B. Mlecnik, W. H. Fridman, F. Pages and J. Galon (2010). "Natural immunity to cancer in humans." *Curr Opin Immunol* 22(2): 215-22.

Bird, R. E., K. D. Hardman, J. W. Jacobson, S. Johnson, B. M. Kaufman, S. M. Lee, T. Lee, S. H. Pope, G. S. Riordan and M. Whitlow (1988). "Single-chain antigen-binding proteins." *Science* 242(4877): 423-6.

Birtalan, S., R. D. Fisher and S. S. Sidhu (2010). "The functional capacity of the natural amino acids for molecular recognition." *Mol Biosyst* 6(7): 1186-94.

Birtalan, S., Y. Zhang, F. A. Fellouse, L. Shao, G. Schaefer and S. S. Sidhu (2008). "The intrinsic contributions of tyrosine, serine, glycine and arginine to the affinity and specificity of antibodies." *J Mol Biol* 377(5): 1518-28.

Bjorkman, P. J., M. A. Saper, B. Samraoui, W. S. Bennett, J. L. Strominger and D. C. Wiley (1987). "The foreign antigen binding site and T cell recognition regions of class I histocompatibility antigens." *Nature* 329(6139): 512-8.

Bjorkman, P. J., M. A. Saper, B. Samraoui, W. S. Bennett, J. L. Strominger and D. C. Wiley (1987). "Structure of the human class I histocompatibility antigen, HLA-A2." *Nature* 329(6139): 506-12.

Boder, E. T., K. S. Midelfort and K. D. Wittrup (2000). "Directed evolution of antibody fragments with monovalent femtomolar antigen-binding affinity." *Proc Natl Acad Sci U S A* 97(20): 10701-5.

Boder, E. T., M. Raeeszadeh-Sarmazdeh and J. V. Price (2012). "Engineering antibodies by yeast display." *Arch Biochem Biophys*.

Boder, E. T. and K. D. Wittrup (1997). "Yeast surface display for screening combinatorial polypeptide libraries." *Nat Biotechnol* 15(6): 553-7.

Bogan, A. A. and K. S. Thorn (1998). "Anatomy of hot spots in protein interfaces." *J Mol Biol* 280(1): 1-9.

Borbulevych, O. Y., K. H. Piepenbrink and B. M. Baker (2011). "Conformational melding permits a conserved binding geometry in TCR recognition of foreign and self molecular mimics." *J Immunol* 186(5): 2950-8.

Borbulevych, O. Y., K. H. Piepenbrink, B. E. Gloor, D. R. Scott, R. F. Sommese, D. K. Cole, A. K. Sewell and B. M. Baker (2009). "T cell receptor cross-reactivity directed by antigen-dependent tuning of peptide-MHC molecular flexibility." *Immunity* 31(6): 885-96.

Bothmann, H. and A. Pluckthun (1998). "Selection for a periplasmic factor improving phage display and functional periplasmic expression." *Nat Biotechnol* 16(4): 376-80.

Bothmann, H. and A. Pluckthun (2000). "The periplasmic Escherichia coli peptidylprolyl cis,trans-isomerase FkpA. I. Increased functional expression of antibody fragments with and without cis-prolines." *J Biol Chem* 275(22): 17100-5.

Boulter, J. M., M. Glick, P. T. Todorov, E. Baston, M. Sami, P. Rizkallah and B. K. Jakobsen (2003). "Stable, soluble T-cell receptor molecules for crystallization and therapeutics." *Protein Eng* 16(9): 707-11.

Bradbury, A. R., S. Sidhu, S. Dubel and J. McCafferty (2011). "Beyond natural antibodies: the power of in vitro display technologies." *Nat Biotechnol* 29(3): 245-54.

Brekke, O. H. and I. Sandlie (2003). "Therapeutic antibodies for human diseases at the dawn of the twenty-first century." *Nat Rev Drug Discov* 2(1): 52-62.

Bridgeman, J. S., A. K. Sewell, J. J. Miles, D. A. Price and D. K. Cole (2011). "Structural and biophysical determinants of alphabeta T-cell antigen recognition." *Immunology* 135(1): 9-18.

Brinkmann, U., Y. Reiter, S. H. Jung, B. Lee and I. Pastan (1993). "A recombinant immunotoxin containing a disulfide-stabilized Fv fragment." *Proc Natl Acad Sci U S A* 90(16): 7538-42.

Brischwein, K., B. Schlereth, B. Guller, C. Steiger, A. Wolf, R. Lutterbuese, S. Offner, M. Locher, T. Urbig, T. Raum, P. Kleindienst, P. Wimberger, R. Kimmig, I. Fichtner, P. Kufer, R. Hofmeister, A. J. da Silva and P. A. Baeuerle (2006). "MT110: a novel bispecific single-chain antibody construct with high efficacy in eradicating established tumors." *Mol Immunol* 43(8): 1129-43.

Bulek, A. M., D. K. Cole, A. Skowera, G. Dolton, S. Gras, F. Madura, A. Fuller, J. J. Miles, E. Gostick, D. A. Price, J. W. Drijfhout, R. R. Knight, G. C. Huang, N. Lissin, P. E. Molloy, L. Wooldridge, B. K. Jakobsen, J. Rossjohn, M. Peakman, P. J.

Rizkallah and A. K. Sewell "Structural basis for the killing of human beta cells by CD8(+) T cells in type 1 diabetes." *Nat Immunol* 13(3): 283-9.

Bulek, A. M., D. K. Cole, A. Skowera, G. Dolton, S. Gras, F. Madura, A. Fuller, J. J. Miles, E. Gostick, D. A. Price, J. W. Drijfhout, R. R. Knight, G. C. Huang, N. Lissin, P. E. Molloy, L. Wooldridge, B. K. Jakobsen, J. Rossjohn, M. Peakman, P. J. Rizkallah and A. K. Sewell (2012). "Structural basis for the killing of human beta cells by CD8(+) T cells in type 1 diabetes." *Nat Immunol* 13(3): 283-9.

Celis, E., V. Tsai, C. Crimi, R. DeMars, P. A. Wentworth, R. W. Chesnut, H. M. Grey, A. Sette and H. M. Serra (1994). "Induction of anti-tumor cytotoxic T lymphocytes in normal humans using primary cultures and synthetic peptide epitopes." *Proc Natl Acad Sci U S A* 91(6): 2105-9.

Chames, P., S. E. Hufton, P. G. Coulie, B. Uchanska-Ziegler and H. R. Hoogenboom (2000). "Direct selection of a human antibody fragment directed against the tumor T-cell epitope HLA-A1-MAGE-A1 from a nonimmunized phage-Fab library." *Proc Natl Acad Sci U S A* 97(14): 7969-74.

Chen, J. L., G. Stewart-Jones, G. Bossi, N. M. Lissin, L. Wooldridge, E. M. Choi, G. Held, P. R. Dunbar, R. M. Esnouf, M. Sami, J. M. Boulter, P. Rizkallah, C. Renner, A. Sewell, P. A. van der Merwe, B. K. Jakobsen, G. Griffiths, E. Y. Jones and V. Cerundolo (2005). "Structural and kinetic basis for heightened immunogenicity of T cell vaccines." *J Exp Med* 201(8): 1243-55.

Chen, Y., C. Wiesmann, G. Fuh, B. Li, H. W. Christinger, P. McKay, A. M. de Vos and H. B. Lowman (1999). "Selection and analysis of an optimized anti-VEGF antibody: crystal structure of an affinity-matured Fab in complex with antigen." *J Mol Biol* 293(4): 865-81.

Chervin, A. S., D. H. Aggen, J. M. Raseman and D. M. Kranz (2008). "Engineering higher affinity T cell receptors using a T cell display system." *J Immunol Methods*.

Chlewicki, L. K., P. D. Holler, B. C. Monti, M. R. Clutter and D. M. Kranz (2005). "High-affinity, peptide-specific T cell receptors can be generated by mutations in CDR1, CDR2 or CDR3." *J Mol Biol* 346(1): 223-39.

Chodorge, M., L. Fourage, G. Ravot, L. Jermutus and R. Minter (2008). "In vitro DNA recombination by L-Shuffling during ribosome display affinity maturation of an anti-Fas antibody increases the population of improved variants." *Protein Eng Des Sel* 21(5): 343-51.

Chung, S., K. W. Wucherpfennig, S. M. Friedman, D. A. Hafler and J. L. Strominger (1994). "Functional three-domain single-chain T-cell receptors." *Proc Natl Acad Sci U S A* 91(26): 12654-8.

Clackson, T., H. R. Hoogenboom, A. D. Griffiths and G. Winter (1991). "Making antibody fragments using phage display libraries." *Nature* 352(6336): 624-8.

Claverie, J. M., A. Prochnicka-Chalufour and L. Bougueleret (1989). "Implications of a Fab-like structure for the T-cell receptor." *Immunol Today* 10(1): 10-4.

Cohen, C. J., N. Hoffmann, M. Farago, H. R. Hoogenboom, L. Eisenbach and Y. Reiter (2002). "Direct detection and quantitation of a distinct T-cell epitope derived from tumor-specific epithelial cell-associated mucin using human recombinant antibodies endowed with the antigen-specific, major histocompatibility complex-restricted specificity of T cells." *Cancer Res* 62(20): 5835-44.

Cole, D. K., B. Laugel, M. Clement, D. A. Price, L. Wooldridge and A. K. Sewell (2012). "The molecular determinants of CD8 co-receptor function." *Immunology* 137(2): 139-48.

Cole, D. K., N. J. Pumphrey, J. M. Boulter, M. Sami, J. I. Bell, E. Gostick, D. A. Price, G. F. Gao, A. K. Sewell and B. K. Jakobsen (2007). "Human TCR-binding affinity is governed by MHC class restriction." *J Immunol* 178(9): 5727-34.

Cole, D. K., F. Yuan, P. J. Rizkallah, J. J. Miles, E. Gostick, D. A. Price, G. F. Gao, B. K. Jakobsen and A. K. Sewell (2009). "Germline-governed recognition of a cancer epitope by an immunodominant human T-cell receptor." *J Biol Chem*.

Coloma, M. J. and S. L. Morrison (1997). "Design and production of novel tetravalent bispecific antibodies." *Nat Biotechnol* 15(2): 159-63.

Cormier, J. N., Y. M. Hijazi, A. Abati, P. Fetsch, M. Bettinotti, S. M. Steinberg, S. A. Rosenberg and F. M. Marincola (1998). "Heterogeneous expression of melanoma-associated antigens and HLA-A2 in metastatic melanoma in vivo." *Int J Cancer* 75(4): 517-24.

Coulie, P. G., V. Brichard, A. Van Pel, T. Wolfel, J. Schneider, C. Traversari, S. Mattei, E. De Plaen, C. Lurquin, J. P. Szikora, J. C. Renauld and T. Boon (1994). "A new gene coding for a differentiation antigen recognized by autologous cytolytic T lymphocytes on HLA-A2 melanomas." *J Exp Med* 180(1): 35-42.

Cox, A. L., J. Skipper, Y. Chen, R. A. Henderson, T. L. Darrow, J. Shabanowitz, V. H. Engelhard, D. F. Hunt and C. L. Slingluff, Jr. (1994). "Identification of a peptide recognized by five melanoma-specific human cytotoxic T cell lines." *Science* 264(5159): 716-9.

Davis, M. M. and P. J. Bjorkman (1988). "T-cell antigen receptor genes and T-cell recognition." *Nature* 334(6181): 395-402.

Davis, M. M., J. J. Boniface, Z. Reich, D. Lyons, J. Hampl, B. Arden and Y. Chien (1998). "Ligand recognition by alpha beta T cell receptors." *Annu Rev Immunol* 16: 523-44.

de Bruin, R., K. Spelt, J. Mol, R. Koes and F. Quattrocchio (1999). "Selection of high-affinity phage antibodies from phage display libraries." *Nat Biotechnol* 17(4): 397-9.

de Kruif, J., E. Boel and T. Logtenberg (1995). "Selection and application of human single chain Fv antibody fragments from a semi-synthetic phage antibody display library with designed CDR3 regions." *J Mol Biol* 248(1): 97-105.

De Pascalis, R., N. R. Gonzales, E. A. Padlan, P. Schuck, S. K. Batra, J. Schlom and S. V. Kashmiri (2003). "In vitro affinity maturation of a specificity-determining region-grafted humanized anticarcinoma antibody: isolation and characterization of minimally immunogenic high-affinity variants." *Clin Cancer Res* 9(15): 5521-31.

Degano, M., K. C. Garcia, V. Apostolopoulos, M. G. Rudolph, L. Teyton and I. A. Wilson (2000). "A functional hot spot for antigen recognition in a superagonist TCR/MHC complex." *Immunity* 12(3): 251-61.

Dhimolea, E. and J. M. Reichert (2012). "World Bispecific Antibody Summit, September 27-28, 2011, Boston, MA." *MAbs* 4(1): 4-16.

DiBrino, M., T. Tsuchida, R. V. Turner, K. C. Parker, J. E. Coligan and W. E. Biddison (1993). "HLA-A1 and HLA-A3 T cell epitopes derived from influenza virus proteins predicted from peptide binding motifs." *J Immunol* 151(11): 5930-5.

Ding, Y. H., B. M. Baker, D. N. Garboczi, W. E. Biddison and D. C. Wiley (1999). "Four A6-TCR/peptide/HLA-A2 structures that generate very different T cell signals are nearly identical." *Immunity* 11(1): 45-56.

Ding, Y. H., K. J. Smith, D. N. Garboczi, U. Utz, W. E. Biddison and D. C. Wiley (1998). "Two human T cell receptors bind in a similar diagonal mode to the HLA-A2/Tax peptide complex using different TCR amino acids." *Immunity* 8(4): 403-11.

Dolezal, O., R. De Gori, M. Walter, L. Doughty, M. Hattarki, P. J. Hudson and A. A. Kortt (2003). "Single-chain Fv multimers of the anti-neuraminidase antibody NC10: the residue at position 15 in the V(L) domain of the scFv-0 (V(L)-V(H)) molecule is primarily responsible for formation of a tetramer-trimer equilibrium." *Protein Eng* 16(1): 47-56.

Donermeyer, D. L., K. S. Weber, D. M. Kranz and P. M. Allen (2006). "The study of high-affinity TCRs reveals duality in T cell recognition of antigen: specificity and degeneracy." *J Immunol* 177(10): 6911-9.

Dong, J., A. Sereno, D. Aivazian, E. Langley, B. R. Miller, W. B. Snyder, E. Chan, M. Cantele, R. Morena, I. B. Joseph, A. Boccia, C. Virata, J. Gamez, G. Yco, M. Favis, X. Wu, C. P. Graff, Q. Wang, E. Rohde, R. Rennard, L. Berquist, F. Huang, Y. Zhang, S. X. Gao, S. N. Ho, S. J. Demarest, M. E. Reff, K. Hariharan and S. M. Glaser (2011). "A stable IgG-like bispecific antibody targeting the epidermal growth factor receptor and the type I insulin-like growth factor receptor demonstrates superior anti-tumor activity." *MAbs* 3(3): 273-88.

Dreier, T., G. Lorenczewski, C. Brandl, P. Hoffmann, U. Syring, F. Hanakam, P. Kufer, G. Riethmuller, R. Bargou and P. A. Baeuerle (2002). "Extremely potent, rapid and costimulation-independent cytotoxic T-cell response against lymphoma cells catalyzed by a single-chain bispecific antibody." *Int J Cancer* 100(6): 690-7.

Dunn, S. M., P. J. Rizkallah, E. Baston, T. Mahon, B. Cameron, R. Moysey, F. Gao, M. Sami, J. Boulter, Y. Li and B. K. Jakobsen (2006). "Directed evolution of human T cell receptor CDR2 residues by phage display dramatically enhances affinity for

cognate peptide-MHC without increasing apparent cross-reactivity." *Protein Sci* 15(4): 710-21.

Ehrlich, P. (1906). Collected studies on immunity, New York: Wiley & Sons.

Falk, K., O. Rotzschke, M. Takiguchi, B. Grahovac, V. Gnau, S. Stevanovic, G. Jung and H. G. Rammensee (1994). "Peptide motifs of HLA-A1, -A11, -A31, and -A33 molecules." *Immunogenetics* 40(3): 238-41.

Fellouse, F. A., K. Esaki, S. Birtalan, D. Raptis, V. J. Cancasci, A. Koide, P. Jhurani, M. Vasser, C. Wiesmann, A. A. Kossiakoff, S. Koide and S. S. Sidhu (2007). "High-throughput generation of synthetic antibodies from highly functional minimalist phage-displayed libraries." *J Mol Biol* 373(4): 924-40.

Fellouse, F. A., B. Li, D. M. Compaan, A. A. Peden, S. G. Hymowitz and S. S. Sidhu (2005). "Molecular recognition by a binary code." *J Mol Biol* 348(5): 1153-62.

Fellouse, F. A., C. Wiesmann and S. S. Sidhu (2004). "Synthetic antibodies from a four-amino-acid code: a dominant role for tyrosine in antigen recognition." *Proc Natl Acad Sci U S A* 101(34): 12467-72.

Fields, B. A., B. Ober, E. L. Malchiodi, M. I. Lebedeva, B. C. Braden, X. Ysern, J. K. Kim, X. Shao, E. S. Ward and R. A. Mariuzza (1995). "Crystal structure of the V alpha domain of a T cell antigen receptor." *Science* 270(5243): 1821-4.

Finkel, T. H., J. C. Cambier, R. T. Kubo, W. K. Born, P. Marrack and J. W. Kappler (1989). "The thymus has two functionally distinct populations of immature alpha beta + T cells: one population is deleted by ligation of alpha beta TCR." *Cell* 58(6): 1047-54.

Foote, J. and G. Winter (1992). "Antibody framework residues affecting the conformation of the hypervariable loops." *J Mol Biol* 224(2): 487-99.

Fremont, D. H., M. Matsumura, E. A. Stura, P. A. Peterson and I. A. Wilson (1992). "Crystal structures of two viral peptides in complex with murine MHC class I H-2Kb." *Science* 257(5072): 919-27.

Fremont, D. H., W. A. Rees and H. Kozono (1996). "Biophysical studies of T-cell receptors and their ligands." *Curr Opin Immunol* 8(1): 93-100.

Garboczi, D. N., P. Ghosh, U. Utz, Q. R. Fan, W. E. Biddison and D. C. Wiley (1996). "Structure of the complex between human T-cell receptor, viral peptide and HLA-A2." *Nature* 384(6605): 134-41.

Garboczi, D. N., D. T. Hung and D. C. Wiley (1992). "HLA-A2-peptide complexes: refolding and crystallization of molecules expressed in Escherichia coli and complexed with single antigenic peptides." *Proc Natl Acad Sci U S A* 89(8): 3429-33.

Garboczi, D. N., U. Utz, P. Ghosh, A. Seth, J. Kim, E. A. VanTienhoven, W. E. Biddison and D. C. Wiley (1996). "Assembly, specific binding, and crystallization of a human TCR-alphabeta with an antigenic Tax peptide from human T lymphotropic virus type 1 and the class I MHC molecule HLA-A2." *J Immunol* 157(12): 5403-10.

Garcia, K. C., M. Degano, R. L. Stanfield, A. Brunmark, M. R. Jackson, P. A. Peterson, L. Teyton and I. A. Wilson (1996). "An alphabeta T cell receptor structure at 2.5 A and its orientation in the TCR-MHC complex." *Science* 274(5285): 209-19.

Gascoigne, N. R., C. C. Goodnow, K. I. Dudzik, V. T. Oi and M. M. Davis (1987). "Secretion of a chimeric T-cell receptor-immunoglobulin protein." *Proc Natl Acad Sci U S A* 84(9): 2936-40.

Gascoigne, N. R., T. Zal and S. M. Alam (2001). "T-cell receptor binding kinetics in T-cell development and activation." *Expert Rev Mol Med* 2001: 1-17.

Gaugler, B., B. Van den Eynde, P. van der Bruggen, P. Romero, J. J. Gaforio, E. De Plaen, B. Lethe, F. Brasseur and T. Boon (1994). "Human gene MAGE-3 codes for an antigen recognized on a melanoma by autologous cytolytic T lymphocytes." *J Exp Med* 179(3): 921-30.

Gebauer, M. and A. Skerra (2009). "Engineered protein scaffolds as next-generation antibody therapeutics." *Curr Opin Chem Biol* 13(3): 245-55.

Graff, C. P., K. Chester, R. Begent and K. D. Wittrup (2004). "Directed evolution of an anti-carcinoembryonic antigen scFv with a 4-day monovalent dissociation half-time at 37 degrees C." *Protein Eng Des Sel* 17(4): 293-304.

Grakoui, A., S. K. Bromley, C. Sumen, M. M. Davis, A. S. Shaw, P. M. Allen and M. L. Dustin (1999). "The immunological synapse: a molecular machine controlling T cell activation." *Science* 285(5425): 221-7.

Greenwood, J., G. J. Hunter and R. N. Perham (1991). "Regulation of filamentous bacteriophage length by modification of electrostatic interactions between coat protein and DNA." *J Mol Biol* 217(2): 223-7.

Gregoire, C., N. Rebai, F. Schweisguth, A. Necker, G. Mazza, N. Auphan, A. Millward, A. M. Schmitt-Verhulst and B. Malissen (1991). "Engineered secreted T-cell receptor alpha beta heterodimers." *Proc Natl Acad Sci U S A* 88(18): 8077-81.

Griffiths, A. D., M. Malmqvist, J. D. Marks, J. M. Bye, M. J. Embleton, J. McCafferty, M. Baier, K. P. Holliger, B. D. Gorick, N. C. Hughes-Jones and et al. (1993). "Human anti-self antibodies with high specificity from phage display libraries." *Embo J* 12(2): 725-34.

Griffiths, A. D., S. C. Williams, O. Hartley, I. M. Tomlinson, P. Waterhouse, W. L. Crosby, R. E. Kontermann, P. T. Jones, N. M. Low, T. J. Allison and et al. (1994). "Isolation of high affinity human antibodies directly from large synthetic repertoires." *Embo J* 13(14): 3245-60.

Guo, H. C., T. S. Jardetzky, T. P. Garrett, W. S. Lane, J. L. Strominger and D. C. Wiley (1992). "Different length peptides bind to HLA-Aw68 similarly at their ends but bulge out in the middle." *Nature* 360(6402): 364-6.

Haidar, J. N., B. Pierce, Y. Yu, W. Tong, M. Li and Z. Weng (2009). "Structure-based design of a T-cell receptor leads to nearly 100-fold improvement in binding affinity for pepMHC." *Proteins* 74(4): 948-60.

Hammond, S. A., R. Lutterbuese, S. Roff, P. Lutterbuese, B. Schlereth, E. Bruckheimer, M. S. Kinch, S. Coats, P. A. Baeuerle, P. Kufer and P. A. Kiener (2007). "Selective targeting and potent control of tumor growth using an EphA2/CD3-Bispecific single-chain antibody construct." *Cancer Res* 67(8): 3927-35.

Hanes, J. and A. Pluckthun (1997). "In vitro selection and evolution of functional proteins by using ribosome display." *Proc Natl Acad Sci U S A* 94(10): 4937-42.

Hanes, J., C. Schaffitzel, A. Knappik and A. Pluckthun (2000). "Picomolar affinity antibodies from a fully synthetic naive library selected and evolved by ribosome display." *Nat Biotechnol* 18(12): 1287-92.

Hawkins, R. E., S. J. Russell and G. Winter (1992). "Selection of phage antibodies by binding affinity. Mimicking affinity maturation." *J Mol Biol* 226(3): 889-96.

Hawkins, R. E. and G. Winter (1992). "Cell selection strategies for making antibodies from variable gene libraries: trapping the memory pool." *Eur J Immunol* 22(3): 867-70.

Hilyard, K. L., H. Reyburn, S. Chung, J. I. Bell and J. L. Strominger (1994). "Binding of soluble natural ligands to a soluble human T-cell receptor fragment produced in Escherichia coli." *Proc Natl Acad Sci U S A* 91(19): 9057-61.

Ho, M., R. J. Kreitman, M. Onda and I. Pastan (2005). "In vitro antibody evolution targeting germline hot spots to increase activity of an anti-CD22 immunotoxin." *J Biol Chem* 280(1): 607-17.

Hoet, R. M., E. H. Cohen, R. B. Kent, K. Rookey, S. Schoonbroodt, S. Hogan, L. Rem, N. Frans, M. Daukandt, H. Pieters, R. van Hegelsom, N. C. Neer, H. G. Nastri, I. J. Rondon, J. A. Leeds, S. E. Hufton, L. Huang, I. Kashin, M. Devlin, G. Kuang, M. Steukers, M. Viswanathan, A. E. Nixon, D. J. Sexton, H. R. Hoogenboom and R. C. Ladner (2005). "Generation of high-affinity human antibodies by combining donor-derived and synthetic complementarity-determining-region diversity." *Nat Biotechnol* 23(3): 344-8.

Holler, P. D., L. K. Chlewicki and D. M. Kranz (2003). "TCRs with high affinity for foreign pMHC show self-reactivity." *Nat Immunol* 4(1): 55-62.

Holler, P. D., P. O. Holman, E. V. Shusta, S. O'Herrin, K. D. Wittrup and D. M. Kranz (2000). "In vitro evolution of a T cell receptor with high affinity for peptide/MHC." *Proc Natl Acad Sci U S A* 97(10): 5387-92.

Holler, P. D. and D. M. Kranz (2003). "Quantitative analysis of the contribution of TCR/pepMHC affinity and CD8 to T cell activation." *Immunity* 18(2): 255-64.

Holliger, P. and P. J. Hudson (2005). "Engineered antibody fragments and the rise of single domains." *Nat Biotechnol* 23(9): 1126-36.

Holliger, P., T. Prospero and G. Winter (1993). ""Diabodies": small bivalent and bispecific antibody fragments." *Proc Natl Acad Sci U S A* 90(14): 6444-8.

Hoo, W. F., M. J. Lacy, L. K. Denzin, E. W. Voss, Jr., K. D. Hardman and D. M. Kranz (1992). "Characterization of a single-chain T-cell receptor expressed in Escherichia coli." *Proc Natl Acad Sci U S A* 89(10): 4759-63.

Hoogenboom, H. R., A. D. Griffiths, K. S. Johnson, D. J. Chiswell, P. Hudson and G. Winter (1991). "Multi-subunit proteins on the surface of filamentous phage: methodologies for displaying antibody (Fab) heavy and light chains." *Nucleic Acids Res* 19(15): 4133-7.

Hoogenboom, H. R. and G. Winter (1992). "By-passing immunisation. Human antibodies from synthetic repertoires of germline VH gene segments rearranged in vitro." *J Mol Biol* 227(2): 381-8.

Horwitz, A. H., C. P. Chang, M. Better, K. E. Hellstrom and R. R. Robinson (1988). "Secretion of functional antibody and Fab fragment from yeast cells." *Proc Natl Acad Sci U S A* 85(22): 8678-82.

Hosse, R. J., A. Rothe and B. E. Power (2006). "A new generation of protein display scaffolds for molecular recognition." *Protein Sci* 15(1): 14-27.

Huang, J., V. I. Zarnitsyna, B. Liu, L. J. Edwards, N. Jiang, B. D. Evavold and C. Zhu (2010). "The kinetics of two-dimensional TCR and pMHC interactions determine T-cell responsiveness." *Nature* 464(7290): 932-6.

Hulsmeyer, M., P. Chames, R. C. Hillig, R. L. Stanfield, G. Held, P. G. Coulie, C. Alings, G. Wille, W. Saenger, B. Uchanska-Ziegler, H. R. Hoogenboom and A. Ziegler (2005). "A major histocompatibility complex-peptide-restricted antibody and t cell receptor molecules recognize their target by distinct binding modes: crystal structure of human leukocyte antigen (HLA)-A1-MAGE-A1 in complex with FAB-HYB3." *J Biol Chem* 280(4): 2972-80.

Hunt, D. F., R. A. Henderson, J. Shabanowitz, K. Sakaguchi, H. Michel, N. Sevilir, A. L. Cox, E. Appella and V. H. Engelhard (1992). "Characterization of peptides bound to the class I MHC molecule HLA-A2.1 by mass spectrometry." *Science* 255(5049): 1261-3.

Huppa, J. B., M. Axmann, M. A. Mortelmaier, B. F. Lillemeier, E. W. Newell, M. Brameshuber, L. O. Klein, G. J. Schutz and M. M. Davis (2010). "TCR-peptide-MHC interactions in situ show accelerated kinetics and increased affinity." *Nature* 463(7283): 963-7.

Hurwitz, H., L. Fehrenbacher, W. Novotny, T. Cartwright, J. Hainsworth, W. Heim, J. Berlin, A. Baron, S. Griffing, E. Holmgren, N. Ferrara, G. Fyfe, B. Rogers, R. Ross and F. Kabbinavar (2004). "Bevacizumab plus irinotecan, fluorouracil, and leucovorin for metastatic colorectal cancer." *N Engl J Med* 350(23): 2335-42.

Huston, J. S., D. Levinson, M. Mudgett-Hunter, M. S. Tai, J. Novotny, M. N. Margolies, R. J. Ridge, R. E. Bruccoleri, E. Haber, R. Crea and et al. (1988). "Protein engineering of antibody binding sites: recovery of specific activity in an anti-digoxin single-chain Fv analogue produced in Escherichia coli." *Proc Natl Acad Sci U S A* 85(16): 5879-83.

Irvine, D. J., M. A. Purbhoo, M. Krogsgaard and M. M. Davis (2002). "Direct observation of ligand recognition by T cells." *Nature* 419(6909): 845-9.

Irving, R. A., A. A. Kortt and P. J. Hudson (1996). "Affinity maturation of recombinant antibodies using E. coli mutator cells." *Immunotechnology* 2(2): 127-43.

Ishizuka, J., G. B. Stewart-Jones, A. van der Merwe, J. I. Bell, A. J. McMichael and E. Y. Jones (2008). "The structural dynamics and energetics of an immunodominant T cell receptor are programmed by its Vbeta domain." *Immunity* 28(2): 171-82.

Jager, E., M. Ringhoffer, J. Karbach, M. Arand, F. Oesch and A. Knuth (1996). "Inverse relationship of melanocyte differentiation antigen expression in melanoma tissues and CD8+ cytotoxic-T-cell responses: evidence for immunoselection of antigen-loss variants in vivo." *Int J Cancer* 66(4): 470-6.

Janeway, C. A., Jr., P. Travers, M. Walport and E. al. (2001). Immunobiology: The Immune System in Health and Disease. 5th Edition.

Jungbluth, A. A., S. Ely, M. DiLiberto, R. Niesvizky, B. Williamson, D. Frosina, Y. T. Chen, N. Bhardwaj, S. Chen-Kiang, L. J. Old and H. J. Cho (2005). "The cancer-testis antigens CT7 (MAGE-C1) and MAGE-A3/6 are commonly expressed in multiple myeloma and correlate with plasma-cell proliferation." *Blood* 106(1): 167-74.

Karanikas, V., C. Lurquin, D. Colau, N. van Baren, C. De Smet, B. Lethe, T. Connerotte, V. Corbiere, M. A. Demoitie, D. Lienard, B. Dreno, T. Velu, T. Boon and P. G. Coulie (2003). "Monoclonal anti-MAGE-3 CTL responses in melanoma patients displaying tumor regression after vaccination with a recombinant canarypox virus." *J Immunol* 171(9): 4898-904.

Kawakami, Y., S. Eliyahu, C. H. Delgado, P. F. Robbins, L. Rivoltini, S. L. Topalian, T. Miki and S. A. Rosenberg (1994). "Cloning of the gene coding for a shared human melanoma antigen recognized by autologous T cells infiltrating into tumor." *Proc Natl Acad Sci U S A* 91(9): 3515-9.

Kawakami, Y., S. Eliyahu, C. H. Delgado, P. F. Robbins, K. Sakaguchi, E. Appella, J. R. Yannelli, G. J. Adema, T. Miki and S. A. Rosenberg (1994). "Identification of a human melanoma antigen recognized by tumor-infiltrating lymphocytes associated with in vivo tumor rejection." *Proc Natl Acad Sci U S A* 91(14): 6458-62.

Kawakami, Y., S. Eliyahu, C. Jennings, K. Sakaguchi, X. Kang, S. Southwood, P. F. Robbins, A. Sette, E. Appella and S. A. Rosenberg (1995). "Recognition of multiple epitopes in the human melanoma antigen gp100 by tumor-infiltrating T lymphocytes associated with in vivo tumor regression." *J Immunol* 154(8): 3961-8.

Kawakami, Y., S. Eliyahu, K. Sakaguchi, P. F. Robbins, L. Rivoltini, J. R. Yannelli, E. Appella and S. A. Rosenberg (1994). "Identification of the immunodominant peptides of the MART-1 human melanoma antigen recognized by the majority of HLA-A2-restricted tumor infiltrating lymphocytes." *J Exp Med* 180(1): 347-52.

Kersh, E. N., A. S. Shaw and P. M. Allen (1998). "Fidelity of T cell activation through multistep T cell receptor zeta phosphorylation." *Science* 281(5376): 572-5.

Kessels, H. W., M. D. van Den Boom, H. Spits, E. Hooijberg and T. N. Schumacher (2000). "Changing T cell specificity by retroviral T cell receptor display." *Proc Natl Acad Sci U S A* 97(26): 14578-83.

Kieke, M. C., E. V. Shusta, E. T. Boder, L. Teyton, K. D. Wittrup and D. M. Kranz (1999). "Selection of functional T cell receptor mutants from a yeast surface-display library." *Proc Natl Acad Sci U S A* 96(10): 5651-6.

Kieke, M. C., E. Sundberg, E. V. Shusta, R. A. Mariuzza, K. D. Wittrup and D. M. Kranz (2001). "High affinity T cell receptors from yeast display libraries block T cell activation by superantigens." *J Mol Biol* 307(5): 1305-15.

Kipriyanov, S. M., S. Dubel, F. Breitling, R. E. Kontermann and M. Little (1994). "Recombinant single-chain Fv fragments carrying C-terminal cysteine residues: production of bivalent and biotinylated miniantibodies." *Mol Immunol* 31(14): 1047-58.

Kisielow, P. and A. Miazek (1995). "Positive selection of T cells: rescue from programmed cell death and differentiation require continual engagement of the T cell receptor." *J Exp Med* 181(6): 1975-84.

Kjer-Nielsen, L., C. S. Clements, A. G. Brooks, A. W. Purcell, M. R. Fontes, J. McCluskey and J. Rossjohn (2002). "The structure of HLA-B8 complexed to an immunodominant viral determinant: peptide-induced conformational changes and a mode of MHC class I dimerization." *J Immunol* 169(9): 5153-60.

Kjer-Nielsen, L., C. S. Clements, A. W. Purcell, A. G. Brooks, J. C. Whisstock, S. R. Burrows, J. McCluskey and J. Rossjohn (2003). "A structural basis for the selection of dominant alphabeta T cell receptors in antiviral immunity." *Immunity* 18(1): 53-64.

Knappik, A., L. Ge, A. Honegger, P. Pack, M. Fischer, G. Wellnhofer, A. Hoess, J. Wolle, A. Pluckthun and B. Virnekas (2000). "Fully synthetic human combinatorial antibody libraries (HuCAL) based on modular consensus frameworks and CDRs randomized with trinucleotides." *J Mol Biol* 296(1): 57-86.

Kohler, G. and C. Milstein (1975). "Continuous cultures of fused cells secreting antibody of predefined specificity." *Nature* 256(5517): 495-7.

Korn, T., D. M. Nettelbeck, T. Volkel, R. Muller and R. E. Kontermann (2004). "Recombinant bispecific antibodies for the targeting of adenoviruses to CEA-expressing tumour cells: a comparative analysis of bacterially expressed single-chain diabody and tandem scFv." *J Gene Med* 6(6): 642-51.

Kortt, A. A., M. Lah, G. W. Oddie, C. L. Gruen, J. E. Burns, L. A. Pearce, J. L. Atwell, A. J. McCoy, G. J. Howlett, D. W. Metzger, R. G. Webster and P. J. Hudson (1997). "Single-chain Fv fragments of anti-neuraminidase antibody NC10 containing five- and ten-residue linkers form dimers and with zero-residue linker a trimer." *Protein Eng* 10(4): 423-33.

Krebber, A., J. Burmester and A. Pluckthun (1996). "Inclusion of an upstream transcriptional terminator in phage display vectors abolishes background expression of toxic fusions with coat protein g3p." *Gene* 178(1-2): 71-4.

Kristensen, P. and G. Winter (1998). "Proteolytic selection for protein folding using filamentous bacteriophages." *Fold Des* 3(5): 321-8.

Kwong, K. Y., S. Baskar, H. Zhang, C. L. Mackall and C. Rader (2008). "Generation, affinity maturation, and characterization of a human anti-human NKG2D monoclonal antibody with dual antagonistic and agonistic activity." *J Mol Biol* 384(5): 1143-56.

Lamminmaki, U., S. Pauperio, A. Westerlund-Karlsson, J. Karvinen, P. L. Virtanen, T. Lovgren and P. Saviranta (1999). "Expanding the conformational diversity by random insertions to CDRH2 results in improved anti-estradiol antibodies." *J Mol Biol* 291(3): 589-602.

Laugel, B., J. M. Boulter, N. Lissin, A. Vuidepot, Y. Li, E. Gostick, L. E. Crotty, D. C. Douek, J. Hemelaar, D. A. Price, B. K. Jakobsen and A. K. Sewell (2005). "Design of soluble recombinant T cell receptors for antigen targeting and T cell inhibition." *J Biol Chem* 280(3): 1882-92.

Laugel, B., H. A. van den Berg, E. Gostick, D. K. Cole, L. Wooldridge, J. Boulter, A. Milicic, D. A. Price and A. K. Sewell (2007). "Different T cell receptor affinity thresholds and CD8 coreceptor dependence govern cytotoxic T lymphocyte activation and tetramer binding properties." *J Biol Chem* 282(33): 23799-810.

Lawrence, M. C. and P. M. Colman (1993). "Shape complementarity at protein/protein interfaces." *J Mol Biol* 234(4): 946-50.

Lee, C. M., N. Iorno, F. Sierro and D. Christ (2007). "Selection of human antibody fragments by phage display." *Nat Protoc* 2(11): 3001-8.

Lefranc, M. P., V. Giudicelli, C. Ginestoux, J. Bodmer, W. Muller, R. Bontrop, M. Lemaitre, A. Malik, V. Barbie and D. Chaume (1999). "IMGT, the international ImMunoGeneTics database." *Nucleic Acids Res* 27(1): 209-12.

Li, B., H. Xi, L. Diehl, W. P. Lee, L. Sturgeon, J. Chinn, L. Deforge, R. F. Kelley, C. Wiesmann, M. van Lookeren Campagne and S. S. Sidhu (2009). "Improving therapeutic efficacy of a complement receptor by structure-based affinity maturation." *J Biol Chem* 284(51): 35605-11.

Li, Y., R. Moysey, P. E. Molloy, A. L. Vuidepot, T. Mahon, E. Baston, S. Dunn, N. Liddy, J. Jacob, B. K. Jakobsen and J. M. Boulter (2005). "Directed evolution of human T-cell receptors with picomolar affinities by phage display." *Nat Biotechnol* 23(3): 349-54.

Liddy, N., G. Bossi, K. J. Adams, A. Lissina, T. M. Mahon, N. J. Hassan, J. Gavarret, F. C. Bianchi, N. J. Pumphrey, K. Ladell, E. Gostick, A. K. Sewell, N. M. Lissin, N. E. Harwood, P. E. Molloy, Y. Li, B. J. Cameron, M. Sami, E. E. Baston, P. T. Todorov, S. J. Paston, R. E. Dennis, J. V. Harper, S. M. Dunn, R. Ashfield, A. Johnson, Y. McGrath, G. Plesa, C. H. June, M. Kalos, D. A. Price, A. Vuidepot, D. D. Williams, D. H. Sutton and B. K. Jakobsen (2012). "Monoclonal TCR-redirected tumor cell killing." *Nat Med* 18(6): 980-7.

Liddy, N., P. E. Molloy, A. D. Bennett, J. M. Boulter, B. K. Jakobsen and Y. Li (2010). "Production of a soluble disulfide bond-linked TCR in the cytoplasm of Escherichia coli trxB gor mutants." *Mol Biotechnol* 45(2): 140-9.

Lillemeier, B. F., M. A. Mortelmaier, M. B. Forstner, J. B. Huppa, J. T. Groves and M. M. Davis (2009). "TCR and Lat are expressed on separate protein islands on T cell membranes and concatenate during activation." *Nat Immunol* 11(1): 90-6.

Linley, A. J., M. Ahmad and R. C. Rees "Tumour-associated antigens: considerations for their use in tumour immunotherapy." *Int J Hematol* 93(3): 263-73.

Linley, A. J., M. Ahmad and R. C. Rees (2011). "Tumour-associated antigens: considerations for their use in tumour immunotherapy." *Int J Hematol* 93(3): 263-73.

Liu, J. K., Q. Teng, M. Garrity-Moses, T. Federici, D. Tanase, M. J. Imperiale and N. M. Boulis (2005). "A novel peptide defined through phage display for therapeutic protein and vector neuronal targeting." *Neurobiol Dis* 19(3): 407-18.

Lo Conte, L., C. Chothia and J. Janin (1999). "The atomic structure of protein-protein recognition sites." *J Mol Biol* 285(5): 2177-98.

Loffler, A., P. Kufer, R. Lutterbuse, F. Zettl, P. T. Daniel, J. M. Schwenkenbecher, G. Riethmuller, B. Dorken and R. C. Bargou (2000). "A recombinant bispecific single-chain antibody, CD19 x CD3, induces rapid and high lymphoma-directed cytotoxicity by unstimulated T lymphocytes." *Blood* 95(6): 2098-103.

Loset, G. A., E. Lunde, B. Bogen, O. H. Brekke and I. Sandlie (2007). "Functional phage display of two murine alpha/beta T-cell receptors is strongly dependent on fusion format, mode and periplasmic folding assistance." *Protein Eng Des Sel* 20(9): 461-72.

Low, N. M., P. H. Holliger and G. Winter (1996). "Mimicking somatic hypermutation: affinity maturation of antibodies displayed on bacteriophage using a bacterial mutator strain." *J Mol Biol* 260(3): 359-68.

Lowe, D. C., S. Gerhardt, A. Ward, D. Hargreaves, M. Anderson, F. Ferraro, R. A. Pauptit, D. V. Pattison, C. Buchanan, B. Popovic, D. K. Finch, T. Wilkinson, M. Sleeman, T. J. Vaughan and P. R. Mallinder "Engineering a high-affinity anti-IL-15 antibody: crystal structure reveals an alpha-helix in VH CDR3 as key component of paratope." *J Mol Biol* 406(1): 160-75.

Lowe, D. C., S. Gerhardt, A. Ward, D. Hargreaves, M. Anderson, F. Ferraro, R. A. Pauptit, D. V. Pattison, C. Buchanan, B. Popovic, D. K. Finch, T. Wilkinson, M. Sleeman, T. J. Vaughan and P. R. Mallinder (2011). "Engineering a high-affinity anti-IL-15 antibody: crystal structure reveals an alpha-helix in VH CDR3 as key component of paratope." *J Mol Biol* 406(1): 160-75.

Lucas, S. and P. G. Coulie (2008). "About human tumor antigens to be used in immunotherapy." *Semin Immunol* 20(5): 301-7.

Madden, D. R. (1995). "The three-dimensional structure of peptide-MHC complexes." *Annu Rev Immunol* 13: 587-622.

Madden, D. R., D. N. Garboczi and D. C. Wiley (1993). "The antigenic identity of peptide-MHC complexes: a comparison of the conformations of five viral peptides presented by HLA-A2." *Cell* 75(4): 693-708.

Madden, D. R., J. C. Gorga, J. L. Strominger and D. C. Wiley (1991). "The structure of HLA-B27 reveals nonamer self-peptides bound in an extended conformation." *Nature* 353(6342): 321-5.

Mallender, W. D. and E. W. Voss, Jr. (1994). "Construction, expression, and activity of a bivalent bispecific single-chain antibody." *J Biol Chem* 269(1): 199-206.

Marks, J. D., A. D. Griffiths, M. Malmqvist, T. P. Clackson, J. M. Bye and G. Winter (1992). "By-passing immunization: building high affinity human antibodies by chain shuffling." *Biotechnology (N Y)* 10(7): 779-83.

Marks, J. D., H. R. Hoogenboom, T. P. Bonnert, J. McCafferty, A. D. Griffiths and G. Winter (1991). "By-passing immunization. Human antibodies from V-gene libraries displayed on phage." *J Mol Biol* 222(3): 581-97.

Martinez-Hackert, E., N. Anikeeva, S. A. Kalams, B. D. Walker, W. A. Hendrickson and Y. Sykulev (2006). "Structural basis for degenerate recognition of natural HIV peptide variants by cytotoxic lymphocytes." *J Biol Chem* 281(29): 20205-12.

Mason, D. (1998). "A very high level of crossreactivity is an essential feature of the T-cell receptor." *Immunol Today* 19(9): 395-404.

Matsui, K., J. J. Boniface, P. Steffner, P. A. Reay and M. M. Davis (1994). "Kinetics of T-cell receptor binding to peptide/I-Ek complexes: correlation of the dissociation rate with T-cell responsiveness." *Proc Natl Acad Sci U S A* 91(26): 12862-6.

McCafferty, J., A. D. Griffiths, G. Winter and D. J. Chiswell (1990). "Phage antibodies: filamentous phage displaying antibody variable domains." *Nature* 348(6301): 552-4.

McCall, A. M., L. Shahied, A. R. Amoroso, E. M. Horak, H. H. Simmons, U. Nielson, G. P. Adams, R. Schier, J. D. Marks and L. M. Weiner (2001). "Increasing the affinity for tumor antigen enhances bispecific antibody cytotoxicity." *J Immunol* 166(10): 6112-7.

McKee, M. D., J. J. Roszkowski and M. I. Nishimura (2005). "T cell avidity and tumor recognition: implications and therapeutic strategies." *J Transl Med* 3: 35.

McKeithan, T. W. (1995). "Kinetic proofreading in T-cell receptor signal transduction." *Proc Natl Acad Sci U S A* 92(11): 5042-6.

McLafferty, M. A., R. B. Kent, R. C. Ladner and W. Markland (1993). "M13 bacteriophage displaying disulfide-constrained microproteins." *Gene* 128(1): 29-36.

Meng, W. S., H. von Grafenstein and I. S. Haworth (1997). "A model of water structure inside the HLA-A2 peptide binding groove." *Int Immunol* 9(9): 1339-46.

Michaelson, J. S., S. J. Demarest, B. Miller, A. Amatucci, W. B. Snyder, X. Wu, F. Huang, S. Phan, S. Gao, A. Doern, G. K. Farrington, A. Lugovskoy, I. Joseph, V. Bailly, X. Wang, E. Garber, J. Browning and S. M. Glaser (2009). "Anti-tumor activity of stability-engineered IgG-like bispecific antibodies targeting TRAIL-R2 and LTbetaR." *MAbs* 1(2): 128-41.

Molek, P., B. Strukelj and T. Bratkovic (2011). "Peptide phage display as a tool for drug discovery: targeting membrane receptors." *Molecules* 16(1): 857-87.

Monks, C. R., B. A. Freiberg, H. Kupfer, N. Sciaky and A. Kupfer (1998). "Three-dimensional segregation of supramolecular activation clusters in T cells." *Nature* 395(6697): 82-6.

Moore, P. A., W. Zhang, G. J. Rainey, S. Burke, H. Li, L. Huang, S. Gorlatov, M. C. Veri, S. Aggarwal, Y. Yang, K. Shah, L. Jin, S. Zhang, L. He, T. Zhang, V. Ciccarone, S. Koenig, E. Bonvini and S. Johnson (2011). "Application of dual affinity retargeting molecules to achieve optimal redirected T-cell killing of B-cell lymphoma." *Blood* 117(17): 4542-51.

Morris, G. P. and P. M. Allen (2012). "How the TCR balances sensitivity and specificity for the recognition of self and pathogens." *Nat Immunol* 13(2): 121-8.

Muller, B. H., A. Savatier, G. L'Hostis, N. Costa, M. Bossus, S. Michel, C. Ott, L. Becquart, A. Ruffion, E. A. Stura and F. Ducancel (2011). "In vitro affinity maturation of an anti-PSA antibody for prostate cancer diagnostic assay." *J Mol Biol* 414(4): 545-62.

Murphy, K., P. Travers and M. Walport, Eds. (2008). Janeway's Immunobiology.

Nielsen, U. B., G. P. Adams, L. M. Weiner and J. D. Marks (2000). "Targeting of bivalent anti-ErbB2 diabody antibody fragments to tumor cells is independent of the intrinsic antibody affinity." *Cancer Res* 60(22): 6434-40.

Nissim, A., H. R. Hoogenboom, I. M. Tomlinson, G. Flynn, C. Midgley, D. Lane and G. Winter (1994). "Antibody fragments from a 'single pot' phage display library as immunochemical reagents." *Embo J* 13(3): 692-8.

Novellino, L., C. Castelli and G. Parmiani (2005). "A listing of human tumor antigens recognized by T cells: March 2004 update." *Cancer Immunol Immunother* 54(3): 187-207.

Novotny, J., R. K. Ganju, S. T. Smiley, R. E. Hussey, M. A. Luther, M. A. Recny, R. F. Siliciano and E. L. Reinherz (1991). "A soluble, single-chain T-cell receptor fragment endowed with antigen-combining properties." *Proc Natl Acad Sci U S A* 88(19): 8646-50.

Nuttall, S. D. and R. B. Walsh (2008). "Display scaffolds: protein engineering for novel therapeutics." *Curr Opin Pharmacol* 8(5): 609-15.

O'Callaghan C, A., M. F. Byford, J. R. Wyer, B. E. Willcox, B. K. Jakobsen, A. J. McMichael and J. I. Bell (1999). "BirA enzyme: production and application in the

study of membrane receptor-ligand interactions by site-specific biotinylation." *Anal Biochem* 266(1): 9-15.

Onda, T., D. LaFace, G. Baier, T. Brunner, N. Honma, T. Mikayama, A. Altman and D. R. Green (1995). "A phage display system for detection of T cell receptor-antigen interactions." *Mol Immunol* 32(17-18): 1387-97.

Orcutt, K. D., M. E. Ackerman, M. Cieslewicz, E. Quiroz, A. L. Slusarczyk, J. V. Frangioni and K. D. Wittrup "A modular IgG-scFv bispecific antibody topology." *Protein Eng Des Sel* 23(4): 221-8.

Padlan, E. A. (1994). "Anatomy of the antibody molecule." *Mol Immunol* 31(3): 169-217.

Pansri, P., N. Jaruseranee, K. Rangnoi, P. Kristensen and M. Yamabhai (2009). "A compact phage display human scFv library for selection of antibodies to a wide variety of antigens." *BMC Biotechnol* 9: 6.

Parker, K. C., M. A. Bednarek, L. K. Hull, U. Utz, B. Cunningham, H. J. Zweerink, W. E. Biddison and J. E. Coligan (1992). "Sequence motifs important for peptide binding to the human MHC class I molecule, HLA-A2." *J Immunol* 149(11): 3580-7.

Parkhurst, M. R., M. L. Salgaller, S. Southwood, P. F. Robbins, A. Sette, S. A. Rosenberg and Y. Kawakami (1996). "Improved induction of melanoma-reactive CTL with peptides from the melanoma antigen gp100 modified at HLA-A*0201-binding residues." *J Immunol* 157(6): 2539-48.

Paschen, A. (2009). T Cell Antigens in Cancer. Tumor-Associated Antigens: Identification, Characterizatio, and Clinical Application. O. Gires and B. Seliger**:** 3-22.

Paschke, M. and W. Hohne (2005). "A twin-arginine translocation (Tat)-mediated phage display system." *Gene* 350(1): 79-88.

Pavoni, E., M. Flego, M. L. Dupuis, S. Barca, F. Petronzelli, A. M. Anastasi, V. D'Alessio, A. Pelliccia, P. Vaccaro, G. Monteriu, A. Ascione, R. De Santis, F. Felici, M. Cianfriglia and O. Minenkova (2006). "Selection, affinity maturation, and characterization of a human scFv antibody against CEA protein." *BMC Cancer* 6: 41.

Pawson, T. and P. Nash (2000). "Protein-protein interactions define specificity in signal transduction." *Genes Dev* 14(9): 1027-47.

Perez, P., R. W. Hoffman, S. Shaw, J. A. Bluestone and D. M. Segal (1985). "Specific targeting of cytotoxic T cells by anti-T3 linked to anti-target cell antibody." *Nature* 316(6026): 354-6.

Perez, P., J. A. Titus, M. T. Lotze, F. Cuttitta, D. L. Longo, E. S. Groves, H. Rabin, P. J. Durda and D. M. Segal (1986). "Specific lysis of human tumor cells by T cells coated with anti-T3 cross-linked to anti-tumor antibody." *J Immunol* 137(7): 2069-72.

Pluckthun, A. (2012). "Ribosome display: a perspective." *Methods Mol Biol* 805: 3-28.

Pluckthun, A. and A. Skerra (1989). "Expression of functional antibody Fv and Fab fragments in Escherichia coli." *Methods Enzymol* 178: 497-515.

Purbhoo, M. A., D. J. Irvine, J. B. Huppa and M. M. Davis (2004). "T cell killing does not require the formation of a stable mature immunological synapse." *Nat Immunol* 5(5): 524-30.

Purbhoo, M. A., Y. Li, D. H. Sutton, J. E. Brewer, E. Gostick, G. Bossi, B. Laugel, R. Moysey, E. Baston, N. Liddy, B. Cameron, A. D. Bennett, R. Ashfield, A. Milicic, D. A. Price, B. J. Classon, A. K. Sewell and B. K. Jakobsen (2007). "The HLA A*0201-restricted hTERT(540-548) peptide is not detected on tumor cells by a CTL clone or a high-affinity T-cell receptor." *Mol Cancer Ther* 6(7): 2081-91.

Purbhoo, M. A., D. H. Sutton, J. E. Brewer, R. E. Mullings, M. E. Hill, T. M. Mahon, J. Karbach, E. Jager, B. J. Cameron, N. Lissin, P. Vyas, J. L. Chen, V. Cerundolo and B. K. Jakobsen (2006). "Quantifying and imaging NY-ESO-1/LAGE-1-derived epitopes on tumor cells using high affinity T cell receptors." *J Immunol* 176(12): 7308-16.

Rabinowitz, J. D., C. Beeson, D. S. Lyons, M. M. Davis and H. M. McConnell (1996). "Kinetic discrimination in T-cell activation." *Proc Natl Acad Sci U S A* 93(4): 1401-5.

Reinke, S., P. Koniger, G. Herberth, H. Audring, H. Wang, J. Ma, Y. Guo, W. Sterry and U. Trefzer (2005). "Differential expression of MART-1, tyrosinase, and SM5-1 in primary and metastatic melanoma." *Am J Dermatopathol* 27(5): 401-6.

Reiser, J. B., C. Darnault, A. Guimezanes, C. Gregoire, T. Mosser, A. M. Schmitt-Verhulst, J. C. Fontecilla-Camps, B. Malissen, D. Housset and G. Mazza (2000). "Crystal structure of a T cell receptor bound to an allogeneic MHC molecule." *Nat Immunol* 1(4): 291-7.

Reiser, J. B., C. Gregoire, C. Darnault, T. Mosser, A. Guimezanes, A. M. Schmitt-Verhulst, J. C. Fontecilla-Camps, G. Mazza, B. Malissen and D. Housset (2002). "A T cell receptor CDR3beta loop undergoes conformational changes of unprecedented magnitude upon binding to a peptide/MHC class I complex." *Immunity* 16(3): 345-54.

Reiter, Y., I. Kurucz, U. Brinkmann, S. H. Jung, B. Lee, D. M. Segal and I. Pastan (1995). "Construction of a functional disulfide-stabilized TCR Fv indicates that antibody and TCR Fv frameworks are very similar in structure." *Immunity* 2(3): 281-7.

Richman, S. A., D. H. Aggen, M. L. Dossett, D. L. Donermeyer, P. M. Allen, P. D. Greenberg and D. M. Kranz (2009). "Structural features of T cell receptor variable regions that enhance domain stability and enable expression as single-chain ValphaVbeta fragments." *Mol Immunol* 46(5): 902-16.

Riechmann, L. and M. Weill (1993). "Phage display and selection of a site-directed randomized single-chain antibody Fv fragment for its affinity improvement." *Biochemistry* 32(34): 8848-55.

Rinderknecht, M., A. Villa, K. Ballmer-Hofer, D. Neri and M. Detmar (2010). "Phage-derived fully human monoclonal antibody fragments to human vascular endothelial growth factor-C block its interaction with VEGF receptor-2 and 3." *PLoS One* 5(8): e11941.

Robins, H. S., P. V. Campregher, S. K. Srivastava, A. Wacher, C. J. Turtle, O. Kahsai, S. R. Riddell, E. H. Warren and C. S. Carlson (2009). "Comprehensive assessment of T-cell receptor beta-chain diversity in alphabeta T cells." *Blood* 114(19): 4099-107.

Romero, P., N. Gervois, J. Schneider, P. Escobar, D. Valmori, C. Pannetier, A. Steinle, T. Wolfel, D. Lienard, V. Brichard, A. van Pel, F. Jotereau and J. C. Cerottini (1997). "Cytolytic T lymphocyte recognition of the immunodominant HLA-A*0201-restricted Melan-A/MART-1 antigenic peptide in melanoma." *J Immunol* 159(5): 2366-74.

Rondot, S., J. Koch, F. Breitling and S. Dubel (2001). "A helper phage to improve single-chain antibody presentation in phage display." *Nat Biotechnol* 19(1): 75-8.

Roosnek, E. and A. Lanzavecchia (1989). "Triggering T cells by otherwise inert hybrid anti-CD3/antitumor antibodies requires encounter with the specific target cell." *J Exp Med* 170(1): 297-302.

Rothe, C., S. Urlinger, C. Lohning, J. Prassler, Y. Stark, U. Jager, B. Hubner, M. Bardroff, I. Pradel, M. Boss, R. Bittlingmaier, T. Bataa, C. Frisch, B. Brocks, A. Honegger and M. Urban (2008). "The human combinatorial antibody library HuCAL GOLD combines diversification of all six CDRs according to the natural immune system with a novel display method for efficient selection of high-affinity antibodies." *J Mol Biol* 376(4): 1182-200.

Rudolph, M. G., R. L. Stanfield and I. A. Wilson (2006). "How TCRs bind MHCs, peptides, and coreceptors." *Annu Rev Immunol* 24: 419-66.

Russel, M., H. B. Lowman and T. Clackson (2004). Introduction to phage display biology and phage display. Phage Display. T. Clackson and H. B. Lowman**:** 1-11.

Salgaller, M. L., A. Afshar, F. M. Marincola, L. Rivoltini, Y. Kawakami and S. A. Rosenberg (1995). "Recognition of multiple epitopes in the human melanoma antigen gp100 by peripheral blood lymphocytes stimulated in vitro with synthetic peptides." *Cancer Res* 55(21): 4972-9.

Sami, M., P. J. Rizkallah, S. Dunn, P. Molloy, R. Moysey, A. Vuidepot, E. Baston, P. Todorov, Y. Li, F. Gao, J. M. Boulter and B. K. Jakobsen (2007). "Crystal structures of high affinity human T-cell receptors bound to peptide major histocompatibility complex reveal native diagonal binding geometry." *Protein Eng Des Sel* 20(8): 397-403.

Saper, M. A., P. J. Bjorkman and D. C. Wiley (1991). "Refined structure of the human histocompatibility antigen HLA-A2 at 2.6 A resolution." *J Mol Biol* 219(2): 277-319.

Scanlan, M. J., A. J. Simpson and L. J. Old (2004). "The cancer/testis genes: review, standardization, and commentary." *Cancer Immun* 4: 1.

Schamel, W. W., I. Arechaga, R. M. Risueno, H. M. van Santen, P. Cabezas, C. Risco, J. M. Valpuesta and B. Alarcon (2005). "Coexistence of multivalent and monovalent TCRs explains high sensitivity and wide range of response." *J Exp Med* 202(4): 493-503.

Schier, R., A. McCall, G. P. Adams, K. W. Marshall, H. Merritt, M. Yim, R. S. Crawford, L. M. Weiner, C. Marks and J. D. Marks (1996). "Isolation of picomolar affinity anti-c-erbB-2 single-chain Fv by molecular evolution of the complementarity determining regions in the center of the antibody binding site." *J Mol Biol* 263(4): 551-67.

Schlereth, B., I. Fichtner, G. Lorenczewski, P. Kleindienst, K. Brischwein, A. da Silva, P. Kufer, R. Lutterbuese, I. Junghahn, S. Kasimir-Bauer, P. Wimberger, R. Kimmig and P. A. Baeuerle (2005). "Eradication of tumors from a human colon cancer cell line and from ovarian cancer metastases in immunodeficient mice by a single-chain Ep-CAM-/CD3-bispecific antibody construct." *Cancer Res* 65(7): 2882-9.

Schmid, D. A., M. B. Irving, V. Posevitz, M. Hebeisen, A. Posevitz-Fejfar, J. C. Sarria, R. Gomez-Eerland, M. Thome, T. N. Schumacher, P. Romero, D. E. Speiser, V. Zoete, O. Michielin and N. Rufer (2010). "Evidence for a TCR affinity threshold delimiting maximal CD8 T cell function." *J Immunol* 184(9): 4936-46.

Schodin, B. A., C. J. Schlueter and D. M. Kranz (1996). "Binding properties and solubility of single-chain T cell receptors expressed in E. coli." *Mol Immunol* 33(9): 819-29.

Schofield, D. J., A. R. Pope, V. Clementel, J. Buckell, S. Chapple, K. F. Clarke, J. S. Conquer, A. M. Crofts, S. R. Crowther, M. R. Dyson, G. Flack, G. J. Griffin, Y. Hooks, W. J. Howat, A. Kolb-Kokocinski, S. Kunze, C. D. Martin, G. L. Maslen, J. N. Mitchell, M. O'Sullivan, R. L. Perera, W. Roake, S. P. Shadbolt, K. J. Vincent, A. Warford, W. E. Wilson, J. Xie, J. L. Young and J. McCafferty (2007). "Application of phage display to high throughput antibody generation and characterization." *Genome Biol* 8(11): R254.

Scott, A. M., J. D. Wolchok and L. J. Old (2012). "Antibody therapy of cancer." *Nat Rev Cancer* 12(4): 278-87.

Scott, J. K. and G. P. Smith (1990). "Searching for peptide ligands with an epitope library." *Science* 249(4967): 386-90.

Sewell, A. K. (2002). "Breaking the kinetic window of T-cell activation." *Trends Immunol* 23(2): 67.

Sewell, A. K. (2012). "Why must T cells be cross-reactive?" *Nat Rev Immunol* 12(9): 669-77.

Shinohara, N. and H. Fukuda (2002). "Isolation of monoclonal antibodies recognizing rare and dominant epitopes in plant vascular cell walls by phage display subtraction." *J Immunol Methods* 264(1-2): 187-94.

Shiroishi, M., K. Tsumoto, Y. Tanaka, A. Yokota, T. Nakanishi, H. Kondo and I. Kumagai (2007). "Structural consequences of mutations in interfacial Tyr residues of a protein antigen-antibody complex. The case of HyHEL-10-HEL." *J Biol Chem* 282(9): 6783-91.

Shusta, E. V., P. D. Holler, M. C. Kieke, D. M. Kranz and K. D. Wittrup (2000). "Directed evolution of a stable scaffold for T-cell receptor engineering." *Nat Biotechnol* 18(7): 754-9.

Silver, M. L., H. C. Guo, J. L. Strominger and D. C. Wiley (1992). "Atomic structure of a human MHC molecule presenting an influenza virus peptide." *Nature* 360(6402): 367-9.

Skerra, A. (2000). "Engineered protein scaffolds for molecular recognition." *J Mol Recognit* 13(4): 167-87.

Skerra, A. and A. Pluckthun (1988). "Assembly of a functional immunoglobulin Fv fragment in Escherichia coli." *Science* 240(4855): 1038-41.

Skerra, A. and A. Pluckthun (1991). "Secretion and in vivo folding of the Fab fragment of the antibody McPC603 in Escherichia coli: influence of disulphides and cis-prolines." *Protein Eng* 4(8): 971-9.

Skipper, J. C., P. H. Gulden, R. C. Hendrickson, N. Harthun, J. A. Caldwell, J. Shabanowitz, V. H. Engelhard, D. F. Hunt and C. L. Slingluff, Jr. (1999). "Mass-spectrometric evaluation of HLA-A*0201-associated peptides identifies dominant naturally processed forms of CTL epitopes from MART-1 and gp100." *Int J Cancer* 82(5): 669-77.

Slamon, D. J., B. Leyland-Jones, S. Shak, H. Fuchs, V. Paton, A. Bajamonde, T. Fleming, W. Eiermann, J. Wolter, M. Pegram, J. Baselga and L. Norton (2001). "Use of chemotherapy plus a monoclonal antibody against HER2 for metastatic breast cancer that overexpresses HER2." *N Engl J Med* 344(11): 783-92.

Smith, G. P. (1985). "Filamentous fusion phage: novel expression vectors that display cloned antigens on the virion surface." *Science* 228(4705): 1315-7.

Smith, G. P. and V. A. Petrenko (1997). "Phage Display." *Chem Rev* 97(2): 391-410.

Spagnoli, G. C., C. Schaefer, T. E. Willimann, T. Kocher, A. Amoroso, A. Juretic, M. Zuber, U. Luscher, F. Harder and M. Heberer (1995). "Peptide-specific CTL in tumor infiltrating lymphocytes from metastatic melanomas expressing MART-1/Melan-A, gp100 and Tyrosinase genes: a study in an unselected group of HLA-A2.1-positive patients." *Int J Cancer* 64(5): 309-15.

Staerz, U. D., O. Kanagawa and M. J. Bevan (1985). "Hybrid antibodies can target sites for attack by T cells." *Nature* 314(6012): 628-31.

Starr, T. K., S. C. Jameson and K. A. Hogquist (2003). "Positive and negative selection of T cells." *Annu Rev Immunol* 21: 139-76.

Steidl, S., O. Ratsch, B. Brocks, M. Durr and E. Thomassen-Wolf (2008). "In vitro affinity maturation of human GM-CSF antibodies by targeted CDR-diversification." *Mol Immunol* 46(1): 135-44.

Stern, L. J. and D. C. Wiley (1994). "Antigenic peptide binding by class I and class II histocompatibility proteins." *Structure* 2(4): 245-51.

Stone, J. D., A. S. Chervin and D. M. Kranz (2009). "T-cell receptor binding affinities and kinetics: impact on T-cell activity and specificity." *Immunology* 126(2): 165-76.

Storb, U., H. M. Shen, N. Michael and N. Kim (2001). "Somatic hypermutation of immunoglobulin and non-immunoglobulin genes." *Philos Trans R Soc Lond B Biol Sci* 356(1405): 13-9.

Strong, R. K., D. M. Penny, R. M. Feldman, L. P. Weiner, J. J. Boniface, M. M. Davis and P. J. Bjorkman (1994). "Engineering and expression of a secreted murine TCR with reduced N-linked glycosylation." *J Immunol* 153(9): 4111-21.

Tait, B. D. (2000). "HLA class I expression on human cancer cells. Implications for effective immunotherapy." *Hum Immunol* 61(2): 158-65.

Thompson, J., T. Pope, J. S. Tung, C. Chan, G. Hollis, G. Mark and K. S. Johnson (1996). "Affinity maturation of a high-affinity human monoclonal antibody against the third hypervariable loop of human immunodeficiency virus: use of phage display to improve affinity and broaden strain reactivity." *J Mol Biol* 256(1): 77-88.

Timmers, E., M. M. Hermans, M. E. Kraakman, R. W. Hendriks and R. K. Schuurman (1993). "Diversity of immunoglobulin kappa light chain gene rearrangements and evidence for somatic mutation in V kappa IV family gene segments in X-linked agammaglobulinemia." *Eur J Immunol* 23(3): 619-24.

Tomlinson, I. M., G. Walter, J. D. Marks, M. B. Llewelyn and G. Winter (1992). "The repertoire of human germline VH sequences reveals about fifty groups of VH segments with different hypervariable loops." *J Mol Biol* 227(3): 776-98.

Topp, M. S., P. Kufer, N. Gokbuget, M. Goebeler, M. Klinger, S. Neumann, H. A. Horst, T. Raff, A. Viardot, M. Schmid, M. Stelljes, M. Schaich, E. Degenhard, R. Kohne-Volland, M. Bruggemann, O. Ottmann, H. Pfeifer, T. Burmeister, D. Nagorsen, M. Schmidt, R. Lutterbuese, C. Reinhardt, P. A. Baeuerle, M. Kneba, H. Einsele, G. Riethmuller, D. Hoelzer, G. Zugmaier and R. C. Bargou (2011). "Targeted therapy with the T-cell-engaging antibody blinatumomab of chemotherapy-refractory minimal residual disease in B-lineage acute lymphoblastic leukemia patients results in high response rate and prolonged leukemia-free survival." *J Clin Oncol* 29(18): 2493-8.

Traversari, C., P. van der Bruggen, I. F. Luescher, C. Lurquin, P. Chomez, A. Van Pel, E. De Plaen, A. Amar-Costesec and T. Boon (1992). "A nonapeptide encoded by human gene MAGE-1 is recognized on HLA-A1 by cytolytic T lymphocytes directed against tumor antigen MZ2-E." *J Exp Med* 176(5): 1453-7.

Trefzer, U., M. Hofmann, S. Reinke, Y. J. Guo, H. Audring, G. Spagnoli and W. Sterry (2006). "Concordant loss of melanoma differentiation antigens in synchronous

and asynchronous melanoma metastases: implications for immunotherapy." *Melanoma Res* 16(2): 137-45.

Tsai, C. J., S. L. Lin, H. J. Wolfson and R. Nussinov (1997). "Studies of protein-protein interfaces: a statistical analysis of the hydrophobic effect." *Protein Sci* 6(1): 53-64.

Tynan, F. E., N. A. Borg, J. J. Miles, T. Beddoe, D. El-Hassen, S. L. Silins, W. J. van Zuylen, A. W. Purcell, L. Kjer-Nielsen, J. McCluskey, S. R. Burrows and J. Rossjohn (2005). "High resolution structures of highly bulged viral epitopes bound to major histocompatibility complex class I. Implications for T-cell receptor engagement and T-cell immunodominance." *J Biol Chem* 280(25): 23900-9.

Tynan, F. E., H. H. Reid, L. Kjer-Nielsen, J. J. Miles, M. C. Wilce, L. Kostenko, N. A. Borg, N. A. Williamson, T. Beddoe, A. W. Purcell, S. R. Burrows, J. McCluskey and J. Rossjohn (2007). "A T cell receptor flattens a bulged antigenic peptide presented by a major histocompatibility complex class I molecule." *Nat Immunol* 8(3): 268-76.

Valitutti, S. and A. Lanzavecchia (1997). "Serial triggering of TCRs: a basis for the sensitivity and specificity of antigen recognition." *Immunol Today* 18(6): 299-304.

Valitutti, S., S. Muller, M. Cella, E. Padovan and A. Lanzavecchia (1995). "Serial triggering of many T-cell receptors by a few peptide-MHC complexes." *Nature* 375(6527): 148-51.

Valmori, D., J. F. Fonteneau, C. M. Lizana, N. Gervois, D. Lienard, D. Rimoldi, V. Jongeneel, F. Jotereau, J. C. Cerottini and P. Romero (1998). "Enhanced generation of specific tumor-reactive CTL in vitro by selected Melan-A/MART-1 immunodominant peptide analogues." *J Immunol* 160(4): 1750-8.

van Baren, N., F. Brasseur, D. Godelaine, G. Hames, A. Ferrant, F. Lehmann, M. Andre, C. Ravoet, C. Doyen, G. C. Spagnoli, M. Bakkus, K. Thielemans and T. Boon (1999). "Genes encoding tumor-specific antigens are expressed in human myeloma cells." *Blood* 94(4): 1156-64.

van der Bruggen, P., C. Traversari, P. Chomez, C. Lurquin, E. De Plaen, B. Van den Eynde, A. Knuth and T. Boon (1991). "A gene encoding an antigen recognized by cytolytic T lymphocytes on a human melanoma." *Science* 254(5038): 1643-7.

van der Merwe, P. A. and S. J. Davis (2003). "Molecular interactions mediating T cell antigen recognition." *Annu Rev Immunol* 21: 659-84.

van der Merwe, P. A. and O. Dushek (2011). "Mechanisms for T cell receptor triggering." *Nat Rev Immunol* 11(1): 47-55.

van Oers, M. H., M. Van Glabbeke, L. Giurgea, R. Klasa, R. E. Marcus, M. Wolf, E. Kimby, M. van t Veer, A. Vranovsky, H. Holte and A. Hagenbeek (2010). "Rituximab maintenance treatment of relapsed/resistant follicular non-Hodgkin's lymphoma: long-term outcome of the EORTC 20981 phase III randomized intergroup study." *J Clin Oncol* 28(17): 2853-8.

van Wyngaardt, W., T. Malatji, C. Mashau, J. Fehrsen, F. Jordaan, D. Miltiadou and D. H. du Plessis (2004). "A large semi-synthetic single-chain Fv phage display library based on chicken immunoglobulin genes." *BMC Biotechnol* 4: 6.

Varela-Rohena, A., P. E. Molloy, S. M. Dunn, Y. Li, M. M. Suhoski, R. G. Carroll, A. Milicic, T. Mahon, D. H. Sutton, B. Laugel, R. Moysey, B. J. Cameron, A. Vuidepot, M. A. Purbhoo, D. K. Cole, R. E. Phillips, C. H. June, B. K. Jakobsen, A. K. Sewell and J. L. Riley (2008). "Control of HIV-1 immune escape by CD8 T cells expressing enhanced T-cell receptor." *Nat Med* 14(12): 1390-5.

Vaughan, T. J., A. J. Williams, K. Pritchard, J. K. Osbourn, A. R. Pope, J. C. Earnshaw, J. McCafferty, R. A. Hodits, J. Wilton and K. S. Johnson (1996). "Human antibodies with sub-nanomolar affinities isolated from a large non-immunized phage display library." *Nat Biotechnol* 14(3): 309-14.

Velappan, N., H. E. Fisher, E. Pesavento, L. Chasteen, S. D'Angelo, C. Kiss, M. Longmire, P. Pavlik and A. R. Bradbury (2010). "A comprehensive analysis of filamentous phage display vectors for cytoplasmic proteins: an analysis with different fluorescent proteins." *Nucleic Acids Res* 38(4): e22.

Vesely, M. D., M. H. Kershaw, R. D. Schreiber and M. J. Smyth (2011). "Natural innate and adaptive immunity to cancer." *Annu Rev Immunol* 29: 235-71.

Virnekas, B., L. Ge, A. Pluckthun, K. C. Schneider, G. Wellnhofer and S. E. Moroney (1994). "Trinucleotide phosphoramidites: ideal reagents for the synthesis of mixed oligonucleotides for random mutagenesis." *Nucleic Acids Res* 22(25): 5600-7.

Viti, F., F. Nilsson, S. Demartis, A. Huber and D. Neri (2000). "Design and use of phage display libraries for the selection of antibodies and enzymes." *Methods Enzymol* 326: 480-505.

Wang, J., Y. Liu, T. Teesalu, K. N. Sugahara, V. R. Kotamrajua, J. D. Adams, B. S. Ferguson, Q. Gong, S. S. Oh, A. T. Csordas, M. Cho, E. Ruoslahti, Y. Xiao and H. T. Soh (2011). "Selection of phage-displayed peptides on live adherent cells in microfluidic channels." *Proc Natl Acad Sci U S A* 108(17): 6909-14.

Wang, W., P. H. Gulden, R. A. Pierce, J. Shabanowitz, S. T. Man, D. F. Hunt and V. H. Engelhard (1997). "A naturally processed peptide presented by HLA-A*0201 is expressed at low abundance and recognized by an alloreactive CD8+ cytotoxic T cell with apparent high affinity." *J Immunol* 158(12): 5797-804.

Ward, E. S. (1991). "Expression and secretion of T-cell receptor V alpha and V beta domains using Escherichia coli as a host." *Scand J Immunol* 34(2): 215-20.

Ward, E. S., D. Gussow, A. D. Griffiths, P. T. Jones and G. Winter (1989). "Binding activities of a repertoire of single immunoglobulin variable domains secreted from Escherichia coli." *Nature* 341(6242): 544-6.

Weber, K. S., D. L. Donermeyer, P. M. Allen and D. M. Kranz (2005). "Class II-restricted T cell receptor engineered in vitro for higher affinity retains peptide specificity and function." *Proc Natl Acad Sci U S A* 102(52): 19033-8.

Webster, R. (2001). Filamentous Phage Display. Phage Display: A Laboratory Manual. C. F. Barbas, 3rd., D. R. Burton, J. K. Scott and G. J. Silverman**:** 1.1-1.37.

Weidanz, J. A., K. F. Card, A. Edwards, E. Perlstein and H. C. Wong (1998). "Display of functional alphabeta single-chain T-cell receptor molecules on the surface of bacteriophage." *J Immunol Methods* 221(1-2): 59-76.

Weisser, N. E. and J. C. Hall (2009). "Applications of single-chain variable fragment antibodies in therapeutics and diagnostics." *Biotechnol Adv* 27(4): 502-20.

Wells, J. A. (1990). "Additivity of mutational effects in proteins." *Biochemistry* 29(37): 8509-17.

Willcox, B. E., G. F. Gao, J. R. Wyer, J. E. Ladbury, J. I. Bell, B. K. Jakobsen and P. A. van der Merwe (1999). "TCR binding to peptide-MHC stabilizes a flexible recognition interface." *Immunity* 10(3): 357-65.

Willcox, B. E., G. F. Gao, J. R. Wyer, C. A. O'Callaghan, J. M. Boulter, E. Y. Jones, P. A. van der Merwe, J. I. Bell and B. K. Jakobsen (1999). "Production of soluble alphabeta T-cell receptor heterodimers suitable for biophysical analysis of ligand binding." *Protein Sci* 8(11): 2418-23.

Williams, S. C. and G. Winter (1993). "Cloning and sequencing of human immunoglobulin V lambda gene segments." *Eur J Immunol* 23(7): 1456-61.

Withoff, S., M. N. Bijman, A. J. Stel, L. Delahaye, A. Calogero, M. W. Jonge, B. J. Kroesen and L. Leij (2001). "Characterization of BIS20x3, a bi-specific antibody activating and retargeting T-cells to CD20-positive B-cells." *Br J Cancer* 84(8): 1115-21.

Wooldridge, L., J. Ekeruche-Makinde, H. A. van den Berg, A. Skowera, J. J. Miles, M. P. Tan, G. Dolton, M. Clement, S. Llewellyn-Lacey, D. A. Price, M. Peakman and A. K. Sewell (2012). "A single autoimmune T cell receptor recognizes more than a million different peptides." *J Biol Chem* 287(2): 1168-77.

Wooldridge, L., H. A. van den Berg, M. Glick, E. Gostick, B. Laugel, S. L. Hutchinson, A. Milicic, J. M. Brenchley, D. C. Douek, D. A. Price and A. K. Sewell (2005). "Interaction between the CD8 coreceptor and major histocompatibility complex class I stabilizes T cell receptor-antigen complexes at the cell surface." *J Biol Chem* 280(30): 27491-501.

Wu, H., G. Beuerlein, Y. Nie, H. Smith, B. A. Lee, M. Hensler, W. D. Huse and J. D. Watkins (1998). "Stepwise in vitro affinity maturation of Vitaxin, an alphav beta3-specific humanized mAb." *Proc Natl Acad Sci U S A* 95(11): 6037-42.

Wu, H., D. S. Pfarr, Y. Tang, L. L. An, N. K. Patel, J. D. Watkins, W. D. Huse, P. A. Kiener and J. F. Young (2005). "Ultra-potent antibodies against respiratory syncytial virus: effects of binding kinetics and binding valence on viral neutralization." *J Mol Biol* 350(1): 126-44.

Wulfing, C. and A. Pluckthun (1994). "Correctly folded T-cell receptor fragments in the periplasm of Escherichia coli. Influence of folding catalysts." *J Mol Biol* 242(5): 655-69.

Yang, W. P., K. Green, S. Pinz-Sweeney, A. T. Briones, D. R. Burton and C. F. Barbas, 3rd (1995). "CDR walking mutagenesis for the affinity maturation of a potent human anti-HIV-1 antibody into the picomolar range." *J Mol Biol* 254(3): 392-403.

Yewdell, J. W. (2001). "Not such a dismal science: the economics of protein synthesis, folding, degradation and antigen processing." *Trends Cell Biol* 11(7): 294-7.

Zemlin, M., M. Klinger, J. Link, C. Zemlin, K. Bauer, J. A. Engler, H. W. Schroeder, Jr. and P. M. Kirkham (2003). "Expressed murine and human CDR-H3 intervals of equal length exhibit distinct repertoires that differ in their amino acid composition and predicted range of structures." *J Mol Biol* 334(4): 733-49.

Zhao, Y., A. D. Bennett, Z. Zheng, Q. J. Wang, P. F. Robbins, L. Y. Yu, Y. Li, P. E. Molloy, S. M. Dunn, B. K. Jakobsen, S. A. Rosenberg and R. A. Morgan (2007). "High-affinity TCRs generated by phage display provide CD4+ T cells with the ability to recognize and kill tumor cell lines." *J Immunol* 179(9): 5845-54.

Zinkernagel, R. M. and P. C. Doherty (1974). "Immunological surveillance against altered self components by sensitised T lymphocytes in lymphocytic choriomeningitis." *Nature* 251(5475): 547-8.

Zubovits, J., E. Buzney, L. Yu and L. M. Duncan (2004). "HMB-45, S-100, NK1/C3, and MART-1 in metastatic melanoma." *Hum Pathol* 35(2): 217-23.